GROUNDBORNE VIBRATIONS CAUSED BY RAILWAY CONSTRUCTION AND OPERATION IN BUILDINGS: DESIGN, IMPLEMENTATION AND ANALYSIS OF MEASUREMENT FOR ASSESSMENT OF HUMAN EXPOSURE.

Gennaro SICA

PH.D. THESIS **2014**

GROUNDBORNE VIBRATIONS CAUSED BY RAILWAY CONSTRUCTION AND OPERATION IN BUILDINGS: DESIGN, IMPLEMENTATION AND ANALYSIS OF MEASUREMENT FOR ASSESSMENT OF HUMAN EXPOSURE.

Gennaro SICA

Acoustics Research Centre

School of Computing, Science and Engineering

University of Salford, Salford, UK

Submitted in Partial fulfilment of the Requirements of the

Degree of Doctor of Philosophy, March 2014

"A part of me is gonna always be with you,

A part of you is gonna always be with me."

To Vale

TABLE OF CONTENTS

LIST OF FIGURES

LIST OF TABLES

LIST OF NOMENCLATURE

ADC = Analogue to Digital Converter

ANC = Association of Noise Consultant

BS = British Standard

CP = Control Position

CWD = Choi-Williams distribution

Defra = Department environment food and rural affairs

ERRAC = European Railway Research Advisory Council

ERT = Electrical Resistivity Tomography

EXT = Accelerometer outside the house

FRF = Frequency Response Function

GIS = Geographic Information System

GPR = Ground Penetration Radar

GPS = Global Positioning System

HVSR = Spectral Ratio between Horizontal and Vertical components

INT = Accelerometer inside the house

IRF = Impulse Response Function

ISO = International Standard Organization

KB = Weighting curve from DIN 4150-2

LSSTA = Logarithmic Smoothed Short Term Average

LTA = Long Term Average

MASW = Multichannel Analysis of Surface Waves

MIMO = Multi Input Multi Output

ML = Measurement line

MLS = Maximum Length Sequence

MSC = magnitude squared coherence

PCA = Principal Component Analysis

PPA = Peak Particle Acceleration

PPV = Peak Particle Velocity

RMQ = Root Mean Quad

RMS = Root Mean Square

RSPWVD = Reassigned-Smoothed-Pseudo-Wigner-Ville Distribution

SASW = Spectral Analysis of Surface Waves

SDF = Seismic Direction Finding

SDM = Spectral Density Matrix in the frequency domain

SESAME = Site EffectS assessment using AMbient Excitations

SFTF = Short Time Fourier Transform

SISO = Single Input Single Output

SPAC = SPatial AutoCorrelation

SPWVD = Smoothed-Pseudo-Wigner-Ville distribution

SSTA = Smoothed Short Term Average

STA = Short Term Average

STF = Standard Transfer Function

SVD = Singular Value Decomposition

TF = Time Frequency distribution

TLM = Thin Layer Method

TRL = Transport Research Laboratory

TVANE = Train Vibration And Noise Effects

USGS = U.S. Geological Survey

VDV = Vibration Dose Value

W PPA = Weighted PPA

W RMQ = Weighted RMQ

W RMS = Weighted RMS

W_b = Weighting curve from BS 6472-1:2008 applied in vertical direction

W_d =Weighting curve from BS 6472-1:2008 and ISO 2361-1:1997 applied in horizontal direction

W_k = Weighting curve from ISO 2361-1:1997 applied in vertical horizontal direction

W_m = Weighting curve from ISO 2361-1:2003 applied in any direction

WVD = Wigner-Ville distribution

LIST OF SYMBOLS

A = accelerance

$A(d)$ = magnitude acceleration at d

$A(d_0)$ = magnitude acceleration at d_0

A_k = vibration measured at distance d_k

a_{ref} = reference acceleration

$a_w(t)$ = frequency weighted acceleration signal

$a_{w,95}$ = statistical maximum weighted acceleration

$a_{w,\max}$ = maximum 1-second average weighted acceleration

$\langle a_{w,\max} \rangle$ = mean value of the maximum weighted acceleration

$|A(f)|$ = averaged Fourier magnitude spectrum of an event at the control position

α = vibration attenuation

α_M = pseudo attenuation coefficient

α_0 = initial guess of α

B = bending stiffness

$|B(f)|$ = average Fourier magnitude spectrum of an internal event

$B_{pred}(f)$ = predicted complex Fourier spectrum of an internal event

c_1, c_2 = damping coefficients model apparent mass

C_n = crest factor

$C[x(t,f)]$ = general Cohen's class formulation

$C_{EI}(f)$ = magnitude-squared function between $\{E_n\}$ and $\{I_n\}$

$C_{I_i D_{Mj}}(f)$ = virtual coherence function

d = distance

d_0 = reference distance Barkan's law

d_S = distance between sleepers

D = soil material damping

D_M = general principal component matrix formulation

$D_M(f)$ = principal component matrix in the frequency domain

$D_{Mj}(f)$ = j-th principal component in the frequency domain

$\overline{D_{SE}}$ = distance between the source and the accelerometer outside the property

$\overline{D_{SB}}$ = distance between the source and the building

$\overline{D_{EI}}$ = distance between the two sensors

$\overline{D_{SC}}$ = distance between the source and the CP

Δ = matrix of singular values

Δt = sampling interval

e = triaxial event

e_p = predicted value of the internal exposure

e_r = true value of the internal exposure

$\{E_n\} = e(t)$ = signal recorded at EXT

$E(f)$ = double sided "non smoothed" Fourier spectrum for $\{E_n\}$

$E_q(f)$ = spectral estimation for the slice q for EXT

$EE_{ij}(f) = EE(f)$ = autopower matrix for the triaxial signal at EXT

E_fh = error function

$\varepsilon_{\exp}$ = relative error

$\xi\{\ \}$ = expectation value

f = frequency

f_0 = frequency range between 0 to 80 Hz

f_d = passage frequency

f_e = excitation frequency due to wheel-rail interaction

f_k = fundamental excitation frequency generated by fixed lengths in the train

$f(t)$ = external force

$\hat{f}(f,t)$ = frequency centroid of the SPWVD distribution

g = Acceleration due to gravity

G = second Lamé constant, shear modulus

$G_{EE}(f)$ = auto spectra of $\{E_n\}$

$G_{II}(f)$ = auto spectra of $\{I_n\}$

$G_{EI}(f)$ = cross spectrum between $\{E_n\}$ and $\{I_n\}$

$\gamma_{EI}(f)$ = complex coherence function between the two signals $\{E_n\}$ and $\{I_n\}$

H = set of the pile hits

$H(f)$ = magnitude only transmissibility or velocity ratio

$H_{est}(f)$ = interpolated double sided transmissibility $H(f)$

$H_{est}(f)$ = average interpolated transmissibility over $A(f)$

$H_{ave}(f)$ = average transmissibility function per case study

$H2(f)$ = cross spectrum transmissibility

$H1(f)$ = cross spectrum transmissibility or direct transmissibility

$H2_{VI_i}(f)$ = cross spectrum virtual transmissibility

$H_{VI_i}(f)$ = magnitude only virtual transmissibility

h_1, h_2 = window functions

$i_{pred}(t)$ = predicted internal time history

$I_{pred}(f)$ = predicted internal spectra

$\{I_n\}$ = signal recorded at *INT*

$II_{ij}(f)$ = autopower matrix for the triaxial signal at *INT* at f

$IE_{ij}(f) = IE(f)$ = cross power matrix between *INT* and *EXT* at f

$IE'_{ij}(f) = IE'(f)$ = virtual cross power spectra matrix between *INT* and *EXT* at f

$I[x_1(t, f), x_2(t, f)]$ = interference term between two signals

k = bending wave number

k_1, k_2 = stiffness coefficients model apparent mass

l = length of the beam

l_k = fixed length in the train

L = set of linearities L_j

L_j = linearity for a j dual channel measurement

λ = wavelength

λ_L = first Lamé constant

$\lambda_1^q, \lambda_2^q, \lambda_3^q$ = eigenvalues of the cross energy matrix M in the time window q

m = mass

m_1, m_2 = mass coefficients model apparent mass

m_{2a} = specific apparent mass of standing human body

m' = linear density

M = cross energy matrix

$Mi \quad i = 1 \ldots 4$ = measurement positions

M_0 = exposure metric at distance d_0

M_{2a} = general apparent mass of standing human body

$M(d)$ = exposure metric at distance d

μ = mean value of a stochastic process

n = variables

n_C = number of channels

N = number of vibration events

N_T = number of passing train

N_R = number of the triaxial rise events

N_q = length of time window

N_e = length of the piling event

$N_{\Delta t}^{e}$ = number of overlapped time windows

N_{fbin} = number of the frequency bins for RSPWVD

N_{SPT} = number of blow count of the SPT

$N_0^e(f_0)$ =time bins that exceed the polarization threshold at f_0

o = overlap

off_H = end of the interval where $LSSTA \geq -1dB$

off_L = end of the interval where $LSSTA \geq -20dB$

on_H = start of the interval where $LSSTA \geq -1dB$

on_L = start of the interval where $LSSTA \geq -20dB$

O = origin

ω = angular frequency

p = observations

P,Q = line of pile installation

$Pi,Qi \quad i=1\ldots4$ = pile positions

$P(f)$ = degree of polarization in frequency domain

$P(t_k, f_0)$ = polarization degree in time frequency domain

$PL(q)$ = planarity in the time window q

$P_{WVD}[x(t,f)]$ = WVD of x

$P_{WVD}[x_1(t,f), x_2(t,f)]$ = cross WVD of two signals

$P_{RSPWVD}[x(t,f)]$ = RSPWD of x

$P_{SPWVD}[x(t,f)]$ = SPWD of x

$P_{CWD}[x(t,f)]$ = CWD of x

$P^e_{HP}(f_0)$ = probability that frequency bins with polarization above 0.8

$P^e_{MP}(f_0)$ = probability that frequency bins have polarization between 0.5 and 0.8

$\overline{P_{HP}(f_0)}$ = average $P^e_{HP}(f_0)$ at each frequency f_0

$\overline{P^{N0}_{HP}(f_p)}$ = average $P^e_{HP}(f_0)$ at each frequency f_0 discarding the zeroes

$\overline{P^{MAX}_{HP}(f_0)}$ = max $P^e_{HP}(f_0)$ at each frequency f_0

$\overline{P^{W}_{HP}(f_0)}$ = weighted average $P^e_{HP}(f_0)$ at each frequency f_0

$\phi_{t-f}(t,f)$ = kernel function

$\phi_{CW}(t,f,\sigma)$ = Choi and Williams kernel function

$\varphi(q)$ = incidence or deep angle in the time window q

$\varphi(t_k, f_0)$ = incidence angle in time frequency domain

$\overline{\varphi_{HR}^{k}}$ = average value of azimuth with a polarization above 0.8

$\overline{\varphi_{HP}^{e}(f_0)}$ = statistical incidence angles with a polarization above 0.8

q = time window/slice

Q^T = eigenvector matrix of R

r = viscous friction

r^T = triaxial event's rise signal

R_C = covariance matrix

R_{SL} = STA\LTA

R_X = autocorrelation of $\{X_n\}$

$RL(q)$ = rectlinearity in the time window q

$\overline{RL_{HR}^{k}}$ = average value of rectilinearity which exceeds 0.8

ρ = density

s = spring

S = vibration source

$S(f)$ = SDM

$S_p(t_k, f_0)$ = time frequency SDM

$S_{lm}(t_k, f_0)$ = elements of $S_p(t_k, f_0)$

$\overline{S_p(t_k, f_o)}$ = smoothed estimation of $S_p(t, f)$

σ_X^2 = variance of a stochastic process

σ_a = standard deviation of the maximum 1-second average weighted acceleration

σ_v = standard deviation of the maximum 1-second average weighted velocity

t = time

t_k = time sample

t_{HR}^k = time interval where the rectilinearity exceeds 0.8

$t_0^e(f_0)$ = time bins at a fixed frequency f_0 for an event

$\hat{t}(f,t)$ = temporal centroid of the SPWVD distribution

tr = trace of the matrix

T = duration

T_E = r.m.s evaluation period

T_r = KB evaluation period

$T_{e,j}$ = exposure period of the j^{th} event

τ = lag

$\vartheta(q)$ = azimuth angle in the time window q

$\vartheta(t_k, f_0)$ = azimuth angle in time frequency domain

$\overline{\vartheta_{HR}^k}$ = average value of azimuth which exceeds 0.8

$\overline{\vartheta_{HP}^e(f_0)}$ = statistical azimuth angles with a polarization above 0.8

$\overline{\vartheta_{HP}^W(f_0)}$ = weighted azimuth average $\overline{\vartheta_{HP}^j(f_0)}$ at each frequency f_0

u_1^q = eigenvector corresponding to the largest eigenvalue in the time window q

$u_{11,}^q u_{21,}^q u_{31}^q$ = three direction cosines of eigenvector u_1^q in the time window q

U = orthonormal matrix

$U(f)$ = matrix of the eigenvectors for a frequency f

v = train speed

v_b = velocity loaded floor with human body

v_{fs} = velocity unloaded floor

$v_{w,\max}$ = maximum 1-second average weighted velocity

$v_{w,95}$ = statistical maximum weighted velocity

$\langle v_{w,\max} \rangle$ = mean value of the maximum weighted velocity

V = vibration magnitude

V_P = P waves speed

V_S = S waves speed

V_R = Rayleigh wave speed

V_L = Love waves speed

V_{SO} = low-amplitude shear wave velocity

w_T = windowing function

W_r = set of the triaxial rise events

x_{rms} = r.m.s. value

x_a = analytic signal of x

$x = x(t)$ = time history

$x_w(t)$ = weighted time history

$x^T(t)$ = row vector of a triaxial recording in the time domain

$x_e(i), x_n(i), x_z(i)$ = three signals of the triaxial recording

$x(f)$ = vector of a triaxial recording in the frequency domain

X = original set of data

$X_q(f)$ = spectral estimation for the slice q

$X(f)$ = spectrum of the signal $\{X_n\}$

$\{X_n\}$ = vibration signal as a stochastic process

$y(t)$ = absolute motion of the mass

Y = new data set from PCA

Y_B = mobility human body

Y_F = floor mobility

$z(t)$ = relative motion between mass and ground

ACKNOWLEDGEMENTS

The PhD is a challenge that can be only overcome through a process of intellectual and human growth. This entire document is the proof of the intellectual growth and these pages acknowledge the people who have contributed, in one way or another, to this intellectual and human process.

First of all I have to thank my family for their unconditional love, trust and support.

The knowledge, guidance and patience of Prof. Andy Moorhouse has been fundamental for the achievement of my PhD and it has been a privilege working with him. On the other hand, I was not able to improve as a person without the support and love of Valentina Maini. I thank her for the 5 years spent together.

I am very grateful to Dr. David Waddington who gave me the opportunity to undertake the PhD at Salford University and to take part in projects like NANR209, CargoVibes and FNM2013. I thank him for his experimental experience (including his toolbox), availability and sense of humour.

NANR209 was an extensive and exciting project that could not be delivered without the team effort. The "V-Team" was not just a team; it was a family with which I shared academic success, endless days, food, laughs and tears. Therefore I have to thank Dr. James Woodcock, Dr. Eulalia Peris, Dr. Jenna Condie, Zbgniew Koziel and Calum Sharp. Moreover, I thank Natalia Szczepanczyk, Valentin Le Bescond and George Perkins for their vital support during the vibration survey. I cannot forget to mention the social scientists from S.U.S.H.U, managed by Prof. Andy Steele, working on NANR209 with special thanks to Nathan Whittle and his black van.

Thanks to Defra for founding both NANR209 and FNM2013. It has been exciting working with noise experts like Richard Perkins, Paul Shield and Chris Skinner and with two legends in the field of groundborne vibration: Colin Stanworth and Rupert Thornely Taylor.

I have to thank Guralp ltd for the assistance and support in the design and the delivery of the instrumentation used during NANR209 without which it could have been difficult to deliver such large field work.

The post graduate office, rooms G10 and G11 in the Newton Building, is a good working environment where it is possible to learn about new topics, discuss and find help and I'm very pleased to have crossed my life and academic path with my colleagues Dr. Charlie "Boy" Mydlarz, Dr. Rodolfo "The Machine" Venegas, Dr. Andrew Elliot, Ian Cushing, Dr. Neil Bruce, Dr. Anthon Krinkin, Dr. Tomos Pentre, Dr. Ben Piper, Dr. Konstantinos Dadiotis, Dr. Micheal Sturm, Micheal Hudelmeir, Dr. Richard Hughes, Dr. Sarah Payne, Dr. Liam Kelly, Heo YongHwa, John Braiden, Paul Power, Darius Satongar, Dr. Jonathan Sheaffer, Micheal Lotinga, Dr. Julian Romero, Linda Gedemer, Tobias Ackroyd, Fotis Georgiou, Nikos Zafeiropolus, Andrew King, Steven Wheeler, Dr. Paul Kendrick, Dr. Rob Oldfield and Dr. Jonathan Hargreaves. A special mention is due to my fellow Italian colleagues Dr. Diego Turo and Massimo Serafini for their constant support and because it is always better to discuss either silly or important things in your mother tongue and in front of a pasta dish.

It was not possible to deliver the large and complex field works of NANR209 and FNM2013 without the support, help and refuge provided by the laboratories of the Acoustic Research Centre. I am really thankful to Danny McCaul, Ian Rattigan, Henric Mattson; and particular mention is due to Claire Lomax and Gary Philips who give me the possibility to work and learn at the Calibration Laboratory and to my colleague James Massaglia for being an excellent acousticians and a great saxophone player.

I thank my dear friend Dr. Mauro Palo for his suggestions and assistance in the development of the polarization analysis.

I'm very grateful to Prof. Trevor Cox, Dr. Bruno Fazenda and Dr. Iian Jackson for the short work experience in the Good Recording project. I'm thankful to Dr. Francis Li for rejecting my PhD application otherwise I could have been written

another story. It has been a pleasure to chat about geotechnical problems with Dr. Gareth Swift and Dr. Laurence Weeks.

I'm really thankful to all the experts in the field of acoustic, noise and vibration with who I have discussed in these years with a particular mention to Dr. Eng Jorge De Avillez, Dr. Bruno Zuada Coelho, Alessandro Sabato, Dr. Umberto Berardi, Prof. Gaetano Licitra, Dorothee Stiebel, Eng. Serafino Di Rosario, Julien Violleau, Heather Billin, Dr. Hamid Masoumi, Dr. Saverio Savio, Carel Ostendorf, Graham Parry, Michelle Villot, Arnold Koopman, Roger Muller, Dr. Davide Bonsi, Bernd Asmussen, Nick Craven, Dr. Oliver Bewes, Eric Thalheimer, Ilaria Grossoni, Eng. Marco Acquati and all the acousticians who attended the IOA seminars and ANC presentation regarding the NANR209 project.

A special thanks goes to my scouse friend Phil Kamara and the people of the Crescent Pub.

A special mention is due to my PhD examiners (Dr. Mark Avis, Dr. Hugh Hunt and Prof. Yu Lam) who gave me one of the hardest days of my life but they also provided me with an important improvement of the quality of this manuscript.

I'm greatful to my "new" colleagues at HS2 Ltd Techinical Directorate for the support shown with a special mention to the Acoustics team: Tom Marshall, Pamela Lowery, Dr. Phil Brewer and Jeremy Newton.

A thank is due to my friends spread around the world for just believing in me: The Italians (Elisa, Daniele, Carmela, Qrli, Elena, Alessio, Prof. Castagnolo & Bea, Lucia, Mara and Sara Vicari), The Original Walworth Road Residence (Fabrizio, Il Prof, Fabio and Adriano & Irina), Francesca La Rom, Laps, Sero, Emma, Dan DNA & The Bunker Studio, Peppe il Punkabestia, Eleonora, Tamburrino & Fede, Marco Cesario, Aliena, Cipriano & Mary P, Massimo D'Agostino, Frizzy Pazzy, Pierdomenico Romano, Martellone & Ilaria, Gargano, Valerio De Felice, Ivana, Rab, Mio Fratello Pifano, Zero, Puccettone, Bagnoli, Lambros, Il Nero, Youthman, Masone, Anacleto Vitolo, Soundblast, Pio, Rad, Huru, Sandro Digital, Smetz, Lo Smilzo, Piera, Elisa, Elena, Chiara, Il Massiccio, Domenico, Il Prez, T70, Morfuco,

Wicked Boys, Dj Arnold, Kam & Erica, Enzo & Annarita, Fusco, Francesco Marra, Enrico Tiberi & Citanò, Martin Sullivan, Pironti family, Valentina Sada, Samy, Daniele De Gruttola, Gerardo & Samanta & Giovanni, Salerno Sound Boys & Sound Systems and all the other… you are really too many!

The last but not least thank goes to the people that take part to the social and acoustics survey during NANR209 and FNM2013. I'm very grateful to all of them for their trust, their hospitality and for sharing their stories.

LIST OF PUBLICATIONS

JOURNALS

G. Sica, E. Peris, J. Woodcock, A. Moorhouse and D. Waddington, "Design of measurement methodology for the evaluation of human exposure to vibration in residential environments," *Science of the Total Environment*, In Press, Corrected Proof, Available online 26 July 2013; http://dx.doi.org/10.1016/j.scitotenv.2013.07.006

E. Peris, J. Woodcock., G. Sica, A. Moorhouse, and D. Waddington, "Annoyance due to railway vibrations at different times of the day," *Journal of the Acoustical Society of America*, vol. 131, no. 2, pp. EL191-EL196, 2012; http://dx.doi.org/10.1121/1.3679390

E. Peris, J. Woodcock., G. Sica, C. Sharp, A. Moorhouse, and D. Waddington, "Effects of situational, attitudinal and demographic factors on railway annoyance in residential areas," *Journal of the Acoustical Society of America*, vol. 135 , pp. 194, 2014; http://dx.doi.org/10.1121/1.4836495

C. Sharp, J. Woodcock., G. Sica, E. Peris, A. Moorhouse, and D. Waddington, "Exposure-response relationships for annoyance due to freight and passenger railway vibration exposure in residential environments," *Journal of the Acoustical Society of America*, vol. 135, pp. 205, 2014; http://dx.doi.org/10.1121/1.4836115

D. Waddington, J. Woodcock, E. Peris, J. Condie, G. Sica, A. Moorhouse and A. Steele, "Human response to vibration in residential environments," *Journal of the Acoustical Society of America*, vol. 135, pp. 182, 2014; http://dx.doi.org/10.1121/1.4836496

CONFERENCE PROCEEDINGS (AS FIRST AUTHOR)

G. Sica, J. Woodcock, E. Peris, A. Moorhouse, and D. Waddington, "New methodologies for determining exposure in residential environments from overground railway vibration and evaluation of uncertainties in measurement and estimation.," in *Internoise*, Lisbon, 2010.

G. Sica, J. Woodcock, E. Peris, Z. Koziel, A. Moorhouse, and D. Waddington, "Estimation of vibration exposure in residential environments," in *ICBEN*, London, 2011.

G. Sica, J. Woodcock, E. Peris, A. Moorhouse, and D. Waddington, "On the assessment of the human exposure from vibration caused by railway construction," in *Internoise 2012*, New York, 2012.

G. Sica, A. Moorhouse, J. Woodcock, E. Peris, C. Sharp, and D. Waddington, "Measurement of ground-to-building frequency response functions for assessment of human exposure to vibration from railway vibration," in *ISMA*, Leuven, 2012.

TECHNICAL REPORTS

D. Waddington, A. Moorhouse, A. Steele, J. Woodcock, J. Condie, E. Peris, G. Sica, and Z. Koziel, "Human Response to Vibration in Residential Environements (NANR209), Final Project Report," Defra, London, 2011.

E. Peris, G. Sica, J. Woodcock, Z. Koziel, A. Elliott, R. Venegas, A. Moorhouse, and D. Waddington, "Human Response to Vibration in Residential Environments (NANR209), Technical Report 1: Measurement of vibration exposure," Defra, London, 2011.

G. Sica, J. Woodcock, E. Peris, A. Moorhouse, and D. Waddington, "Human Response to Vibration in Residential Environments (NANR209), Technical Report 3: Calculation of Vibration Exposure," Defra, London, 2011.

Z. Koziel, M. Smith, G. Sica, J. Woodcock, E. Peris, A. Moorhouse, and D. Waddington,"Human Response to Vibration in Residential Environments (NANR209), Technical Report 4: Calculation of noise exposure", Defra, London, 2011.

J. Woodcock., E. Peris, J. Condie, G. Sica, A. Moorhouse, and D. Waddington, "Human Response to Vibration in Residential Environments (NANR209), Technical Report 6: Determination of Exposure-Response Relantionships.," Defra, London, 2011.

FOREWORD

The work presented in Part 1 of this thesis reports the results of a group exercise based upon a project funded by the Department of Environment, Food and Rural Affairs to investigate the human response to vibration in residential environments. The author's individual contributions to this project were as follows (numbers in brackets define the author's percentage contribution to joint tasks):

- Identified sites for vibration exposure and response assessment (75 %)
- Developed measurement strategies for vibration exposure assessment for railway operations and construction
- Developed methodology for vibration exposure assessment from railway traffic
- Developed and implemented methodology for vibration exposure from railway construction
- Coordination between additional research assistants and with social science team (50%)
- Field measurements (50 %)
- Calibration/equipment maintenance/downloading data/ raw storage (75 %)
- Investigated the influence of mounting conditions (33 %)
- Investigated the influence of human load of floor vibration
- Developed uncertainty analysis for the evaluation of the vibration exposure in residential environments
- Authored technical report (report 3 of 6 for the whole project)

Part 2 of this dissertation represents analysis of the data for which the author was entirely responsible. The analyses, results, views, and conclusions presented in this thesis are those of the author and do not necessarily represent the views of the Department of Food, Environment and Rural Affairs.

ABSTRACT

Environmental issues surrounding railway operation and construction have become more prominent in recent years, increasing the need for administrators and researchers to understand how residents living around railways respond to the noise and vibration generated by them.

Within this context, the University of Salford, within the project funded by Defra "Human response to vibration in residential environments" (NANR209), has derived exposure response relationships for railway traffic and construction for a population sample of 1281 people: 931 for railway traffic and 350 for railway construction. Vibration measurements within residences have been used for assessing human exposure to vibration alongside a social study questionnaire based on face-to-face interviews for quantifying the human response.

The first part of this work is concerned with the exposure side of NANR209. The design and implementation of measurement methodologies are presented and discussed, which provide exposure data suitable for building an exposure response relationship for vibration caused by the sources mentioned above.

In light of the large amount of vibration data gathered during the project, the analysis of vibration signals is considered in the second part of the dissertation. Two aspects connected with the assessment of the human exposure to vibration are investigated: wave field assessment and ground to building transmissibility analysis.

1 INTRODUCTION

1.1 MOTIVATION

Since the 1820s, railway trains have been a form of transportation for people and materials. Nowadays, the needs of a well-connected society have pushed the design of railway systems closer to living environments; several examples of these situations can be found in the Cross rail project in London, the Metro link extension in Manchester and the U.K. HS2 project. The factors listed above combined with the raising of vehicle speeds, the increasing of vehicle loads and the growing of traffic flows have generated concern about the environmental issues caused by vibration from railway construction and operation and their effects on people.

Thus, the influence of vibrations on working and living environments has become an important problem in technologically advanced societies (Xia et al. [1]) and the problem of knowing how communities respond to environmental vibration has caught the attention of administrators and researchers.

A favoured way to explore community reaction to environmental vibration is to derive an exposure response relationship which describes the response of a percentage of the population, expressed in annoyance, as a function of the level of vibration to which it is exposed. These relationships, since the seminal work done by Schultz [2], are widely used in environmental noise but less for vibration. Therefore, there is a need to produce a robust exposure-response dataset for human exposure to vibration (Elias and Villot [3]), and to evaluate the most suitable index to be used to express associated levels of vibration (Waddington et al. [4]).

The research needs have been satisfied by the activity of the University of Salford in the project "Human response to vibration in residential environment" (NANR209) (Waddington et al. [4]), funded by the Department for Environment, Food and Rural Affairs (Defra), providing an exposure response relationship for

vibration outside the respondent's control like railway construction and operation affecting the living environment.

In order to assess the human exposure, the approach suggested by the standards, 24 hour internal recording, does not seem to be practical for its implementation in a "large scale" survey. In fact, the standard approach would require an extensive number of sensors in order to cover the population sample, which was 1281 people, and to fit within the time scales of the project, three years. Moreover, the requirement of 24 hour internal recordings is too demanding for all the participants of the survey.

Therefore, new measurement strategies need to be developed for satisfying both project and standard requirements. In order to achieve this objective several fields have to be explored such as: planning and implementation of field work, the most recent sensors, measurement methods, community engagement methods and signal processing.

Apart from providing input data for exposure response relationships, a by-product of the exposure methodologies based on measurement is the generation of one of the largest databases of vibration caused by railway vibration.

1.2 RESEARCH OBJECTIVES

The main objective of the work upon which this thesis is based is the development and implementation of methodologies in order to provide exposure data suitable for building an exposure response relationship for vibration caused by railway construction and operation.

As already pointed out in section 1.1, the standard methods for assessing the exposure cannot be applied for an assessment on a "large scale" like the one of the project "Human response to vibration in residential environments" with almost 1300 case studies. Therefore, new strategies need to be adopted in order to assess the human exposure.

In the case of railway traffic the methodology is oriented in the experimental estimation of the internal exposure based on a very intensive field work. On the other hand, for construction sources the exposure assessment is more oriented towards a semi empirical approach typically used in the construction environment. Both methodologies represent a novelty in the field.

In order to provide a robust sample of the population affected by railway vibration, an identification of the sites for collecting both response and exposure is needed. This is a very important task belonging to the design of the measurement protocol together with the choice of the most suitable instrument for measuring the human exposure.

As mentioned in 1.1, one advantage of an experimental exposure methodology is the creation of one of the biggest databases for railway vibration. The latter can open up several possibilities for analysis, potentially leading to improved understanding of some of the factors related to the vibration exposure. Among those, the author has focussed his attention on two aspects strongly correlated with the assessment of the human exposure: wave field assessment and transmissibility analysis.

The latter is used for evaluating the transmission of the vibration from the soil to the residence in the exposure measurement procedures and the former is adopted for identifying the groundborne vibration components generated by the source.

1.3 DISSERTATION OUTLINE

Considering the research objectives mentioned above, the thesis structure can be summarized using the following topics: Design, Implementation and Analysis.

The first two subjects are treated in the first part of the dissertation; from chapter 2 to 5 the design and implementation of measurement methodologies used for the exposure assessment in NANR209 are described and discussed. The analyses of the factors related to the human exposure to vibration are considered in the second part of the thesis from chapter 6 to 8.

The first chapter provides the motivation, the research objectives and an outline of the dissertation. The second chapter is a review of the assessment of exposure to vibration in buildings. The third chapter describes the design of the exposure measurements. The implementation of the exposure methodologies for railway traffic and construction are described in chapters 4 and 5. Chapter 6 provides a review of waves in soils. Chapters 7 and 8 are oriented towards the analysis of the measurement data: the former is about the wave field assessment whereas the latter considers the analysis of the transmissibility. Although a section presenting the conclusions from each chapter is provided at the end of each chapter, chapter 9 is devoted to the discussion and conclusions about the whole thesis.

PART ONE: DESIGN AND IMPLEMENTATION OF MEASUREMENTS FOR ASSESSMENT OF HUMAN EXPOSURE

"If you look at frequencies...

the human hear would probably hear down to

what recognize 70 and 60 Hz...

but between 50 and 30 Hz

It's a vibration...

It's something that the waveform slows so slow

that the hear does not pick it up

but the body does... and it's moving the body."

Brian Nordhoff - Groove Corporation

from "Dub Echoes"

2 REVIEW OF THE ASSESSMENT OF EXPOSURE TO VIBRATION IN BUILDINGS

2.1 INTRODUCTION

In this chapter a brief review of the human response to vibration in buildings is given. First a description of how the human body responds to vibration is presented in section 2.2 focussing on two elements: the biodynamic and the annoyance response. Then, in section 2.3 the evaluation of the human exposure in buildings is considered. An overview of how the standards manage the human exposure is in section 2.3.1 whereas the state of art of the research is in section 2.3.2 highlighting the strategy for assessing the vibration exposure for annoyance evaluation. Conclusions are drawn in section 2.4.

2.2 HUMAN RESPONSE TO VIBRATION

Whole-body vibration occurs when the body is supported on a surface which is vibrating and is usually said to occur when the whole environment is undergoing motion and the effect of interest is not local to any particular point of contact. This is the case for vibration sources in residential environments.

It is possible that vibrations can be transmitted to the human body through a chair or bed. Local vibration occurs when one or more parts of the body are in contact with a vibrating surface. Both whole-body and local vibration can cause vibration throughout the body. The latter is highly sensitive to many types of motions and a living environment close to a railway can produce sufficient whole-body vibrations for there to be a need to assess its impact and effects. The effects of whole-body vibration from railway are well described in BS ISO 14837-1:2005 [5]:

"Structural vibration inside the buildings can be detected by human occupants and can affect them in many ways: their quality life can be reduced as can their working efficiency. The level of vibration generated inside buildings close to rail system are such that in some

situations they give rise to (in order of magnitude) annoyance, discomfort, activity disturbance and, at extreme levels, might in rare cases affect health"

Fundamental research, described in section 2.2.1 and 2.2.2, carried out by several researchers has identified the range of frequencies usually associated with the effects of whole body vibration on health, activity and comfort between 1 Hz and 80 Hz. This frequency range has been standardised in national and international guidance such as BS ISO 14837-1:2005 [5]. In the following sections the biodynamic and the annoyance response to vibration are considered.

2.2.1 BIODYNAMIC RESPONSE TO VIBRATION

In order to minimise undesirable influences of vibration on the human body, an understanding of how the body moves when exposed to vibration is needed. Consequently, experimental studies of the biodynamic responses to vibration and impact have been conducted to observe body dynamic behaviour and develop mathematical models (Matsumoto and Griffin [6]) representing specific aspects of body response.

Even so, the mechanisms of the dynamic responses of the body are not yet fully understood. The complexity of the structure of the human body, difficulties in making measurements and differences in responses within and between individuals have impeded understanding. The responses of the seated human body have been investigated in many studies, but there have been few investigations with standing subjects.

If we consider the human body as a mechanical system it may, at low frequencies and low levels of vibration, be roughly approximated by a linear lumped parameter system (Rasmussen [7]), of the type shown in Figure 1. One of the most important parts of this system with respect to vibration and shock effect seems to be the part marked "thorax-abdomen system". This is due to a distinct resonance effect occurring in the 3-6 Hz range as indicated in Figure 2 and Figure 3, which makes efficient vibration isolation of a seated or standing person very difficult.

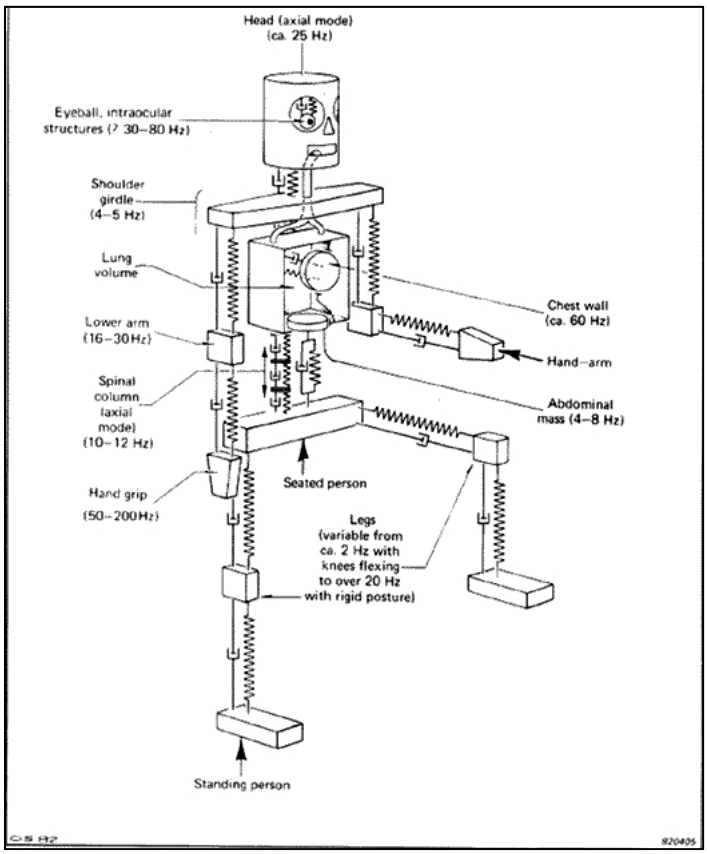

FIGURE 1 – SIMPLIFIED MECHANICAL SYSTEM REPRESENTING THE HUMAN BODY STANDING ON A VERTICAL VIBRATING PLATFORM (FROM RASMUSSEN [7])

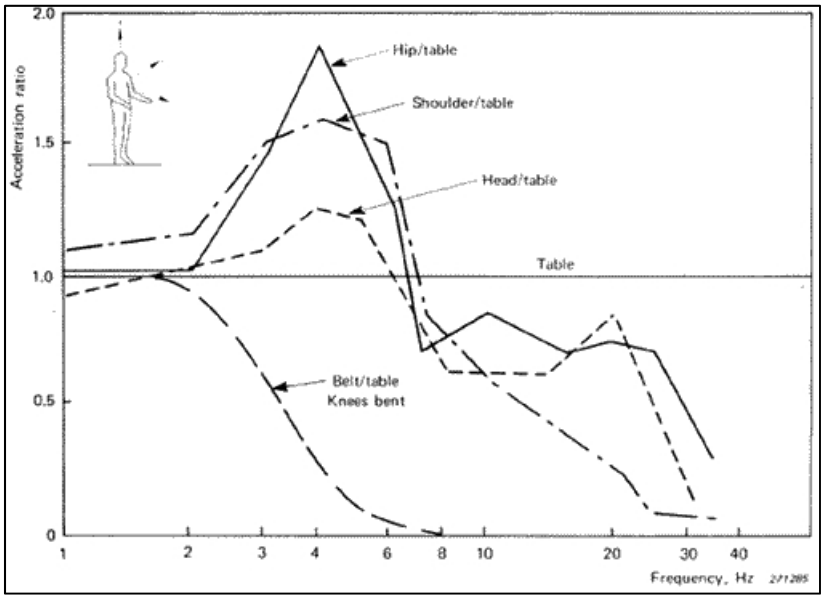

FIGURE 2 – TRANSMISSIBILITY OF VERTICAL VIBRATION FROM A TABLE TO VARIOUS PART OF THE BODY OF A STANDING HUMAN SUBJECT (FROM RASMUSSEN [7])

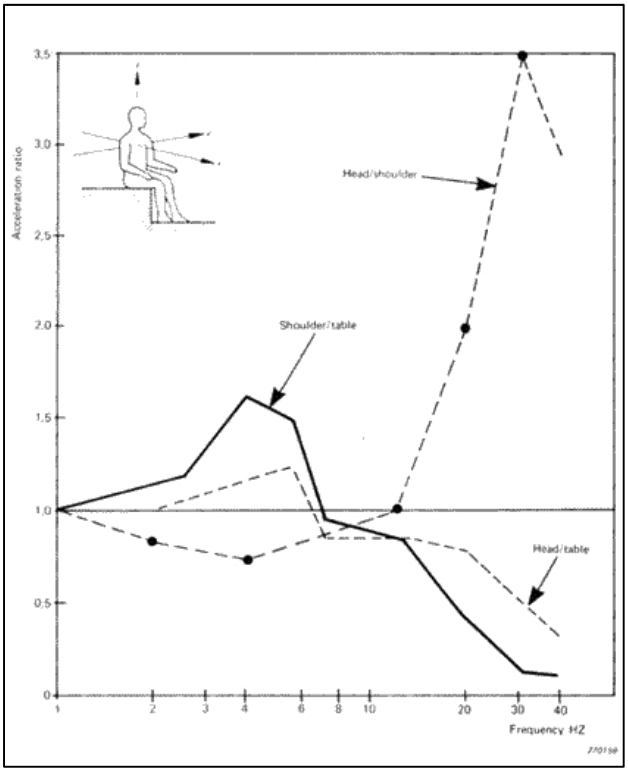

FIGURE 3 - TRANSMISSIBILITY OF VERTICAL VIBRATION FROM A TABLE TO VARIOUS PARTS OF THE BODY OF A SEATED HUMAN SUBJECT (FROM RASMUSSEN [7]).

From Figure 2 and Figure 3 we can also notice that the effects of vertical vibrations are often similar to those in the seated position except that seating vibration can generate local vibration of the head. A comparison of the dynamic response of the human body in standing position and in sitting position has been done by Matsumoto and Griffin [8] and Holmund et al. [9].

As described in the 'Handbook of Human Vibration' (Griffin [10]), a person may lie either on one side of the body, or on the front (i.e. prone), or on the back (i.e. supine) or in some variation on these positions (e.g. semi-supine). The full length of the body (from feet to head) may be exposed to the same vibration or parts may be well isolated from the motion. A couch may either provide stability to resist horizontal motion or allow substantial movement. The variations in the conditions of recumbent persons are considerable and the number of relevant studies is small.

A factor that can change the amount of vibration transmitted to the human body is the posture. For seated person a small alteration in position or muscle tension may

help to reduce vibration severity in the region of the body resonance. In the standing position the influence of frequencies above about 3 Hz may be greatly reduced by bending at the knees. Several studies about the influence of posture for standing body subject to vertical whole-body vibration have been carried out by Matsumuto and Griffin [11], Subashi et all. ([12] and [13]).

Another factor to take into account is the differences in biodynamic response between different genders. The latter is thought to be due to differences in body structure and fat distribution between females and males (Holmund and Lundstrom [14]).

2.2.2 ANNOYANCE RESPONSE TO VIBRATION

A parameter that plays an important part, especially if we are interested in understanding parameters like annoyance and discomfort, is the amount, in terms of duration and magnitude, of the vibrations to which the human body is exposed.

Weighted W_k r.m.s. acceleration (ms^{-2})	Reaction
Less than 0.315	Not uncomfortable
0.315 to 0.63	A little uncomfortable
0.5 to 1.0	Fairly uncomfortable
0.8 to 1.6	Uncomfortable
1.25 to 2.5	Very uncomfortable
Greater than 2	Extremely uncomfortable

TABLE 1 - VIBRATION MAGNITUDE AND DISCOMFORT REACTION (FROM ISO 2631-1:1997) IN PUBLIC TRANSPORT. THE VALUES ARE WEIGHTED ACCORDING TO THE FREQUENCY RANGE 1-80 HZ AND WEIGHTING DEFINED IN ISO 2631-1:1997.

The effects of duration and magnitude on the vibration exposure are generally related to how humans perceive vibration where both physical and psychological factors need to be taken in account. A review of the studies on vibration perception can be found in Woodcock et al. [15] and Elias & Villot [3].

Regarding discomfort to whole body vibration, accepted values are provided in ISO 2631-1:1997 [16] and reported in Table 1 - VIBRATION MAGNITUDE AND DISCOMFORT REACTION (FROM ISO 2631-1:1997) IN PUBLIC TRANSPORT. THE VALUES ARE WEIGHTED ACCORDING TO THE FREQUENCY RANGE 1-80 HZ AND WEIGHTING DEFINED IN ISO 2631-1:1997.

. The latter shows approximate indications of likely reactions to various magnitudes of overall vibration total values in public transport. With respect to comfort in residential building, ISO 2631-2:1997 [16] points out that in many countries occupants are likely to complain if the vibration magnitude is only slightly above the perception threshold. In ISO 2631-2:1997 [16], the absolute threshold of perception of W_k-weighted vertical vibration is reckoned to be about 0.015 m/s^2. It represents the median peak magnitude detectable by "alert, fit persons" (interquartile range: 0.01 – 0.02 m/s^2) (Elias & Villot [3]).

Although there is standardization about the perception threshold of vibration, the understanding of the various possible effects of the duration of vibration exposure is far from complete. Experimental studies take much time; there are many potential conditions to study and many artefacts which might dominate the findings. While both interesting and useful experimental research has been conducted, in no area is there yet sufficient evidence for any time dependency to be used without qualification. Most studies of the effects of vibration on comfort and annoyance have been concerned with conditions in which the magnitude, frequency and duration of vibration have been constant within each exposure. In contrast, the vibration induced in buildings by passing trains is intermittent and may have variable characteristics (Howarth and Griffin [17]).

For periodic vibration and stationary random vibration the r.m.s. frequency weighted acceleration often provides a sufficiently useful indication of the relative

severities of different motions. With transient vibration, shocks, and non-stationary vibration the period of time over which an r.m.s. value is determined affects its magnitude. If the form of these motions is well known it may be possible to devise a simple criterion defining the appropriate measurement period. However, in general, r.m.s measurements are primarily restricted to the assessment of motions which are continuous, statistically stationary and do not contain shocks. Considering intermittent events, the effective total daily exposure time is simply obtained by adding up the individual exposure times expressed in r.ms.

The peak acceleration (or velocity) is sometimes used if a motion has a highly constrained form, but the peak value will not be useful unless the vibration has been frequency weighted, and the peak value obtained after frequency weighting can be highly dependent on the manner in which the weighting is implemented. Peak values do not take the duration of the event into account.

For the assessment of some effects of transient, shock and non-stationary motions the root-mean-quad (r.m.q.) and vibration dose value (VDV), both expressing a fourth power law dependency, appear more appropriate than either r.m.s. or peak values. As with r.m.s. and peak measures, the acceleration must be frequency weighted before determining the r.m.q. or VDV.

A comparison between r.m.s and VDV for the evaluation of annoyance from intermittent events, like railway vibrations in buildings, was investigated by Howarth and Griffin [17] in two experiments. The first experiment was conducted to determine the manner in which annoyance caused by railway-induced building vibration depends on how frequently trains pass. It also investigated how annoyance depends on the magnitude of the vibration. The second experiment was conducted to confirm that the relation between the number of passing trains and the magnitude of vibration could be used to predict conditions which will cause similar annoyance. The findings of the first study were employed to determine a trade-off between the number of passing trains, N_T and the magnitude of the vibration, V. The relation was determined as approximately

$N_T \propto V^{-4}$ for equal annoyance. This was confirmed by the results of the second experiment in which r.m.s. evaluation of the vibration (i.e., $N_T \propto V^{-2}$) was found to be less satisfactory. The relation ($V^4 N_T$ = constant) for equal annoyance is consistent with the use of the vibration dose value VDV proposed for vibration assessment.

2.3 HUMAN EXPOSURE TO VIBRATION IN BUILDINGS

2.3.1 STANDARDS AND GUIDELINES

The response of the human body to vibration depends, as shown in the previous section, on different parameters like vibration axes, posture and gender. On the other hand, parameters such as duration, frequency content and vibration type are essential in order to evaluate the vibration exposure.

As a consequence, there is no a standard approach for the evaluation of the human exposure in residential environments. Some countries have their own approach to the assessment and regulation of vibration in residential environments, for example:

- United Kingdom with BS 6472-1:2008 [18].
- United States with FTA guidelines [19].
- Norway with NS 8176:1999 [20].
- Sweden with DNR.S02-4235/SA60 [21].
- Germany with DIN 4150-2:1999 [22].

Otherwise rules are sometimes adopted from existing guidelines provided either by institutions or other countries. The most significant guidelines related to the evaluation of the human response in buildings can be found in the following documents:

- ISO 2631-2:2003 [23].
- ANSI S3.29-1983 (R2001) [24].

- Nordtest Method NT ACOU-082 [25].
- DIN 4150-2:1999 [22].

A comprehensive comparison of national and international standards related to the evaluation of the human exposure to vibration in building can be found in two documents: appendix D of Zapfe et al. [26] and in Elias & Villot [3]. Although standards differ from country to country, it is possible to identify some common points in the exposure assessments as:

- measurement point
- frequency weighting
- exposure metric
- exposure evaluation.

All the regulations agree on the idea that the vibration exposure has to be measured or predicted in one position in one room. Vibrations are generally quantified at the point of entry defined as the contact surface between the human body and the vibrating receiver (floor). Standards encourage the assessment of the vibration exposure in mid-room or mid-span, the location that is likely to represent the worst case. The Nordtest method [25] quantifies the uncertainty of the exposure measurement using one sensor as ± 5 dB and is related to the variability of the vibration level along the floor. In order to minimize this uncertainty multiple measurement positions on the floor should be used. For external excitation such as ground-borne vibrations, the U.K. standard BS 6472-1:2008 [18] suggests one or two measurement points on the floor for determining its vibration response: in the central part within one-third and two-thirds of the width/length. Apart for the measurement points suggested in BS 6472-1:2008 [18], the ANC guidelines [27] advise that it may be necessary to take measurements in all occupied rooms in order to determine the variation of vibration within the building. Measurements should be made if possible in the absence of occupant. Where prolonged direct measurements are not practicable they may be made on a surface other than the point of entry to (taken as meaning supporting) the human subjects. In that case a transfer function is required and tri-axial measurements are

necessary at both locations to establish it. In ANC guidelines [27] issues about the mounting conditions and the human load on the floor are pointed out as well.

The French transport operator RATP[1] measures the floor vibration close to the load-bearing wall in order to minimize the uncertainty due to the measurement position on the floor [3].

For estimating the effects of vibrations on humans in residential environments, Hirao et al. [28] developed a wireless measurement system for simply and accurately measuring vibration in two- and three-story detached houses of wooden or steel construction. In this system, five wireless vibration measurement devices (installed with a data recorder in the building) are controlled simultaneously by outdoor mobile PC or laboratory PC via wireless LAN and an Internet connection. It sends the vibration acceleration waveforms recorded in the building over the network to the laboratory PC. The system was able to measure vibration accelerations at the ground near the foundations and floors in the houses.

Frequency weightings are curves which are applied to the vibration signals, either acceleration or velocity, for reflecting the sensitivity of humans to the perception of vibration at different frequencies. BS 6472-1:2008 [18] recommends two frequency weighting curves: W_b and W_d are applied to vertical and horizontal vibration respectively. The W_b curve has its maximum sensitivity in the frequency range 4Hz to 12.5Hz whereas for the W_d curve the maximum sensitivity can be found in the frequency range 1Hz to 2Hz. In ISO 2631-1:1997 [16] two weighting curves are recommended for acceleration signals: the W_k weighting curve in the vertical direction and the W_d curve in the horizontal direction. The W_k weighting curve is not so different from the W_b weighting defined in BS 6472-1:2008 [18]. ISO 2631-2:2003 [23] recommends the use of the W_m weighting curve which is applied to acceleration signals in any direction. DIN 4150-2 [22] recommends the use of the *KB* weighting curve applied to velocity signals. As U.K. and Germany, Japan has

[1] Régie Autonome des Trasports Parisiens.

.

developed its frequency weighting curves that differ from the W_k and W_d weighting (Ellias and Villot [3]). The W_b, W_d, W_k, and W_m weighting curves are illustrated in Figure 4.

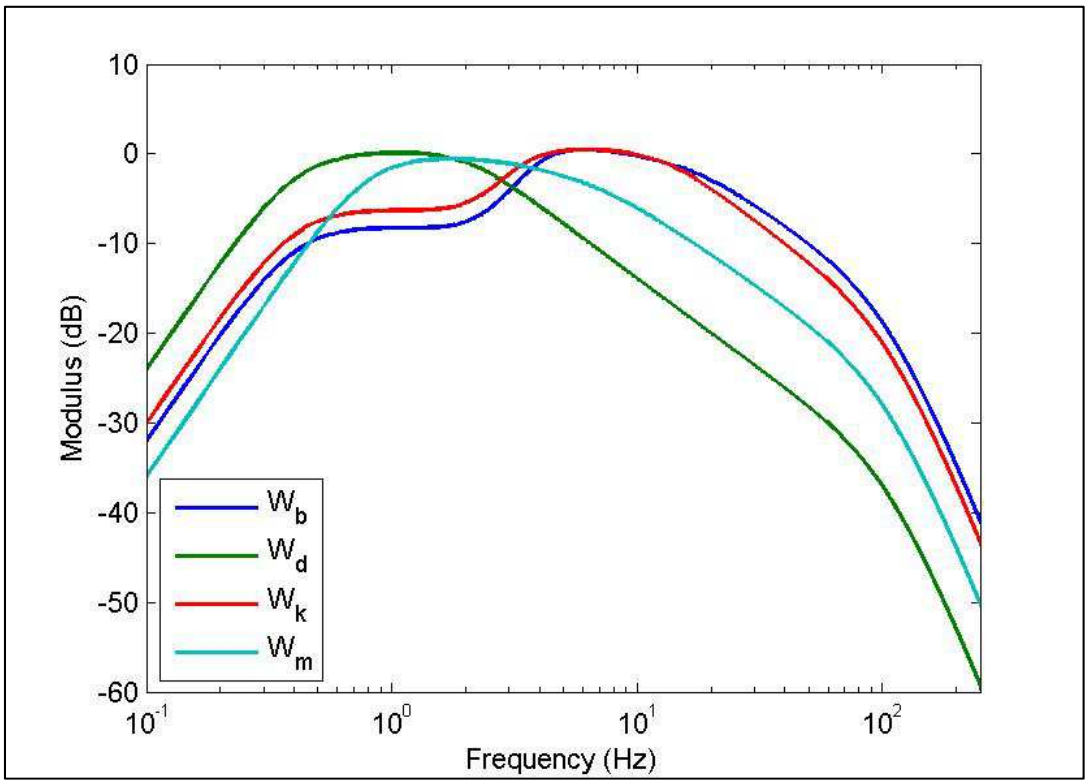

FIGURE 4 – FREQUENCY WEIGHTING CURVES. W_B (BLUE LINE) AND W_D (GREEN LINE) FROM BS 6472-1:2008. W_K (RED LINE) AND W_M (LIGHT BLUE LINE) FROM ISO 2631-1:2003.

Apart the frequency weighting curves, International Standard such as ISO 2631-2:2003 [23] and ANSI S2.71-1983 (R2006) [29] provide vibration perception threshold base curves. The latter were also presented in BS 6472-1:1992 [30]. These base curves are intended to represent the threshold at which 50% of the population will be able to perceive vibration. As already stated in section 2.2.2, In ISO 2631-1:1997 [16] the absolute threshold of perception of W_k-weighted vertical vibration is quantified as 0.015 m/s^2. The same value is stated in BS 6472-1:2008.

The exposure is expressed, in all the standards, with a single figure parameter defined as a metric. The FTA guidelines provide an exposure metric in frequency domain too.

The most common metric for assessing the human exposure to vibration is the r.m.s. value calculated on the weighted vibration signal measured in terms of either acceleration or velocity depending on the country where the standard is used.

$$x_{rms} = \sqrt{\frac{1}{T_E}\int_{o}^{T_E} x_w^2(t)\cdot dt} \tag{2.1}$$

Where x_w is considered the weighted time history, expressed in velocity or acceleration, and T_E is the evaluation period. The widely use time period is 1 second which can be found in ISO 2631-1:1997, ISO 2631-2:2003, Italy, Spain, Norway, Sweden and USA. In Japan the time constant is 0.63 s whereas in Netherlands (Osterndorf [31]) and Germany the period is 0.125 s.

United Kingdom suggests a different exposure metric instead: the Vibration Dose Value or VDV. The latter is based on laboratory studies (Howarth and Griffin [17]) and satisfy, as explained in section 2.2.2, the following relationship:

$$N_T V^4 \propto annoyance \tag{2.2}$$

The VDV for a frequency-weighted, acceleration signal $a_w(t)$, using W_b or W_d as appropriate, measured in m/s^2 , with a duration T is:

$$VDV_{b/d,day/night} = \left[\int_0^T a_w^4(t)\,dt\right]^{0.25} \tag{2.3}$$

The measurement unit for VDV is m/s$^{1.75}$ and provides an indication of the total strength of a vibration appropriately accumulated over time and not merely the average value as is the case with the r.m.s (Howarth and Griffin [17]).

The exposure evaluation can be divided in two main categories: maximum level of time dependent running r.m.s. and/or mean energy-based value (Elias & Villot [3]). Most standards determine the exposure as the maximum level of the highest

value among the measured metrics for all the vibration events. This kind of approach can be found, for example, in Spain, Italy, Sweden and USA.

In Norway (NS 8176:1999 [20]) and the Netherlands (SBR-Part B:2002 [32]) instead, the maximum value is derived using a statistical method from the measurement ensemble.

For the Norwegian standard in for railway traffic, a minimum of 30% of 15 measured trains passing shall be selected from the train type that gives the highest values of weighted velocity or acceleration (most often goods trains). Under the assumption that the data are distributed in a log normal way the exposure is evaluated using the statistical maximum weighted acceleration or velocity level ($a_{w,95}$ or $v_{w,95}$) from 1 second averages of acceleration or velocity signals (Turunen-Rise [33]). The exposure is assessed for velocity or acceleration as follows:

$$\begin{aligned} v_{w,95} &= \left\langle v_{w,\max} \right\rangle + 1.8\sigma_v \\ a_{w,95} &= \left\langle a_{w,\max} \right\rangle + 1.8\sigma_a \end{aligned} \tag{2.4}$$

Where $v_{w,\max}$ and $a_{w,\max}$ are the maximum 1-second average weighted velocity or acceleration level for a single train passage. $\left\langle v_{w,\max} \right\rangle$ and $\left\langle a_{w,\max} \right\rangle$ are the mean value of the maximum weighted velocity and acceleration respectively for all train events belonging to the statistical ensemble. σ_v and σ_a are the standard deviations of the maximum 1-second average weighted velocity or acceleration level of the statistical ensemble.

The other approach used for the exposure evaluation is an energy based approach. The latter can be considered as a cumulative value calculated over all the events recorded during the measurement period and it is used in the U.K. standard BS 6472-1:2008. Considering N events of various durations t_n during the evaluation period (day or night) the VDV is obtained according to the formula:

$$VDV_{b/d,day/night} = \left(\sum_{n=1}^{N} VDV_{b/d,t_n}^4 \right)^{1/4} \tag{2.5}$$

Another "cumulative" exposure evaluation appears in DIN 4150-2 where the KB_{FTr} value is defined as:

$$KB_{FTr} = \sqrt{\frac{1}{T_r}\sum_j T_{e,j} KB^2_{FTm,j}} \tag{2.6}$$

where T_r is the evaluation period (day or night), $T_{e,j}$ is the exposure period of the j^{th} event, and $KB^2_{FTm,j}$ is the average of the maximum 0.125 s running average r.m.s. velocity for each 30 second period of an event.

Generally the exposure is evaluated for different times of the day, which can change depending on the standards. Limit values are set for those time periods and for different types of buildings divided in different areas like: residential, office, industrial etc., etc. The limits values for the British standard are presented below in Table 2 for residential buildings.

Place and time	**Low probability of adverse comment[2]** m/s$^{1.75}$	**Adverse comment possible** m/s$^{1.75}$	**Adverse comment probable[3]** m/s$^{1.75}$
Residential buildings 16*hr* day	0.2 – 0.4	0.4 – 0.8	0.8 – 1.6
Residential buildings 8*hr* night	0.1 – 0.2	0.2 – 0.4	0.4 – 0.8

TABLE 2 - VIBRATION DOSE VALUE RANGES WHICH MIGHT RESULT IN VARIOUS PROBABILITIES OF ADVERSE COMMENT WITHIN RESIDENTIAL BUILDINGS. TAKEN FROM BS 6472-1:2008

The American FTA guidelines [19] set different limit values for vibration and ground-borne noise depending on the frequency of transit trains. The categories are: less than 30, 30-70 and more than 70 events per day.

The guidelines provided above are applicable to vibration sources different from transportation such as internal and construction vibration. For large construction

[2] Below these ranges adverse comment is not expected.
[3] Above these ranges adverse comment is very likely.

works like the Channel Tunnel Rail Link (CRTL) and Crossrail[4] specific limits have been set which lie within the BS 6472-1:2008 ranges.

An attempt to relate exposure and response to vibration in residential environments for construction vibration has been done in BS 5228-2:2009 annex B [34] using PPV (Peak Particle Velocity) as a descriptor for the exposure. According to the standard, it is considered more appropriate to provide guidance in terms of the PPV instead of using the VDV of the weighted acceleration signal, since this parameter is likely to be more routinely measured through the more usual concern over potential building damage. Furthermore, since many of the empirical vibration predictors yield a result in terms of PPV, it is necessary to understand what the consequences might be of any predicted levels in terms of human perception and disturbance.

2.3.2 RESEARCH

The research about the human response to vibration can be broadly divided in three areas: biodynamic, perception and community response.

The biodynamic response of the human body to vibration has been briefly treated in section 2.2.1 whereas a literature review about the study on vibration perception can be found in Woodcock et al. [15] and Elias & Villot [3] as already stated in 2.2.2.

Both the research areas mentioned above and the criteria for evaluating the human exposure to vibration in the standards are based on laboratory studies which may not reflect the behaviour and the perception of a resident inside his property subject to vibration sources outside his control.

This problem can be approached understanding how the community responds to the vibration source. As already said in section 1.2, the main "tool" for exploring this issue is to build an exposure response relationship. For a given sample of the population, in order to build this relationship, the response is generally measured

[4] Crossrail Ltd (CRL) is a fully owned subsidiary of Transport for London (TfL).

through socio-acoustic questionnaire whereas the exposure is the result either of vibration measurements or estimations.

With respect to environmental noise, there are a fewer studies on the derivation of exposure response relationships for vibration. The latter have been derived only for transportation sources, like road and railway traffic, because the quasi permanent nature of vibration generated are repeatable and predictable facilitating such studies. It is worth to stress that all the exposure response relationships derived until now describe steady state situation. This means that the vibration source is already included in the living environment. Exposure response relationships have not been developed yet for new railway lines or for existing lines where rail services are altered. Furthermore, exposure response relationships have not been derived yet for large construction process affecting living environment such as railways, underground and tram line.

Below field studies for deriving exposure response relationship from environmental vibration are presented focussing the attention on the strategy adopted for the determination of the vibration exposure.

The importance of road traffic ground-borne vibrations in terms of disturbance were studied by Watts [35] in a study for the TRL. A questionnaire (Watts [36]) was designed in order to study the vibration nuisance. Approximately 30 people were interviewed for 50 residential sites in UK. For each site a median vibration nuisance were determined as an overall rating of noise nuisance. At one house per site external noise and window vibration were recorded for 15 minutes every hour over 24 hours. At later stage a deeper vibration assessment was done on a small number of houses, just 5 sites, where vibration was likely to be perceptible: the assessment consisted of vibration recording close to the facade and in the middle of the ground floor. The houses with the vibration level at the foundation above the perception threshold were close to significant surface irregularities. Moreover, the results showed a good correlation between the 18-hour noise levels at the facades of the dwellings with the vibration nuisance implying that the acoustically coupled vibration needed to be investigated.

Woodroof & Griffin [37] conducted a survey of annoyance caused by railway induced vibration in buildings in Scotland. A sample of 720 potential respondents was drawn from the adult population of Scotland who live within 100 meters of a railway line. The respondents were clustered in 24 sites, each containing 30 potential respondents. A questionnaire was designed to determine the number of residents who feel railway-induced building vibration in their home, and to find the amount of annoyance this caused. Of the 720 potential respondents, 459 were interviewed. A total of 160 reported noticing railway-induced building vibration and most of these, 133, lived at one of 12 sites. Vibration was recorded continuously for 24 hours in three orthogonal axes in 52 of the dwellings at the 12 sites, in buildings occupied by one of the 133 respondents who noticed vibration. It was found that the annoyance was well correlated with the number of train passages in 24 hours. The results also suggested that 35% of residents within 100 m of the railway line perceived vibration.

A large study in Norway (Turunen-Rise et al. [38], Klaeboe and Turunen-Rise [39], Klaeboe et al. [40]) was conducted for deriving an exposure response relationship for vibration from road and rail traffic. The response was quantified through telephone interview for 1503 respondents. On the other hand, for 1427 respondents of the sample population the exposure was estimated using a semi empirical model developed by Madshus et al. [41]. An important finding from this study was that there were no significant differences in annoyance caused by road and railway vibration sources.

The most recent study in terms of developing exposure response relationships for railway traffic was done in North America by the Transit Cooperative Research Program (Zapfe et al. [26]). In this study the responses of 1306 residents were assessed with a telephone interview in five cities: New York, Sacramento, Dallas, Toronto and Boston. Clearly it was not feasible to measure noise and vibration inside the residence of each respondent. Instead, measurements were made at 41 residences, and ground-surface measurements were made at an additional 100 locations. Grid measurements were interpolated to estimate vibration levels at each interview location based on its position along the alignment, and

perpendicular distance from the alignment. The calculated exterior vibration levels were then adjusted to estimate the vibration and noise levels inside each residence, based on the exterior and interior measurements at the 41 residential measurement sites. At each site, the field measurements were performed over a three to five day period. In this study, around 200 different noise and vibration metrics were considered as potential independent variables for an exposure-response relationship. It was found that all of the calculated metrics were highly correlated with each other and it was therefore concluded that any one of the metrics would be as good a predictor as any other of annoyance.

Exposure response relationships have been developed for super-fast train as well. The most recent study for evaluating the community response to Shinkansen railway vibration has been carried out in Japan by Yokoshima et al. [42]. For the study three separate social surveys were considered in the following areas: Kanagawa Prefecture (848 respondents), Fukuoka Prefecture (721 respondents), and City of Nagoya (174 respondents) in Japan. After the social survey was completed, measurements of noise and vibration were made to estimate noise exposures associated with each of the respondents' residences on a site-by-site basis. Maximum vibration level in the vertical direction and sound pressure level were measured on the ground for 24 hour at several points at different distances from the track. Vibration exposure (LVmax) was calculated from the averaged value among the top 50% of the measured maximum vibration levels. One or two distance reduction equations for each of noise and vibration metrics were formulated to describe the relationship between distance and the metric. The exposures in each dwelling were then estimated on the basis of the corresponding formula. Exposure response relationships were provided for each survey area.

Considered as the negative evaluation of environmental conditions by residents (Condie et al. [43]) , the annoyance is use as main measurement of the response due to its applicability for policy and guideline but it just one approach for understanding the problem of the psychological effect of the vibration exposure. Peris et al. [44] and other studies suggest that exposure to vibration during the night provoke a higher annoyance response than exposure during the evening or

day and that vibration generated by transportation sources causes disturbance to rest and sleep which is expected to be the most serious adverse health effect for vibrations and vibration induced noise. Unfortunately, only few laboratory and field studies exist on the argument.

Among them, it is worth to mention the large Swedish project TVANE (Ogren and Öhrström [45], Öhrström et al. [46]) (Train vibration and noise effects) which investigated the combined effects of railway noise and vibration on sleep. The socio-acoustics survey involved 980 residents living at different distances from the railway line in areas without train vibrations and in areas with different levels of vibrations (0.1 – 1.43 mm/s) induced by trains. The effects of noise and vibration on the residents from railway traffic was evaluated through a postal questionnaire whereas the exposure was assessed with empirical studies in the field in areas with similar railway noise exposure and different levels of railway vibration and with experimental studies on sleep performed in laboratory. The field survey for the combined exposure evaluation was conducted on 4 sites: 2 with a weak presence of vibration and 2 with a strong presence of vibration. Preliminary noise estimation for each residential building at each measurement site was done with the calculation program Cadna and measurements for controlling noise and vibration were performed before the final selection of the study areas. Vibration levels were measured outside and inside 5 houses in the two sites where the ground motion was considered strong. Results from field studies confirm the strong effects of railway vibrations on sleep. An interaction effect exists between noise and vibration and general annoyance to railway noise increase when combined with railway vibration.

Sleep disturbance is a parameter that can be evaluated through physiological measurement, such as polysomnography, and the latter can be an alternative way to annoyance survey for evaluating the effects of noise and vibration on sleep. In this sense, a German study conducted by Elemenhorst et al. [47] investigated event-related awakening reaction during sleep in a field study on nocturnal railway noise with a comparison with similar study on aircraft noise. 33 healthy participants (mean age 36.2 years ± 10.3 (SD); 22 females) living alongside railway

tracks around Cologne/Bonn (Germany) were, for the first time, polysomnographically investigated during nine consecutive nights. The probability of noise-induced awakenings was analysed basing on 8,866 recorded noise events which were recorded during the night at the sleeper's ear using class-1-sound level at 27 different homes. The study provided an exposure response relationship for nocturnal railway noise and showed that nocturnal freight train noise leads to significantly increased awakening probabilities which are higher than for aircraft noise, supporting the order found in the laboratory and contrasting the findings of annoyance surveys. It is worth to note that during the field survey vibration levels were measured outside and inside the property but, until now, just the noise data have been presented.

As pointed out in the White paper for European transport [48] the aim of the European rail operators is to increase the market share of goods traffic from 8 % in 2001 to 15 % in 2020. The nightly time slots will play an important in this since there are scientific evidences, through the studies presented above, that freight traffic increase the overall annoyance and is the main cause of sleep disturbance for residence living close to the railway lines.

In this framework, it can be mentioned the activity of two European projects: RIVAS and Cargovibes. At the time of this writing both projects are not completed yet. The RIVAS project [49] aims at reducing, below or near the human perception threshold, the environmental impact of ground-borne vibration, focussing on freight traffic, while safeguarding the commercial competitiveness of the railway sector. Instead, the Cargovibes project [50] has as main aim to develop and validate of measures to ensure acceptable levels of vibration for residents living in the vicinity of freight railway lines. In RIVAS the exposure response relationship will be used for evaluating the effectiveness of the mitigation measure whereas in Cargovibes the relationship will be derived for assessing the community response to railway vibration. Another important objective of the project Cargovibes is to publish a good practice guide on the assessment of the human response to vibration in residential environments. The aim of the guidance will be to provide end users with a set of practical tools to

assess the human impact of "steady state" railway vibration primarily in terms of annoyance and sleep disturbance. Encompassing the current state of knowledge regarding the human response to vibration in residential environments alongside the practical outputs of the Cargovibes project, it is intended that this document will serve to promote policy and standard development in this field. The development of this document included a workshop held at the University of Salford in May 2013, the outcomes of which will be incorporated in the guidance (Moorhouse et al. [51]).

2.4 CONCLUSION

In this chapter a review on the human response to vibration has been given.

The physical response to vibration depends on several parameters such as: vibration axes, posture and gender. For evaluating the vibration exposure parameters like amplitude, duration, frequency content and vibration type are essential especially for evaluating annoyance where both physical and psychological response need to be considered. Due to the complexity of the human response, there is not a standardisation of how to measure the vibration exposure. The standards generally agree on measurement position and the use of frequency weighting, but there are differences on the exposure metric, the method for evaluating the exposure and the limits for the annoyance evaluation. The latter are mainly based on thresholds that were established for perception due to vibration on humans in laboratory situations. It is not clear whether these guidelines are relevant for assessing human response including annoyance in real life (Waddington et al. [4]).

A better knowledge of the human response in living environment can be achieved assessing the response of the community to the vibration source with an exposure response relationship. The response is generally evaluated with socio acoustic questionnaire whereas the exposure is estimated with measurement or prediction. In spite of environmental noise, few studies have been conducted for environmental vibration for deriving exposure response relationships which were

mainly focussed on transportation sources. It can be said that in all the studies considered in section 2.3.2, which represent the state of art of the field, the estimation of the internal exposure relies on few internal measurement completed by either model or extrapolation method for assessing the exposure in the rest of the dwellings.

The knowledge of the human response to vibration in residential environments can be improved with the design and implementation of new measurement strategies. In this way reliable experimental data for the derivation of robust exposure response relationships for railway operations, railway construction can be collected and the most suitable vibration metric for describing annoyance can be investigated.

3 EXPOSURE MEASUREMENT DESIGN

3.1 INTRODUCTION

The derivation of an exposure response relationship for vibration in residential environments was the main aim of the three year project "Human response to vibration in residential environments" (NANR209) (see **Error! Reference source not found.**). The latter required the collection of a large amount of experimental data for quantifying both physical (exposure) and psychological (response) reaction of almost 1500 residents to different vibration sources outside their control. This chapter describes the design process for the exposure measurement where the author was primarily involved.

Taking into account that the data collection required half of the time needed for completing the present project, the planning side of the measurement campaign was an important task that cannot be underestimated: logistical and technical issues must be considered in the design of a practical measurement protocol (Woodcock et al. [52]). Two major tasks are considered in this chapter: the site identification for providing a robust sample of the residents affected by vibration in living environments and the selection of the best instrumentation for measuring the human exposure.

Design challenges site identification
Definition residential environment
Definition general criteria for site identification
Definition source specific criteria for site identification

TABLE 3 – DESIGN CHALLENGE SITE IDENTIFICATION

Design challenges for instrument design
Definition of human exposure and exposure measurement
General requirements for measuring human exposure
Practical requirements for field work
Installation, calibration and mounting

TABLE 4 – DESIGN CHALLENGE INSTRUMENT DESIGN

The design challenges related to the former and latter tasks are listed in Table 3 and Table 4.

In order to satisfy the design challenges listed above the problem of the exposure measurement needs to be formulated (see section 3.3). Then, in section 3.4, the task of the identification of the measurement site is considered whereas in 3.5 the instrumentation for measuring the human exposure to vibration is described.

3.2 NANR209

3.2.1 BACKGROUND

"Human response to vibration in residential environments" is the final part of a seven year project funded by the Department of Food and Rural Affair (Defra) UK (Perkins et al. [53]): its aim was to find a relationship between exposure to vibration in residential areas and human response quantified in terms of annoyance. The project was developed in three stages: a scoping stage undertaken by David Trevor-Jones Associates, a pilot study (Arup Acoustics and Temple Group [54]) conducted by Arup Acoustics, Temple Group, TRL & ISVR and a main study with the University of Salford as main investigator. The scope of the University of Salford was to derive an exposure response relationship for vibration in residential environments outside the resident's control and to evaluate the most suitable index to be used for expressing the associated levels of

vibration. The vibration sources considered in the study were railway operation and construction. The study consisted of the quantification of the response with a social survey questionnaire based on face-to-face interviews followed by vibration measurements in order to obtain a measure of the exposure. In the framework of the main study different methodologies have been developed for determining both response and exposure to vibration.

3.2.2 DETERMINATION OF RESPONSE

Annoyance has been defined as a psychological phenomenon: it's largely considered as the negative evaluation of environmental conditions by residents [43]. The latter was taken as the main measurement of response due to its applicability for developing policy guidance and international standard.

A social survey questionnaire was developed to measure residents' self-reported annoyance and to provide data for establishing exposure response relationship between levels of annoyance and the levels of vibration. Residents' self-reported annoyance for noise was also covered in this social survey questionnaire, due to vibration and noise often being experienced together. Furthermore, the survey aimed to collect data on number of other factors that may be influential, for example, vibration and noise sensitivity, self-reported ratings of acceptability and satisfaction with the home. In order to avoid influencing responses and reasons for participation in the research, the survey was presented as a survey of neighbourhood satisfaction. Within the social survey questionnaire the following definitions were used to describe the three vibration sources investigated:

- Railway – defined as '*the railway, including passenger trains, freight trains, track maintenance or any other activity from the railway*'.
- Construction activity – defined as '*construction activity, including demolition, piling, road works, drilling, surface activity such as bulldozers and loading trucks and any other construction activity*'.

The social survey was carried out with 1281 residents: 931 respondents for railway traffic and 350 respondents for railway construction. It was undertaken in areas

where the residents were already exposed to vibration and in different periods from the vibration survey in order to avoid bias. The development and implementation of the questionnaire is described in Condie et al .[43] and Condie and Steele [55].

3.2.3 DETERMINATION OF EXPOSURE

Vibration exposure was obtained through measurement and prediction in order to obtain, where possible, an estimation of internal vibration exposure for each residence in which a questionnaire was completed. The source specific methodologies employed for the determination of the exposure can be found in the chapters 4 and 5.

3.2.4 INDIVIDUAL CONTRIBUTION TO THE RESEARCH

In the framework of NANR209 the author has been involved in the following areas:

- Measurement planning and site identification.
- Design and implementation of measurement protocols.
- Downloading data, storage and equipment maintenance.
- Exposure calculation
- Uncertainty analysis
- Writing final reports.

3.3 FORMULATION OF THE PROBLEM

3.3.1 THE VIBRATION EXPOSURE

The exposure is defined as the 'quantity' of vibration to which a hypothetical resident is exposed inside their property from vibration sources that are outside their control, assuming that they remain indoors during the period of exposure. Specifically, the total amount of vibration energy absorbed by a respondent over a given time period is defined as vibration dose. Therefore, in this work the terms vibration exposure and vibration dose have the same meaning because they are

evaluated over the same time period. Due to the lack of information related to the activities of the community, it seems more useful to consider exposure-response relationships instead of dose-response relationships from a policy/planning point of view (Woodcock et al. [15]).

3.3.2 VIBRATION TYPES AND VIBRATION SOURCES

Different types of vibration may affect a living environment and can be grouped in the following categories according to the time history of the vibration input to the subject (BS 6472-1:2008 [18]):

- Continuous.
- Intermittent.
- Occasional.

Each of these categories can be characterised by one of the following vibration: constant, variable or impulsive amplitude. However, in order to evaluate human exposure, the vibration needs to be considered in the frequency range encompassing the range of human sensitivity. There are a number of objective features, represented in Figure 5, of vibration exposure which can influence human response including the amplitude, direction, frequency content, duration, and envelope characteristics of the vibration.

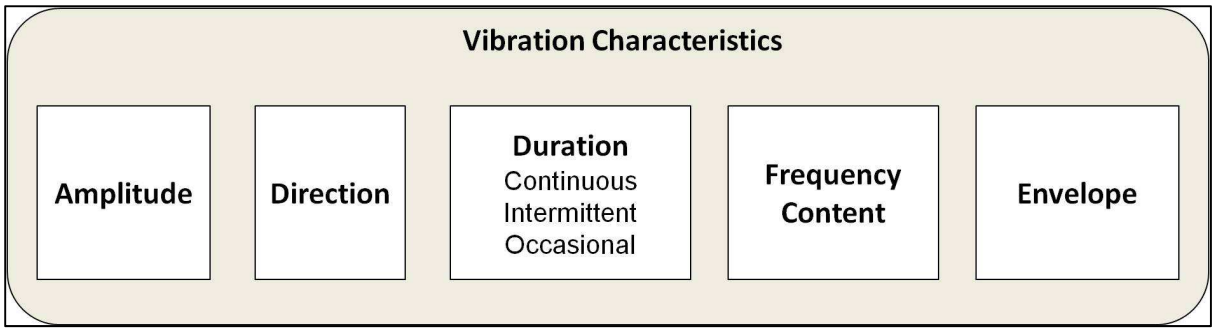

FIGURE 5 - VIBRATION CHARACTERISTICS

The vibration considered in NANR209 consists of the ground and structural vibrations caused by manmade processes, specifically:

- Railway activity.

- Construction activity.

3.3.3 RESIDENTIAL ENVIRONMENT AND EXPOSURE ESTIMATION

The living environment has been defined as a dense group of dwellings within a radius of 100 meters from the vibration source. In these situations it can be helpful to break down the generation, transmission and perception of vibration into the following elements (See Figure 6):

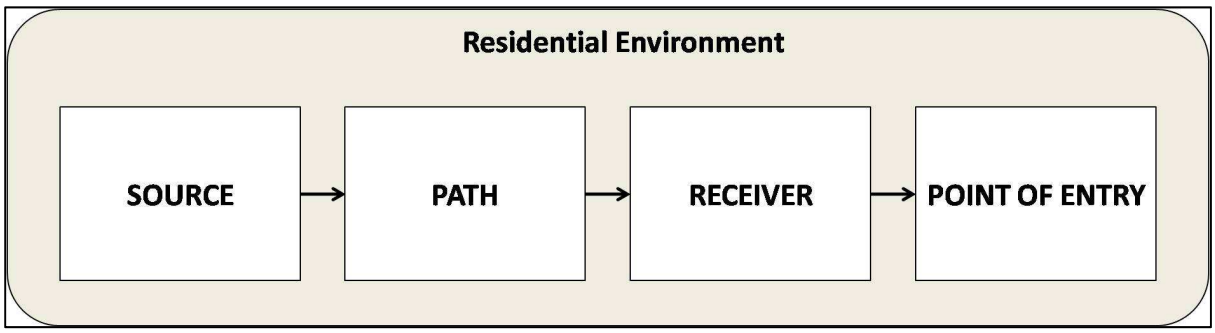

FIGURE 6 - BLOCK DIAGRAM OF A RESIDENTIAL ENVIRONMENT

- Source – defined as the region where the vibration is create and transferred into the ground.
- Path – defined as the soil profile where the vibration is propagated.
- Receiver – comprises the soil which interacts with the building foundation, the sub-structure linked with the foundation like floors, walls and ceilings which might generate re-radiated noise and other effects like moving objects (mirrors/clattering glasses).
- Point of entry – the point in the building at which the vibration 'enters' the human body. The latter is most sensitive to vibration in the frequency range from 1 to 80 Hertz (BSI ISO 14837-1:2005 [5]).

For the activities considered in the study, the source is external to the property and each region (source, path and receiver) is involved in the process of vibration transmission and may either magnify or reduce the level of vibration during its passage. Therefore, these factors need to be taken into account for a complete understanding and estimation of the exposure.

It must also be recognized that vibration activity can affect the residential environments in a more or less permanent way, such as in the case of railway traffic, or may be transitory such as the vibration from construction sites. Therefore, this last characteristic has to be considered in the evaluation of the exposure. As well as potentially affecting the annoyance from vibration it also has major implications for the measurement of exposure. With permanent sources, like railways, it is possible to estimate exposure from internal measurements in the homes of survey respondents. On the other hand, this is not possible for transitory sources because of a logistical 'catch-22': the survey must precede measurements to avoid biased responses; however, the survey of annoyance must occur after the exposure and the measurement during the exposure. It is not possible to satisfy all these criteria simultaneously so large scale internal measurement are not possible for construction sites.

3.3.4 EXPOSURE MEASUREMENT

The evaluation of exposure is mainly done for each vibration source using a novel measurement methodology described in Sica et. al. [56] and Peris et. al. [57]. As explained in section 1.1, the methodology used in this work is oriented on the direct estimation of the internal vibration exposure using extensive field work, the latest generation accelerometers, and novel community engagement methods. This approach made it possible to estimate vibration exposure from railway operation for 522 dwellings over a population sample of 931 people. As discussed in section 2.3.2, this approach is in contrast with the one used in the previous field studies where the exposure is estimated using a limited number of internal measurements and extrapolation/empirical methods.

The exposure assessment relies on two types of measurement:

- Long term measurement.
- Short term measurement.

Long term measurements, taken at 'control positions', are conducted close to the residential environment with the aim of capturing the full time history of the

sources over at least a 24 hour period. On the other hand, short term measurement, usually with an average duration of thirty minutes, have been used for evaluating the impact of the vibration within the respondent's property, as close as possible to the point of entry. External short term measurements arranged in an array configuration were also used for assessing the vibration attenuation through the residential environment. The methods used for evaluating the exposure for each sources are described in more detail in chapters 4 and 5.

3.4 SITE SELECTION

Considering the design challenges for the site selection listed in Table 3, the site selection needs to be based on general (see 3.4.1) and source specific criteria (see 3.4.2) for gathering both response and exposure measurement as the first step for deriving an exposure response relationship.

3.4.1 GENERAL CRITERIA

As stated in the section 3.3, the residential environment is defined as the dense group of dwellings within a radius of 100 meters from the vibration source, according to the study done by Woodroof and Griffin [37]; from this definition we can identify two parameters necessary for the selection of the site: the distance from the vibration source and the density of dwellings. The latter is chosen to maximise the number of potential interviews for each site. The actual number of successful interviews also depends on the success rate of the interviewer. A success rate of one completed questionnaire per ten houses visited was established from the preliminary field trial where 33 interviews were gathered over 349 properties. This figure was used to estimate the number of successful questionnaire before visiting a site. Sites at different distances from the vibration source with different property types have been chosen for achieving a wide range of exposure to the vibration for the potential number of respondents. Measurement sites were chosen, as far as possible, to provide a representative overall socio-demographics sample (Condie et. al. [43]) but this aspect is outside the scope of this thesis. The main features for selecting the exposure measurement sites are summarised in the points below:

- A high concentration of residential properties in close proximity to the source with a probability that vibration would be perceptible in the residences.
- As far as possible, residences were required to be exposed only to the source of vibration of interest – there would be no interference from other sources.
- A sufficient number of respondents were required in the locality exposed to the vibration.
- The measurement site needed to be easily accessible and without the risk of compromising the health, safety and welfare of the survey personnel.

At the first stage the measurement sites were identified using online map service like Google maps using the density of dwelling and the distance from the vibration source as main parameters for selecting the potential site. The following step was to have a site reconnaissance for assessing their suitability and safety. The measurement site selection also considered the time necessary for the field work and the budget.

In this section the general criteria used for identifying site for measuring annoyance and exposure have been presented. Specific criteria also need to be adopted for identifying sites subjected to the vibration source under investigation which are discussed in the following section.

3.4.2 SOURCE SPECIFIC CRITERIA

3.4.2.1 RAILWAY ACTIVITY

The semi-permanent nature of the railway activity made the selection of the site not so difficult. In fact railway lines are frequently surrounded by living environments. The site identification was carried out according to the general criteria listed in section 3.4.1 combined with specific criteria listed below:

- The sites were required to have high railway traffic.
- Properties within a distance of 70 meters to the railway were mainly targeted to ensure a high enough vibration level perceptible for the respondents.

The potential locations satisfying the requirement listed above were identified following the West Coast main line of the UK concentrated in the North West and Midlands areas. A total of twelve sites were chosen at which the social survey and the vibration measurements were conducted.

3.4.2.2 CONSTRUCTION ACTIVITY

In spite of the permanent nature of the railway source, construction activity has a transitory characteristic which makes the identification of the measurement site difficult. The construction activity needed to potentially affect a sufficient population to yield responses from several hundred residents and the feasibility of measurement also had to be taken into account. These requirements led to the adoption of a different framework of site identification based on:

- The stage of the construction activity. The major part of this activity needed to be placed during spring, summer and autumn of 2010.
- It required the cooperation of the construction site management, due to the transitory nature of the source.
- The vibration activity needed ideally to comprise different types of construction sources.

Many of the identified sites were rejected as they did not meet the requirements or they proved to be impractical for the implementation of the measurement protocol. The only potential measurement site was found considering construction work from light rail installation. The measurement sites were identified in two areas of Manchester.

3.5 INSTRUMENTATION

In this section the instrumentation, and its characteristics, used for measuring the human exposure to vibration is discussed in order to satisfy the design challenges listed in Table 4.

3.5.1 GENERAL REQUIREMENT

In the framework of the project 'Human response to vibration in residential environments', the assessment of the exposure has been done through measurement. The characteristics of the measurement system need to be chosen carefully in order to obtain an accurate evaluation of the exposure. BS 6472-1 [18] requires the recording of acceleration time history in order to derive the VDV as exposure metrics. The frequency range for assessment of human sensitivity to vibration has been standardised as 1-80 Hz. The assessment of the human response to vibration in building does not only depend on whole body vibration but it should be also considering the perception of groundborne noise. As a consequence, the instrumentation needs to be able to predict ground-borne noise from vibration measurements as required by BS ISO 14837-1:2005 [5] even if the human response to groundborne noise is outside the scope of NANR209.

Regarding dynamic range, the lower limit of the problem can be identified as the threshold of perception which needs to be measured cleanly, and consequently a noise-floor significantly lower is required. In order to measure all non-perceivable vibration, the transducer would require a noise floor of 3×10^{-6} ms^{-2}, which is the lower limit identified in BS ISO 14837-1:2005 [5] for measuring groundborne vibration, for achieving a signal-to-noise-ratio of 20 dB (Arup Acoustics and Temple Group [54]).

The upper bound depends on the type and the position of the measurement. Because the exposure measurement would be mainly unattended at a large number of locations; the overload of the measurement system should be avoided. BS ISO 4866:2010 [58] gives a guidance regarding typical structural response magnitudes for various event types: excluding blasting and earthquakes, the upper bound for interior measurements is expected to be below 1 g[5]. From the discussion above the range necessary for measuring the human exposure is between 3×10^{-6} ms^{-2} and 10 ms^{-2} demanding a dynamic range greater than 130 dB. Theoretical dynamic ranges for 16 and 24 bit ADCs are 96 and 144dB respectively.

[5] With the term g is indicated the acceleration due to gravity ~ 10 ms^{-2}

Therefore 24 bit systems will be preferable for this study together with a transducer with an unusually low noise floor. Beyond the general characteristic listed above, the measurement system needs to be robust, portable, weather resistant and with a good capacity to store data in order to measure vibration at multiple outdoor locations per day. Seismic recorders/transducers have proven track records with respect to long-term stability, reliability and weather resistance, as they are typically required to work under such conditions.

3.5.2 SEISMIC TRANSDUCER

Seismic transducers measure ground motion relative to an inertial reference (a suspended mass). An inertial seismometer converts ground motion into an electric signal but its properties cannot be described by a single scale factor, such as output volts per millimetre of ground motion. The response of a seismometer to a ground motion depends not only on the amplitude of the ground motion but also on its time scale. This is because the seismic mass has to be kept in place by a mechanical or electromagnetic restoring force (Bormann [59]).

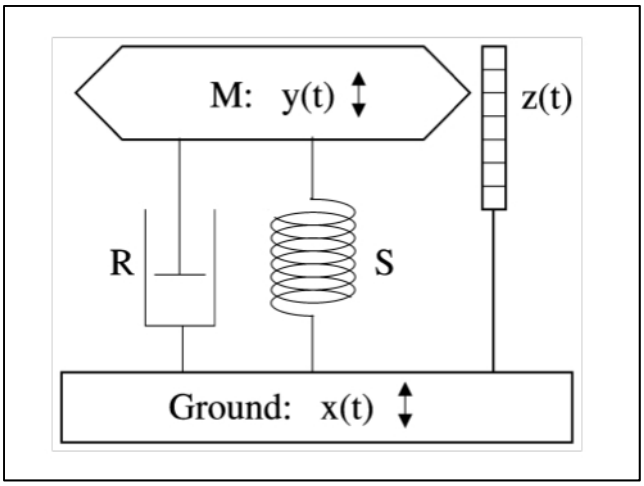

FIGURE 7- DAMPED HARMONIC OSCILLATOR

There are many different types of sensors design to measure different frequency bands and ground motion amplitudes. High gain sensors, or seismographs, are used to measure small local, moderate regional and teleseismic earthquakes. These record ground motions (usually velocity) that are too small to be felt (weak motion typical clip 1cm/s). Low gain sensors, or strong motion accelerometers, are used

to measure strong motion produced by large local earthquakes that would clip the high gain sensors (typical clip 2*g*). There are no fundamental differences in the physics of the two sensors and they can be simply modelled as a mass and spring system with viscous damping (Bormann [59]) shown in Figure 7.

We assume that the seismic mass performs a pure translation. The mechanical elements of the system are a mass m, a spring with stiffness s and a damping element with a constant of viscous friction r. The time dependent ground motion is express as $x(t)$, the absolute motion of the mass $y(t)$ and its relative motion $z(t) = y(t) - x(t)$. An acceleration of the mass caused by an external force $f(t)$ can be expressed as:

$$m\ddot{y}(t) = f(t) - sz(t) - r\dot{z}(t) \tag{3.1}$$

Equation (3.1) can be rearranged since we are interested in the relationship between $z(t)$ and $x(t)$

$$m\ddot{z}(t) + r\dot{z}(t) + sz(t) = f(t) - m\ddot{x}(t) \tag{3.2}$$

The acceleration $\ddot{x}(t)$ of the ground has the same effect as an external force of magnitude $f(t) = -m\ddot{x}(t)$ acting on the mass in the absence of ground acceleration. A ground motion $x(t)$ can be simulated by applying a force $-m\ddot{x}(t)$ to the mass while the ground is not moving. The force is normally generated by sending a current through an electromagnetic transducer, but it may also be applied mechanically. Nowadays seismic instrumentation works using a force-feedback loop. These systems are similar to standard seismometers, but they usually have a displacement transducer to measure the motion of the seismometer mass. In addition, they add an electromagnetic force system that has the role of minimizing the motion of the mass with respect to the seismometer case. The force applied to the mass for keeping it stationary is simply equal and opposite of the ground acceleration. The essential feature of these systems is that the dynamic range of the instrument is dictated by the dynamic range of the electronic feedback system, and

not by the dynamic range of the mechanical seismometer. This characteristic allows them to achieve a wide dynamic range often up 140 dB. However, the electronic feedback system can also be designed to provide the desired instrument response. An example of this feature is the possibility to design seismic instrumentation that behaves as a weak motion seismometer in a certain frequency range whereas in another the sensor works as strong motion accelerometer as is the case for the Guralp 3TB/5TB (Guralp [60]).

Seismic transducers generally consist of a sensing unit and a recording unit. Current state-of-art is to record output voltages from the sensing system with a digital data logger, which typically consists of an analogue to digital converter (ADC) and some type of digital computer for processing, storage and communication (the recording unit).

3.5.3 MEASUREMENT SYSTEM

The most appropriate measurement system for exploring the human exposure to vibration in residential environments, among the ones commercially available, is the Guralp CMD-5TD (Figure 8). The latter is a three-axis strong-motion force feedback accelerometer combining low-noise components with high feedback loop gain to provide a linear, precision transducer with a very large dynamic range (Guralp [61]).

FIGURE 8 - GURALP CMD-5TD

The noise floor of ~10 μms^{-2} across the frequency range of interest completely satisfies the requirements given in section 3.4.1. From Figure 9 it can be seen that the background noise of the instrument coincides (orange line) with the upper bound of the USGS low noise model[6] (yellow line labelled with HNM in Figure 9). On the other hand, the sensitivity in the standard configuration for the unit corresponds to 5 V output for 1*g* acceleration in input, meeting the requirement of the upper bound chosen for unattended measurements.

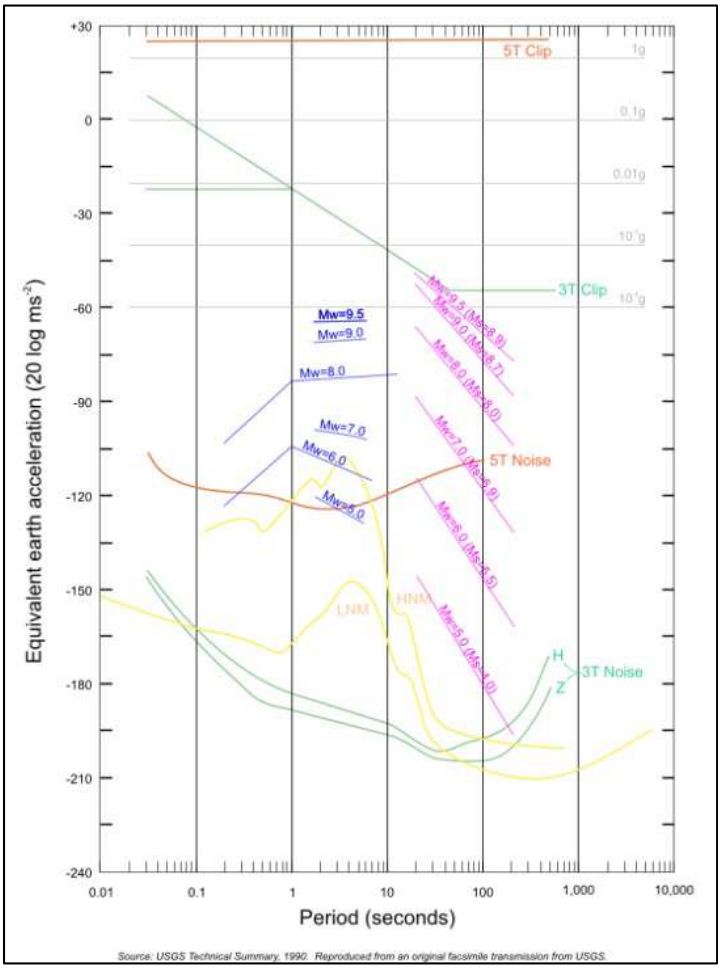

FIGURE 9 - BACKGROUND NOISE OF THE SENSOR (ORANGE LINE) AS A FUNCTION OF THE PERIOD. LINE LABELLED HNM: UPPER BOUND OF USGS NOISE MODEL. COURTESY OF GURALP LTD.

Since the sensor has a force feedback transducer, its dynamic range is greater than 140 dB for the frequency interval between 0.005 to 0.5 Hz and greater than 127 dB

[6] The USGS Low Noise Model [214] summarizes the lowest observed vertical seismic noise levels throughout the seismic frequency band. It is useful as a reference for assessing the quality of seismic stations, for predicting the ability to detect small signals, and for the design of seismic sensors.

between 3 to 30 Hz. Furthermore, the frequency response of the sensor is designed to be flat in the frequency range between 0 and 100 Hz. The unit has a built-in low pass filter at 100 Hz which starts rolling off from 80 Hz. The low-pass filter is implemented in the feedback loop and is completely described by the poles and zeroes of the instrument's response which are available in the calibration sheet provided by the manufacturer.

The CMG-5TD has an in-built 24-bit digitizer (CMG-DM24/3) with a sample frequency of 200 Hz coupled with the transducer satisfying the other general requirement stated in section 3.4.1. Thus, the CMG-5TD sensor system has a large dynamic range, combining the 140 dB of the sensor with the 132 dB noise-free resolution of the digitizer.

Moreover, vibration data is recorded and stored in the memory of the unit which has a capacity of 4 GB allowing long-term measurement to be made without the need of an external acquisition system. A tri-axial 24 hours measurement sampled at 250 Hz will generate approximately 520 MB which means that the unit can record continuously for more than 8 days.

The last but not least feature of the measurement system is its size: 140 mm height and 180 mm diameter with a mass of 3.8 Kg. These are good characteristics, considering the large number of measurements that are needed for deriving the exposure response relationships, which makes the instrument extremely portable and it does not occupy too much space during the monitoring phase.

3.5.4 CALIBRATION

The primary objective of the calibration of an instrument, such as an accelerometer, is to determine its sensitivity over the amplitude and frequency range over which the instrument is to be used. The sensitivity of an accelerometer is obtained by placing the transducer with its sensitivity axis parallel to the direction of motion of the vibration generator, measuring the motion or input applied by the vibration generator, and measuring the output of the transducer.

A vibration generator may be a support for tilting the transducer relative to the pull of gravity, a centrifuge, an electrodynamic vibration generator, or the anvil of a ballistic pendulum. The tilting support and centrifuge are used for a calibration at zero frequency. Rotational calibration is used for low-frequency calibration using the Earth's gravitational field. An electrodynamic vibration generator is normally used for steady-state sinusoidal calibrations (BS ISO 16063:1998 [62]).

The level of the calibration is limited by the accuracy of the measurements of the excitation provided by the vibration generator. This is at the base of the distinction between 'primary' and 'secondary' calibration.

The response of the CMG-5TD (in V/ms^{-2}) is measured at the production stage by tilting the sensor through 90° and measuring the acceleration due to gravity. Local *g* at the Guralp Systems production facility is known to an accuracy of 5 digits. This technique is considered to be a primary calibration according to BS ISO 16063:1998 [62]. In addition, sensors are subjected to the "wagon wheel" test, where they are slowly rotated about a vertical axis. The response of the sensor traces out a sinusoid over time, which is calibrated at the factory to range smoothly from 1g to -1g without clipping (Guralp [61]).

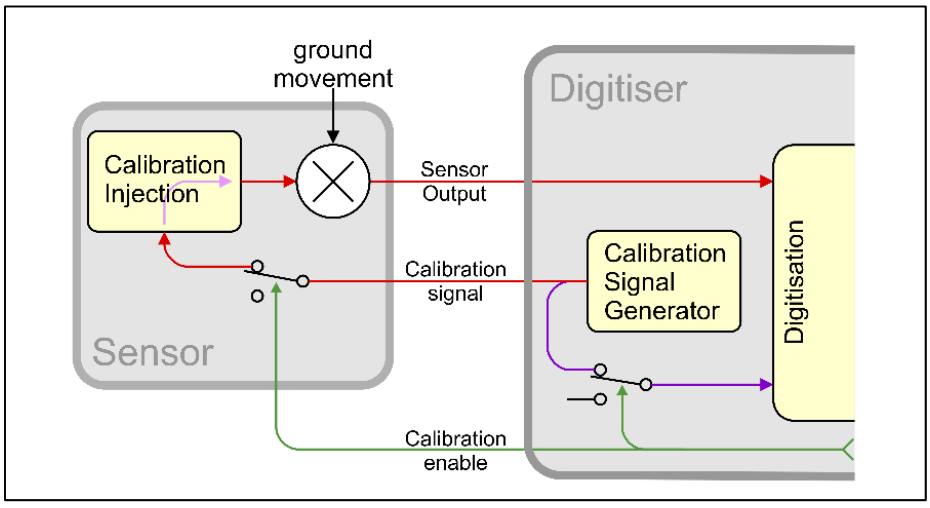

FIGURE 10 – SCHEMATIC OF GURALP 5TD CALIBRATION CHECK TAKEN FROM WWW.GURALP.COM.

However, the sensor response can be checked using the manufacturer's interface by injecting a known electrical calibration signal into the sensor. This gives rise to an equivalent acceleration (see Figure 10) that is added to the measured

acceleration to provide the sensor output. The signal injected into the sensor can then be compared with the sensor output to determine if the sensitivity of the sensor is consistent with the value provided by Guralp. This procedure was performed off-site before starting each set of field measurements to ensure the accelerometers were properly functioning.

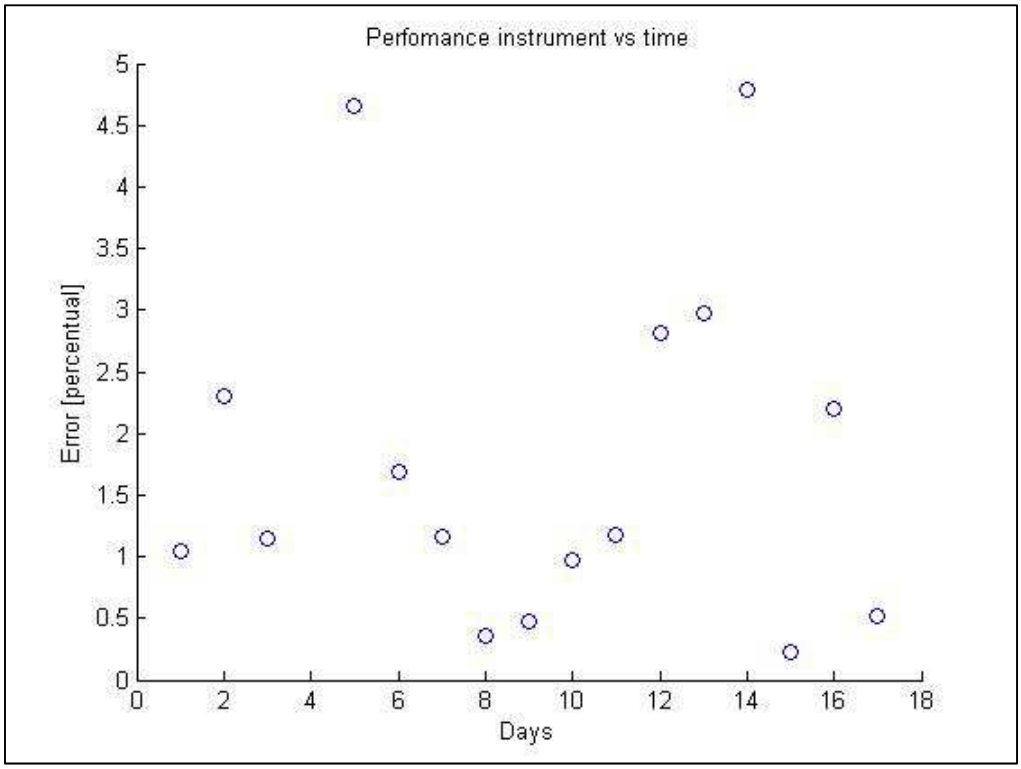

FIGURE 11 – PERCENTAGE CALIBRATION ERROR AS THE DIFFERENCE BETWEEN INJECTED REFERENCE ACCELERATION AND MEASURED ACCELERATION OVER TIME IN DAYS.

Figure 11 shows the evolution of the calibration error factor over time of one instrument. The error is the difference between the injected reference acceleration and the measured acceleration. The graph suggests an average behaviour of the instrument of less than 3% error. The two spikes at around 5% are thought to be mainly due to the variation in the background level. The performance of all the instruments resulted in errors between 3% - 3.5%. The calibration error is explained by the variation in the background level in the measured signal. The latter is very low due to the sensitivity of the instrumentation, shown in Figure 9, and can be influenced by variation in environmental parameters like temperature or anthropic activity

3.5.5 SYNCHRONISATION

The internal clock of the measurement system is set either by receiving timing signal from the GPS satellite network via an attached GPS antenna, or by taking information from an external clock or GPS emulator. Synchronisation between the units is essential for assuring "phase locked" measurements.

The antenna method has been mainly used for the long term monitoring position. The antenna was generally installed in an open air location although installations enclosed space with thin roof/wall or with a small window like a garage or shed could also be used. Time synchronisation with the satellite network is achieved when at least three satellites (with a maximum of six) are detected by the antenna. The digitizer makes a continuous polling to the antenna in order to synchronise as many satellites as possible in order to obtain better information about the location of the instrument expressed in latitude, longitude and elevation.

Due to logistical problems associated with running cables outside properties through the windows during internal measurements, it was not often practicable to setup GPS antennas required to synchronise the internal clocks of the units. Moreover, it was observed that the internal clocks of the instrumentation would tend to drift over long durations and changes in ambient temperature if the antenna was not plugged into the unit. To overcome this problem, the manufacturer introduced an external clock or GPS emulator which consists of a microprocessor-controlled, temperature compensated quartz oscillator. Once synchronised by the GPS time source, the GPS emulator can keep time to an accuracy of 1.2×10^{-8} s and has been shown to perform with a drift of less than 1 ms over a period of 48 hours. The GPS emulators were synchronised overnight in the laboratory, thus avoiding the need to connect any GPS during internal measurement.

3.5.6 TRANSDUCER INSTALLATION

The installation of the sensor depends on the type of measurement which can be either long or short term.

Long term measurements were generally conducted outside the resident's house such as in the garden next to the facade most exposed to the vibration source. Seismic transducer cannot be directly installed on soil because soil and/or weathered rock layers between the sensor and the bedrock will modify seismic amplitudes and waveforms (Bormann [59]). Ideally, the instrument will be installed in hand-dug pits or machine-augered holes. Once a level base is made in the floor using cement or plaster, the accelerometer can be sited there and covered with a box or bucket (Guralp [61]). This type of installation has been considered impractical because it is time consuming and can create disruption to the property which might upset the resident. Therefore, the only requirement for the outside installation of the unit was to find a solid surface. A location like a garage or shed was the best solution to the problem providing a secure place for the instrumentation and a protection from the weather.

Short term monitoring measurements were mainly performed inside the resident's house. The current methods for installing accelerometers on structure are described in BS ISO 5348:1998 [63] but they are impracticable due to the characteristics of the sensor in terms of mass, dimension and design. Furthermore, as the requirement of the project involved measurement inside occupied residences, some of the installation methods employed must not cause damage or leave permanent marks on any surface. When an internal measurement was allowed the vibration inside the property was measured, if possible in the room where the respondent says that they are worst affected according to BS 6472-1:2008 [18] and ANC guidelines [27]. However, due to the mass of the Guralp CMG-5TD instruments (3.8 Kg), any resonances due to different mounting surfaces, e.g. carpet, had to be considered. The results of an investigation into the mounting conditions for different surfaces are presented in the following section 3.5.6.1 and a theoretical evaluation of the human load on the vibration measurement is given in section 3.5.6.2.

3.5.6.1 MOUNTING CONDITIONS

One of the most commonly encountered variables when mounting the accelerometers in dwellings is whether the units are mounted on a rigid floor (i.e. a timber or concrete floor) or a floor with a compliant covering (i.e. carpet or linoleum). A simple laboratory study was conducted to determine the effect of mounting the Guralp accelerometers on different types of carpet and any action that could be taken to reduce these effects.

The material under investigation was laid on a concrete slab and a Guralp accelerometer was mounted on it either directly, on a ceramic tile (4mm x 300mm x 300 mm), or on a circular metal plate (5mm thick x 210 mm diameter). Two B&K type 4379 accelerometers were mounted directly onto the slab orientated in the direction of interest (tests were conducted for the vertical and in-plane components). The slab was excited by striking it ten times with a sledgehammer in the vertical and horizontal directions. The effect of the different mounting methods was evaluated by examining the ratio between the magnitude Fourier spectra averaged over 10 hammer blows of the acceleration measured by the Guralp system and the B&K system. The experiment was conducted for 15 mm, 10 mm, and 7 mm thick carpets as well as a control measurement which was taken with the Guralp unit mounted directly onto the concrete slab.

The findings of this experiment confirmed there to be large differences in response between rigid and carpet mounting. In general it was found that by using a steel plate the effect of mounting the Guralp accelerometers on compliant covering was greatly reduced. Based on the results, the following guidance was adopted when mounting the Guralp accelerometers:

- On rigid surface such as concrete, timber floors, the accelerometers were mounted directly on the surface.
- On compliant surface such as carpets and linoleum, the accelerometers were mounted on a metal plate.

Full details about these investigations can be found in Woodcock et. al. [52] and Peris et. al. [57].

3.5.6.2 HUMAN LOAD

As assessed in section 3.5.5, the internal vibration measurements were taken in unoccupied room even though the individual perceives vibration at the point of entry. Thus, the influence of the standing human body on the vibration measurement in terms of frequency and magnitude was explored.

This problem has been approached in a similar way to the problem of the vibration transmission of machinery; in this way, the ratio between the loaded and the unloaded velocity can be expressed for every point of the structure as a function of the mobilities of the human body and the structure. This ratio reflects the influence of the human body on the structure. The influence of the standing human body on a floor is determined using the relation that links the ratio between the velocity of the loaded (v_b) and unloaded (v_{fs}) floor with the mobilities of a floor (Y_F), and the human body (Y_B).

$$\frac{v_b}{v_{fs}} = \frac{1}{1 + Y_F Y_B^{-1}} \tag{3.3}$$

The mobility of the floor is approximated by the mobility of a beam as, in the proximity of a beam, the mobility of a timber floor is similar to the mobility of a beam (Mayer and Nightingale [64]). In this way Y_F, is expressed by (3.4) (Xin [65]) and the mobility of the human body Y_B, comes from (3.7) derived by the apparent mass in (3.5).

$$\begin{aligned} Y_F(\omega) &= -\frac{j\omega}{2BK}\left(\frac{\sinh(kx)\sinh(k(l-x_0))}{\sinh(kl)} - \frac{\sin(kx)\sin(k(l-x_0))}{\sin(kl)}\right) \quad 0 \le x \le x_0 \\ Y_F(\omega) &= -\frac{j\omega}{2BK}\left(\frac{\sinh(kx_0)\sinh(k(l-x))}{\sinh(kl)} - \frac{\sin(kx_0)\sin(k(l-x))}{\sin(kl)}\right) \quad x_0 \le x \le l \end{aligned} \tag{3.4}$$

Where $k = \left(\omega^2 m'/B\right)^{1/4}$ is the bending wave number, m' the linear density, B the bending stiffness, ω the angular frequency and l the length of the beam. The apparent mass of the human body is given by Matsumoto and Griffin [6]:

$$M_{2a}(i\omega)=\frac{(ic_1\omega+k_1)\left[m_1\left(-m_2\omega^2+ic_2\omega+k_2\right)+m_2\left(ic_2\omega+k_2\right)\right]}{-\left[m_1\omega+i\left(c_1+c_2\right)\omega+\left(k_1+k_2\right)\right]\left(-m_2\omega^2+ic_2\omega+k_2\right)^2} \quad (3.5)$$

Where k_1=4.39 x 10^{-3} $Nm^{-1}kg^{-1}$, k_2=5.53 x 10^{-2} $Nm^{-1}kg^{-1}$, m_1=5.74 x 10^{-1}, m_2 =3.94 x 10^{-1}, c_1 =3.71 x 10^{1} $Nsm^{-1}kg^{-1}$, c_2 =1.18 x 10^{1} $Nsm^{-1}kg^{-1}$ are parameters of the linear lumped two degree of freedom model in Figure 12. Nominal corresponding parameters for a specific static mass of the body may be obtained by multiplying the parameters listed above by the static mass.

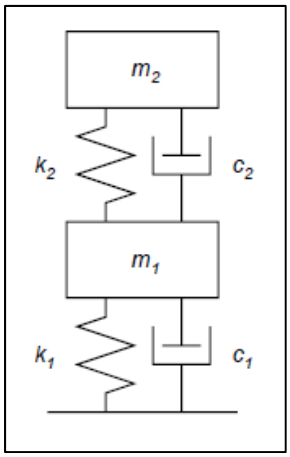

FIGURE 12 – LINEAR LUMPED 2 D.O.F. APPARENT MASS OF STANDING HUMAN SUBJECTED TO WHOLE BODY VIBRATION

The accelerance A is obtained from the specific apparent mass m_{2a}:

$$A=\frac{1}{m_{2a}} \quad (3.6)$$

Therefore, the mobility of the human body in the standing position is:

$$Y_B=\frac{A}{j\omega} \quad (3.7)$$

A better understanding of the influence of the human load is obtained by showing the trend of the ratio in (3.1) in the frequency domain for a wood beam with a length of 4.55 m, width 0.096 m, height 0.192 m and with $x=x_0$=2.275 and for persons of various masses (see Figure 13). The ratio is almost 1 for frequencies above 50 Hz whereas it oscillates between 2 and 0.2 for frequencies below 50 Hz.

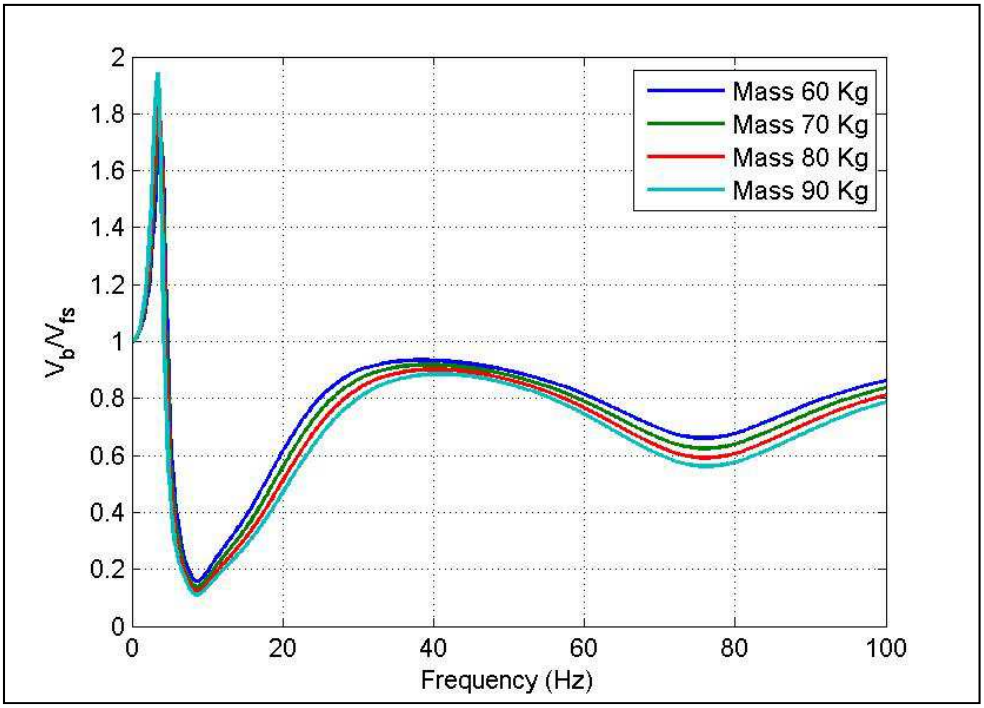

FIGURE 13 - INFLUENCE OF THE HUMAN LOAD ON A WOODEN BEAM EXPRESSED AS THE RATIO BETWEEN THE VELOCITY OF THE LOADED BEAM (V_B) AND THE VELOCITY OF THE UNLOADED BEAM (V_{FS}) FOR DIFFERENT VALUES OF STATIC MASS. FROM THE TOP TO THE BOTTOM 60, 70, 80 AND 90 KG

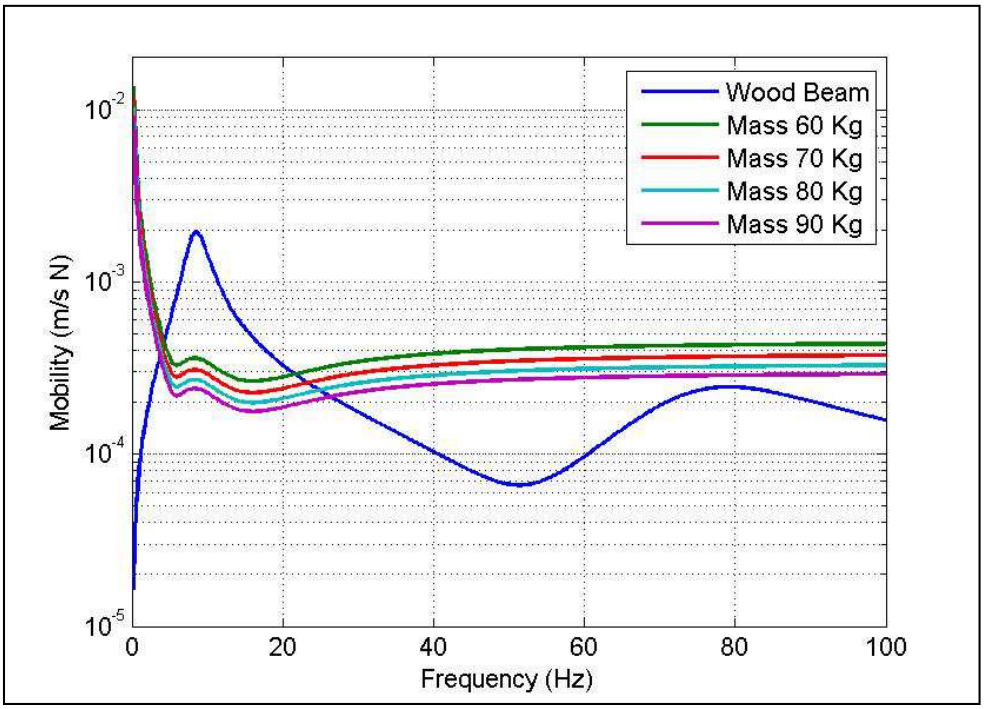

FIGURE 14 - MOBILITY COMPARISON. FROM THE TOP TO THE BOTTOM: MOBILITY UNLOADED WOOD BEAM AND MOBILITY OF HUMAN BODY ON A STANDING POSITION WITH STATIC MASS FROM 60 KG TO 90 KG.

For frequencies below around 50 Hz, the beam has a higher mobility with respect to the human body in the standing position, especially around its first vibration

mode as shown in Figure 14. Therefore, when vibration is measured on the unloaded beam of a timber floor, an overestimation of the vibration transmitted to the human body (i.e. when the beam is subject to a human load) is expected.

Note that the damping ratio of a real wooden floor will be considerably higher than that used for a single beam in this analysis. This will have the effect of suppressing the resonance peak of the beam at around 10 Hz and therefore the load of the person will be less influential than as shown in Figure 13 and Figure 14. Thus, in order to estimate accurately the influence of a human load a reliable estimate of the damping is required.

A detailed investigation of this problem can be found in Peris et al. [57].

3.5.7 USE AND RELIABILITY

Due to the large number of measurements required in the project, the ease of use of the instrumentation in the field was a decisive factor. The setup of the Guralp CMG-5TD in the field was a fast and easy process: orient the instrument to the North with a compass, ensure the unit is correctly levelled, plug in the antenna or the GPS emulator and supply power to the unit using lead acid battery. Once the power is supplied, the units were configured to begin recording time history data to its flash memory without any further interaction required by the operator. The Guralp CMG-5TD equipment proved to be robust and reliable under the conditions encountered during field measurements.

3.6 CONCLUSION

A large scale assessment of both exposure and response to vibration in residential environments involve a number of logistical and technical challenges.

The problem of the exposure determination needs to be formulated (See 3.3) taking into account the concept of human exposure itself, the residential environment and its components: source, path, receiver and human.

The design stage of the both response and exposure measurement starts with the site selection. General (See 3.4.1) and source specific (See 3.4.2) requirements need to be declared in order to identify the sample of the population affected by vibration. The site selection procedure includes off-site studies and fieldwork. Off-site, or "desk" studies are relatively inexpensive and should be performed first (Bormann [59]). Then, many potential sites will be eliminated for one reason or another through a reconnaissance. In order to measure the human exposure to vibration in residential environments, the right instrumentation needs to be chosen (See 3.5). The main criteria are an extremely low noise floor for recording well below the threshold of perception and a 24 bit digitizer (144 dB) for avoiding overload in unattended measurement. Moreover, practical requirement like portability, ease of use, storage capacity, mounting without damage to floor etc have to be considered. All these requirements were completely satisfied in the choice of a seismic transducer: a force feedback strong motion accelerometer. The importance of correct installation, synchronization and calibration of the instrument has also been highlighted.

4 EXPOSURE ESTIMATION FOR RAILWAY OPERATIONS

4.1 INTRODUCTION

The main study of the project "Human response to vibration in residential environments" (NANR209) was oriented, in its first part, to the derivation of an exposure response relationship for railway vibration.

This chapter describes the methodology used for measuring and assessing the vibration exposure from railway operations for almost 1000 case studies which satisfies one of the research objectives of this dissertation (See 1.2).

In order to handle this large number of case studies a novel approach (Woodcock et. al [52], Sica et. al [56], Peris et. al [57], Sica et. al [66]) has been implemented for meeting the specification of the standard: the methodology is oriented towards the experimental determination of the internal exposure taking advantage of the semi-permanent nature of the vibration source , as explained in section 3.3.3.

The current guidance for measuring vibration and evaluating vibration for assessing the likelihood of adverse comment is outlined in BS 6472-1:2008 [18] and ANC guidelines [27]. Both sources of guidance recommend recording acceleration time histories as close to the point of entry as possible, therefore taking measurement inside residences. Internal measurement should be taken at each residences studied because the vibration level may vary from one residence to another depending on foundations (rigidity, mass, natural frequencies), structure and number of floors as suggested by Madshus et al. [41].

The characteristics of the vibration source are described in section 4.2 whereas the measurement approach and the exposure assessment can be found in section 4.3 and 4.4. In section 4.5 the procedure for obtaining the internal vibration exposure is shown; in section 4.6 the results of the novel approach are presented. Conclusions are drawn in section 4.7.

4.2 SOURCE CHARACTERISTICS

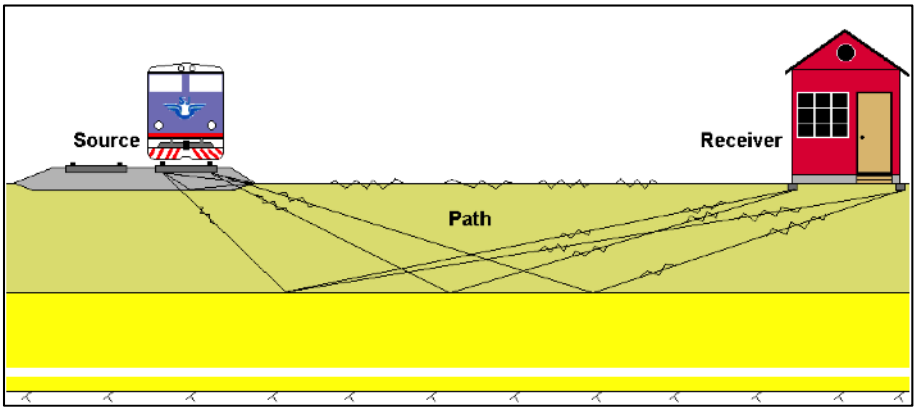

FIGURE 15 – RESIDENTIAL ENVIRONMENT SCHEME SUBJECT TO RAILWAY VIBRATION (FROM BAHREKAZEMI [68]).

Railway vibration is a source that affects residential environments externally as explained in section 3.3.3. According to Stiebel [67], during the pass-by of a train, mechanical vibrations are generated at the wheel-rail contact. Then, the vibrations are transferred via track, soil and foundation into surrounding buildings and lead to an excitation of floors and walls. As a consequence, annoyance due to vibrations (1-80 Hz) and to ground-borne noise (16-250 Hz) may occur.

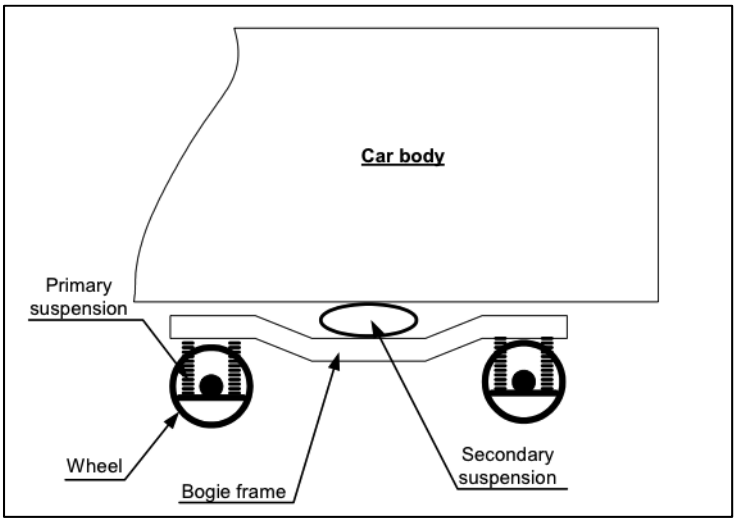

FIGURE 16 - MAIN PARTS OF A TRAIN BOGIE (FROM BAHREKAZEMI [68])

The framework source-path-receiver in Figure 15 can be useful for describing the vibration propagation phenomena where the vibration at source is generated by the interaction of the following components:

- Train (carriage, bogie, wheel) (See Figure 16)
- Track (track, sleepers, ballast, sub ballast)
- Sub structure (embankment/cutting)

Considering the complexity of these interactions, a brief description of the source mechanisms generating the vibration is needed because they are the "trigger points" or what is felt by the residents inside their property. In terms of vibration generation, the weight of the train provides a basic stress field in the ground, while the unsprung mass and the suspension characteristics of the vehicle, together with their speed, will determine the extent to which track and rolling stock characteristics enhance this stress field (Dawn & Stanworth [69]). The vibration generated by the train-track interaction is generally mitigated by the structure underneath the rail: ballast, sub ballast and the embankment.

There are several mechanisms of generating ground vibration which may contribute to the total level of vibration in different frequency bands (Krylov [70]). Among these mechanisms it is worth mentioning the wheel-axle (bogie plus wheel set) pressure on to the track, the effects of joints in unwelded rails, the unevenness of wheel or rails (all these mechanism cause vibration at train-speed-dependent frequencies); dynamically induced forces of the carriage (such as bouncing, pitching and yawing) and wheel-axle bending vibrations excited mainly by unevenness of wheels and rails (these occur at their natural frequencies).

The most common generation mechanism is a pressure of wheel-axles onto the track (Krylov [70]). It is always present whereas all other mechanisms may theoretically be eliminated if rail and wheels could be made perfectly smooth and no carriage or wheel-axle-bending vibration occurs. In the ideal conditions described above, the wheel-axle pressure mechanism is probably major contributor to train-speed-dependent components of the low frequency vibration spectra (up to 50 Hz), including the so called passage frequency $f_d = v/d_s$ where v is the speed of the train and d_S is the distance between the sleepers.

The dynamic excitations at the wheel-rail contact points come from irregular vertical profile of the wheel and the rail running surface. The variations in the vertical profiles of either surface introduce a relative displacement input to the vehicle and track systems. A wavelength λ generates a frequency of excitation $f_e = v/\lambda$; where v denotes the train speed range of 36-250 km/h (10-70 m/s) and the important wavelengths lie within the range of 0.125-14 m (Sheng et al. [71]).

According to Kouroussis et al. [72] and Mirza et al. [73], the dynamic deflection induced by the irregularity in the rail profile and wheel out-of-roundness plays an important role in the transmission of ground vibrations to locations farther from the track amplifying the axle load effect which belongs to the quasi static contribution of the source. Furthermore, the dynamic load strongly depends on two parameters: the speed of the train and the vehicle dynamics.

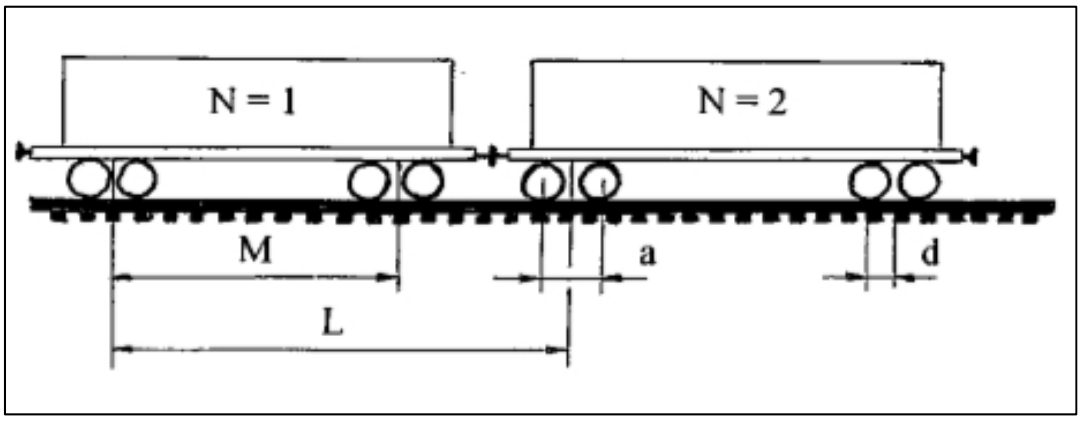

FIGURE 17 – SCHEME OF THE LENGHTS INVOLVED IN THE QUASI STATIC LOAD (FROM KRYLOV [70])

Summarising, as shown in Figure 17, in the train there are some fixed lengths l_k such as the length of the train, the length of the car, the distance between the wheels, the distance between the sleepers etc that when the train travelling at a speed v generate a vibration components with a fundamental frequency f_k according to:

$$f_k = \frac{v}{l_k} \tag{4.1}$$

The mass of the car on its suspension spring also causes a resonance frequency, typically of a few Hertz. In motion this generates an additional harmonic component due to the pitching of the car. These oscillatory components belong to the quasi statics contribution due to the moving load. On the other hand, the other sub-structure (ballast and embankment/cutting) can be also modelled as a mass spring damper system. If a resonance occurs with the train-wheel-track system, this will generate amplification of the energy content in the band of the resonance frequency. Furthermore, all the complex mechanism that generate the vibration (train-wheel-track-substructure) are purely mechanical and subjected to ageing over time such as unevenness of rail and wheels or the joint in unwelded tracks, introducing non linearity into the system. However, we need to take in account the singularity in the railway track such as switches and crossings work, expansion joints, wheel burns on the rail, cable ducts beneath the track and many other that will increase the level of complexity of the vibration generation. All these contributions belong to the dynamic load.

Both quasi static and dynamic loads contribute to the randomness of the vibration source in a broadband of frequency range inside the physical human perception. The quasi static loads produce large displacements under the track but, for train speeds lower than the wave speeds in the ground, these form a near field which does not propagate into the far field. Nevertheless for location close to the track and low frequencies the quasi-static loads may still be important (Triepaischjonsak et al. [74]).

Ground vibrations generated from the source are in the range of 0-10 Hz for cohesive soils, and higher frequencies for soils of friction material according to a Swedish report written by Hannelius (in Bahrekazemi [68]). The latter also notices that vibration in the ground increases with decreasing mass of the bank-fill material, and increasing depth to the bedrock.

Especially at low frequencies, Dawn and Stanworth [69] suggested that the excitation of ground vibration generated by freight train depends on the total mass of the vehicle, not just the unsprung mass and the wheelset. This is

evidenced by a large measured difference between loaded and unloaded trains; the difference in weights is approximately 12 dB, and the difference in vibration level measured in the building is approximately the same. Although the article is dated 1979, these pioneering experimental observations are still important and largely anticipate the current debate on the effects of the human response from freight vibration.

Several authors such as Krylov [75], Madshus et al. [41] and Kouroussis [72] have recognized the speed of the train as an important factor that influences the amount of energy transmitted from the track to the surroundings. On the other hand according to Dawn [76], the ground vibrations from heavy freight trains on good quality welded tracks have only weak dependence on train speed above 30 km/h. When the speed of the train is less than the Rayleigh waves speed in the ground (which will generally be the case in the residential environments) the dynamic mechanism of vibration generation are more important than the quasi static ones (Sheng et al. [71] and Lombaert & Degrande [77]).

Generally, the system train-wheel-track system can be seen as an incoherent line source of vibration. According to Gutowski & Dym [78], it is reasonable to simulate the passage of the train by using a moving line load, provided that the receiver, i.e., the point of observation, is in the far field of the source but at a distance of less than $1/\pi$ times the length of the train. This approach is similar to the problem of sound propagation formulated by Rathe [79].

Madshus et al. [41] investigated whether a train is a point or a line source. Measurements performed by the NGI[7] indicate that, for low frequency, the vibrations generated by a train are incoherent, if measured at a larger spacing than about 20 m along the track. Therefore, the train should be modelled as a series of statistically independent sources. The variance of the vibration from the whole train should be the sum of the variance from each car, making the train something between a point source and line source. According to Madshus et al. [41], the

[7] Norwegian Geotechnical Institute.

moving load provides the main contribution to the near field of the source, which can be estimated as one wavelength from the source (Auersch and Said [80]).

Once the vibration is generated in the ground it will generally be attenuated or amplified during its propagation through the ground and into the building before being perceived by the human body. Those two aspects will be discussed in the chapters 7 and 8.

4.3 MEASUREMENT APPROACH

Since the railway vibrations affect the residential environments in a semi-permanent way, the measurement approach has been designed with the purpose of determining the internal exposure. The response (See section 3.2.2), on the other hand, has been determined with a face to face questionnaire for a sample population of almost 1000 people. In order to avoid bias in the social survey, the exposure can be assessed only after the responses have been collected; it's important to understand how the social and the vibration team can be co-ordinated so as to achieve the aims of the survey (See 4.3.1). Moreover, a description of the measurement site is given together with the type of the measurement used for deriving the exposure estimation (See 4.3.2).

4.3.1 COORDINATION BETWEEN TEAMS

The nature of the source permitted that the social survey team arrived on the measurement site, selected according to the criteria presented in 3.4.1 and 3.4.2.1, ahead to the vibration team and collecting as many interviews as possible (Condie et al. [43]). During the interview, the social survey team asked to the resident if they would agree to a vibration measurement inside their property. If they agreed, the resident was asked to leave contact details such as name, address and telephone number for organizing the measurement with the vibration team at a later date.

Each questionnaire was identified with a code number or interview code formulated by the initial of the interviewer, the date and the interview number of

that day: for example JC12110901 meant Jenna Condie, 12/11/09, interview 1 of the day (Condie et al. [43]).

The social survey team entered information required by the vibration team such as the interview code, the respondent's name, address and phone number, into the database so as to keep a continuous update of sites of the total number of social survey questionnaires carried out. Twice a week, the system was completely updated before midday so that the vibration team could use the information to make arrangements for taking internal vibration measurements at respondents' properties (Condie et al. [43]).

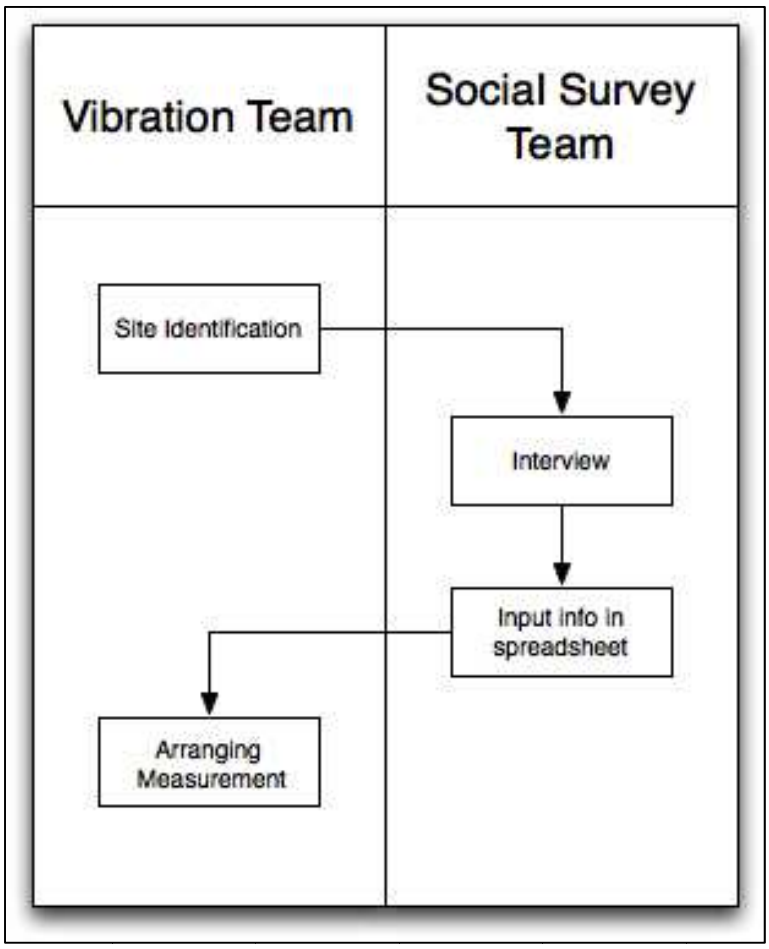

FIGURE 18 – SCHEME REPRESENTING THE COORDINATION BETWEEN VIBRATION AND SOCIAL SURVEY TEAM

This approach, summarised in Figure 18, yielded a success rate of 63% internal measurement from interviewees who agreed to a measurement (Peris et al. [57]).

Another advantage of this approach was the possibility to plan in advance the measurement campaign. With the help of the map, it was possible to identify the dwellings and their distributions along the railway lines so that the measurement survey could be planned to maximize the number of internal measurements. Usually larger streets that had a greater number of respondents were targeted first whereas the sites with a poor density of dwellings were given less priority or discarded.

With this approach, a weekly schedule for the vibration team was created trying to maximize their activity during the period of the fieldwork. The time for the measurement was limited to a specific slot in the overall duration of the project: the gathering of both response and exposure railway data was mainly carried out during the British summer time 2009. The fieldwork also had to be conducted within the budget of the project.

4.3.2 OVERVIEW OF EXPOSURE MEASUREMENT SITE

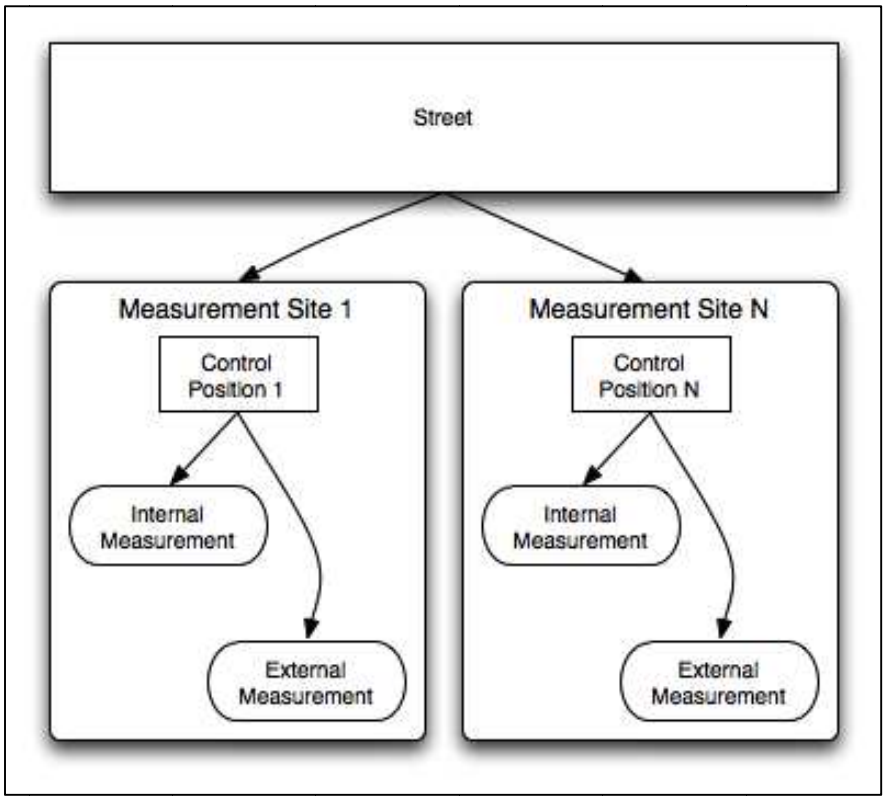

FIGURE 19 - SCHEME REPRESENTING THE MEASUREMENT SITE WITH THE POSSIBLE EXPOSURE MEASUREMENT

Each exposure measurement site (or simply measurement site) is a sample of the residential environment where the residents are potentially affected by vibration. It can represent either the whole or a part of a street where the social survey was taken depending on its dimension (See Figure 19).

Following the site identification (See 3.4.1 and 3.4.2.1) and the social survey, site exposure measurements were conducted in 12 locations in the North-West and Midlands of the U.K.: Birmingham, Coventry, Chester, Stafford, Runcorn, Runcorn east, Leyland, Stockport, South Manchester, Wigan, Crewe and Euxton.

In Table 5 the locations of the exposure sites are reported together with the total interviews, the total of long term and short term measurements and the site characteristics.

At each measurement site can be assigned a configuration describing orientation with respect to the railway line, e.g. parallel (Figure 20), perpendicular (Figure 21) or close (Figure 22).

As already mentioned in section 3.3.3, each residential environment or measurement site can be broken down into four areas: source, path, receiver and human; the exposure at the site can be characterised by a long term position monitoring position outside the property, also known as control position, and short term measurement positions inside the property (See Figure 19).

On arrival on site and the control position was installed according to the guidelines described in section 3.5.6. Where possible, the control position is located at a similar distance from the railway as the affected properties. In fact, the distance of the control position from the line is a compromise between the choice of a secure location for the instrumentation and the distance of the residences from the source. For this reason, it was impossible to install the control position always at the same distance from the line as happened in other measurement approaches used for evaluating the exposure (Madshus [41]). A further discussion about the installation of the control position can be found in section 8.2.

LOCATION	*TOTAL INTERVIEWS*	*TOTAL INTERNAL MEASUREMENTS*	*TOTAL CONTROL POSITIONS*	*% MEASUREMENTS OVER INTERVIEWS*	*% MEASUREMENTS OVER INTERNAL AGREEMENTS*	*CHARACTERISTICS OF THE SITE*
Birmingham	119	69	17	58%	62%	High speed line High % of ethnic minorities
Coventry	29	9	3	31%	35%	High speed line
Chester	9	6	3	67%	86%	High speed line and freight line
Stafford	72	47	14	65%	72%	High speed line and freight line
Runcorn	65	37	13	57%	64%	High speed and freight line
Runcorn East	26	13	7	50%	59%	Underground railway
Leyland	112	69	12	62%	64%	High speed line and freight line
Stockport	159	85	16	53%	80%	High speed line, busy roads and airport nearby.
South Manchester	164	90	31	55%	62%	Low speed line, close to station. High% of ethnic minorities
Wigan	78	48	13	61%	70%	High speed and freight line
Crewe	51	22	8	43%	52%	High speed and freight lines
Euxton	47	27	12	57%	66%	High speed and freight line
TOTAL	**931**	**522**	**149**	**56%**	**63%**	

TABLE 5 - SUMMARY OF THE EXPOSURE MEASURMENT SITES

FIGURE 20 - SITE PARALLEL TO THE RAILWAY LINE

FIGURE 21 - SITE PERPENDICULAR TO THE RAILWAY LINE

FIGURE 22 - SITE WITH A 'CLOSE' ADJACENT TO THE RAILWAY LINE

In order to provide a representative sample of the railway traffic, the control position is installed for 24 hours as done by Woodroof and Griffin [37] and in line with the evaluation of noise indicators (Crocker [81]); there is no basis for assuming that a shorter period will be sufficient to evaluate vibration exposure (Woodcock et al. [52]). A total of 149 control positions (see Table 5) were installed during the fieldwork of the project "Human response to vibration in residential environment" corresponding to almost 3576 hours of recording.

During the 24 hour recording at the control position, short term measurements were conducted as close as possible the point of entry in as many property as possible (Sica et al. [66]). Ideally, the measurements were conducted at the centre of the room where the respondent feels the highest magnitude of vibration as described in section 3.5.5. Since the vibration perception is a subjective feature each internal measurement point could vary from one property to another but the measurement would be consistent with the survey response.

If the respondent was at home or did not allow an internal measurement, according with the protocol, an external measurement might be taken as close to the foundations of the house as possible, if the respondent allowed it. Otherwise, the external measurement might be taken in the pavement of the street at the front or in rear of the property.

NANR209 Internal measurement pro-forma

Site:		**Address:**
Date:	**Start time:**	**End time:**
Acc No:	**Levelled? Y/N**	**Orientated? Y/N**
Room:		**Floor:**
Mounting method:		**Floor type/Floor covering:**
		Approx. thickness of floor covering:
Description of building:		
Sketch of measurement position (Distance from wall. On joist/between joist):		
Notes:		

Event log			
Time	**Event type**	**Time**	**Event type**

FIGURE 23 - MEASUREMENT PRO FORMA

Short term measurements were carried out for 30 minutes at last in order to capture a limited number of train passes, ideally at least five. In the framework of the project 522 internal measurements have been conducted (See Table 5).

For each measurement taken at the site, a measurement pro forma was generated (See Figure 23). The first part of which contained information about the

measurement such as the measurement site, date, address, the number of the accelerometer, start time of the measurement, orientation, levelling, measurement type, location, floor, floor type and mounting condition. The second part was contained a sketch of the measurement and additional notes such as condition of the weather, the presence of a confounding source, the measurement type, the synching method or the GPS position. The last part of the pro forma contained a log sheet section for recording vibration activities occurring during the measurement period together with the time occurrence.

4.4 EXPOSURE ASSESSMENT

As already explained in 4.1 and 2.3.1, the British standard BS 6478 for evaluating the human exposure to vibration in residential environments requires that the exposure should be measured internally at the resident's property for at least 24 hours. Considering the large number of case studies (931), it was impossible to obtain a direct long term internal exposure estimation for each participant and a new strategy [52] was required to meet the needs of both project and standard.

According to BS 6472-1:2008 [18] and ANC guidelines [27], a measurement point other than the point of entry can be used for the long term estimation and a transfer function needs to be declared between this point and the point of entry inside the building. As a consequence, the exposure assessment procedure used in NANR209 can be summarised by the following points:

1. Long-term monitoring at an external position herein referred as the 'control position' (the square in Figure 24).
2. Synchronised short-term snapshot measurement taken in the respondent's dwelling as close the point of entry as possible (the circle in Figure 24).
3. Calculation of a control-to-internal transmissibility (frequency dependent) from 1 and 2.
4. Calculation of long-term vibration exposure inside the dwelling from 1 and 3.

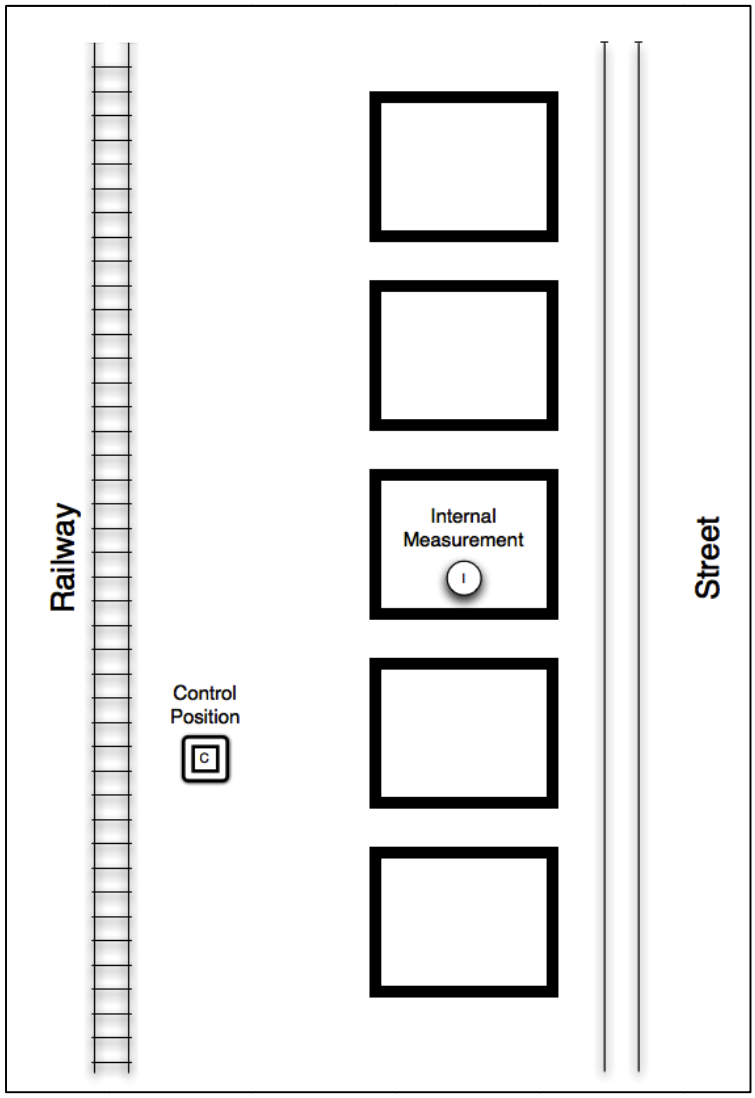

FIGURE 24 - REPRESENTATION OF THE MEASUREMENT APPROACH FOR MEASURING EXPOSURE FROM RAILWAY VIBRATION

The calculation of the exposure is based on the concept that the entire activity recorded at the control position can be 'transferred' to the point of entry inside the property using the measured transmissibility. The main assumption is that there is a fixed relationship over time and space between the signal measured at the control position and that at the point of entry. The validity of this assumption can be influenced by various factors:

1. As mentioned in section 4.2, a train travelling at a finite speed along a given length of track will generate a vibration signal characteristic of the train, track and speed. In general the dominant signal at each measurement position will not necessarily arise from passage over the same section of track. If there are no

significant differences between elements of the train (carriage type, wheel type, wheel condition, etc.) and the total length of the train is longer than any of the normal distances from the track for target properties aligned perpendicularly, there will be a degree of spatial averaging. On the other hand short trains, and trains which have significant differences between their elements will not produce the same effect.

2. There are often singularities or non-uniformities in the railway structure such as culverts, points etc (see section 4.2) that might affect the signal at one position to a greater extent than the other. This effect will be most likely if the two measurement positions are in line parallel to the track.
3. In the near field of the vibration source (see section 4.2) waves in the ground are not fully developed and therefore measurement positions in this region could show greater spatial variations than outside the near field.

The influence of the factors listed above has been mitigated by choosing to keep the control position close to the properties in which exposure is to be estimated. In this way the wave field affecting the control position is similar to that affecting the building. In the surveys, the assessed properties were within a 50 m radius of the control positions so as to "sample" vibration originating from the same part of track as that affecting the properties. Moreover, a general overview of the transmissibility measurement is given in section 8.2.

The methodology presented above therefore provides an approximation of the 24 hour acceleration time history suitable for evaluation of the vibration exposure at the point of entry.

4.5 ANALYSIS

In order to derive exposure response relationships it is necessary to evaluate the long term (24 hour) internal exposure. The calculation of long term internal exposure can be split into three main processes:

1. Identification of the train passages.
2. Computation of the transmissibility or velocity ratio.

3. Adjustment of the control position exposure to the internal position.

Each of those processes requires different signal processing techniques that belong to different areas such as identification of seismic event, spectral analysis and dual channel analysis. Of course, considering the large amount of data that need to be processed, the internal exposure assessments have to be done in the most automated way as possible.

Before considering these processes, a quick description of the data downloading and labelling procedure is given in the following section.

4.5.1 DOWNLOADING AND LABELLING PROCEDURE

During the field measurement, vibration data was recorded and stored in the internal memory of the Guralp CMG-5TD as explained in 3.5.3.

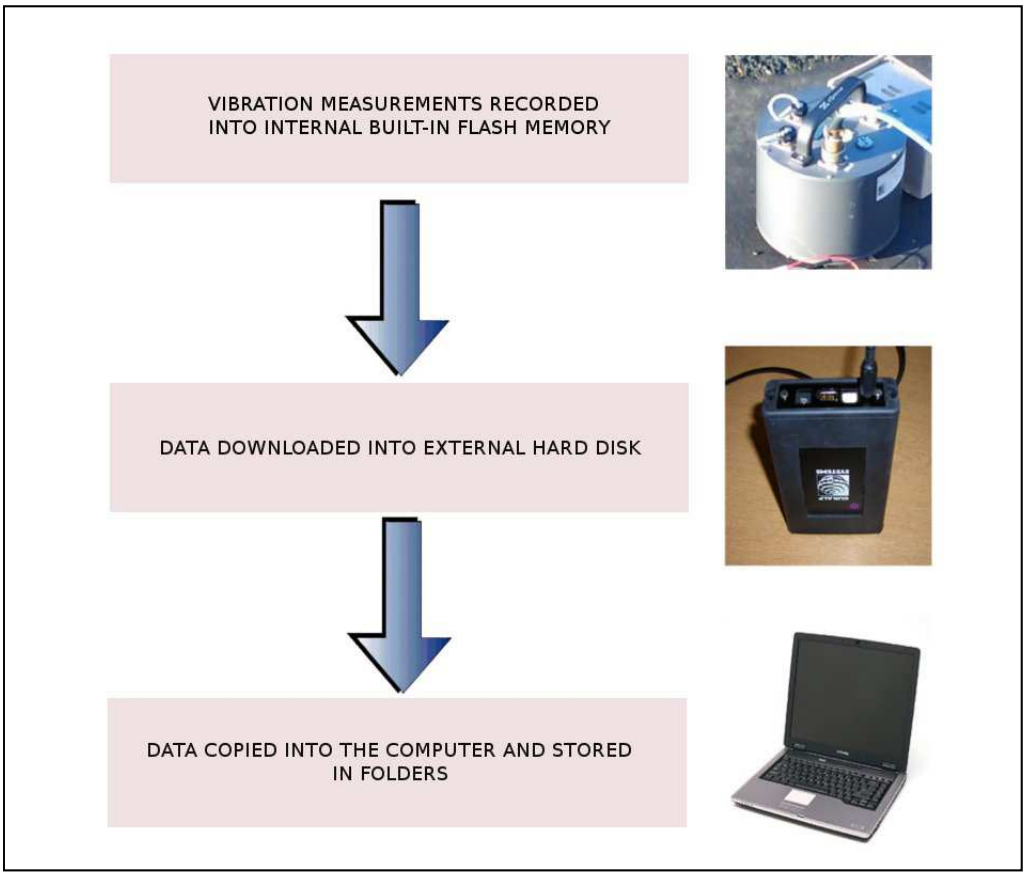

FIGURE 25 – SCHEMATIC OF DATA STORAGE

After completing all the measurements at a site, the data were downloaded through a firewire cable into a SCSI disk using the Guralp PC Interface (known as

Scream!) and a laptop. The data in the laptop were stored in folders with the name of the site and the date (See Figure 25). An integrity check was conducted by checking the recording time history making sure that no errors were presented. All data were also stored to an external disk for security.

Then, the three components of the control position and internal or external measurements for each case study were archived into a single .gcf (Guralp compressed format) files via Scream! (Guralp PC interface). This was then labelled with a unique identifier which links the file with the relevant social survey questionnaire. The labelling procedure is explained in Figure 26.

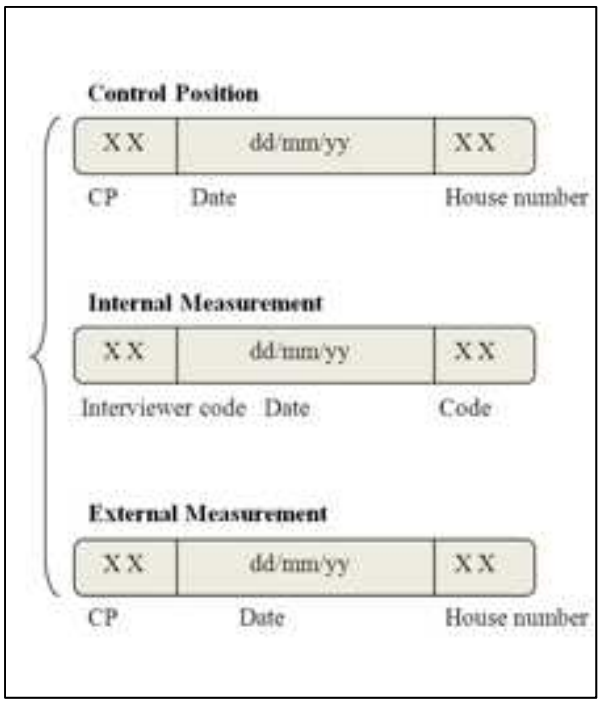

FIGURE 26 – DATA LABELLING PROCEDURE

4.5.2 EVENT IDENTIFICATION

The first step towards the assessment of internal exposure is to identify the relevant vibration events assumed to be the train passages. The data processing procedure described in the following is an improvement over that used in the project and was used for processing data in part 2 of the thesis.

Given an exposure measurement site, the detection of the train passages is done at the long term measurement position for three reasons: a better signal to noise

ratio, less pollution from human activity compared with the short term (internal) measurement and the need to identify, if possible, all railway traffic in order to have the best estimation of the long term internal exposure.

The events are identified from the Z-direction signal in the time domain using the algorithm STA\LTA. The latter is one of the possible trigger algorithms used in seismology for automated event detection (Withers et al. [82]): it consists of an estimation of the signal to noise ratio along the time history evaluating the ratio of short-to-long-term energy density. In detail, the STA\LTA algorithm processes the signal in two moving time windows: a short-time average window (STA) and a long-time average window (LTA). The STA measures the 'instant' amplitude of the signal and watches for the train passes while the LTA takes care of the current average background noise amplitude. When the ratio of both exceeds a pre-set value, an event is 'declared'.

This technique represents the most important part of the event identification procedure. If we define x_k as the time history, STA and LTA are the width of the short and long time windows used for calculating the energy density. The ratio R_{SL} between the short-term average and long term average is defined as follows:

$$R_{SL} = \frac{\sqrt{\frac{1}{STA}\sum_{k=1}^{STA} x_k^2}}{\sqrt{\frac{1}{LTA}\sum_{k=1}^{LTA} x_k^2}} \tag{4.2}$$

Generally, the two windows can be consecutive one to the other or delayed in order to obtain a better statistical independence between the short- and long-term averages allowing quicker recovery from transient (Withers et al. [82]). However, for this analysis the use of overlapping windows has been preferred.

The STA\LTA trigger parameter and associated parameters' settings depend on the goal of the application, on the background noise condition at the site, on the properties of the signals, and on the type of sensor used. All these issues vary broadly among applications and measurement sites. There is no single, general

rule for setting them; instead, the optimal trigger settings for each site must be determined by practical experience. As a consequence, a trial an error method has been used for selecting an effective combination of STA and LTA values which can be applied to each long term measurement position.

A subset of the long term position recordings has been used in order to try different combinations of STA and LTA to train the algorithm to detect events. The latter needs to satisfy two criteria: identifying the maximum number of train events whilst avoiding false events such footfall. For the detection of train passes the optimum values were found to be: STA=1 s and LTA=30 s. A suitable threshold was found to be the average between the 95 and 99 percentile of the STA\LTA (See Figure 27), less its mean value. This approach has been chosen for taking in account of the possible variation of the background noise in the recording used for the analysis.

For the identification of the events at the control position the data are processed in blocks of one hour. The STA\LTA algorithm identifies just a part of the train passes as noted in Figure 28, but for a complete detection of the event other steps are required. Applying a pre and post trigger of 60 seconds, the beginning and the end of the event can be identified evaluating the STA of the portion of the signals that goes from the pre trigger point to the start of the event picked by the STA\LTA and the end of the event picked by the algorithm and the post trigger points (Figure 29): the start and the end of the event can be identified by looking for the point where there is an increment in the background noise evaluated as the 30 percentile of the STA of the two signals.

From the event identified with the procedure above, a further cut has been applied identifying the 10 dB cut points (Zaptfe et al. [26]) from the logarithmic normalized STA of the signal (Mid part Figure 29). In this way all the events identified will have the same signal to noise ratio (Figure 30). However, the 10 dB cut points will give a correct identification of the event only when there is a sharp drop of the waveform into the background noise otherwise if the event drops in the background noise ‘slowly’ the event will contain some additional noise.

For events that happen at the same time in both control and short term monitoring position, the triggering points of the event picked at the control position are used for the identification procedure at the short term monitoring position. However, where there is a time lag due to the propagation time between the two measurements positions the cut points adopted at the control position may not be enough to determine the train pass window for the internal measurement. For this reason a similar approach to the one just described is also used for extracting events at the internal position.

The identification at the internal position starts shifting the triggers identified at the control position by the time lag obtained by the maximum of the correlation between the two signals.

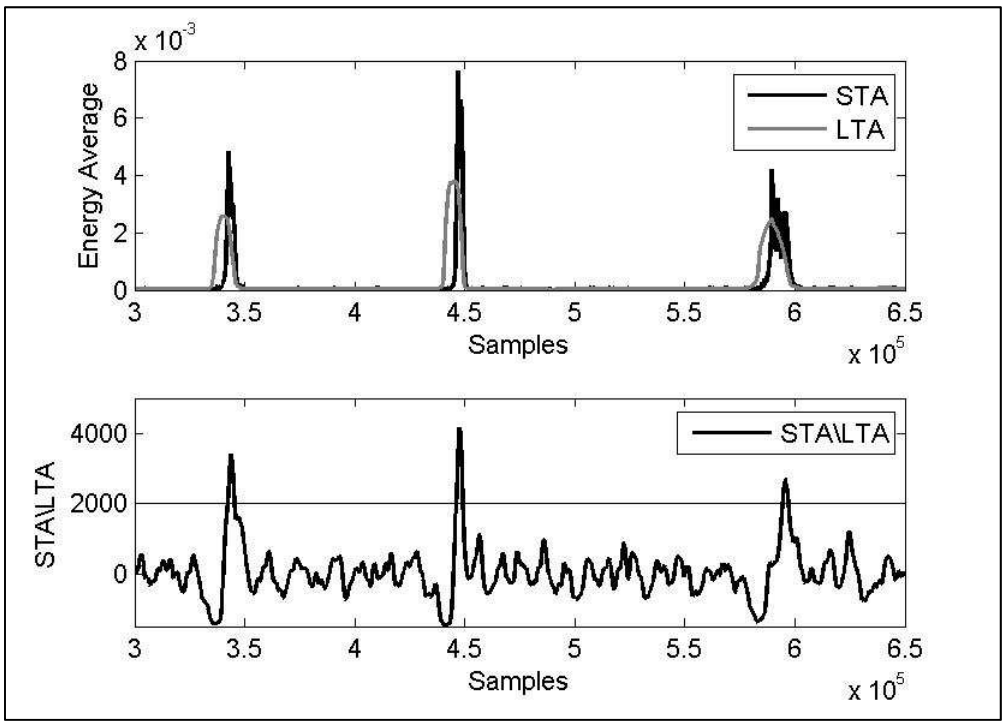

FIGURE 27 – IN THE UPPER PLOT THE TREND OF THE LTA AND STA IS SHOWN FOR SOME ACTVITY RECORDED. THE LOWER PLOT SHOWS THE STA\LTA RATIO FOR THE SAME ACTIVITY.

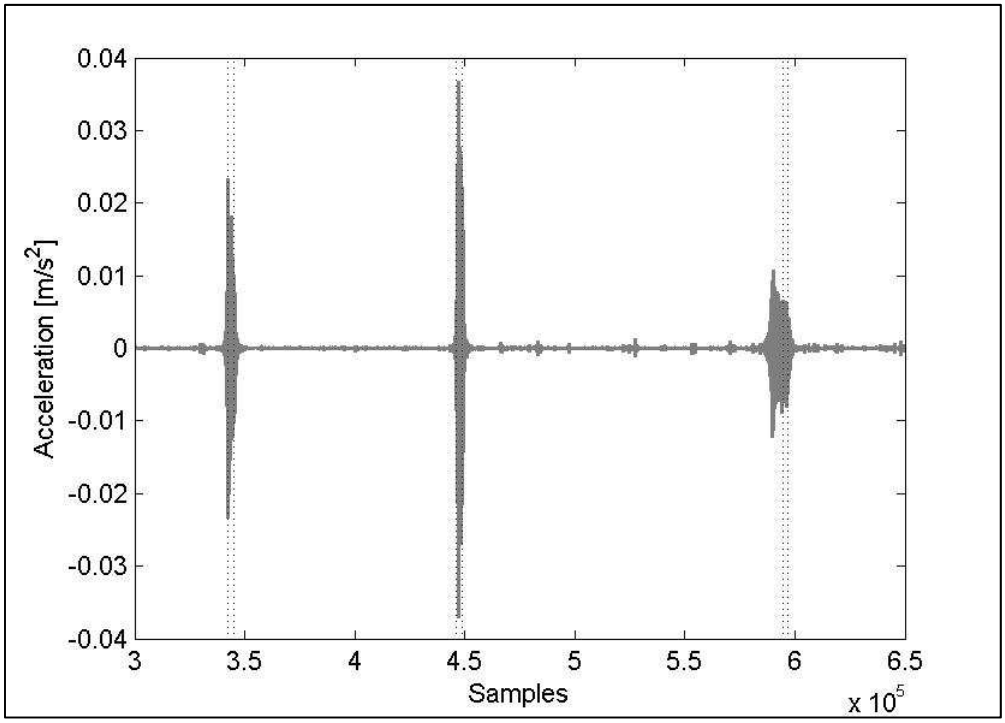

FIGURE 28 - TIME HISTORY OF VIBRATION ACTIVITY AT THE CONTROL POSITION WITH THE TRIGGERS IDENTIFIED BY THE STA\LTA ALGORITHM.

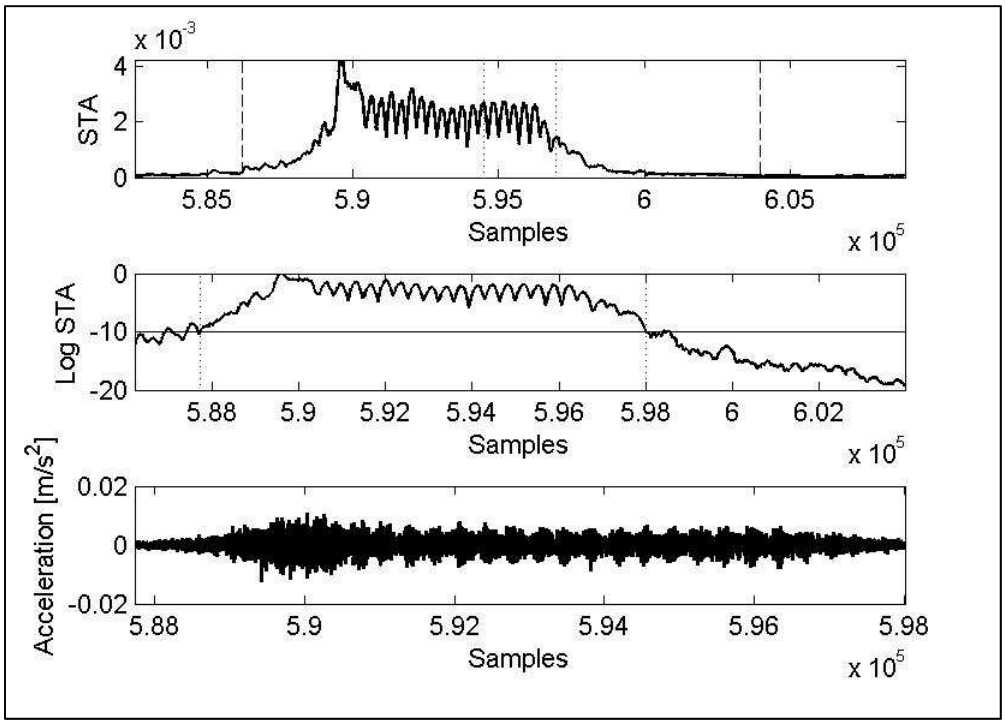

FIGURE 29 – UPPER PANEL: BEGINNING AND END OF AN EVENT IDENTIFIED WITH THE STA\LTA PLUS 60 SECONDS OF PRE AND POST TRIGGERING; MIDDLE PANEL: LOG NORMALIZED STA WITH TRIGGER IDENTIFIED WITH THE 10 CUT DB POINTS; LOWER PANEL: EVENT IDENTIFIED

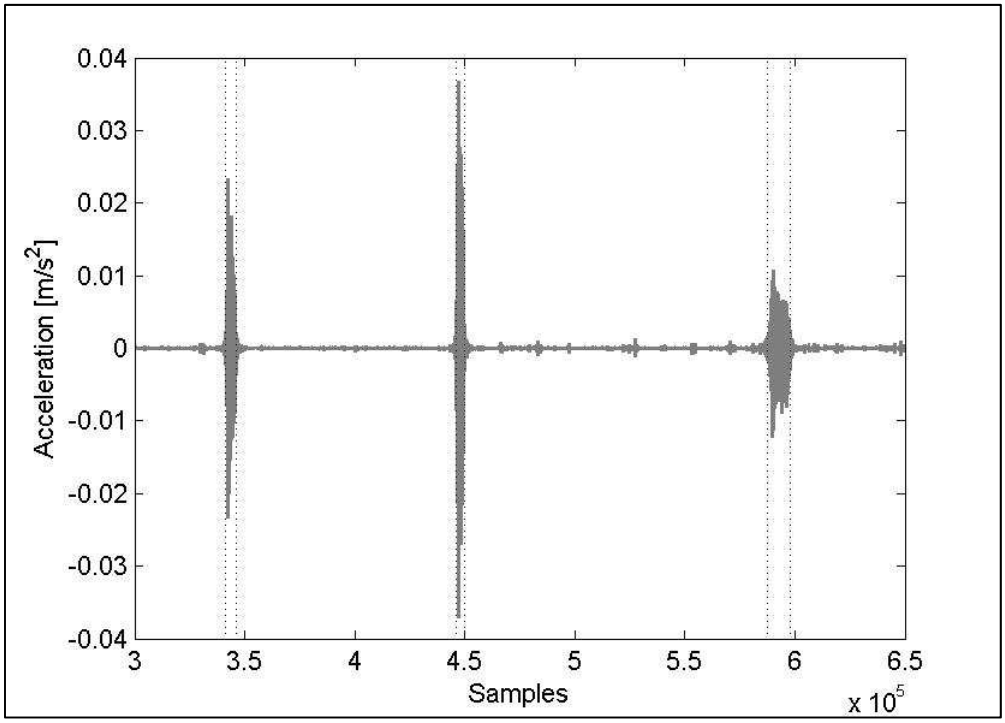

FIGURE 30 – TIME HISTORY WITH THE TRIGGERS IDENTIFIED WITH THE COMPLETE EVENT IDENTIFICATION PROCEDURE.

Then, a pre and post trigger of 60 seconds is applied to the indexes identified above: in this way a better determination of the beginning and the end of the internal event is obtained by evaluating the background noise defined as the 30 percentile of the STA. After this operation, a variable cut between 10 and 6 dB is applied to the normalized logarithmic STA of the event due to the highest background noise that may be found in the internal measurement with respect to the control position. If the cut identified is greater than 6 dB then the internal event is discarded.

The STA\LTA trigger is most effective at "quiet" site with low background noise and less so in the presence of high amplitude man-made events such as bursts or spike type events which may be detected as event but need to be discarded because they are not caused by train passes.

The STA\LTA algorithm identifies events with a success rate of 80% (Sica et al. [66]), but it has been found that clusters of short-term transients such as 30 s of footfalls cause the algorithm to trigger falsely; events such this make up the 20% of the spurious triggers. In an effort to reject false triggers, discrimination based on

crest factor has been employed. Crest factor is defined as the ratio between the peak amplitude and rms of a waveform:

$$C_n = \frac{\left|x_{peak}\right|}{x_{RMS}} \tag{4.3}$$

Highly impulsive signals will result in a high crest factor whereas waveforms with an amplitude envelope that develops slowly over time will exhibit a low crest factor. It has been observed that the vibration measured due to the passage of a train generally has a crest factor lower than ten; by rejecting triggered events with a crest factor higher than ten, the combination of the STA\LTA and crest factor algorithms achieves a 70% successful identification. Then, an integrity check is conducted by manually checking the triggered events and rejecting contaminated data.

4.5.3 TRANSMISSIBILITY

As the internal and external measurement of vibration are synchronised in time with the twenty-four hour control position measurement, it is possible to calculate velocity ratios or transmissibility for each event recorded at both measurement positions.

For the transmissibility used in the study for the evaluation of the internal long term exposure, time histories of the events identified with the algorithm presented above are converted to the frequency domain using a sliding window FFT (a 200 point Hanning window with a 50% overlap in order to obtain a spectral resolution of 1 Hz) from which the magnitudes of the windowed sections are linearly averaged. Further details about the spectral estimation can be found in section 8.3.1.

Then, transmissibilities are calculated using the following equation:

$$H(f) = \frac{\left|B(f)\right|}{\left|A(f)\right|} \tag{4.4}$$

where $|B(f)|$ is the average Fourier magnitude spectrum of an internal event or external event $|A(f)|$ is the averaged Fourier magnitude spectrum of an event at the control position. For each case study, an average velocity ratio is calculated by linearly averaging the velocity ratios calculated for each event.

$$H_{ave}(f) = \frac{1}{N}\sum_{i=1}^{N} H_i(f) \tag{4.5}$$

Where N is the number of events recorded for each case study; a minimum number of 5 train passages are enough for obtaining a reliable velocity ratio. All the velocity ratios have been evaluated with zero phase differences (magnitude only). Further details about this approach are given in section 8.5.5 and in Sica et. al [83].

4.5.4 EXPOSURE ASSESSMENT

The internal exposure needs to be assessed for each property where a questionnaire was taken. An internal vibration measurement may not be taken possible in every residence therefore, in this section, the prediction of the internal exposure from railway vibration is calculated in the following cases:

1. Internal measurement
2. No measurement

In the derivation of the exposure-response relationship only the internal and no measurement case have been considered. The reason is given by the main aim of the study itself that was oriented to the determination of an exposure response relationship for internal vibration especially for this source. The high success rate of internal measurement, around 56% of the total number of interview, has permitted a good "sampling" of the internal vibration activity in all the measurement sites. Furthermore, the measurement methodology together with site configuration allows an estimation of the internal measurement based on similarity assumption as described in section 4.5.4.2. On the other hand, section

4.5.4.1 provides the methods for providing the long term internal exposure using the measured transmissibility with its validation.

4.5.4.1 INTERNAL MEASUREMENT

An average transmissibility is calculated for each case study by linearly averaging the transmissibilities for each individual event according to the method outlined in section 4.5.3.

As shown in section 8.3.4 several transmissibility formulations can be found in literature which can be divided in two categories: real and complex. The main difference among these formulations is that complex transmissibility takes in account of the phase between the two receivers through the cross correlation function.

As discussed in section 8.3.2, experimental evidence provided by several researchers in the field suggests that the normalized cross correlation function is very poor for transmissibility measurement for railway vibration in buildings. This is because both external and internal signals are effectively outputs of a MIMO system, the real inputs being the excitation at the rail track. This makes impossible to obtain a meaningful phase relationship between the two sets of sensors.

Therefore in order to obtain an approximation of the internal signal it is assumed that the phase of the transmissibility is a slowly varying function compared with that of the signal itself and therefore that the internal signal can be approximately reconstructed by applying a filter whose magnitude equals that of the transmissibility and whose phase is zero.

In order to obtain an approximation of the internal vibration, the average transmissibility (magnitude only) for a case study is interpolated to the length of each individual event recorded at the control position. The transmissibility is then applied to the complex Fourier spectrum of the event:

$$B_{pred}(f) = H_{est}(f) \cdot A(f) \tag{4.6}$$

The predicted complex Fourier spectrum of an internal event is $B_{pred}(f)$, $H_{est}(f)$ is the average interpolated transmissibility magnitude calculated for that case study, and $A(f)$ is the measured complex Fourier spectrum of an event at the control position. $H_{est}(f)$ represents the energy ratio (frequency dependent) between the internal and the control position (4.5) used for scaling the spectral content of the event $A(f)$ in order to obtain the $B_{pred}(f)$. The latter can be inverse Fourier transformed back to the time domain for the calculation of parameters such as peak, rms or VDV. Equation (4.6) is repeated for each event recorded at the control position from which the entire 24 hours vibration exposure (caused by railway) can be predicted.

Anticipating the results shown at the end of this section (Table 6), in chapter 8 (Figure 101) and Appendix E (Figure 113, Figure 118 and Figure 123), the method described in this section provides an average maximum error of 20 % on the internal exposure metric like VDV, RMS and Peak. On the other hand, the error introduced on the internal vibration exposure using complex transmissibility function is far greater than one obtained using real one as shown in Figure 102. These results support the use of the zero phase filter as an appropriate strategy for estimating internal exposure.

An application of the methodology for the estimation of the long term exposure from railway operation is provided here for a site which consists of a control position installed at 20 m from the railway line and an internal measurement conducted at the first floor of a semidetached house at 29 m from the source. During the internal measurement 11 train pass bys have been identified using the STA\LTA routine, which is explained in 4.5.2, at both measurement positions. The acceleration time history, z component, of the train events recorded at the control position is reported in Figure 31.

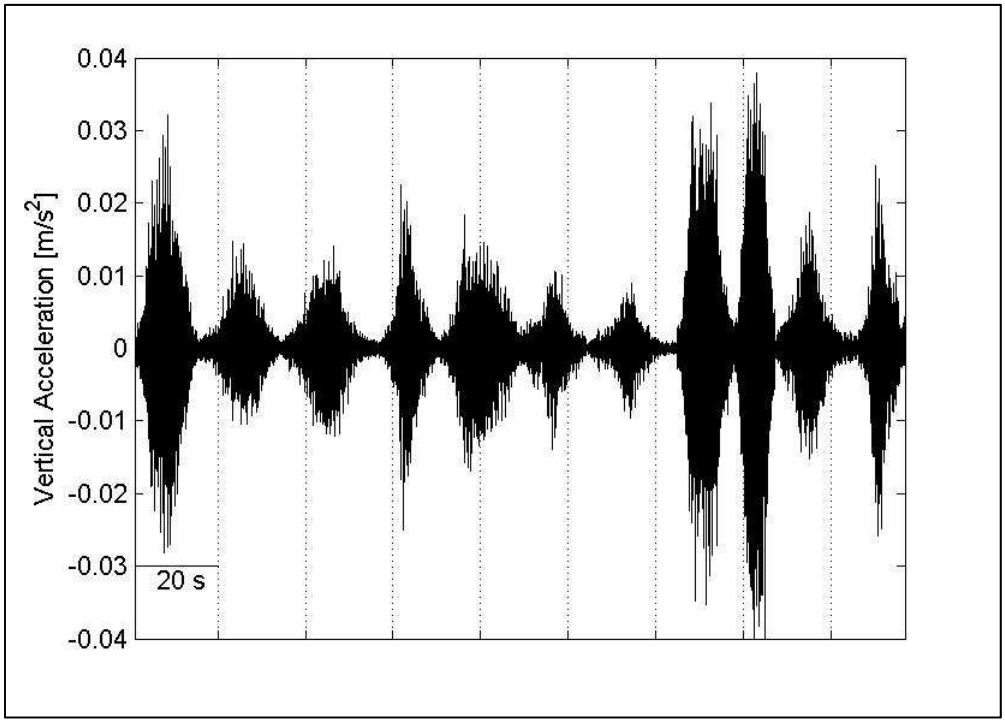

FIGURE 31 - VERTICAL COMPONENT OF THE ACCELERATION TIME HISTORY; TRAIN EVENTS RECORDED AT THE CONTROL POSITION DURING THE INTERNAL MEASUREMENT (PERIODS BETWEEN TRAIN PASSES REMOVED).

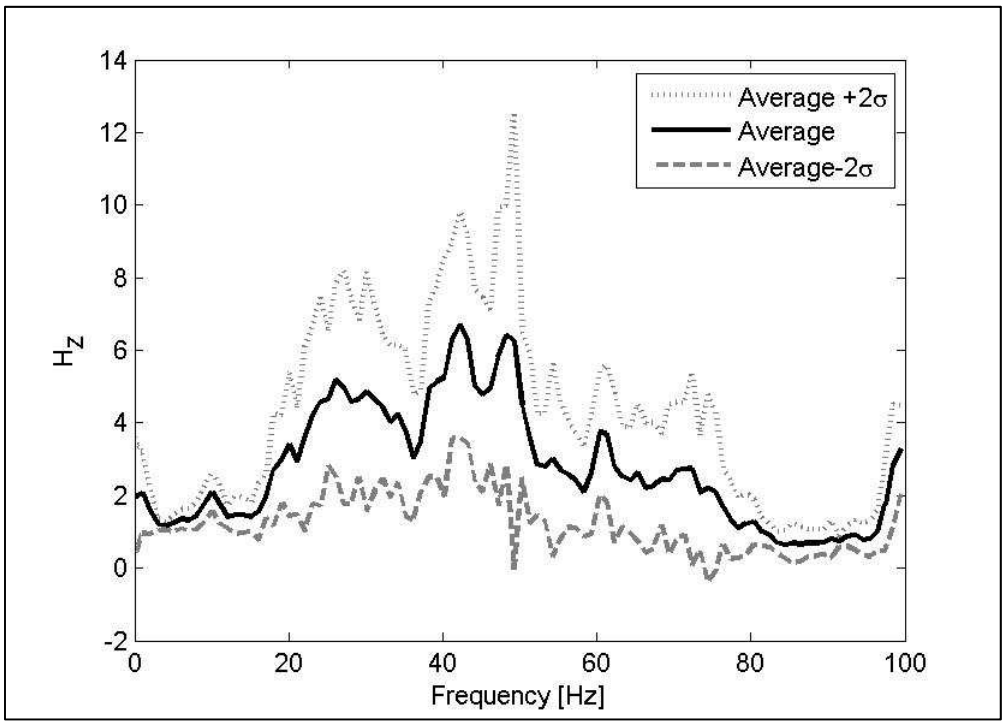

FIGURE 32 - VERTICAL COMPONENT OF THE AVERAGE GROUND TO BUILDING TRANSMISSIBILITY OVER 11 TRAIN PASS BYS; FROM THE TOP TO THE BOTTOM: AVERAGE TRANSMISSIBILITY PLUS AND MINUS 2 TIMES THE STANDARD DEVIATION.

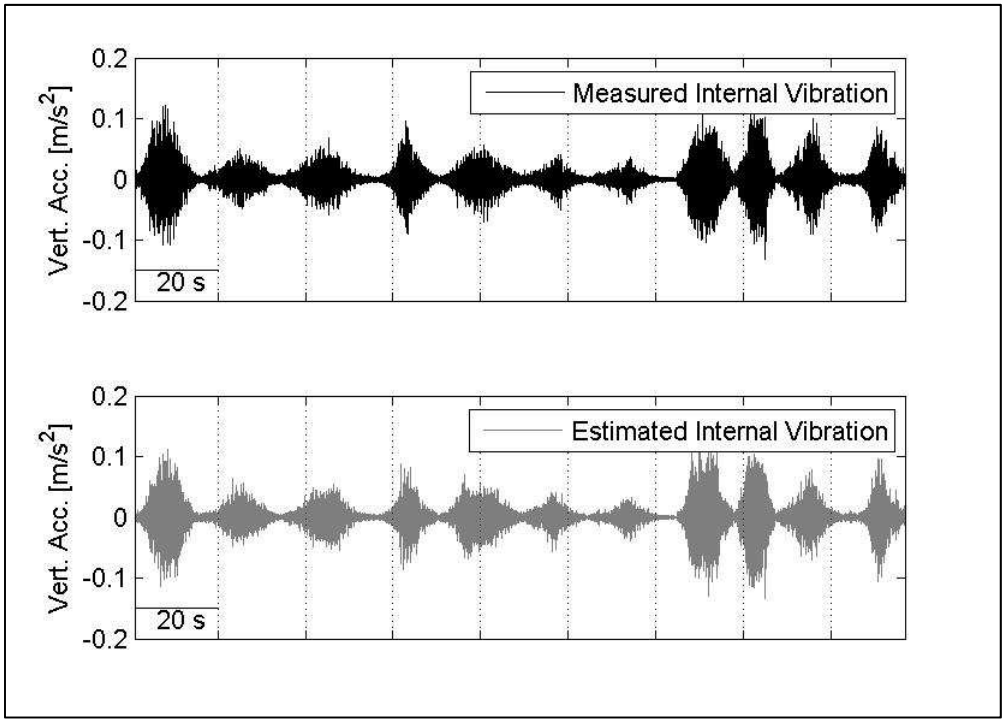

FIGURE 33 - VERTICAL COMPONENT OF THE INTERNAL ACCELERATION TIME HISTORY. UPPER PANEL MEASURED VIBRATION LOWER PANEL ESTIMATED INTERNAL VIBRATION.

In Figure 32 is shown the vertical ground to building transmissibility estimation $H_Z(f)$ obtained by linearly averaging the magnitude only transmissibility for each event recorded at both measurements positions as explained in section 4.5.3.

In Figure 33 an example of the proposed approach is shown: the estimated internal vibration is obtained applying the ground to building transmissibility in Figure 32 to each event recorded at the control position in Figure 31.

It can be seen from Figure 33 that a good prediction can be achieved using this method. Furthermore, the control position by itself is not a good predictor of the long term internal exposure. In fact, as already explained in section 3.3, vibration generated at the source are amplified or attenuated by the building which can only be quantified using the ground-to-building transmissibility.

In Table 6 the exposure metrics RMS, Peak Particle Acceleration (PPA) and VDV with the W_b weighting, have been calculated for both measured and estimated internal vibration showing a maximum absolute error of 9% for the metrics considered which confirms the approach of ignoring transmissibility phase.

Further details about this method and its validation can be found in section 8.5.6.

	W RMS [(m/s^2)]	W PPA [(m/s^2)]	VDV [m/s$^{1.75}$]
Meas. Exposure	0.0070	0.054	0.044
Est. Exposure	0.0075	0.055	0.048
Rel. Error %	-7%	-2%	-9%

TABLE 6 - TABLE SHOWING MEASURED AND PREDICTED INTERNAL VIBRATION EXPOSURE INDICATORS AND PERCENTAGE RELATIVE ERROR.

4.5.4.2 NO MEASUREMENT

If there is no internal measurement available for a given respondent, a search is conducted within the same area for a property of a similar type and a similar distance from the source within the site where an exposure measurement has been taken. The exposure estimated for this property is then assigned to the property for which there was no measurement available. All the properties are in a radius of 50 m from the control position in the measurement site, so the hypothesis of similarity between the properties seems reasonable. The similarity related to the construction between the properties does not imply their likelihood in terms of structural dynamic properties. Therefore, the measured ground to building transmissibility of the nearest house will provide an estimation of the building response where no internal measurement was taken. The similarity for distance from the source can be found in the majority of the configuration of the measurement site where the line of the houses is parallel to the railway line.

This kind of estimation was thought to be more reliable than those obtained from external measurements outside the property (Sica et al. [56]) especially considering the high rate of internal measurement collected during the field work.

4.6 RESULTS

As shown in the section above, the exposure needs to be evaluated for each resident who took part to the survey: for the 56 % of 931 residents annoyed by railway vibration the long term internal exposure is obtained through measurement according to the methodology explained in section 4.4, for the rest of the residents the exposure is estimated using the internal exposure obtained from measurement inside a nearby property of a similar type and at a similar distance from the railway.

In this way an estimation of the internal exposure is obtained for each case study providing a "one to one" relationship with the annoyance. Therefore, the direct consequence of this method is the exposure response relationship for the population affected by railway vibration reported in Woodcock et al. [15] (Figure 34).

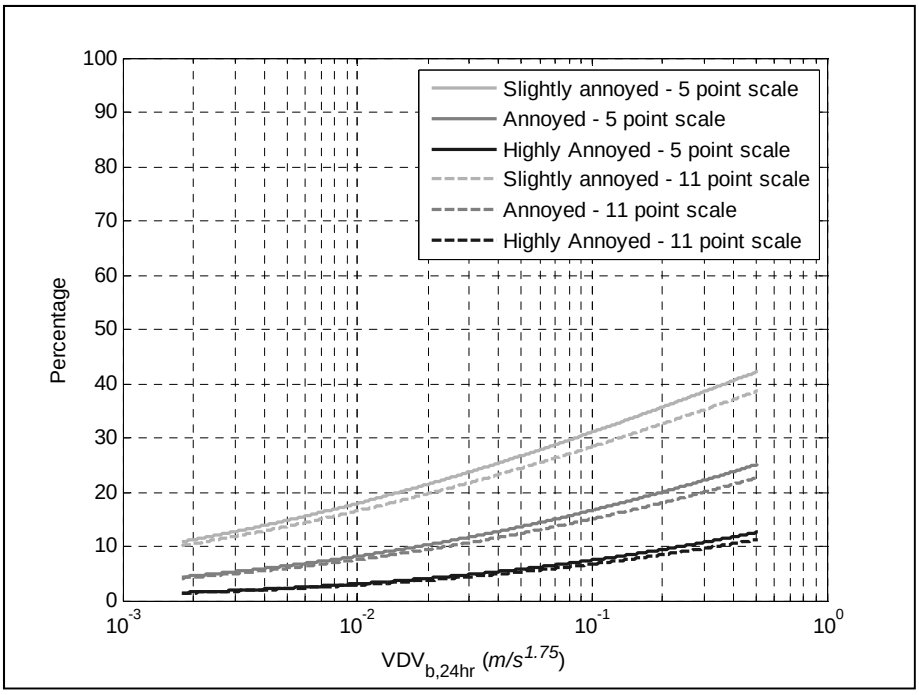

FIGURE 34 - EXPOSURE-RESPONSE RELATIONSHIP FOR ANNOYANCE DUE TO RAILWAY INDUCED VIBRATION CALCULATED USING THE 5-POINT SEMANTIC AND 11-POINT NUMERICAL RESPONSE SCALES (FROM WOODCOCK ET AL. [15]).

4.7 CONCLUSION

In the case of railway vibration, the quasi-permanent nature of the source has logistically made it possible to obtain internal measurement in a large number of

cases in synchronisation with the social survey (See 4.3). The methodology (See 4.4) relies on a 24 hour long term measuring position and synchronized snapshot within the respondent's property. The average transmissibility or velocity ratio (frequency dependent) between the two measurement positions has been used for scaling the activity recorded at the control position inside the property, so an estimation of the internal 24 hours exposure is obtained. Due to the large amount the processing for obtaining the long term internal exposure need to be automated (See 4.5).

For time synchronised internal measurements (about 56 % of 931 residents annoyed by railway vibration) few train passes in each case (generally 5 or more) are captured; then the average (frequency dependent) transmissibility or velocity ratio between the internal and the control position was used to filter the entire time history recorded at the control position. In this way an estimate of the 24 hour exposure inside the property and any exposure metrics can be estimated (See 4.5.4.1). In cases where no internal measurement was possible, the internal exposure has been estimated based on the value obtained from measurement inside a nearby property of similar type at similar distance to the railway (See 4.5.4.2). With the approach presented above, an estimation of the internal exposure is obtained for each case study providing the exposure response relationship for the population affected by railway vibration reported in Woodcock et al. [15].

5 EXPOSURE ESTIMATION FOR RAILWAY CONSTRUCTION

5.1 INTRODUCTION

The aim of this chapter is to provide a methodology for assessing human exposure from vibration due to railway construction activity. This approach will produce exposure data for building an exposure response relationship for 350 residents affected by construction sources satisfying the research objectives related to the project NANR209 (See section 1.2). As explained in chapter 2, construction vibrations can be considered as a non-steady state/transitory source and no exposure response relationship have been derived for this problem prior to the work done by University of Salford.

The strategies for assessing both exposure and response are different to the ones used for the steady state railway source. The exposure estimation relies less on internal measurement, and more on a semi empirical approach based on prediction models for propagating the measured exposure to residences at different distances from the source.

The characteristics of construction vibration are reviewed in section 5.2 whereas the measurement approach can be found in section 5.3. The prediction models are described in sections 5.4 and 0, together with the procedure for obtaining the soil propagation properties from an array of measurements. Finally, the curves derived for prediction of the exposure are presented in 5.6 whereas the conclusions are drawn in section 5.7.

5.2 CONSTRUCTION VIBRATION REVIEW

As for railways, construction vibration is generated externally to the living environment but it has a transitory character. Vibration activity from construction consists of different sources depending on the operations involved on the construction site. According to Wiss [84], the vibration types from construction cover the entire range of vibration affecting the residential environment (See 3.3.2). Construction vibration can be classified as:

- Transitory or impact.
- Steady state or continuous.
- Pseudo-steady state or random.

Impact vibrations occur from blasting or impact pile driving. Steady state vibration may be generated by vibratory pile driving and ground compaction by vibratory rollers. Pseudo-steady vibrations or random vibration are a series of impact vibrations of short intervals approaching a steady state condition. Examples of these sources are pavement breakers, trucks and bulldozers.

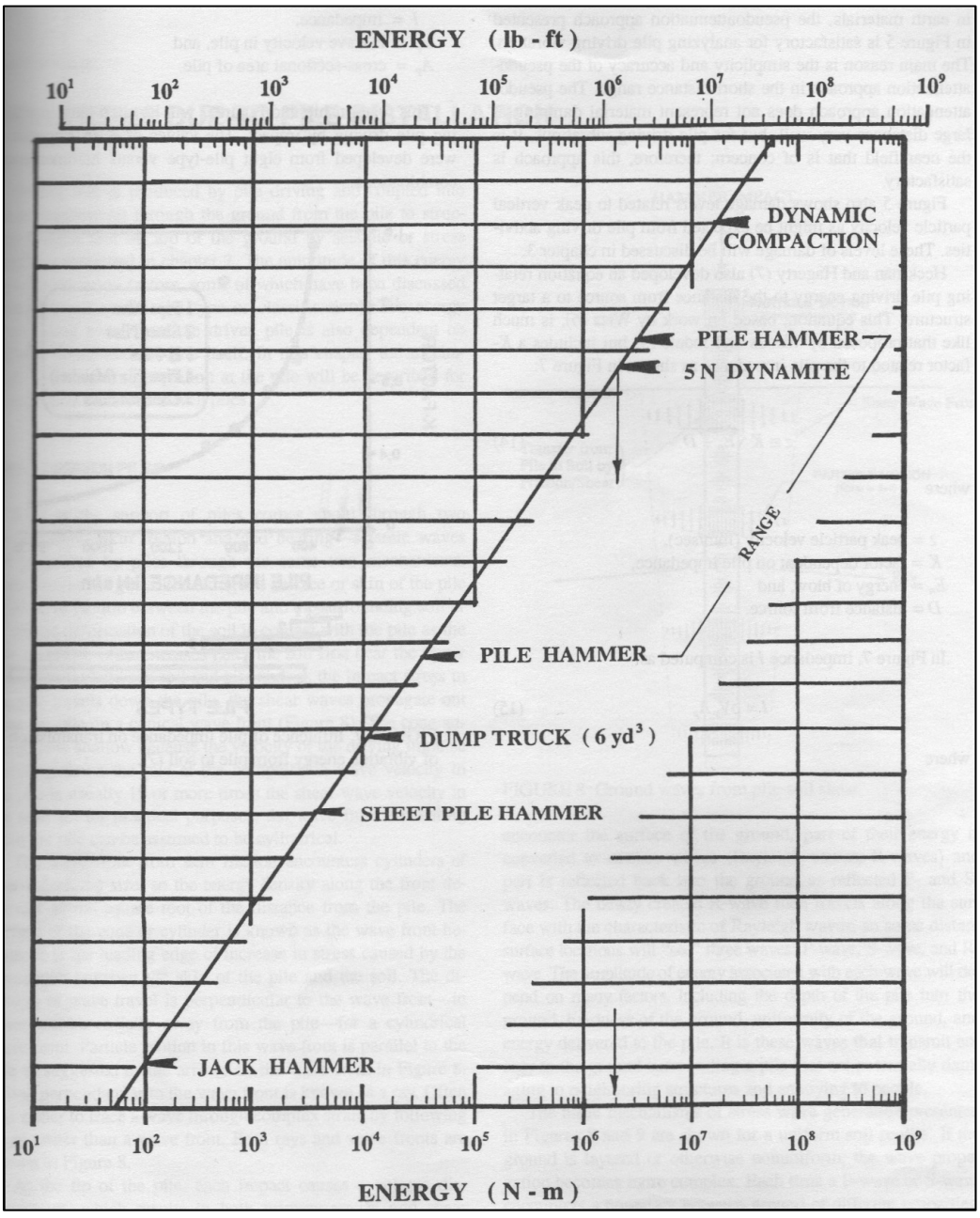

FIGURE 35 - RELATIVE ENERGY SOURCES OF CONSTRUCTION OPERATIONS (FROM WOODS [85]).

The energy of the sources involved in construction activities can be spread over several orders of magnitude as shown in Figure 35 explaining that construction activity can be a matter of concern not only for human response but also in relation of building damage and soil settlement. Sources of construction vibration generate compression, shear and Rayleigh waves (Richart et al. [86]) in homogenous ground but they may also generate Lamb, Love and Stoneley waves in layered ground. However, Rayleigh waves have the largest interest in the evaluation of the human response because building foundations are placed near the ground surface. Furthermore, Rayleigh waves contain roughly 70 % of the total vibration energy and become predominant over the other wave types at comparatively small distances from the vibration sources. For example, pile driving at depths of 4 and 10 *m* generates Rayleigh waves within 0.4 to 3 *m* of the pile, depending on the propagation of Rayleigh and compression waves.

Soil is generally excited at the frequency of the vibration sources. The changes of soil vibrations with distance from the source is caused by the faster attenuation of high frequency components (dispersion) and non-linearity due to near field effects caused by the source mechanism. However, some records cannot be explained by these mechanisms and the effect of soil strata heterogeneity and uncertainties of the geologic profile should be taken in account (Svinkin [87]). The proximity of the soil vibration frequencies to one of the building's natural frequencies generates the condition of resonance causing vibrations into the building substructures such as walls, ceilings and floors with the possibility that such vibrations may be perceived by the resident. Construction vibration is generally expressed as peak particle velocity or PPV.

The evaluation of human exposure is often accomplished by measurement of vibration level, for example expressed in Peak Particle Velocity, and comparison with the requirements of a relevant standard. This approach can be found for example in the works of Clough & Chameau [88] , Woods [85], Athanasopulus & Pelekis [89] especially with regards to vibration from pile driving. A description for the evaluation of human exposure from construction is given in Wiss [84] and

in the book of Dowding [90]. The construction sources considered in the study "Human response to vibration in residential environments" are the following:

- Impact and vibratory pile driving.
- Pavement breaking/shallow excavation.
- Compaction.

5.3 MEASUREMENT APPROACH

In this section the measurement approach for determining the vibration exposure from construction sources is presented. First of all, the coordination between vibration and social teams is described (See 5.3.1), then an explanation of the measurements together with an overview of measurement sites is provided (See 5.3.2 and 5.3.3). Finally, the life cycle of the construction sources is presented (See 5.3.4).

5.3.1 COORDINATION BETWEEN TEAMS

In order to assess exposure and annoyance due to construction vibration it is important to consider the size of the construction site and the duration of the work to ensure that a large sample of residents could potentially be affected by the vibrations. For this reason, the operation from light-railway construction has been chosen as sources for determining both exposure and annoyance in the living environment as already explain in section 3.4.2.2.

Logistically, the approach used for the railway, in which the social survey must be conducted before the vibration measurement in order to avoid biased responses, cannot be adopted: for transient sources, the survey must take place after the exposure has occurred by which time, the source of vibration has already moved on and internal measurements are no longer possible. In this scenario the social and vibration teams work independently. As happened for the railway cases, the interviewers need to input the respondent information' (see section 4.3.1) into the spreadsheet as soon as possible to keep a continuous update of the total number of

social survey questionnaires carried out. Moreover, the information provided was used by the vibration team for deriving the exposure response relationship.

In the planning of the measurement campaign, for both exposure and response, collaboration with the construction manager is vital in order to provide the following information: the time schedule of the operations involved in the construction, the identification of the operations expected to cause annoyance and the most suitable areas of the construction line for conducting both exposure and response measurement. The exposure measurement campaign was carried out during the summer of 2010. In the following sections the derivation of the exposure from construction sources is explained.

5.3.2 EXPOSURE MEASUREMENTS

As described in chapter 4, in the case of railways source it is possible to conduct intensive internal measurement. However, the same approach cannot be adopted for construction sites because the transitory nature of the work causes a logistical 'catch 22' already explained in the previous section.

A different approach is therefore necessary for construction vibration which relies more on the prediction of vibration. The construction sites chosen are of a light rail installation where construction activities move along the route as the work progresses. Essentially the same operations are carried out at every point on the line and the source of vibration moves as sections are completed. In this way, measurements can be taken on one part of the line assuming that essentially the same exposure would occur at other points on the line where surveys are collected independently of the measurements. In comparison with the railway case, far more limited measurements are possible since any properties used for measurement cannot be used for subsequent surveys without biasing the response.

Therefore, measurements were taken at a fixed location on one segment of the linear site as the construction work passed by. The elements of the measurement approach are:

- Control position
- Internal position
- External array.

The purpose of the control position is to capture the entire life cycle of the vibration exposure. It is generally placed at the boundary between the residential environment and the construction site following the guidelines described in section 3.5.6. The measurements lasted for a period of weeks rather than 24 hours as used for railways. For this reason, several units were used for long term monitoring: each week approximately, the instrument was swapped for another one with a new set of batteries. Particular attention was given to the calibration (see section 3.5.4) of the units which was checked before and after the long term installation (despite the fact that there are no guidelines about the calibration of instrumentation for the vibration monitoring in BS 5228-2:2009 [34]). As in the railway case, internal measurements were carried out over a short period for establishing external-to-internal transmissibility or velocity ratio.

The new element introduced in the measurement methodology for construction vibration is the use of an external array to enable simultaneous measurements of the vibration at various distances from the source. These measurements are used for evaluating properties of the soil and thereby to obtain a prediction of the exposure at any distance from the construction line. The development of the propagation method is described in section 5.4. Array and internal measurements are, of necessity, short term and are therefore timed by discussion with construction manager, as said in the previous section, to take place during the day of maximum activity. In this way the signal to noise ratio is as high as possible.

5.3.3 OVERVIEW OF MEASUREMENT SITE

Figure 36 shows one of the sites used for assessing the exposure from construction activity. The site was for the construction of a new tramway and had the form of a linear construction site where different construction operations occurred, usually in sequence on different parts of the line according to the plan and the phase of the construction. Two such linear sites were used, referred to as Site A and Site B.

Social surveys were conducted along the entire length of both sites but measurements were restricted to one section of the line.

FIGURE 36 - CONSTRUCTION SITE A

Site A

The measurement setup for site A is described in Figure 37. The aim of the works was the reconversion of an old railway line to a light rail line. The major parts of the operation were carried out inside the cut where the old track was laid. In this scenario the operation from both impact and vibratory pile driving were measured for the installation of trackside structures. Seven metre tubular piles were driven into soil along both sides of the track at 25 m centres.

The line of the pile P and Q were situated 6.5 m from the centre of the track. The line of the piles Q is taken as the origin of the reference system. From there the distance to the control position is 6 m. The first transducer of the array, denoted $M1$, was placed in line with the other transducers at 10, 20 and 40 m from the first element. Considering the measurement line ML, light blue in Figure 37, as a

datum perpendicular to the line of the piles, the distances between the point O and the piles $P1, P2, P3, P4$ were quantified in -15,10, 35 and 60 m respectively. Because the piling was a localised source it was also important to estimate the distances the each pile $(P1 \ldots P4)$ to each point on the measurement array $(M1 \ldots M4)$. The distances from the pile $Pi \quad i = 1 \ldots 4$ and the measurement points $Mi \quad i = 1 \ldots 4$ from the hypotenuse of the triangles $PiOMj \quad i, j = 1 \ldots 4$ which could be evaluated with Pythagoras's Theorem. The resulting distances are summarized in Table 7.

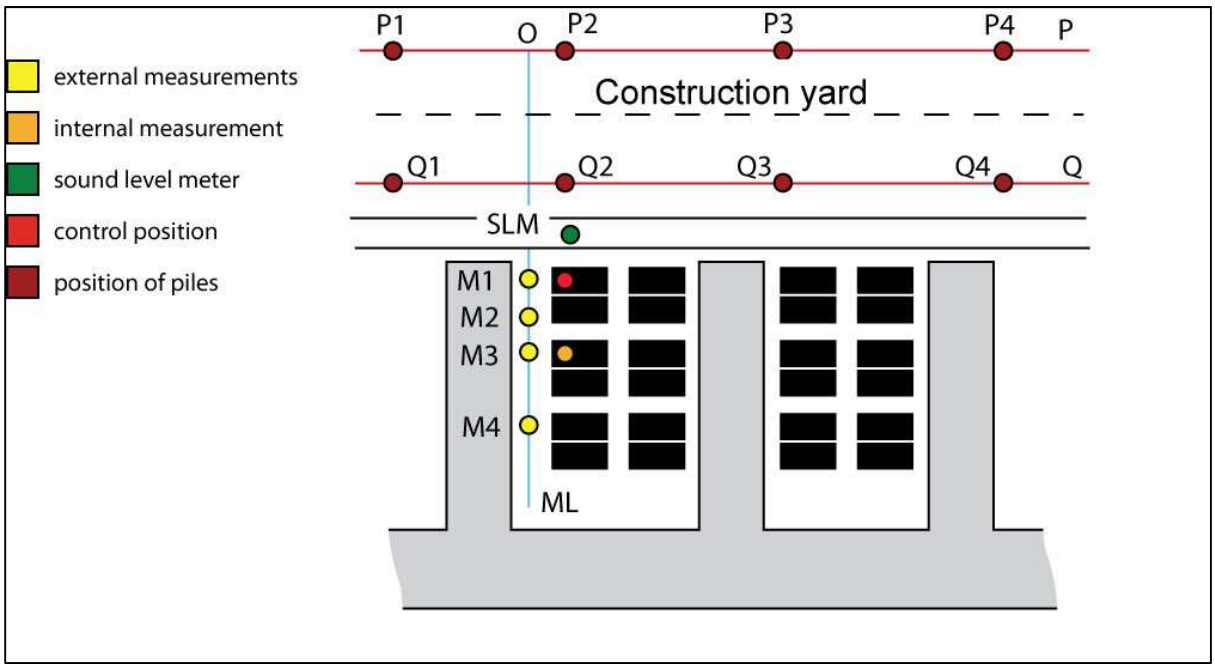

FIGURE 37 - MEASUREMENT SETUP FOR SITE A

	P1	P2	P3	P4
M1	24	21	40	63
M2	33	31	45	67
M3	42	40	52	72
M4	61	60	69	84

TABLE 7 – SITE A DISTANCES BETWEEN MEASUREMENT POSITIONS AND PILE POSITIONS (LINE P FIGURE 37) IN METER

Site B

At site B construction works were carried out for a light rail installation in a residential street. A plan of the measurement layout is given in Figure 38. The works were carried out in strip approximately 100 m long and 8 m wide. The operations involved were:

1. Saw cutting
2. Pavement breaking/Shallow excavation/Material Filling
3. Compaction
4. Slab and Rail installation
5. Tarmac cover

According to the construction manager, item 2 was most likely to be felt by the residents. However, the long term monitoring included items 1, 2 and 3. There were significant differences between the construction activities carried out at Site A and Site B. At Site A the work consisted of a reconversion of the line and the works were carried out in an already existing installation in a typical and quiet residential environment reminiscent of those analysed in the railway survey. The source of vibration, piling, was well localized. Site B was a new installation carried out in a fairly busy main road where the construction operations caused disruption of traffic along the street. This situation might increase the background level of the vibration measurement. Unlike Site A, the vibration sources at Site B were not well localized and were continually moving although always within the strip of land shown in Figure 38.

In this case we defined the datum line, O, at the centre line of the construction strip. The perpendicular distance between the reference system and the control position was estimated at 14 m (Figure 38). As for site A, the first element of the array was installed in line with the control position. The perpendicular distances with respect to the origin (line in Figure 38) of the activity for the array elements are presented in Table 8.

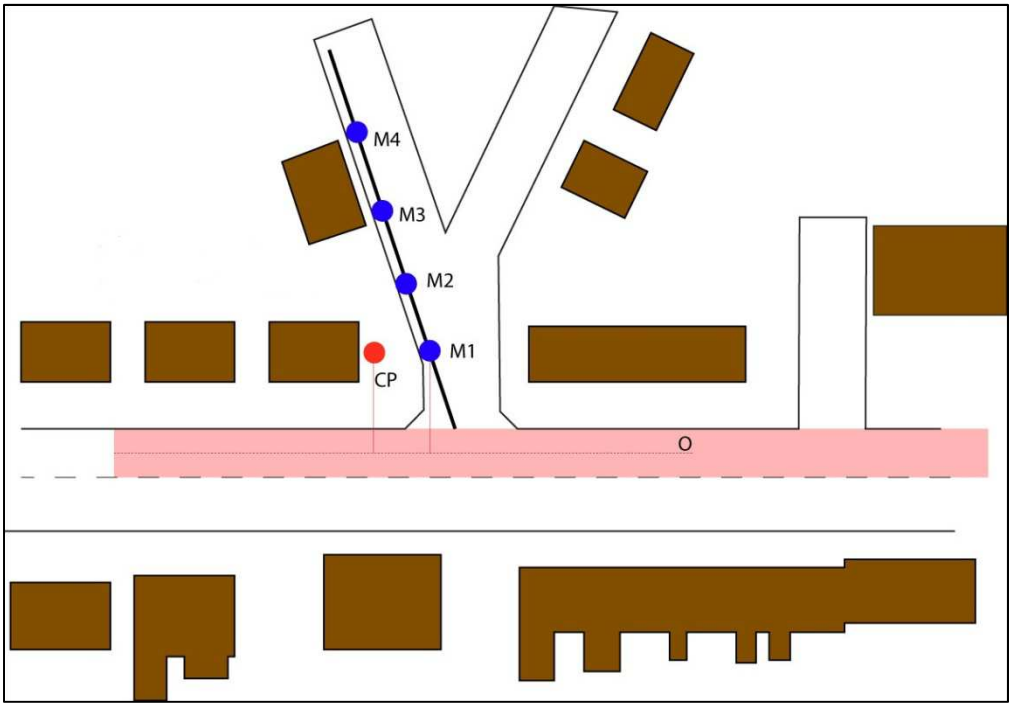

FIGURE 38 – MEASUREMENT SETUP FOR SITE B

M1	M2	M3	M4
14	23	32	42

TABLE 8 - SITE B PERPENDICULAR DISTANCE BETWEEN MEASUREMENT POSITION AND ORIGIN OF THE REFERENCE SYSTEM O

5.3.4 VIBRATION LIFE CYCLE

Continuous records of vibrations were conducted for 63 days at Site A and 36 days at Site B. The life cycle of the construction activity has been analysed by plotting the daily exposure recorded at the control position throughout the monitoring period. Event identification was first carried out manually from the time history in order to identify and remove vibration caused by any local human activity not related to the construction. In Figure 39 is plotted the daily exposure between 08:00 and 18:00 at the control position for Site A expressed in terms of peak particle acceleration (PPA) in the z direction weighted with W_b following the guidance provided by BS 6472-1:2008.

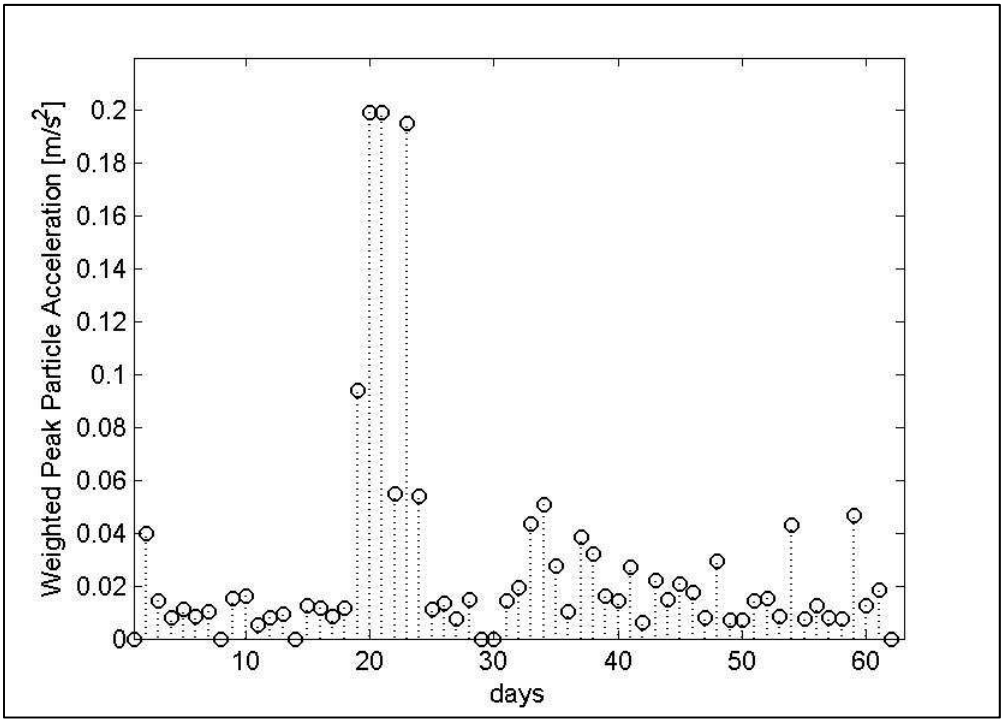

FIGURE 39 - SITE A WEIGHTED W_B PEAK PARTICLE ACCELERATION (Z COMPONENT) OVER 10 HOURS VS MONITORING DAYS. LIFECYCLE OF THE CONSTRUCTION ACTIVITY

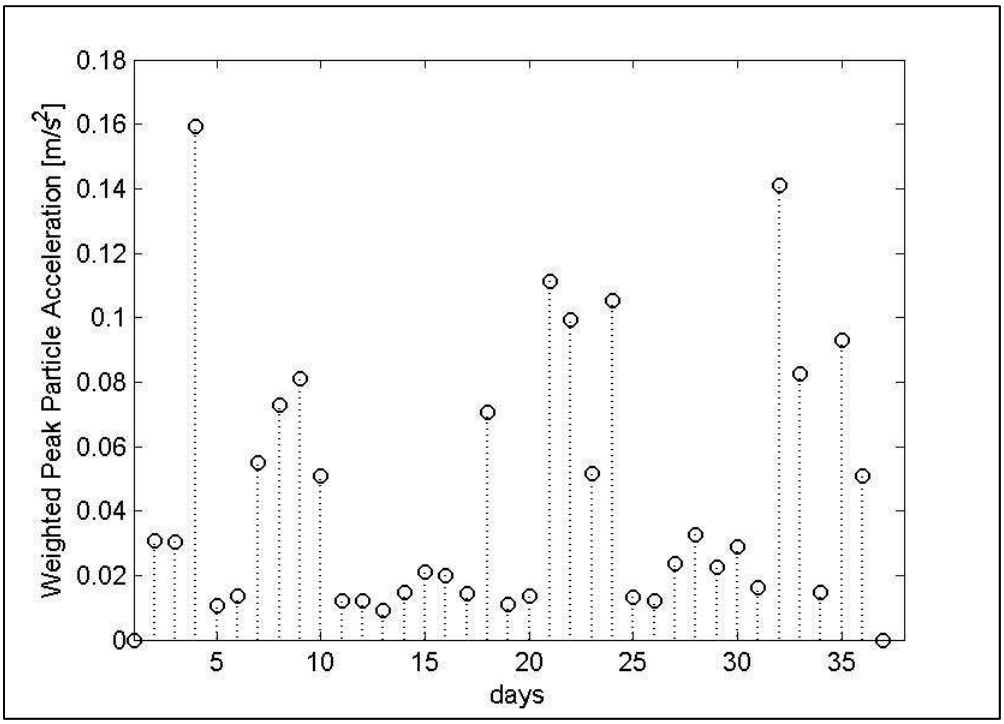

FIGURE 40 - SITE B WEIGHTED W_B PEAK PARTICLE ACCELERATION (Z COMPONENT) OVER 10 HOURS VS MONITORING DAYS. LIFECYCLE OF THE CONSTRUCTION ACTIVITY

The maximum daily value is reached on the 21st day of monitoring with a maximum value of 0.2 m/s² recorded when a pile was driven at position *Q2* very

close to the control position (see Figure 37). On the other hand Figure 40 shows that the maximum of the W_b weighted PPA (z component) is reached at the 4th day of monitoring at Site B with 0.16 m/s^2 due to pavement breaking and shallow excavation. The second highest peak, occurring on the 32nd monitoring day, is probably due to compaction activity.

5.4 EXPOSURE PROPAGATION

In this section the development of the method for predicting the vibration exposure at different distances from the construction site is described. The underlying theory and assumptions are first presented (See section 5.4.1). The method of obtaining damping factors for the soil from the external array measurements is then described in section 5.4.2 and the model validation in 5.4.3. Finally, the propagation of vibration from the ground to the building is discussed (See section 5.4.4).

5.4.1 MODELLING PROPAGATION

The main aim of the array measurements is to derive a propagation law for each measurement site using one of the semi empirical relationships presented in the literature which are discussed in appendix A. Example of methods for predicting ground-borne vibration attenuation with distance for source specific construction operations can be found in BS 5882-2:2009 Table E.1 [34] or in Woods [85] for pile driving. Those relationships can be applied only if a complete set of parameters related to the source is known. This information is not available for either of the sites. Therefore, the most commonly used distance attenuation relationship in literature has been used, known as Barkan's Law [91], which is expressed as:

$$A(d) = A_0 \sqrt{\frac{d_0}{d}} e^{-\alpha(d-d_0)} \tag{5.1}$$

Equation (5.1) describes the approximate formula for amplitudes of spherical waves propagating over the soil surface at large distances from a concentrated source (Barkan [91]). With this relationship Barkan [91] studied experimentally the

propagation of waves under various soil conditions with the aim of understanding the validity limits of theoretically established relationships between soil displacements and distances from the source of waves. Barkan found that the theoretical relationships, which are discussed in section 6.2.1 as Lamb problems, can be valid only if the soil is considered as a solid elastic body. In reality the soil is not a perfect elastic body and the only geometrical attenuation coefficient, introduced in equation A.1 with n=0.5, is not enough for describing the propagation of waves in the soil. A better agreement with the measurement can be achieved taking into account the material attenuation, described in Appendix A, too as described in equation (5.1).

The equation (5.1) relates the magnitude of the acceleration A at a distance d to the level of the known acceleration A_0 at distance d_0 from the source under the assumption that Rayleigh waves dominate the propagation. The attenuation α, measured in 1/m, depends on the material damping D, the Rayleigh wave speed V_R and on the frequency of vibration f according to the simplified relationship (Athanasopoulos et al. [92]) in (5.2).

$$\alpha = \frac{2\pi fD}{V_R} \tag{5.2}$$

Equation (5.2) enables the determination of α knowing soil parameters like D and V_R which were not available during the study, therefore the approach adopted here is to use Barkan's law, equation (5.1), to fit the experimental data obtained from the external array and thereby obtain an empirical estimate for α for the specific site. The assumption that Rayleigh waves dominate the propagation implies that the distance d_0 is in the far field which begins, according to Auersch and Said [80], one wavelength away from the source.

The α-value obtained is then substituted into Barkan's law yielding a model for prediction of the vibration exposure at any distance

5.4.2 CALCULATION OF SOIL PROPERTY

In this section the calculation of the soil property is presented. As mentioned in section 5.4.1, equation (5.1) is used for fitting the array measurements so as to estimate the ground attenuation parameter α . Specifically, α is obtained by minimizing the following error function E_fh:

$$E\_fh = \sum_{k=1}^{N} \left(A_k - A\left(d_k, \alpha_0\right) \right)^2 \tag{5.3}$$

Where A_k is the vibration measured at distance d_k, defined in section 5.3.3, from the source and $A(d_k, \alpha_0)$ is equation (5.1) evaluated at d_k for an initial α_0 guess of α . Therefore the determination of α is obtained using an unconstrained nonlinear optimization implemented in Matlab through the function *fminsearch*.

Figure 41 shows results obtained from the external array at Site A. The z component of Peak Particle Acceleration (PPA) is plotted against distance for times when piling was taking place at different pile positions (See Figure 37). It is noticeable that significantly lower levels are obtained for piling at $P3$ and $P4$. This is thought to be because these positions were shielded from the measurement array by a row of houses whose cellars were acting as wave barriers and therefore causing attenuation of vibration. According to R. Woods [85] a barrier usually must be at least one wavelength deep in order to cause significant screening. Since Barkan's law assumes free field propagation only the contributions coming from $P1$ and $P2$ are considered whereas $P3$ and $P4$ are ignored for fitting of the attenuation parameter. The fit of the experimental data provides an α = 0.0250 1/m for site A (See Figure 42). A similar analysis has been carried out for Site B (see Figure 43). The data fitted with Barkan's law provides an α = 0.0379 1/m for site B.

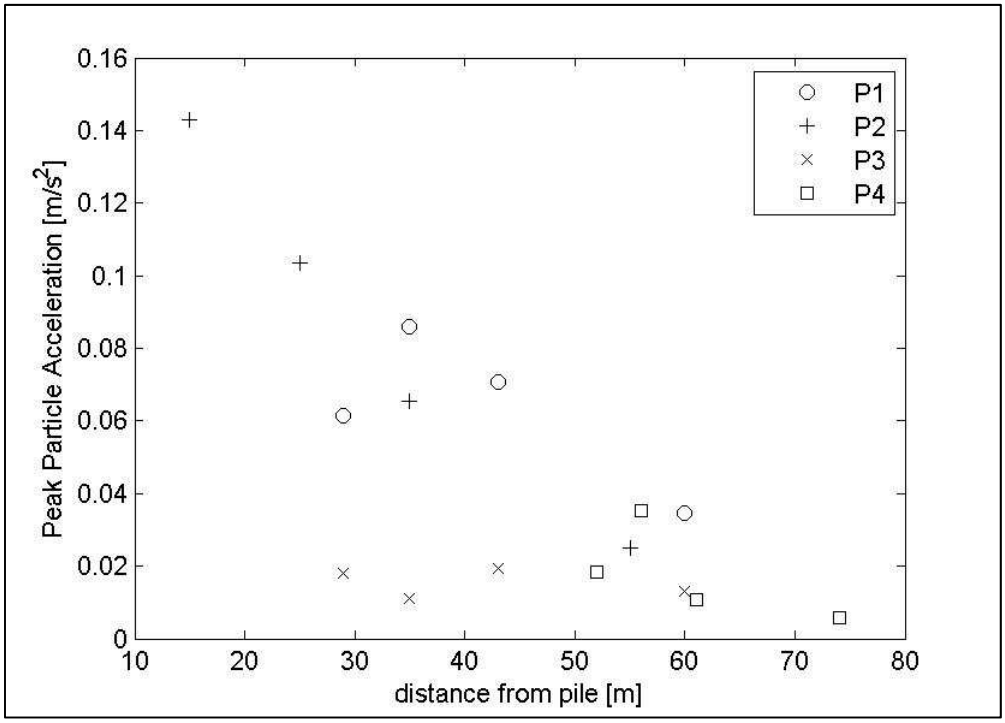

FIGURE 41 – SITE A PEAK PARTICLE ACCELERATION (Z COMPONENT) VS DISTANCE FROM PILE (TABLE 7). P1 P2 P3 P4 PILE POSITIONS (SEE FIGURE 37)

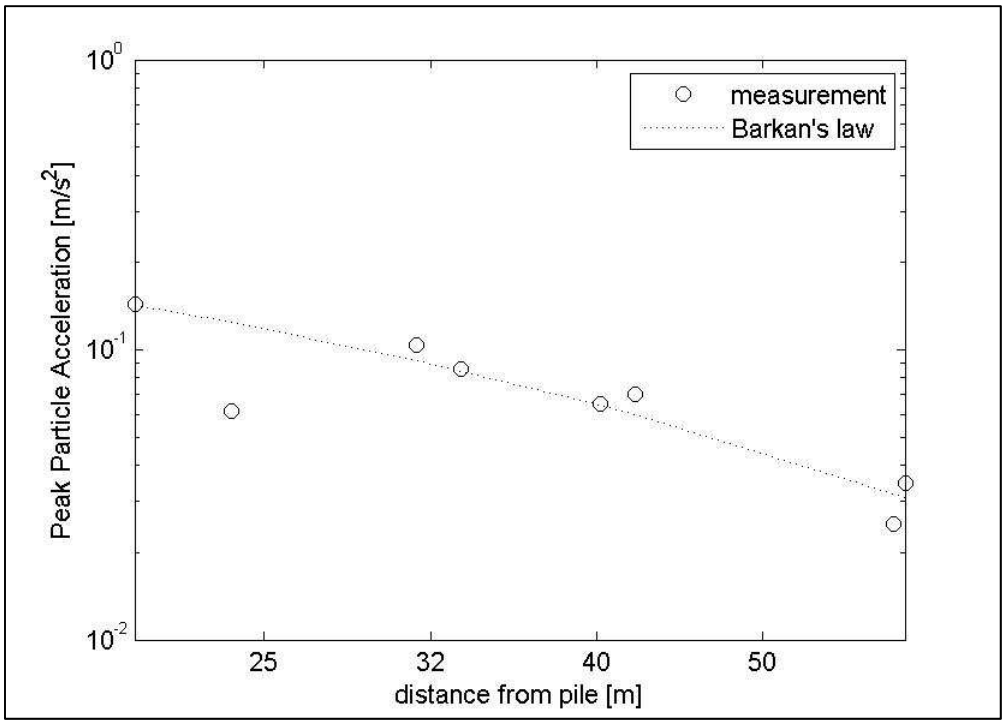

FIGURE 42 - SITE A PEAK PARTICLE ACCELERATION (Z COMPONENT) VS DISTANCE FROM PILE (ONLY CONTRIBUTION P1 AND P2).MEASURED POINT (DOT) EXPERIMENTAL FIT WITH BARKAN'S LAW (LINE). GRAPH IN LOG SCALE

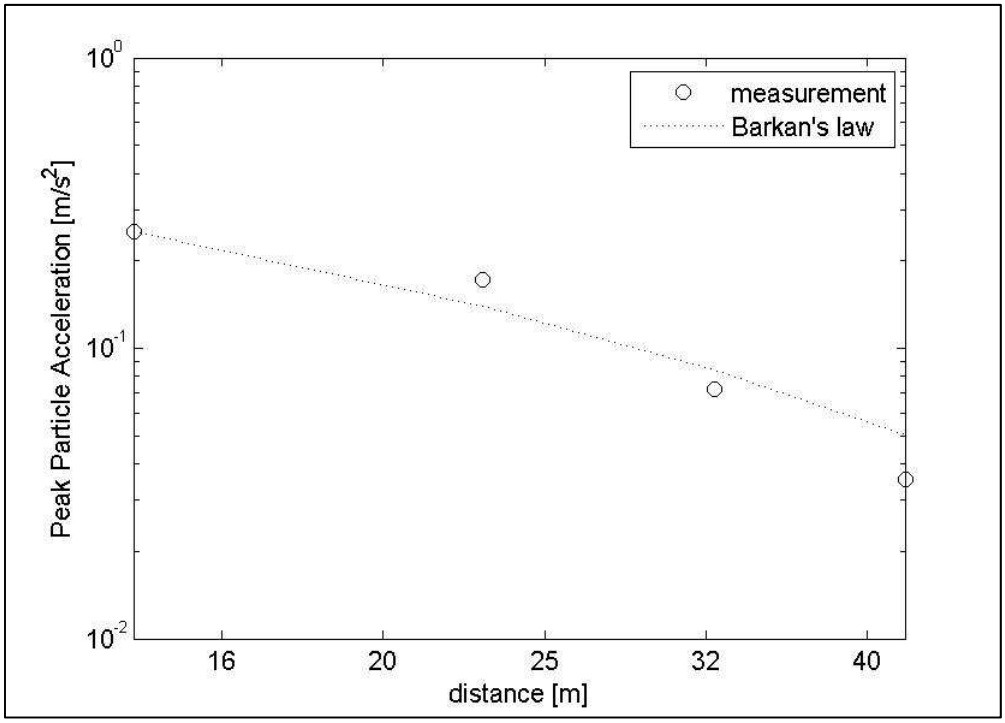

FIGURE 43 – SITE B PEAK PARTICLE ACCELERATION (Z COMPONENT) VS PERPENDICULAR DISTANCE FROM THE ORIGIN (SEE FIGURE 38 AND TABLE 8). MEASURED POINT (DOT) EXPERIMENTAL FIT WITH BARKAN'S LAW (LINE). GRAPH IN LOG SCALE

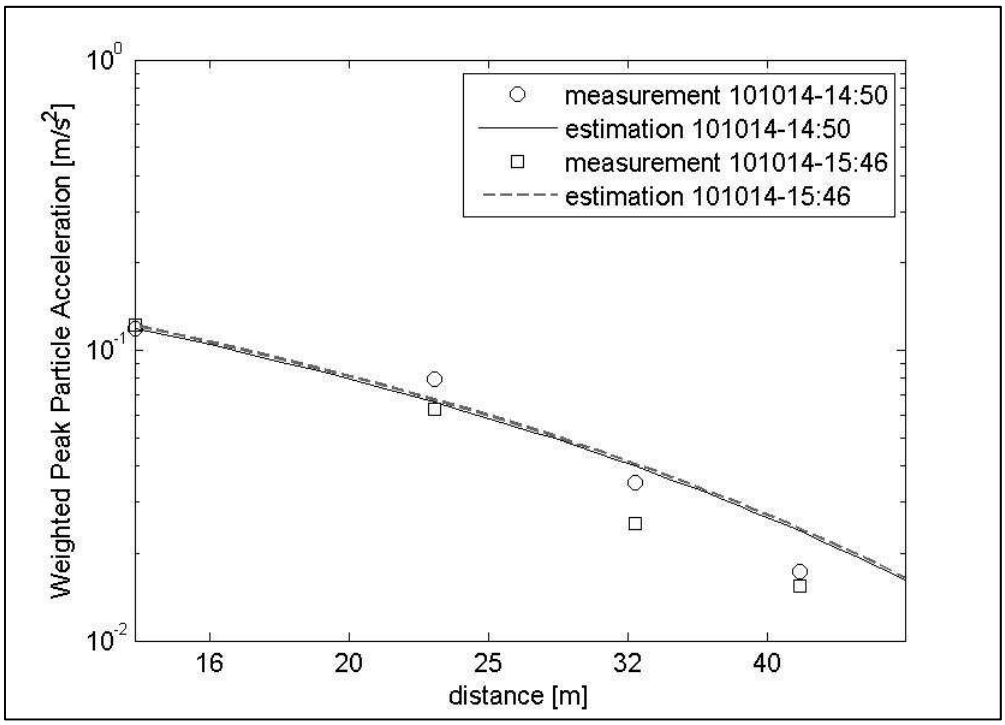

FIGURE 44 - SITE B. EXTERNAL WEIGHTED W_B PEAK PARTICLE ACCELERATION (Z COMPONENT) VS PERPENDICULAR DISTANCE FROM THE ORIGIN (TABLE 8). VARIABILITY OF CONSTRUCTION OPERATIONS AT DIFFERENT TIMES OF THE DAY. MEASUREMENT (DOT AND SQUARE) ESTIMATION WITH BARKAN'S LAW (LINE). GRAPH IN LOG SCALE

One can obtain an idea of the scatter likely to be obtained in the prediction on the two sites by considering the deviation of the measured points from the fitted curve as shown in Figure 43. In addition, Figure 44 plots two decays for data obtained at different times of the day. A slight over-estimation is evident for distances greater than 30 m in one case but not the other. Generally, the accuracy of the prediction is likely to decrease at distances further from the source. In the case studies considered the range of distances goes from 10 to 220 m. On the basis of these results, Barkan's law provides a reasonable approximation of the propagation on soil for the sources considered in this study. However, a quantification of the daily variation of the operation is needed for a better estimation of the uncertainty related to the prediction method. The latter is discussed in Sica et al. [66]. Further insight into the reliability of the results can be gained by carrying out an octave band analysis as reported in the following paragraphs. The approach is essentially the same as that reported at the beginning of the section but is carried out using vibration data that is pre-filtered in octave bands, similar to the one used by Amick [93]. As a consequence the unconstrained nonlinear optimization problem has been implemented minimizing equation (5.3) in each octave band. In this way we should be able to quantify the frequency dependence of the material damping (Rix et al. [94]). In Figure 45 and in Figure 46 the estimated decays using Barkan's law from 4 to 64 Hz are presented for the vibration signal recorded in Site A and B. A strong dependence on frequency is evident. This difference can be assigned to the different nature of the soils, but could also be affected by the level of background vibration especially at high frequencies. The material damping coefficients expressed in octave bands are presented in Table 9.

	4Hz	**8Hz**	**16Hz**	**32Hz**	**64Hz**
α (1/m) Site A	0.0098	0.0254	0.0151	0.0676	0.12
α (1/m) Site B	0.0043	0.0156	0.0313	0.0527	0.061

TABLE 9 – GROUND ATTENUATION PARAMETERS IN OCTAVE BAND FOR BOTH MEASUREMENT SITES

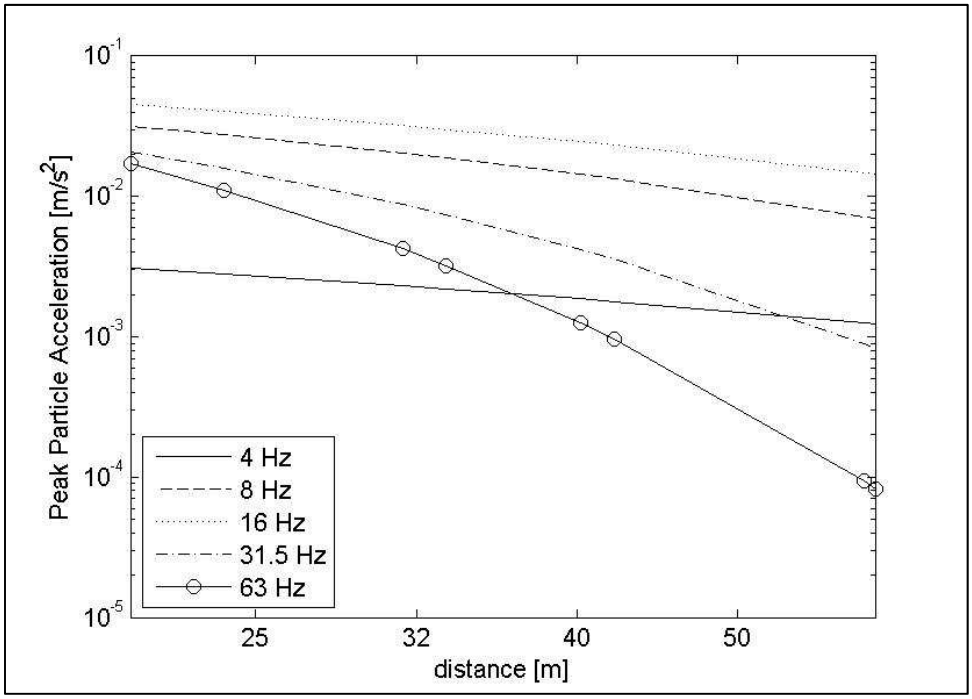

FIGURE 45 - SITE A PEAK PARTICLE ACCELERATION (Z COMPONENT) VS DISTANCE FROM PILE (TABLE 7). ESTIMATED DECAY OF THE PEAK PARTICLE ACCELERATION EXPRESSED IN OCTAVE BAND CENTER FREQUENCIES (4HZ 8HZ 16HZ 31.5HZ AND 63HZ) WITH THE BARKAN'S LAW

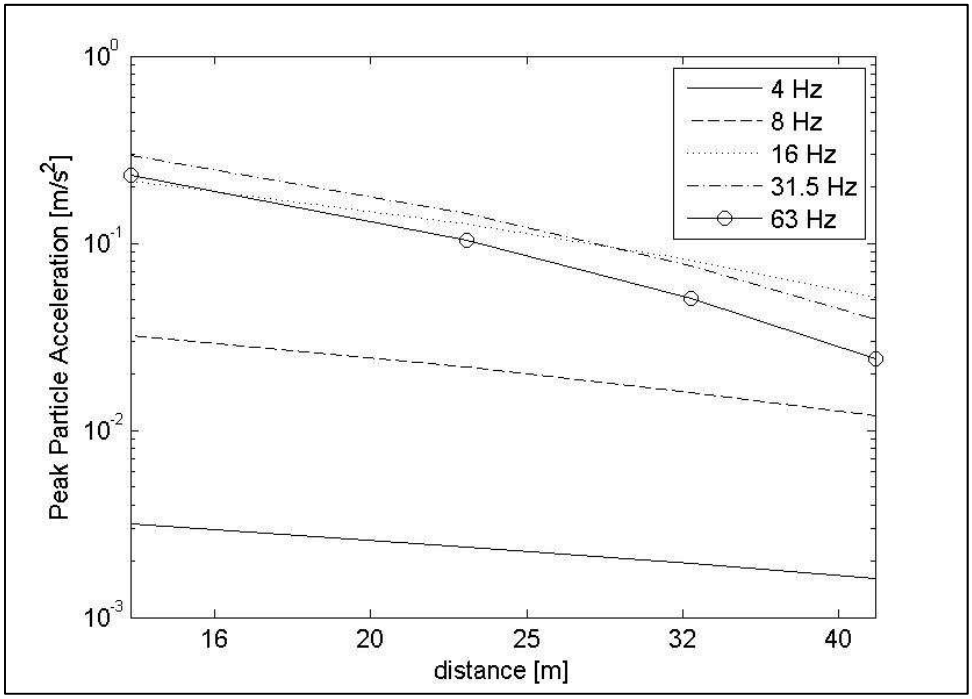

FIGURE 46 - SITE B PEAK PARTICLE ACCELERATION (Z COMPONENT) VS PERPENDICULAR DISTANCE FROM THE ORIGIN (TABLE 8). ESTIMATED DECAY OF THE PEAK PARTICLE ACCELERATION EXPRESSED IN OCTAVE BAND CENTER FREQUENCIES (4HZ 8HZ 16HZ 31.5HZ AND 63HZ) WITH THE BARKAN'S LAW

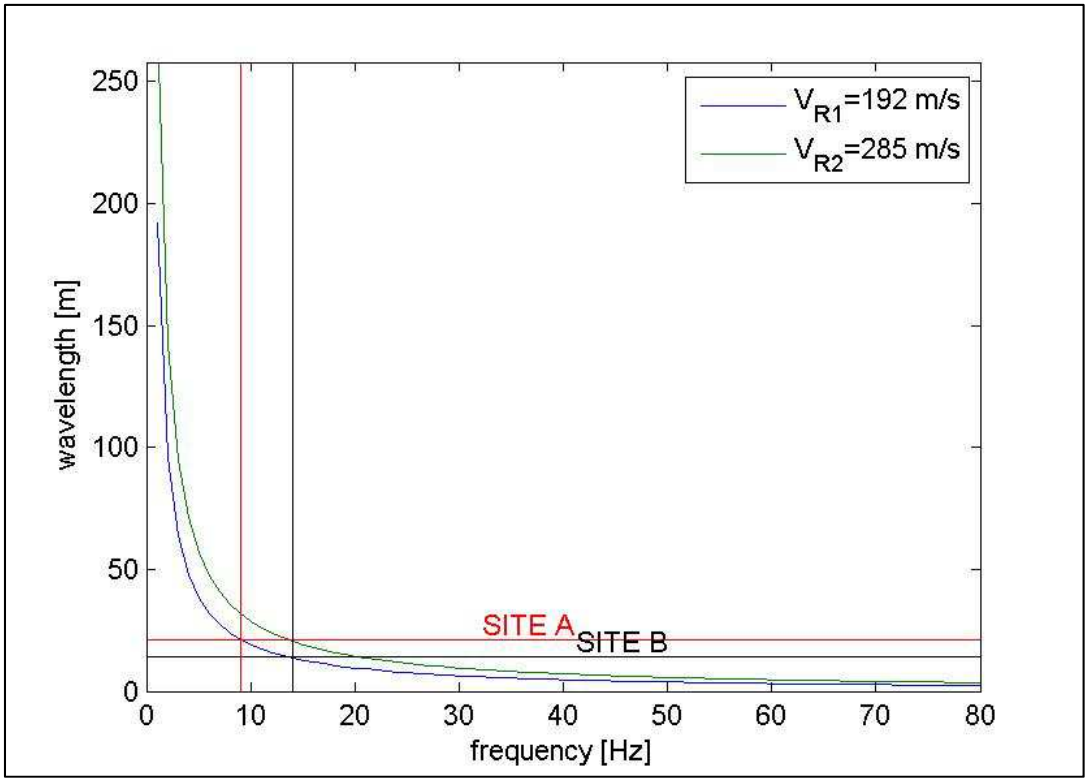

FIGURE 47 – WAVELENGHT VS FREQUENCY FOR DIFFERENT RAYLEIGH WAVES SPEED. BLUE LINE 192 M/S GREEN LINE 285 M/S. RED LINES NEAR FIELD LIMITS FOR SITE A. BLACK LINES NEAR FIELD LIMITS FOR SITE B.

The analysis of the damping coefficient at 4 Hz can give also an evaluation of the soil type by comparison with tabulated values (usually given at 5 Hz). According to the classification done by R.D. Woods & Jadele [95] (Table 17) both sites fall into class II soil types. The latter are also called *Competent Soils* that include sands, sandy clays, silty clays, gravel silts and weathered rock. This is a good description for the soil type in both measurements sites and provides some indications that the curve fitting procedure yields reasonable values. A further confirmation about the soil type can be done only for Site A where borehole data are available.

Since both sites belong to the same class of soil, an estimation of the Rayleigh waves velocity can be obtained using the semi empirical relationship between the low-amplitude shear wave velocity of soil V_{SO} and the number of blow count N_{SPT} of the Standard Penetration Test (Athanasopoulus et al . [92]).

$$V_{SO} = 107.6\left(N_{SPT}\right)^{0.36} \tag{5.4}$$

According to Woods [85], class II soil types correspond to $5 < N_{SPT} < 15$ which correspond to V_{SO} between 192 m/s and 285 m/s. Assuming that the Rayleigh wave speed V_R is V_{SO} and the soil is a homogeneous half space an estimation of the wavelength as a function of the frequency can be obtained and is reported in Figure 47. Considering the measurement position at distance d_0 used for calculating equation (5.1) from both measurement sites, which are 21 m for Site A and 14 m for Site B (See Table 7 and Table 8), and the slowest Rayleigh speed, V_{R_1} from Figure 47, calculated with (5.4) an estimation of the validity of Barkan's Law in the far field region can be obtained from Figure 47. It can be seen that the far field approximation of the Barkan's Law is valid above 9 Hz for site A and above 14 Hz for site B.

A better way to assess the near field of the construction sources, which is important for understanding the validity of Barkan's law, can be achieved with the wave field assessment methods presented in the second part of this work in chapter 7.

5.4.3 VALIDATION OF PROPAGATION MODEL

In the previous section we have analysed the propagation characteristics of the construction vibration using Barkan's law. The first step in the prediction of the exposure is to understand if the semi empirical relationship used in the controlled experiments can be also used for describing the propagation of the vibration metrics used for assessing human exposure. The metrics considered in this case will be: weighted peak particle acceleration (PPA), weighted rms acceleration, VDV and weighted root mean quad (rmq) acceleration. The metrics shown in Table 10 are all calculated with respect to the z component of the acceleration applying the W_b weighting.

For each metric M we have considered the formula:

$$M(d) = M_0 \sqrt{\frac{d_0}{d}} e^{-\alpha_M (d - d_0)} \tag{5.5}$$

Where $M(d)$ is the metric at distance d from the source and M_0 is the metric evaluated at d_0 from the source and α_M is a pseudo attenuation coefficient.

Descriptor	Calculation
Peak particle acceleration (m/s^2)	Maximum deviation of the time series from the mean
Root mean square (m/s^2)	$\ddot{x}_{rms} = \sqrt{\frac{1}{N}\sum_{n=1}^{N}\ddot{x}(n)^2}$
Vibration dose value (m/s$^{1.75}$)	$\ddot{x}_{VDV} = \sqrt[4]{\frac{T}{N}\sum_{n=1}^{N}\ddot{x}(n)^4}$
Root mean quad (m/s^2)	$\ddot{x}_{rmq} = \sqrt[4]{\frac{1}{N}\sum_{n=1}^{N}\ddot{x}(n)^4}$

TABLE 10 - SUMMARY OF VIBRATION EXPOSURE DESCRIPTORS CONSIDERED. WHERE $\ddot{x}(t)$ AN ACCELERATION TIME SERIES, *N* IS THE NUMBER OF SAMPLES IN THE ACCELERATION TIME SERIES, AND *T* IS THE DURATION OF THE EVENT IN SECONDS.

Site A	W RMS	VDV	W PPA	W RMQ
α_M (1/m)	0.017	0.018	0.021	0.02

TABLE 11 - PSEUDO ATTENUATION COEFFICIENT PER WEIGTHED W_B (W) VIBRATION METRICS

The accuracy of the model can be evaluated considering the decay of the exposure metrics from the array measurements and comparing the pseudo attenuation coefficient obtained using (5.5) with the one found in section 5.4.2. The α_M for the site A are reported in Table 5. If the evaluation of the percentage relative error between the pseudo attenuation coefficients of the exposure metrics and the attenuation coefficient is made, it can be seen that a maximum underestimation of 30% of the pseudo coefficients is obtained for the weighted RMS (Sica et al. [96]).

The minimum is for the PPA and RMQ around 16%. Within these limits, it can be assumed that Barkan's law with the soil properties obtained in section 5.4.2 can be used for describing the propagation of all the metrics across the living environment. Similar results have been found for site B.

5.4.4 PROPAGATION INTO BUILDINGS

In the two previous sections the propagation of vibration through the ground has been considered. In addition, when evaluating vibration exposure inside buildings, it is necessary to take in account vibration transmission from the ground into the building. The approach is similar to that conducted for railways: in that case internal and external measurements were made simultaneously for evaluating the ground to building transmissibility. The latter was obtained as an average value over the exposure calculated over several construction events measured at both external and internal positions. In this way an estimation of the variance is possible calculated as twice the standard deviation. A difference from the railway survey is that, for logistical reasons, only a small number of internal measurements were taken for the construction sites.

The property type at site A, in which internal measurement was taken, is a semidetached house for which the frequency dependent external-to-internal transmissibility of weighted W_b PPA (z component) is shown in Figure 48. The measurement was taken at the first floor in the centre of the room.

At site B, two property types have been considered: a terraced house (results Figure 49) where measurements were made at the centre span of the ground floor living room and a semidetached house (Figure 50) where measurements were taken in the hallway at the ground floor.

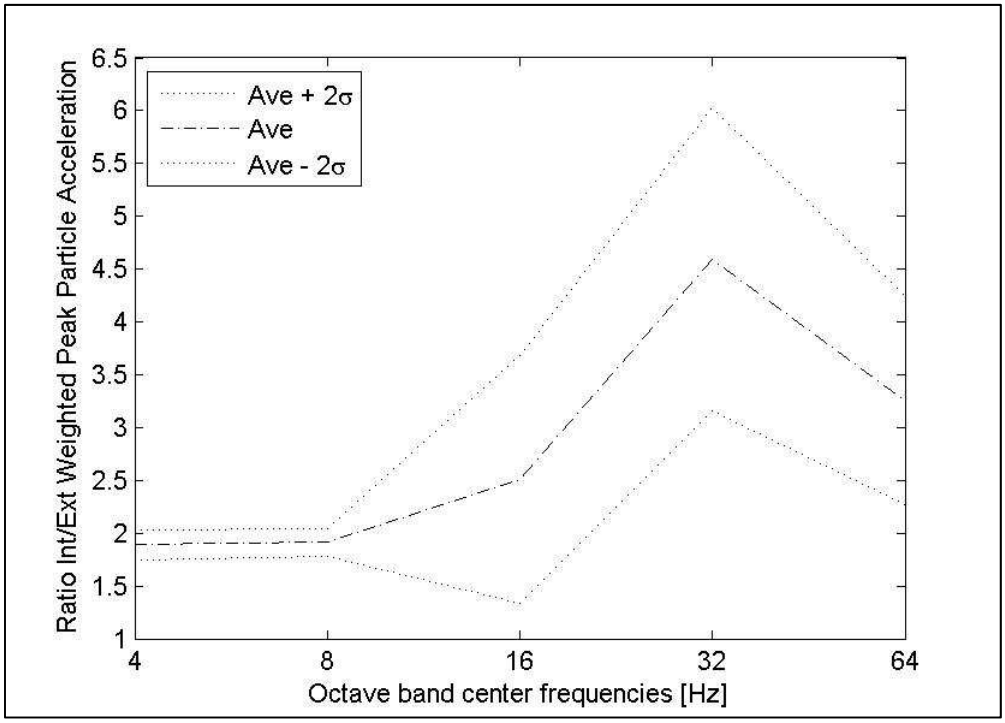

FIGURE 48 - SITE A. RATIO INT/EXT WEIGHTED W_B PEAK PARTICLE ACCELERATION (Z COMPONENT) IN OCTAVE BANDS. SEMIDETACHED HOUSE.INTERNAL MEASUREMENT AT FIRST FLOOR AT THE MID-SPAN

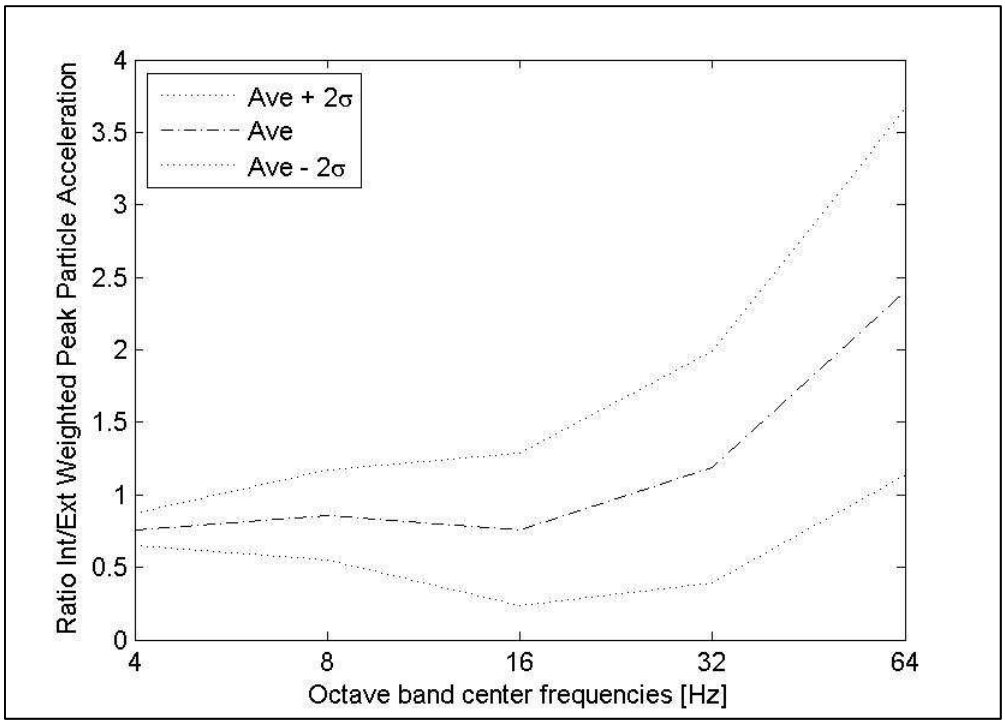

FIGURE 49 - SITE B. RATIO INT/EXT WEIGHTED W_B PEAK PARTICLE ACCELERATION (Z COMPONENT) IN OCTAVE BAND. TERRACED HOUSE.INTERNAL MEASUREMENT AT GROUND FLOOR AT THE MID-SPAN

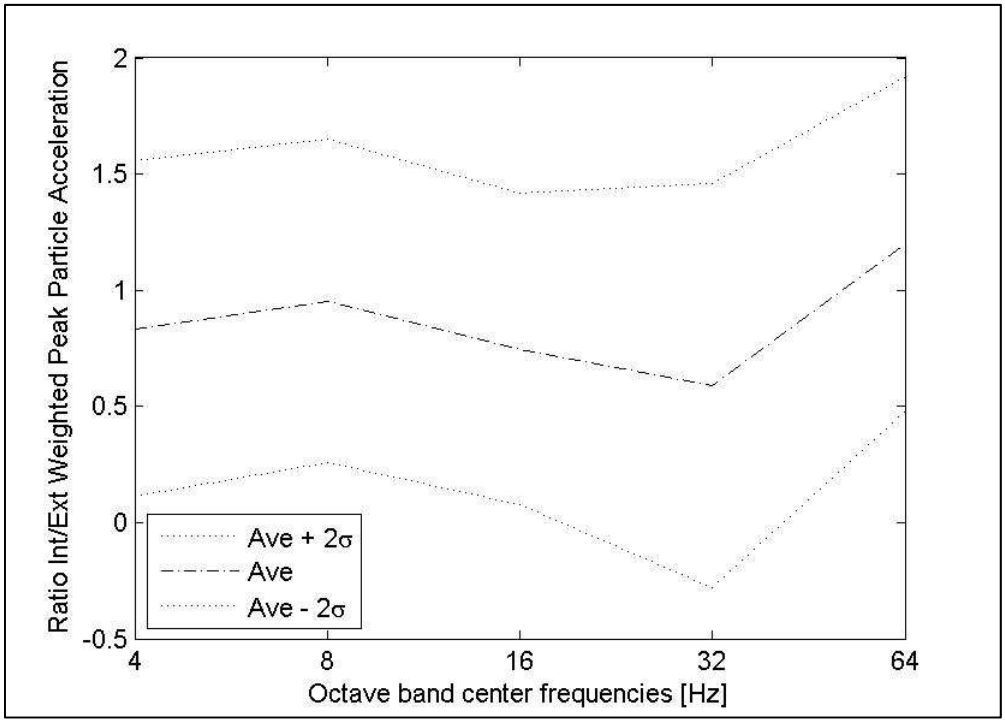

FIGURE 50 - SITE B. RATIO INT/EXT WEIGHTED WB PEAK PARTICLE ACCELERATION (Z COMPONENT) IN OCTAVE BANDS. SEMIDETACHED HOUSE.INTERNAL MEASUREMENT AT GROUND FLOOR IN THE HALLWAY

It can be seen that the octave band transmissibility varies from about 0.6 to 4.5 with the higher values obtained for the first floor and for measurements at the centre span of a larger floor.

Site	Property Type	Amplification factor
A	Semidetached (1st floor)	2.2 ± 0.6
B	Terraced (g. floor)	1.0 ± 0.6
B	Semidetached (g. floor)	0.8 ± 0.8

TABLE 12 – SINGLE FIGURE AMPLIFICATION FACTOR FOR DIFFERENT PROPERTY TYPES

The building responses presented here are evaluated when the distance between the source and the building measured is a minimum: for site A (See Figure 37) this distance is 40 m (Table 7 measurement position $M3$ pile position $P2$) whereas for

site B it is 14 meters (Table 8). It is not known if the building response may change with the distance from the source or with the direction of the source.

A single figure amplification factor is obtained as the ratio between the weighted W_b PPA measured internally and the one measured in the closest external measurement position. Results are shown in Table 12 and are based on only one property type for each type.

5.5 EXPOSURE ASSESSMENT

In order to calculate the daily exposure at different positions we start with the control position measurement which is considered an external measurement. The exposure metrics are calculated from the control position data and then propagated to the appropriate distance using the Barkan's Law (with empirical attenuation parameters identified from the array measurements, section 5.4.2). If an internal exposure is required then it is necessary to apply the external-to-internal transmissibility as described in section 5.4.4. The exposure can be evaluated for the whole monitoring period or by just considering the combination of the maximum daily exposures caused by the set of operation involved in the construction processes.

Considering that the validity of the Barkan's law as a propagator of the exposure has been proved in section 5.4.3, now the goodness of the control position as predictor of external vibration exposure in the residential environment needs to be tested. This is important because the exposure found has to be representative of all sites and not only of the measurement site. The experimental measurements for both sites shown in Figure 42 and Figure 43 have been considered. In Figure 51 the external measurement from site A is compared with the one propagated from the control position using equation (5.5) showing that the control position is a good predictor of external vibration when the source is very close to the residential environment. The equation can be used for assessing external vibration in the worst case scenario described above but an uncertainty has to be defined considering that a difference of a factor of 2 between the measurement and the

prediction from the control position has been found for site B as shown in the Figure 52.

The methodology is tested trying to reproduce two experimental situations where internal exposure has been measured. The predicted internal exposure from the one measured at the control position has been obtained following the steps shown in Figure 53. In the first case we predict the internal exposure measured in the property type of site A in the worst case scenario represented by piling activity measured from position P2. The level of exposure measured at the control position at 15 m is used for estimating the exposure inside the house at 35 m from the source. The results are shown in Table 13. In the second case we have considered an experimental situation encountered at site B. The internal vibration at 32 m from the source is predicted using the level of the exposure from the control position at 14 m. The amplification factor used in this case is the one for the terraced house. Results are shown in Table 14.

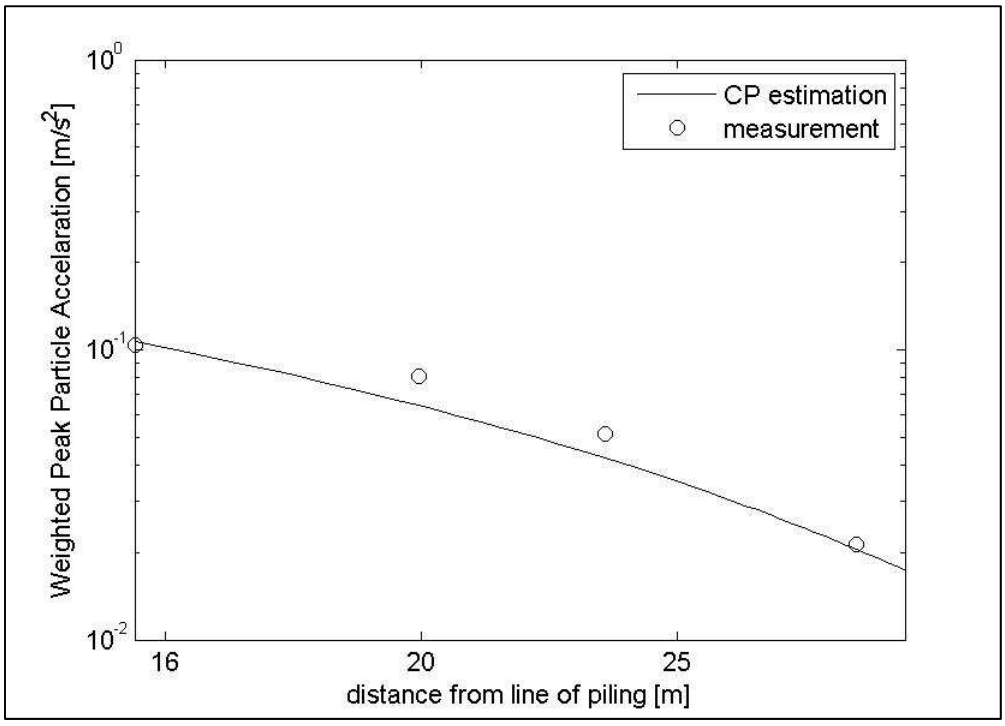

FIGURE 51 - SITE A. WEIGHTED W_B PEAK PARTICLE ACCELERATION VS (Z COMPONENT) DISTANCE FROM THE LINE OF PILING P (FIGURE 10). EXTERNAL WEIGHTED WB PEAK PARTICLE ACCELERATION MEASURED (DOT). ESTIMATED EXTERNAL WEIGHTED W_B PEAK PARTICLE ACCELERATION FROM THE CP USING THE BARKAN'S LAW (LINE).

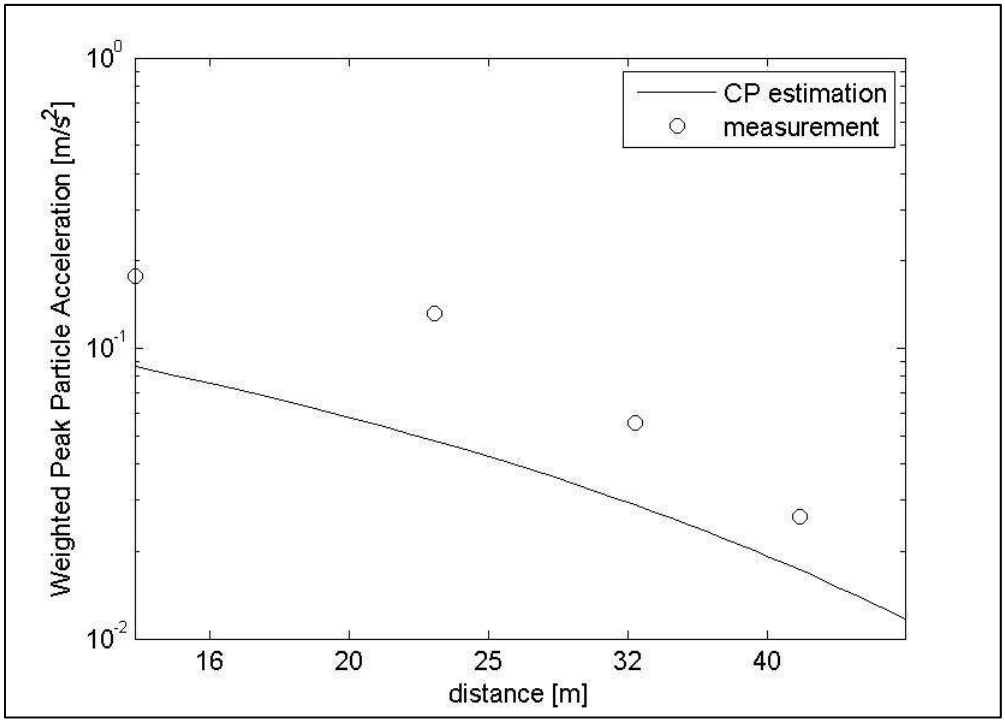

FIGURE 52 - SITE B. W_B WEIGHTED PEAK PARTICLE ACCELERATION (Z COMPONENT) VS DISTANCE FROM THE LINE OF THE WORKS (FIGURE 38). EXTERNAL WEIGHTED W_B PEAK PARTICLE ACCELERATION MEASURED (DOT). ESTIMATED EXTERNAL WEIGHTED W_B PEAK PARTICLE ACCELERATION FROM THE CP USING THE BARKAN'S LAW (LINE).

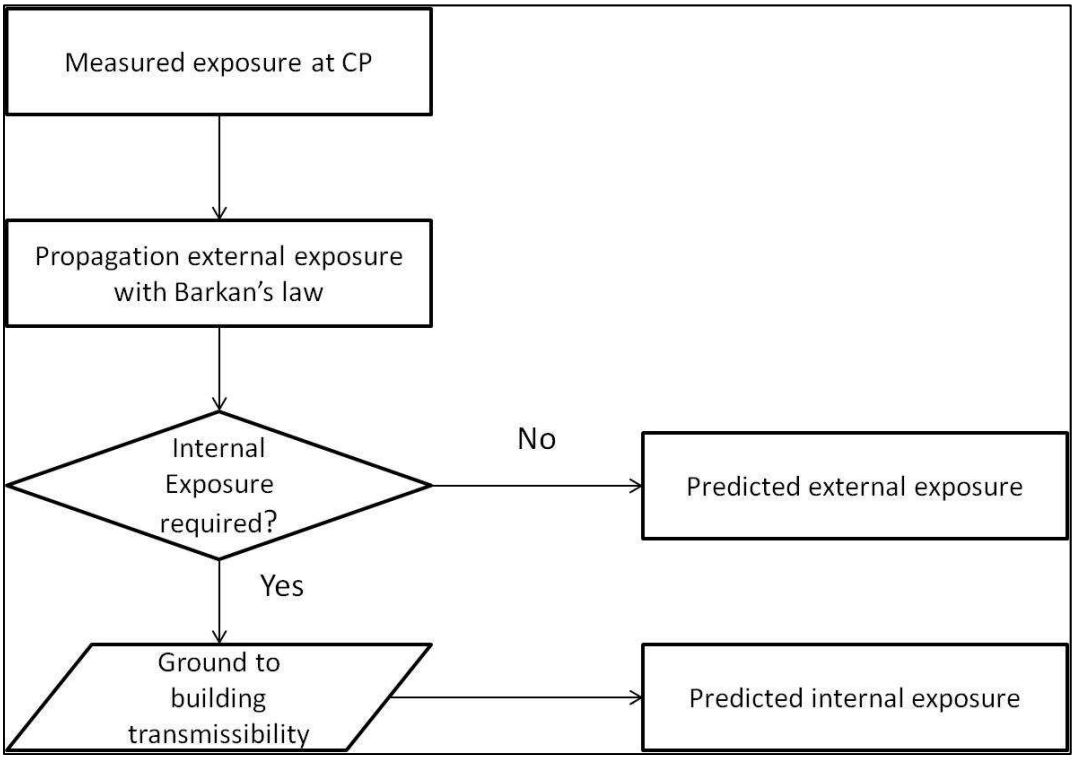

FIGURE 53 - FLOW CHART SHOWING THE STEPS NECESSARY FOR OBTAINING A PREDICTION OF THE EXTERNAL/INTERNAL EXPOSURE FROM A MEASURED ONE AT THE CONTROL POSITION. METHOD APPLICABLE FOR EXPOSURE EXPRESSED AS SINGLE NUMBER OR IN OCTAVE BANDS.

Site A	W RMS	VDV	W PPA	W RMQ
Measured	0.015	0.12	0.12	0.030
Predicted	0.019	0.16	0.16	0.040

TABLE 13 - SITE A PREDICTION OF INTERNAL WEIGHTED WB (W) METRICS COMPARISON

Site B	W RMS	VDV	W PPA	W RMQ
Measured	0.0011	0.048	0.10	0.0057
Predicted	0.0020	0.058	0.10	0.0069

TABLE 14 - SITE B PREDICTION OF INTERNAL WEIGHTED WB (W) METRICS COMPARISON

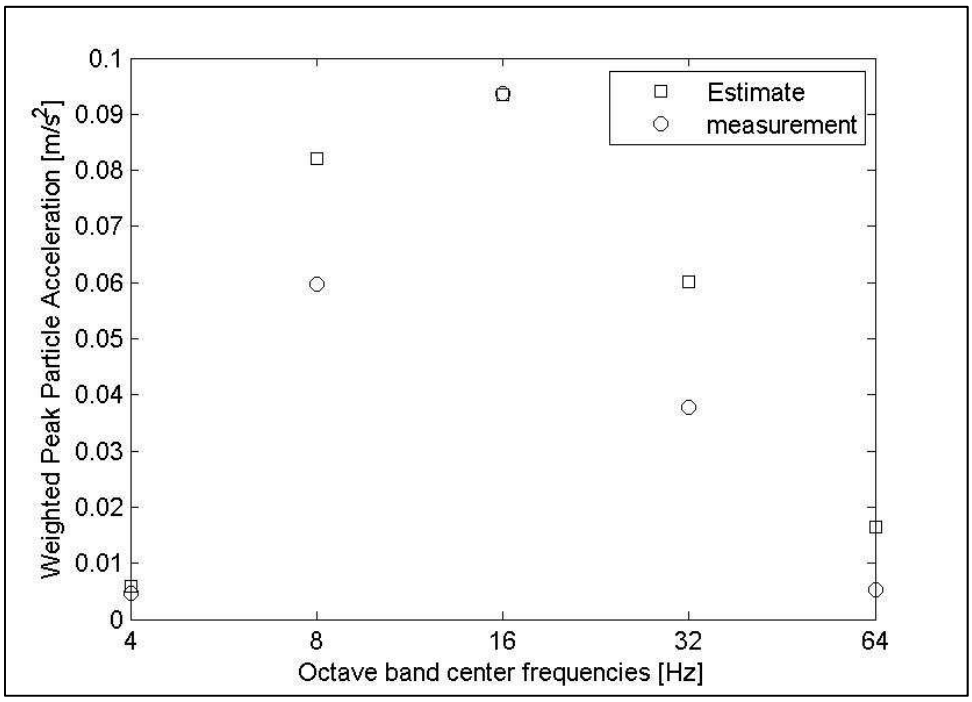

FIGURE 54 - SITE A W_B WEIGHTED PEAK PARTICLE ACCELERATION (Z COMPONENT) IN OCTAVE BANDS. MEASURED INTERNAL EXPOSURE IN W_B WEIGHTED PEAK PARTICLE ACCELERATION (CIRCLE). ESTIMATED INTERNAL EXPOSURE (SQUARE)

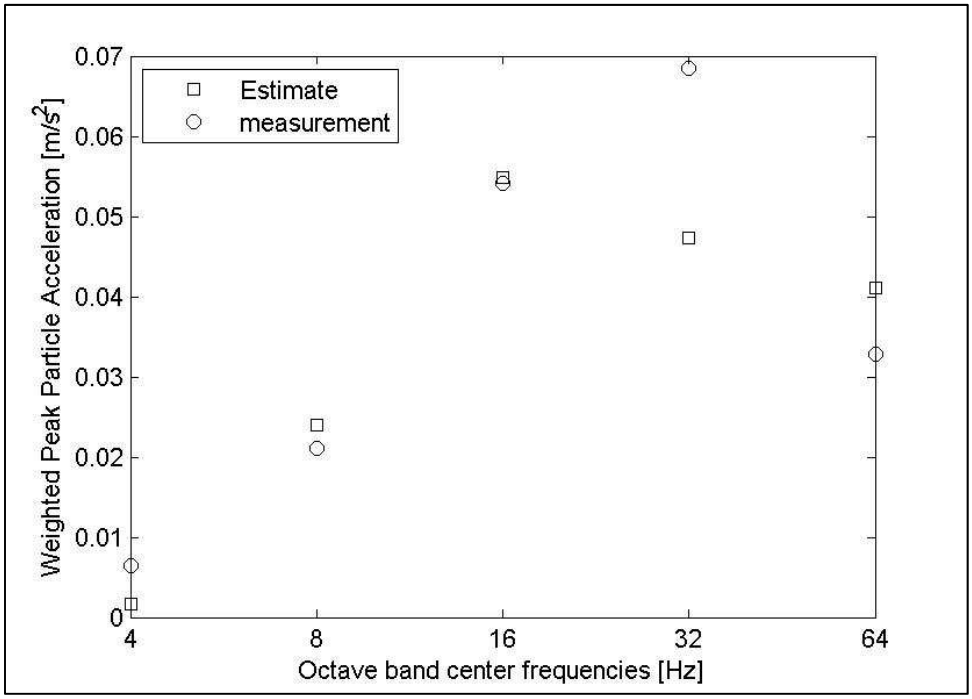

FIGURE 55 - SITE B W_B WEIGHTED PEAK PARTICLE ACCELERATION (Z COMPONENT) IN OCTAVE BANDS. MEASURED INTERNAL EXPOSURE IN W_B WEIGHTED PEAK PARTICLE ACCELERATION (CIRCLE). ESTIMATED INTERNAL EXPOSURE (SQUARE)

The same methodology can be applied for the estimation of the internal exposure in octave bands. Each metric in octave bands, using the Barkan's law, is propagated from the control position using the attenuation coefficients found in the controlled experiments. The exposure is obtained by correcting the exposure level for each band by the ground to building transmissibility defined in 5.4.4. The prediction method has been tested with the same set of data used in the validation of the propagation of single figure metrics. The results of the prediction of the internal exposure expressed in weighted W_b Peak Particle Acceleration (z component) are presented in Figure 54 and Figure 55.

In the prediction of single figure internal metrics the methodology works better for site A where the estimation have been done on a piling source that is more narrowband in comparison with the activity for the other site where the nature of the source is broadband. At site B the largest overestimation is found for the weighted RMS instead the overestimation is smaller for the other metrics. The overestimation can also be assigned in the estimation of the building response using different property type where the measurement position provided a better

estimation of the exposure. The prediction of the metrics in octave bands (Figure 54 and Figure 55) is encouraging for both sites in the estimation of the weighted W_b Peak Particle Acceleration. For site A, Figure 54 shows a slight overestimation in each band preserving the shape of the spectra, whereas for the site B (Figure 55) a better agreement between measurement and estimation has been found with the only exception of the 32 Hz band possibly due to the difference in the actual measurement position and the one used in the estimation of the building response.

Thus, it has been shown that Barkan's law provides reasonable estimates of the external metrics from the control position vibration data with an uncertainty associated with the moving nature of the source. In the case of internal exposure there is less opportunity to validate the results due to the difficulty in obtaining internal measurement positions. For this reason, there is greater confidence in the estimates of the external vibration for the construction sites. This situation is the opposite of that for railways where the internal exposure estimates are based on a dense sampling of internal measurements.

The external and internal exposure estimated for the part of the construction site where the measurement has been taken is assumed to be the same in the other parts of the residential environment exposed to construction activity.

5.6 RESULTS

In this section we finally present the prediction curves used to evaluate the exposure from the construction source. The exposure-response relationships derived from the predicted exposure (Woodcock et al. [97]) are also presented.

First we consider the question of the time period over which the exposure should be calculated. In the case of railway vibration this problem does not occur because the exposure is effectively the same every day (except perhaps weekends), but for the construction sites every day's exposure is different (see Figure 39 and Figure 40). The question then arises as to whether the 'total exposure' accumulated over the entire length of the construction activities would be a more representative indicator of the potential annoyance. The latter would take account of length of

construction programme and it could be argued that this more adequately represents the impact on the residential environment than a daily exposure which takes no account of the length of duration. For example one might expect greater annoyance from a site which continues working for a long period, perhaps years, than one where the work is completed within one day.

If using a daily exposure then a further question arises, since every day's exposure is different, as to which day should be evaluated. One option would be to select a worst case day. An alternative would be to use some measure of the average exposure for the period of construction activities, although in effect, such a measure would relate closely to a total exposure measure. In the absence of definitive information, the exposure has been evaluated on a daily basis, calculated in a 10 hour time window, from 8 a.m. to 6 p.m., which are typical hours of work, for construction during a weekday. In addition, the total exposure has been calculated, although essentially this produces the same data set multiplied by a factor since all residences in the study were assumed to be exposed for the same duration.

Considering the highest daily exposure, for Site A the maximum daily exposure by the piling operations is reached on the 21st day of long term monitoring as shown in Figure 39. In Figure 56 the decay of the external VDV (z component) with distance is presented. The exposure is evaluated from the long term monitoring (control) position at 6 meters from the site boundary (see section 5.3.3) and has been propagated according to Barkan's law incorporating the soil attenuation factors for the site obtained in section 5.4.2. For site B, the maximum daily exposure caused by the pavement breaking/shallow excavation occurs on the third day of long term monitoring from Figure 40. The maximum daily exposure is propagated from the control position data at 14 meters from the origin of the reference system as defined in section 5.3.3. The decay of the external VDV (z component) is also presented in Figure 56.

As the vibration exposure is a cumulative value, the total vibration exposure has been calculated for both sites during the entire monitoring period. For site A, a

total VDV (z component) of 0.27 $m/s^{1.75}$ has been found over 62 days of monitoring whereas for site B the value is 0.19 $m/s^{1.75}$ over 37 days of monitoring. The value obtained has been propagated from the control position using Barkan's law as before. The results are shown for both sites in Figure 57.

The exposure curves presented in this section combined with the annoyance data, gathered trough the response measurement, have been used for building the exposure response relationship for construction sources.

Each resident participating to the survey lives at a certain perpendicular distance from the vibration source in the reference system identified in section 5.3.3, depending on the construction site. Knowing the distance from the source, the associated external exposure is obtained using the relationship (5.5) during the day of maximum activity.

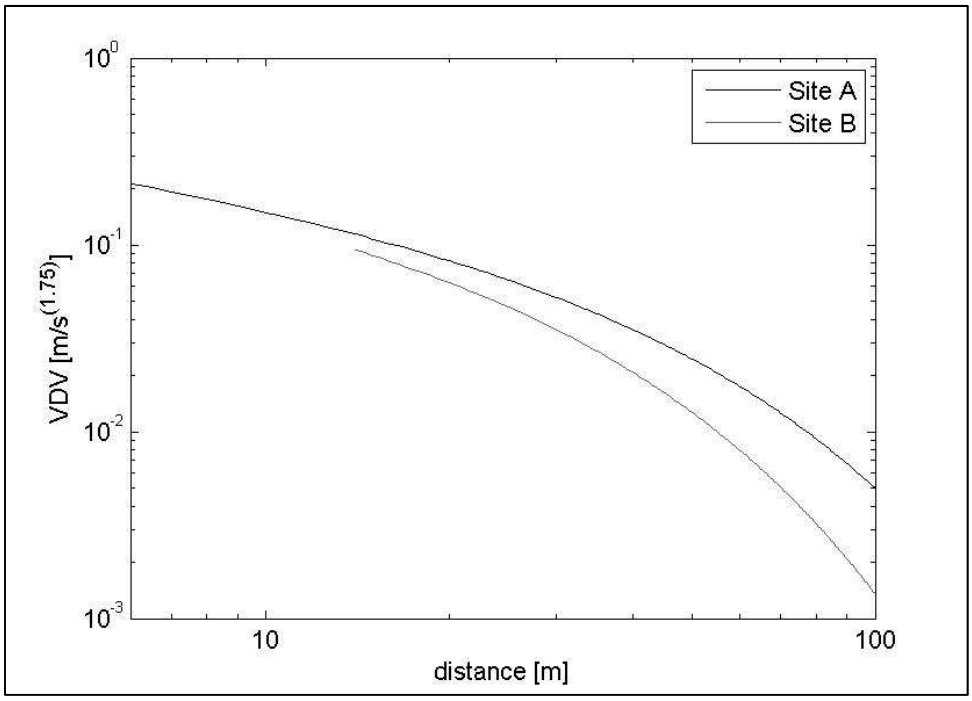

FIGURE 56 - VDV (Z COMPONENT) VS DISTANCE.EXTERNAL MAXIMUM DAILY EXPOSURE FROM CP WITH BARKAN'S LAW. SITE A (BLACK LINE) PILING OPERATION SITE B (GREY LINE) PAVEMENT BREAKING/SHALLOW EXCAVATION. DAILY EXPOSURE CALCULATES OVER 10 HOURS. GRAPH LOG SCALE

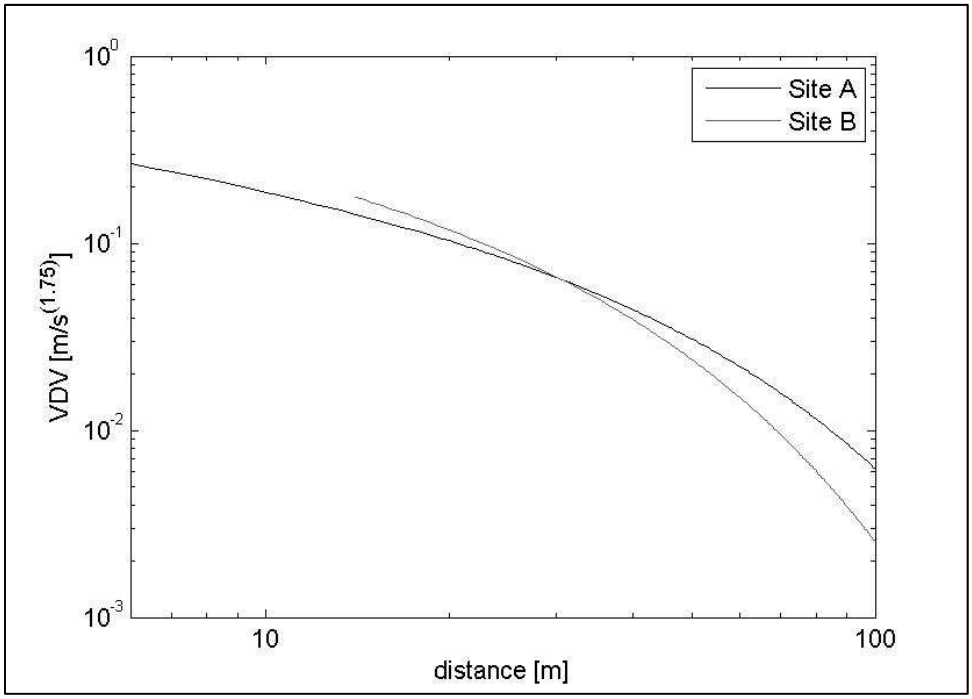

FIGURE 57 - VDV (Z COMPONENT) VS DISTANCE.TOTAL EXTERNAL EXPOSURE PROPAGATED FROM CP WITH BARKAN'S LAW. SITE A (BLACK LINE) EXPOSURE CALCULATED OVER 62 DAYS. SITE B (GREY LINE) EXPOSURE CALCULATED OVER 37 DAYS. GRAPH LOG SCALE

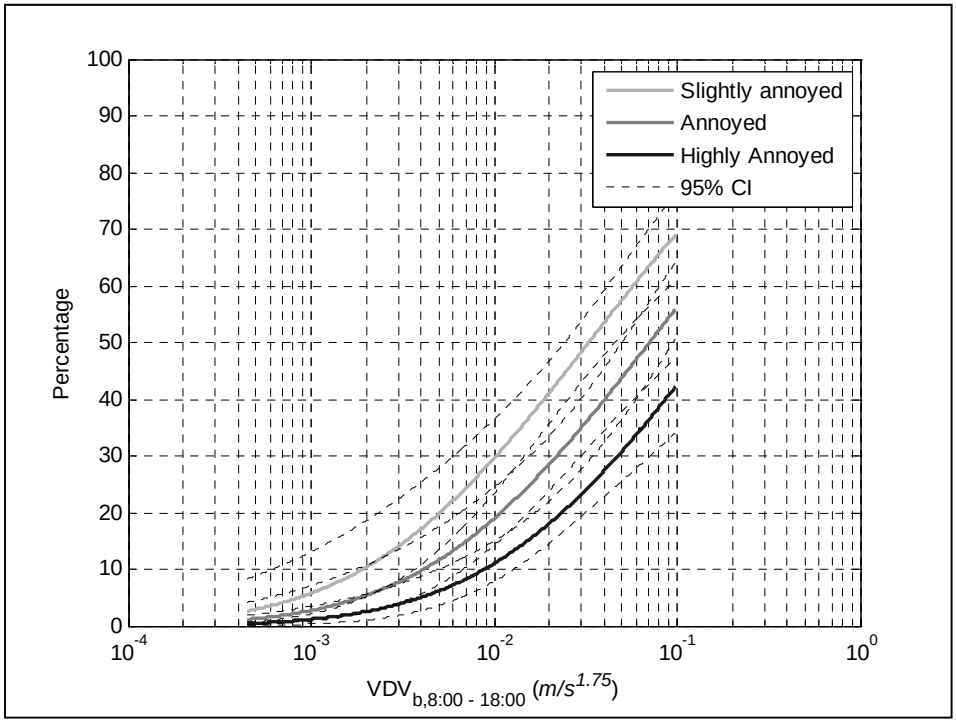

FIGURE 58 - PROPORTION OF PEOPLE REPORTING DIFFERENT DEGREES OF ANNOYANCE FOR A GIVEN VIBRATION EXPOSURE CAUSED BY CONSTRUCTION ACTIVITY (FROM WOODCOCK ET AL. [15]).

Since the exposure propagation curve is valid from the control position, as explained in this section, all the residences with a distance before the long term

monitoring point have been coded with the same value of exposure at the control position. The result of this method provides the exposure-response relationship in Figure 58 for 350 case studies as reported in Woodcock et al. [15].

5.7 CONCLUSION

Construction activity is the product of different operations involved in a construction process. In order to produce a sample of sufficient size it is necessary to consider large scale construction operations, both in terms of dimension and duration of the works. The survey has been conducted using light railway construction works which has the advantage that essentially the same operations are repeated along the length of the track, thereby causing similar vibration exposure in a variety of residential areas. The exposure estimation relies more on prediction which is based on semi-empirical relationships well known in the construction field.

As with railways, a long term monitoring (control) position is employed at the boundary between the construction site and the living environment. Monitoring takes place during the operations which, in consultation with the construction manager, are considered likely to be felt by the residents. The control position is used to record the entire life cycle of the construction operations which required 63 and 36 days respectively on two different sites. More intensive measurements, consisting of an internal position and an external array, have also been conducted alongside the long-term monitoring during the days of major activity. These measurements are then used to estimate the properties of the ground involved in the propagation of the vibration across the residential environment by curve-fitting the well-established semi-empirical relationship, Barkan's law.

Having characterised the ground in this way the exposure recorded at the control position can then be 'propagated' through the residential environment by calculation. The internal exposure is obtained using a velocity ratio to correct for the attenuation from the ground to the internal positions.

The exposure is evaluated both as a 'daily dose' for the day maximum exposure and as a 'total dose' for the entire monitoring period. It has been shown that Barkan's law provide a reliable propagation of the external exposure from the control position with a maximum overestimation of 30% for the exposure metrics considered. Further research is needed for the validation of the methodology in the assessment of the internal exposure.

With the methodology presented in this chapter, the first exposure response relationship has been derived for a "non-steady state" problem. The latter is very important in order to evaluate the community response to vibration in a situation where the source is starting to affect the living environment.

PART TWO: ANALYSIS.

"...It's ok to reach out for wonderful

but on your way to wonderful

you are gonna have to pass thorugh alright

and when you get to alright

take a good look around and get use it

because that maybe as far as you gonna go..."

Bill Whiters from "Still Bill"

6 WAVES IN SOIL: A REVIEW.

6.1 INTRODUCTION

The second part of this dissertation is oriented to the analysis of vibration signals. Two problems, which are correlated to the assessment of the human exposure, are investigated: the wave field assessment and the ground to building transmissibility. The common element of the two issues mentioned above is the propagation of elastic waves in soil. As a consequence, the latter is the main topic of this section providing the "literature background" of the following analysis chapters.

The range of the physical perception of vibration is typically given between 1 and 80 Hz, the upper end of which overlaps with the low frequency part of the audible spectrum. On the other hand the range for the evaluation of the human exposure is also contained in the high frequency range of seismology/geophysics, which is up to 100 Hz, and in the range used in geotechnical engineering that is up to 200 Hz. As a consequence, the problem of human exposure requires a framework that goes beyond what is normally used in acoustics. The use of a seismological/geophysical/geotechnical framework opens different methodologies for soil investigation which might be beneficial to the acoustic community in dealing with groundborne vibration problems. The acoustic community recognized the importance of the local ground response and its influence on the building response for assessing vibration exposure from railways, construction and operation in residential environments.

Geophysics and geotechnicians have developed a large body of techniques for determining local ground properties such as soil layering, wave speed in soil, soil amplification and soil damping. These methods can be divided into laboratory and field or in situ tests, which are grouped into active and passive methods. Active methods are more popular than Passive methods among acoustics researcher.

Passive in situ tests exploit the analysis of ambient vibrations or microtremors for the determination of local ground properties. Ambient vibrations are the upper range of the seismic range (above 1 Hz) which include railway vibration from construction and operation: this implies that these vibration sources can be suitable for ground exploration. A number of applications of seismic passive in situ tests based on vibration from railway construction and operation are discussed in this chapter, together with the description of active and passive in situ tests.

In order to use man made vibrations for investigating soil and propagation characteristics, seismological and geotechnical methods can be used for determining which kind of waves are propagating in the soil. Propagation and wave field assessment methods are also discussed in this chapter together with the ground induced vibration in buildings.

First of all, the problem of the wave propagation in soil is formulated in section 6.2. Then, the methodology for the assessment of soil properties and propagation characteristics are discussed in section 6.3 and 6.4. The wave field assessment is discussed in section 6.5 . Finally, the ground induced vibrations in building are presented in section 6.6.

6.2 FORMULATION OF THE PROBLEM

Considering the scenario described in Figure 6, our attention is going to be focussed on the first two elements of the residential environments: the source and the soil. Depending on the source characteristics explained in 4.2 and 5.2, manmade processes, such as railway or construction, excite the soil generating different waves or propagation modes into the ground.

6.2.1 LAMB PROBLEMS

These problems can be classified, in the first instance, as “Lamb problems” [98]. Lamb investigated the wave motion generated at the surface of an elastic half-

space by the application of concentrated loads at the surface or inside the half space by line load and a point load. A detailed solution of these problems can be found in Achebanch [99], Aki and Richards [100] and Ewing et al. [101].

6.2.2 BODY WAVES AND SUPERFICIAL WAVES

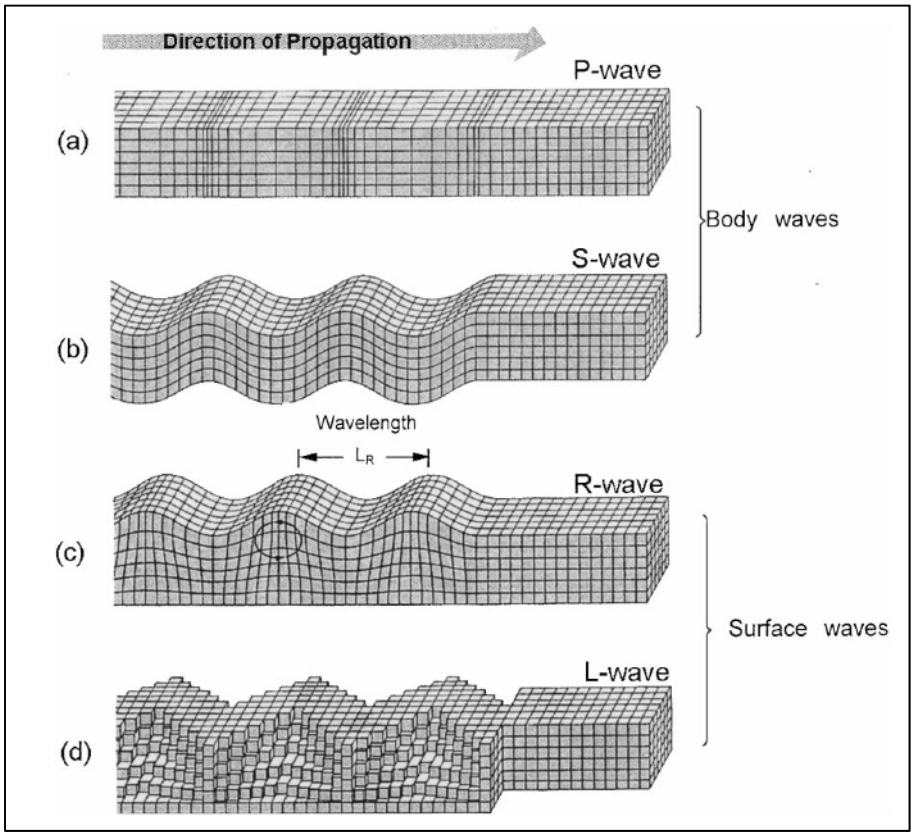

FIGURE 59 - ELASTIC WAVES PROPAGATING ON THE FREE SURFACE: (A) COMPRESSIONAL WAVES; (B) SHEAR WAVES; (C) RAYLEIGH WAVES; (D) LOVE WAVES (FROM ATHANASOPOULS ET AL. [92]) .

If only the activity at the free surface is considered, waves into the ground can be classified in two families: body and superficial waves shown in Figure 59 from Athanasopouls et al. [92].

Body waves are generated in the interior of the ground and can be grouped as P and S waves. P waves (Figure 59 (a)) are longitudinal (or compressional) body waves which pass through a medium as a series of dilations and compressions (Lowrie [102]). Therefore, P waves are pressure waves and they can travel through any type of material with the fastest speed. In soil their speed V_P can be expressed as:

$$V_P = \sqrt{\frac{\lambda + G}{\rho}} \tag{6.1}$$

where λ_L and G are the Lamé constants and ρ is the density. In air, they take the form of sound waves; hence they travel at the speed of sound.

S waves (Figure 59 (b)) are transversal body waves akin to that seen when a rope is shaken. Vertical planes move up and down and adjacent elements of the medium experience shape distortions, changing repeatedly from a rectangle to a parallelogram and back. Adjacent elements of the medium suffer vertical shear (Lowrie [102]). S waves are often referred to as Shear waves or secondary waves because they travel more slowly than a P waves with a speed V_S expressed as:

$$V_S = \sqrt{\frac{G}{\rho}} \tag{6.2}$$

The only elastic property that determines the velocity of the shear wave is the rigidity or shear modulus G. The general shear-wave motion within the plane of the wavefront can be resolved into two orthogonal components: one polarized in the horizontal plane called SH-wave and the other called SV-wave which is polarized in the vertical plane containing the ray path[8].

At the free surface of a medium, groundborne vibration propagates away from the source as a surface waves. In a similar way to the body waves, superficial waves can be divided in two categories sometimes called: Rayleigh waves (R-wave Figure 59 (c)) and Love waves (L-wave Figure 59 (d)). The difference among these wave types can be found in the particle motion of their wavefront.

Rayleigh waves took their name from Lord Rayleigh who studied the propagation of a surface wave along the free surface of a semi-infinite elastic half space in 1885. Rayleigh waves can be considered as a combination of the P and SV waves and are polarized for vibrating in the vertical plane. The particle motion is a retrograde ellipse in the vertical plane with its major axis vertical and minor axis in the

[8] The direction perpendicular to the wavefront is called the seismic ray path.

direction of wave propagation. Particles below the surface are also affected by the passage of the Rayleigh wave with the amplitude decreasing exponentially with the depth in a uniform half space. The speed of the Rayleigh waves depends mainly on the shear-wave velocity V_S: in a homogeneous half-space the Rayleigh-wave velocity V_R is slightly lower than V_S depending on Poisson's ratio (Richart et al. [86]) as shown in (6.3).

$$0.87V_S < V_R < 0.96V_S \tag{6.3}$$

Love waves are surface waves, essentially horizontally polarized waves (SH waves), guided by an elastic layer which is "welded" to an elastic half space on one side while bordering the free surface on the other side. Theory shows that the speed of Love waves with very short wavelengths is close to the slower velocity V_{S1} of the upper layer whereas long wavelengths travel at a speed close to the faster velocity V_{S2}. This dependence between velocity and wavelength or frequency is called dispersion. Therefore, the velocity of the Love waves V_L lies between these two extreme values:

$$V_{S1} < V_L < V_{S2} \tag{6.4}$$

Love waves travel with a slower velocity than P- or S- waves, but faster than Rayleigh waves.

6.2.3 THE EFFECT OF THE SOIL PROFILE

The wave types mentioned above will change their propagation characteristics accordingly with the nature of the medium that they are crossing also known as the soil profile. The simplest situation that can be found is that our soil profile is homogeneous which can be approximated with an elastic half-space. In this case, P-waves and S-waves propagate in all directions away from the source, and hence suffer substantial geometric attenuation, as well as losses due to the damping proprieties of the ground. Manmade sources at the free surface impart most of their energy in surface waves: in a homogeneous half-space, approximately 67% of

the energy of a vertical circular footing, in Figure 60, is radiated as Rayleigh waves (Woods [103]). This is one of the reasons why surface waves often dominate the time histories.

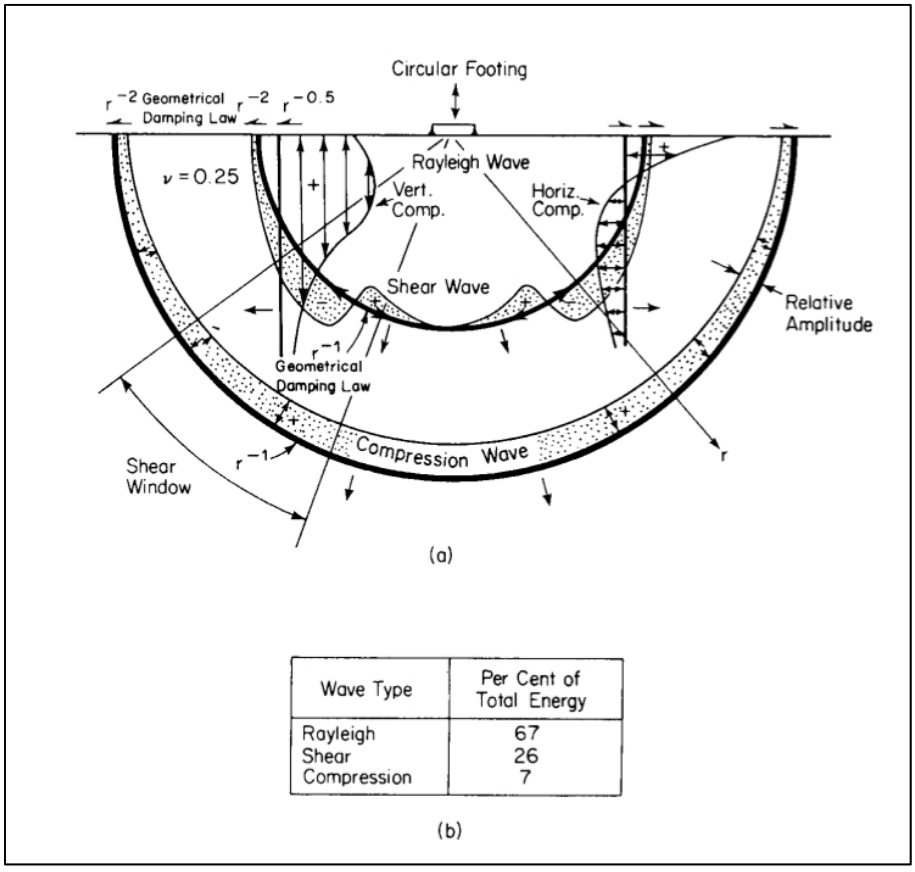

Wave Type	Per Cent of Total Energy
Rayleigh	67
Shear	26
Compression	7

(b)

FIGURE 60 - HARMONIC VERTICAL POINT SOURCE ACTING ON THE SURFACE OF A HOMOGENOUS, ISOTROPIC, LINEAR ELASTIC HALFSPACE: (A) COMPLETE DISPLACEMENT FIELD; (B) PARTITION OF ENERGY BETWEEN DIFFERENT TYPES OF WAVES (FROM WOODS [103]).

In this scenario, Rayleigh waves are not dispersive: there is no dependence of Rayleigh wave velocity on frequency or wavelength, i.e. a homogenous linear elastic medium is characterised by a unique value of Rayleigh wave velocity. Another important remark is that, since the decrease with depth is exponential, the particle motion amplitude becomes rapidly negligible with depth. For this reason it can be assessed that the wave propagation affects a confined superficial zone, hence it is not influenced by mechanical characteristics of layers deeper than about one wavelength (Foti [104]).

In general the medium is heterogeneous and is often modelled by dividing it into parallels layers, in each of which homogeneous conditions are assumed. By

suitable choice of the thickness, density and elastic properties of each layer, real conditions are approximated. One of the particular aspects of S-waves is that in vertically heterogeneous media the propagation is a multimode phenomenon: according to Aki and Richards [94], different modes of propagation can exist at the same frequency, having different distributions of the particle displacements and stresses and having different propagation velocities. From a physical point of view, the existence of different modes of propagation at a given frequency can be explained by the constructive interference occurring among waves (Lai [105]).

The modelling of surface waves in a layered half-space is generally obtained following two approaches: the propagator matrix approach and the method of reflection and transmission coefficients (Lai [105]). The former was originally formulated by Thomson and Haskell and was derived in a finite element formulation, called the dynamic stiffness method, by Kausel and Roësset [106] whereas the latter was initially developed by Kennet.

In a vertically heterogeneous medium, i.e. a layered medium, V_R becomes frequency-dependent and the Rayleigh waves are dispersive. It is related to the layers that are involved in the propagation of a certain wavelength. In fact, the high frequencies (short wavelengths) propagate in thin top layers and their velocity depends on the shallow soil properties whereas the low frequencies (long wavelengths) propagate in thicker layers and their velocity is therefore also influenced by the properties of deeper layers (Socco and Strobbia [107]). In a medium composed of a finite number of homogeneous layers overlaying a homogeneous half-space, the total number of Rayleigh modes of propagation is always finite (Ewing et al. [101]).

It is worth mentioning that the shape of the dispersion curve (Rayleigh phase velocity vs. frequency or wavelength) is strongly related to the variation of stiffness with depth. Usually a distinction is made between a layered system for which the stiffness is monotonically increasing with depth and another one in which there is the presence of stiffer layers over softer ones. The first case is indicated as normally dispersive profile, the latter one as inversely dispersive

profile (Foti [104]). In Figure 61 an idea of the differences between soil profiles mentioned above is shown.

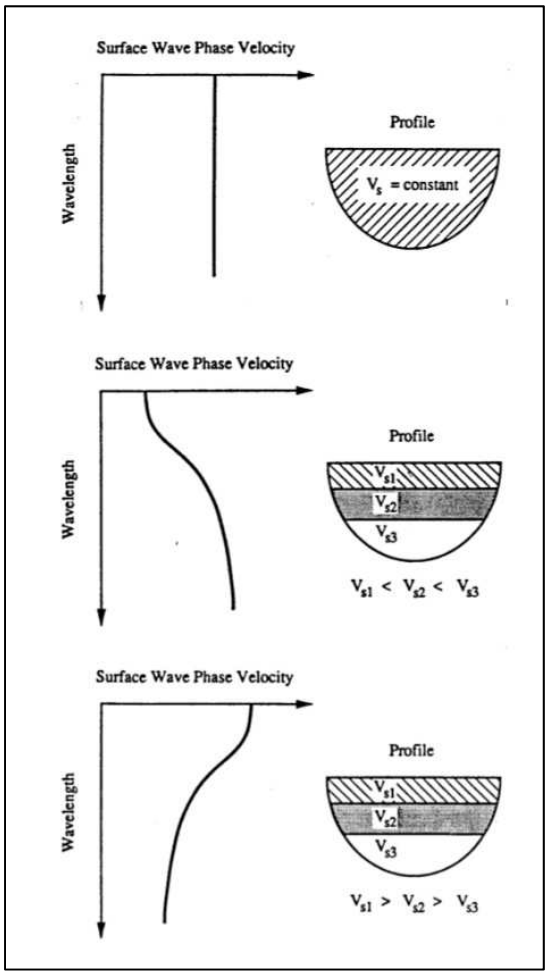

FIGURE 61 – EXAMPLES OF DIFFERENT SOIL PROFILES. FROM THE TOP TO THE BOTTOM: NON DISPERSIVE PROFILE (HOMOGENUOS HALFSPACE), NORMALLY DISPERSIVE AND INVERSELY DISPERSIVE PROFILES (FROM FOTI [104]).

The approaches discussed earlier in the section assumed that the soil layers all run parallel with the surface although this is not always the case. The effect of inclined layers has been investigated by Jones [108] and Jones and Hunt [109] using an approach called thin-layer method (TLM), developed by Kausel in 1994, in relation to groundborne vibration generated by underground trains. The sensitivity of surface vibrations to inclination angle was investigated and the results suggested that small inclination angles of 10^o or less can cause significant variation in rms response of ± 10 dB (Jones and Hunt [109]). This variation was attributed to the refraction of wave energy by the inclined layer.

6.2.4 CONSTITUTE BEHAVIOUR OF SOIL

In the modelling of elastic waves in soil, the latter is usually considered as a linear elastic medium. This linear relationship is called Hooke's law also known as small strain regime which states that the strain in a body is proportional to the stress applied to it. Beyond a certain value of stress, called the proportional limit, Hooke's law no longer holds. Although the material is still elastic the stress-strain relationship is non-linear. If the solid is deformed beyond a certain point, known as elastic limit, it will not recover its original shape when stress is removed. The deformation is said to be plastic. In the plastic range, when the stress is removed the strain does not return to zero; a permanent strain is produced. If the applied stress exceeds the strength of the material a failure occurs (Lowrie [102]). The small strain regime is used for describing the vibration generated by railway traffic in the free field (Houbrechts et al. [110]). This approximation is no longer valid for construction sources like pile driving in the near field because plastic deformations are generated (Masoumi et al. [111]).

6.2.5 THE EFFECT OF WATER

One factor that can change the propagation characteristic of the wave in soil is the presence of water. The latter makes the soil softer encouraging the generation and propagation of low frequency vibrations (Madshus et al. [41]). For taking in account of the water presence, the soil should be modelled as a layered porous isotropic material supported on a homogeneous porous half-space (Nelson [112]). The equations of motion are well described in Biot's original papers concerning wave propagation in porous solids (Biot [113], [114]). For further information please referred to Richart et al. [86].

6.2.6 INHOMOGENEITY AND ANISOTROPY

One of the common approximations done about the soil profile is its homogeneity. Instead, local variabilities are included in the soil properties. According to Jones [108], three sources of soil heterogeneity can readily be identified as: natural inhomogeneity, availability of information and measurement error. Naturally

occurring inhomogeneity is caused by factors such as mineral composition, stress history, moisture content, density, etc. The general trends in soil properties (i.e. significant changes in average properties associated with layering) tend to be accounted for in conventional soil models. Instead, local variations within those layers are difficult to distinguish and it is quite impractical to take sufficient soil samples to accurately map local variations in material properties over the area of interest. Soil profiles must be inferred from a limited number of samples. Finally, measurement and testing errors tend to dilute the value of the samples that have been obtained. A practical method to adequately capture the inherent variation in properties involves a probabilistic model employing random field theory. Jones and Hunt [115] developed a model based on TLM for predicting surface vibration from underground railways through inhomogeneous soil finding that local soil inhomogeneity can significantly affect surface velocity predictions; 90 percent confidence intervals showing 8 dB averages and peak values up to 12 dB are computed.

The approximation of the soil profile through the half space, either homogeneous or layered, is based on the hypothesis of isotropy. This means that the propagation characteristics do not change with the direction. With this assumption it's possible to write the relationships between stress and strain in a simple way. For anisotropic substance this relationships are more complex than in the isotropic case. In fact the elastic parameters are specified by the two parameters λ and G, but as many as 21 parameters may be needed to describe anisotropic elastic behaviour. Wave velocities, which depend on the elastic parameters, vary with direction in an anisotropic medium. Normally, rock can be treated as isotropic (Lowrie [102]).

In this section a general background about the propagation of ground borne vibration in the soil has been given. Considering the point discussed above, it can be said that this phenomenon is complex and it can described only if approximations are used. Since real soils are generally layered, one problem that needs to be considered is the multimode propagation of surface waves. This problem is generally related to the assessment of the soil properties especially in

terms of the soil profile constitution. Another problem is to understand the propagation characteristics of the vibration; in fact, a better knowledge of the wave field components of the perturbation can give us a better knowledge of the soil properties and source mechanisms. Therefore in section 6.3 the assessment of soil properties is considered whereas the assessment of the propagation characteristics is explained in 6.4. The experimental methods for assessing the wave field assessment are presented in section 6.5.

6.3 ASSESSMENT OF SOIL PROPERTIES

In this section an overview of the methods for assessing the soil property is given. The approach used is to divide this methodology in two categories: standard and seismic noise approach.

6.3.1 STANDARD APPROACH

In this section we are going to describe the standard methods that are using for assessing soil properties. These methodologies will be just listed below and will be discussed in details in appendices B, C and D considering Houbrechts et al [110] and Richart et al. [86] as main reference[9]. The standard methods for assessing soil properties are:

- Penetration test - treated in appendix B
- Laboratory tests - treated in appendix B
- Reflection/Refraction survey - treated in appendix C
- Down/up/cross hole tests - treated in appendix C
- Spectral Analysis of Surface Waves (SASW) and Multichannel Analysis of Surface Waves (MASW) - treated in appendix C.
- Imaging techniques (Seismic tomography, Ground Penetration Radar (GPR) and Electrical Resistivity Tomography (ERT)) - treated in appendix D.

[9] Further references will appear if necessary in the appendices

6.3.2 SEISMIC NOISE APPROACH

The methods shown in the previous section can also be defined as "active" because a perturbation is generated for retrieving the soil property. Instead, this section a review of "passive" methods is given where no excitation is used for obtained soil properties. These techniques are based on the study of ambient seismic noise. The origin of the noise itself is not known precisely in the different frequency bands (Larose et al. [116]). For frequencies below 1 Hz, the ambient noise is generally called 'microseisms' and it seems dominated widely by the interaction of the ocean with the solid earth. For frequencies above 1 Hz the noise is identified as 'microtremors'. Around 1 Hz the noise is dominated by the local atmospheric conditions like wind that cannot propagate over large distances. Above 1 Hz the noise consists of manmade processes also known as cultural noise. Since seismic noise has mostly a superficial origin, its predominant part is surface waves. Furthermore, the interest of the analysis of ambient noise recordings became more and more popular over recent decades as it offers a convenient, practical and low cost tool to be used in urbanized areas (Bonnefoy-Claude et al. [117]). As a consequence, these methodologies can be of potential interest to the groundborne vibration community which is more familiar with the methods described in the previous section.

The analysis of seismic noise is generally used for evaluating the effects of the local geology on the ground motion. This effect is called 'site response' and it may modify in a very significant way the effect of ground motion especially in soft soils and it can vary in different part of a city according to the local geology. As a consequence, the site response plays an important role in the definition of the seismic hazard of cities. The latter is generally quantified through the seismic microzonation that is the process of estimating the response of soil layers under earthquake excitations and thus the variation of earthquake characteristics on the ground surface and is the first step for earthquake risk mitigation studies. Furthermore, the study of seismic noise is used for retrieving site response in geotechnical engineering as well. Of course, manmade vibrations are not dangerous like earthquakes but their propagation is affected by the local geology

as pointed out in Dawn and Stanworth [69] and Svinkin [87] therefore these methods can be helpful for a better quantification of the site response, especially in large areas like the one surveyed in NANR209, and decrease the large uncertainties due to the soil profile (Nordtest [25]).

The idea of using noise for ground exploration is not new; in fact it started around the 1950's with the enhancement of seismometers to monitor nuclear tests and the development of seismic arrays. The Japanese seismologist Aki proposed in 1957 an innovative method called spatial autocorrelation (or SPAC) which used ambient vibration measurements to determine the underlying subsoil structure. The explanation of the SPAC method is taken from Chavez-Garcia et al. [118]. The hypotheses done by Aki are two: ambient vibration is stationary in both time and space and the wavefield consists of dispersive waves propagating on the free surface. The microtremors are measured using an array of receivers and the cross correlation function between different pairs of receivers, at the same interstation distance, is measured sampling different orientations on the free surface. Aki showed that the ratio of the average of those different cross correlation functions and the autocorrelation function at a reference station (defined by him as the correlation coefficient) takes the form of a zero-order, first-kind Bessel function. The argument of that Bessel function contains the fixed interstation distance, the frequency, and the phase velocity of the propagating waves.

In recent applications of the SPAC method, such as Chouet et al. [119], the receivers have been disposed on half a circle, with a central station recording simultaneously. This array satisfies a requirement of the method, as it allows the sampling of different azimuths between pairs of stations at the same distance to compute the azimuthal average. With this technique it is then possible to obtain a phase velocity dispersion curve using the records filtered in a series of narrow frequency bands. In 1976, Asten showed that microtremors consisted of Rayleigh waves, and then proceeded to extend the SPAC method to include the possibility of the presence of different modes in the microtremor records. This allowed him to better constrain the geological model deduced from the SPAC measurements

(Chavez-Garcia et al. [118]). The use of SPAC method for obtaining passive seismic tomography from seismic noise is discussed in Larose et al. [116].

The SASW analysis, explained in Appendix C, can be also implemented as passive method. The latter requires recording of microtremors and/or cultural noise by a large number of sensors arranged in two dimensional arrays over the ground surface. Penetration depths with passive methods can range from less than 50 meters with short-period microtremors to several kilometres with long-period microtremors (Tokimatsu in [105]). Passive SASW can be combined with the active method for enhancing the resolution of the analysis in depth (Rix et al. [120]).

As said above, the analysis of seismic noise has its most important application for seismic city microzonation. For this purpose two techniques have been developed: the site-to-reference spectral ratio and the HVSR ratio (the spectral ratio between horizontal and vertical components). The latter will be briefly described because is considered an improvement of the former methodology (Carniel et al. [121]). The HVSR ratio technique was proposed first by Nogoshi and Igarashi in 1971, and then strongly emphasized by Nakamura in 1989 (Bonnefoy-Claude et al. [117]). An explanation of the HVSR method technique can be found in Carniel et al. [121] and Lerno and Chavez-Garcia [122]. The method aims to estimate site response by the spectral ratio between the horizontal and the vertical components of the microtremor motion at the surface (Bonnefoy-Claude et al. [117]). The working hypothesis of Nakamura were: the interpretation of microtremors as Rayleigh waves propagating in a single layer over a half-space and that microtremor motion is due to very local sources, such as traffic in the neighbourhood of the instrument, thus neglecting any contribution from deep sources.

The ability of the HVSR technique to provide reliable information related to site response has been repeatedly shown in the past (Bonnefoy-Claude et al. [117]). However, its theoretical basis is still unclear as two opposite explanations have been proposed. Nakamura, as explained in Bonnefoy-Claude et al. [117], claims that the horizontal to vertical spectral ratio mainly reflects the S-wave resonance in soft surface layer (removing effects of surface waves), and hence that HVSR curves

provide a consistent estimate of the site amplification function. This "body wave" interpretation has been contradicted in several papers (Bonnefoy-Claude et al. [117]) highlighting the relationship between the HVSR and the ellipticity of fundamental mode Rayleigh waves, and thus seriously questioning the existence of any simple direct correlation between HVSR peak value and the actual site amplification factor. This brief summary about the two hypothetical origins of the HVSR peak shows the close link between the composition of the seismic noise wavefield (body or surface waves) and the interpretation of the HVSR curve. The European project called SESAME [123] (Site EffectS assessment using AMbient Excitations), which took place between 2001 and 2004, had as main aim to provide guidelines for a correct use of the Nakamura method in terms of instrumentation, measurement methodology, data processing and interpretation of the HVSR curves. The HVSR method can be performed using a single instrument or in array configuration with the possibility to derive dispersion curve.

For the sources considered in this work, construction and railway traffic, two recent works can be found where the HVSR method is applied.

Harutoonian et al. [124] describe the study of microtremors HVSR based method for assessing compacted ground. Two methods to control this compaction process at a very large site were employed: (a) strictly controlled rolling compaction (b) visually monitored (by naked eye) rolling compaction. The key features of the measured HVSR curves have been studied and analysed to infer useful insights about the compaction achieved by the two methods. Furthermore, the fitting of these measured HVSR curves by trial-and-error forward modelling forms the basis for inferring the shear wave velocity V_S profile and layer thicknesses of the compacted ground. It is shown in this paper that the process of analysing and interpreting the HVSR curves, as well as the forward modelling of the HVSR curves reveal useful information about the quality and consistency of the compacted ground.

Motazedian et al. [125] designed an experiment to observe railway train induced ground vibrations in different site conditions, ten in the Ottawa area, indicating that the durations and amplitudes of the train-induced vibration at the soil sites increased dramatically, in some cases greater than a factor of 100, compared to the reference bedrock site. In the experiment, the HVSR method, among other techniques, was used for estimating site amplification at soil sites. The very high site effect for railway train induced vibration was due to the fact that the speed of train estimated was close to the Rayleigh wave velocity of the soil which was estimated as less than 100 m/s with MASW technique.

Motezedian et al. considered the train as seismic source and the same "vision" is shared by Chen et al. [126] who illustrated that vibrations induced by train, except traditional recognised noises and interference etc., could be used as a seismic source to detect crustal structures with its advantage of abundant frequency spectrum, repeatability and no additional harm to the environment. This approach, as believed by the authors, might bring light to the traditional exploration seismology with the further studies of signal processing and interpretation methods, and related models and new observing systems.

Another seismological approach for the analysis of train vibration can be found by Ditzel et. al [127]. The latter used an array of geophones perpendicular and parallel to the railway for validating his theoretical model for calculating the seismograms generated by a moving train. The predicted vibrations show good agreement with the experimental response; both the computed and measured results clearly show the Doppler effect. Surface waves, generated by oscillating trains, could be observed at large distances from the track, even if the train speed was lower than the speed of the surface waves.

6.4 ASSESSMENT OF PROPAGATION CHARACTERISTICS

6.4.1 MODELLING AND SEMI EMPIRICAL APPROACH

In this section the modelling approach for describing the vibration propagation through the ground caused by manmade process is considered. These problems,

as already said in section 6.2.1, belong to the category of "Lamb problems" and most of the elements essential for analytical studies on the vibration sources and vibration path are contained in his pioneering work of 1904.

Since then, the complexity of the models have grown taking in account the parameters related to both the vibration generation at the source and to the vibration propagation even thanks to the improvements in computational power of the personal computer. For sake of brevity, the modelling of railway vibrations, which is a large subject, will not be treated in this section. More information about the subject can be can be found in the review paper written by Hung and Yang [128] and in the RIVAS report by Mirza et al. [129]

The lack of prediction models for evaluating the environmental effects of construction sources, especially in terms of piling vibration, is highlighted by Masoumi who have proposed, in several papers (Masoumi et al. [111] [130]), prediction models for free field vibration caused by pile driving.

The assessment of the vibration propagation using analytical models can be very difficult due to the complexity of the source mechanisms. Therefore, another way to infer the propagation characteristics is to use theoretical assumptions for fitting experimental data: this approach is called semi empirical. The latter have been used for the exposure assessment caused by construction vibration, see chapter 5, and is treated in Appendix A.

6.4.2 IMPACT METHODS

The methods presented below are based on measurements involving the use of an impact source and series of receivers, geophones or accelerometers, for obtaining the propagation characteristics of the ground. The latter is achieved with the estimation either of the mechanical transfer function or the impulse response function of the soil.

Bovey [131] used the impact method developed mainly for structural work for measuring ground vibration transmission caused by railways. This method measures the mechanical transfer function between various points of a system.

This function gives, as its name implies, the transfer characteristics between two points of the system and yields information in the frequency domain. In order to generate the function, simultaneous analysis must be performed on data signals representing the input force applied at one point of the system and the system response motion measured at the same, or at a different point. The input force is given by a hammer impact whereas the system response is measured by accelerometers. The analysis of data when using the impact method yields the magnitude and phase of the transfer function and also the coherence function, all of which provide information about the quality and reliability of the recorded data.

Nelson and Saurenman [132] developed a method for measuring the soil propagation characteristics ("transfer mobility") from railway traffic. These measurements typically use a large instrumented hammer to generate impulses in the soil. These impulses are measured by an array of accelerometers to characterise the transfer mobility of the ground in a localised area (See Figure 62). These data are then used to develop an estimate of vibration propagation over distance as function of frequency. In fact the impulses are generated along the railways (See Figure 63), in different parts of it simulating a line source, giving also an estimation of the track-bed response. Singleton [133] proposed a modified version of Nelson and Saurenman method (also called winch/weight method) measuring the transfer mobility using MLS excitation generated by a tactile transducer.

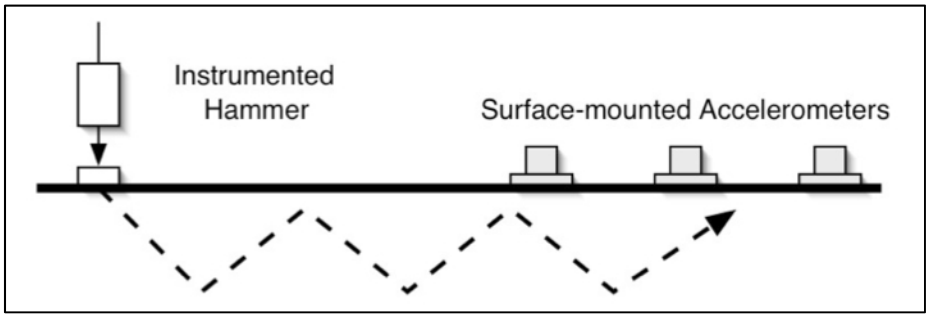

FIGURE 62 – TRANSFER MOBILITY MEASUREMENT SCHEME.

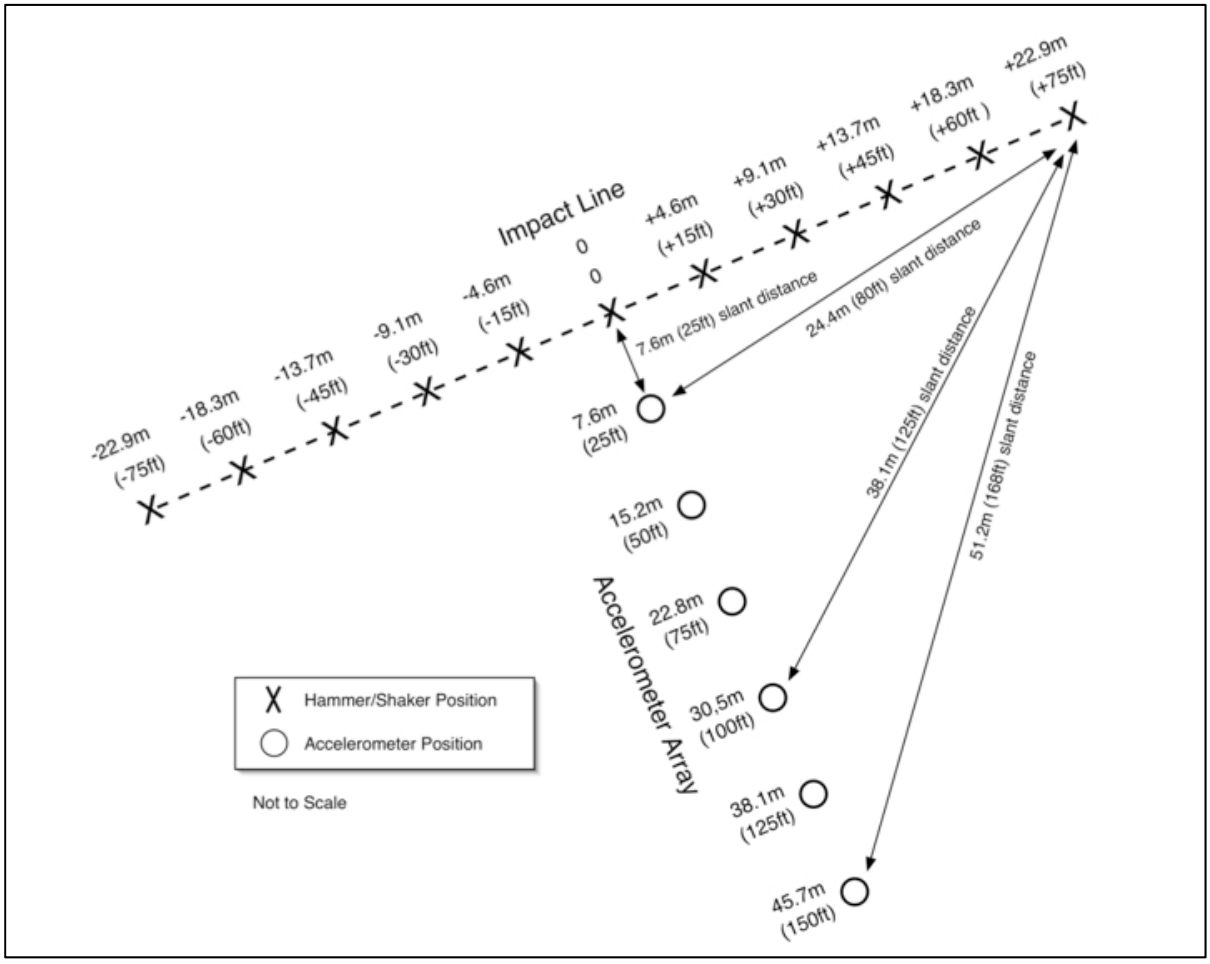

FIGURE 63 – TYPICAL LAYOUT (PLAN VIEW). EXCITATION SOURCE IS PLACED ON "X" POSITIONS TO SIMULATE THE LINE SOURCE. ACCELEROMETERS MEASURE GROUND VIBRATION AT "O" POSITIONS.

In order to predict the vibration in soil and building caused by impact machine Svinkin [87] developed the impulse response function prediction (IRFP) method which is based on the idea of using the impulse response function technique for predicting complete vibration records on existing soils, buildings, and equipment prior to installation of construction and industrial vibration sources under the assumption of small strain. The impulse response function (IRF) estimated experimentally, using the measurement setup in Figure 64, is used for describing the soil and the structures through which waves propagate outward from a vibrating machine foundation. According to the author, experimental IRFs reflect real behaviour of soil and structures without investigation of the soil and structure property. Once the IRF is obtained, the input to the system is the machine foundation motion and the output is the ground motion at any location of interest situated on the surface or within the soil medium or anywhere in a building

subjected to vibrations. Output signals can be obtained, for example, as vibrations records of displacements, velocities, or accelerations at locations of interest.

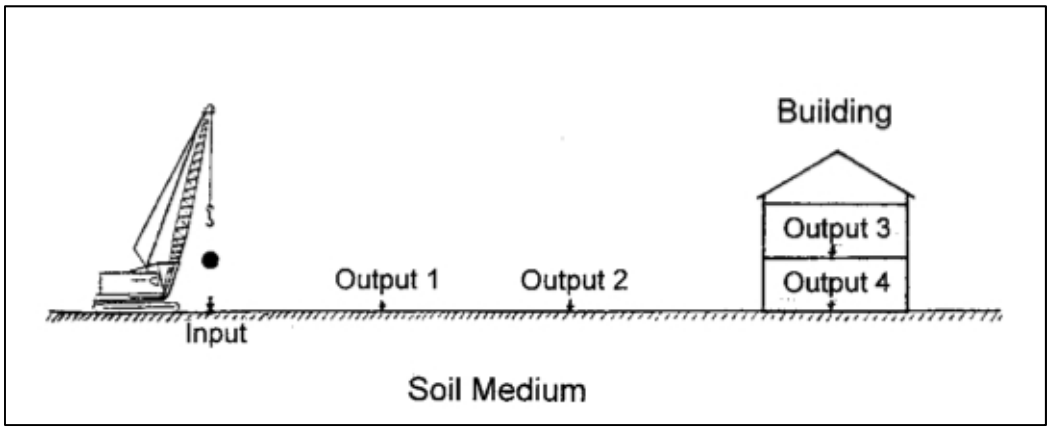

FIGURE 64 - EXPERIMENTAL DETERMINATION OF IMPULSE RESPONSE FUNCTION (FROM SVINKIN [87])

6.5 WAVE FIELD ASSESSMENT

One important aspect of the assessment of the propagation characteristics is to identify which types of wave are included in the disturbance created by the source which is also called wave field assessment. The knowledge of the components of the wave field is strictly linked to the assessment of the dynamic properties of the soil because all the active and passive tests listed in section 6.3 are mainly based either on the estimation of the travel time from body wave or on the estimation of the Rayleigh wave dispersion.

On the other hand, wave field assessment is a useful tool for distinguishing the near field from the far field propagation. Generally, for manmade processes the former is identified with the zone where the propagation characteristics are mainly dominated by the source mechanisms whereas in the latter the wave propagation will mainly reflect the response of the soil dominated by the ground roll and therefore surface waves. Although semi empirical laws, as already shown in Appendix A, can be a way of assessing the wave field, better results can be achieved by analysing the particle motion.

In fact each elastic wave presented in section 6.2.2 “shakes” the soil in a different way characterised by a particular signature generated by the interaction between

the wave and the part of the soil that is excited. This interaction is defined as particle motion which is summarized in the Table 15 for different wave types.

P Wave	Particle motion consists of alternating compression and dilation (extension). Particle motion is parallel to the direction of propagation (longitudinal).
S Wave	Particle motion consists of alternating transverse motion. Particle motion is perpendicular to the direction of propagation (transverse). The Earth's horizontal layers tend to cause mostly SV (in the vertical plane) or horizontal (SH) shear motions.
Rayleigh Wave	Motion is both in the direction of propagation and perpendicular (in a vertical plane), so that the motion is generally elliptical – either prograde or retrograde.
Love Wave	Transverse horizontal motion, perpendicular to the direction of propagation and generally parallel to the Earth's surface.

TABLE 15 - PARTICLE MOTION OF ELASTIC WAVES IN THE GROUND

In the following sections, 6.5.1 and 6.5.2, two experimental method based on the analysis of the particle motion are presented.

6.5.1 PARTICLE MOTION ANALYSIS

When ground vibration data along three orthogonal directions are available, it is possible to plot the particle motion at each point of measurement and obtain valuable information regarding the types of wave propagating away from the source of vibration (Athanasopouls et al. [89]). The particle motion plot is obtained combining the vertical and horizontal time histories of the displacement which can be obtained through singular or double integration depending if ground velocity or acceleration is measured.

Attewell and Farmer [134] introduced the study of the particle motion for assessing the wave field generated by piling vibrations. Analysing the particle motion in the horizontal and vertical plane, they showed that surface vibration induced by driven sheet piles in laminated clay seemed to follow an orbit of retrograde elliptical form similar to but not wholly typical of Rayleigh waves

transmission. In fact the elliptical motion typical of the Rayleigh waves can be clearly seen only at 30 meters from the sources whereas for the other receivers at 10 and 20 meters the particle motion seems more prominent in the horizontal plane indicating a possible mixture of body and surface waves.

Kim and Lee [135] used the velocity particle motion, from a 3D geophone, for inferring the wave type generated by different manmade sources in order to obtain a better characterization of the geometrical attenuation to use in the Barkan's Law which described the vibration attenuation with distance. Analysing the particle motion generated by train induced vibration, they found it was mainly composed of Rayleigh waves with elliptic counter-clockwise motion. However, a significant portion of horizontal shear wave energy was shown in the vertical–transverse plane. The train induced vibration was found to contain 3-directional motions almost evenly, and can be characterized as a mixture of body and surface waves. For piling induced vibration, the particle motions were mostly in the vertical direction, and they can be characterized as a vertical shear wave with a conical wave front. For hydraulic compaction, the particle motions plotted in the vertical–longitudinal and vertical–transverse planes indicated that the major vibrating energy was transmitted by the surface wave with a retrograde ellipse particle motion.

Athanasopoulos and Pelekis [89] analysed the displacement particle motion from sheet pile piling vibration at 2.40 and 11.35 m from the sources. At both distances the elliptical shape of the Rayleigh waves was recognized.

Hwang and Tu [136] presented an extensive study about the ground vibration from dynamic compaction. They showed the particle paths in the plane of vertical and radial directions at 10 meters from the source for different cycle of compaction. The paths of particle motions during the first half cycle looked like flat ellipses rotating in counter clockwise direction. The above characteristics of surface ground motions were almost reproducible in any vibration record of different tamping.

Motazedian et al. [125] analysed the particle motion generated by railway vibration at 500 meters from the source. As noticed by other researchers, the train induced vibration was, however, mainly composed of Rayleigh waves with elliptic counter-clock- wise motion, although the horizontal shear wave energy was also observed in the vertical–transverse plane. They showed that remote train induced vibration was mainly composed of Rayleigh and Love waves, although body waves were present in the particle motion plot.

Foti [104] conducted some experiments to detect the surface wave particle motion that is induced by impulsive sources acting on the ground surface. The main purpose was to investigate their shape in the view of clarifying the relation between Rayleigh waves (that induce an elliptic particle motion) and body waves (that should act as a disturbance when the SASW analysis is performed). At 36 meters from the source the particle motion was elliptical but not retrogrades as expected in a homogeneous elastic medium. Moreover the ellipse axes were not vertical and horizontal as they would have been in a layered elastic medium. At 6 and 12 meters from the source the particle motion was still elliptical but contaminated by incoherent or coherent noise. As a consequence, when the point of detection is moved farther from the source the number of elliptical or quasi-elliptical paths increased. This aspect was associated with mode separation and to the widening of the pulse as the wave travelled along the surface.

6.5.2 POLARIZATION ANALYSIS

As stated in section 6.5, the aim wave field assessment is to identify which types of wave are included in the disturbance generated by manmade processes and is a useful tool for distinguish the near field from the far field propagation. The former is generated by volumetric waves (Arcos et al. [137]) and can be linked to the source mechanism whereas the latter reflects the soil response dominated by surface waves.

As shown in section 6.5.1, particle motion is a tool that is applied for analysing especially construction vibration and in some cases train induced vibration. It is quite a straight forward technique which just relies in plotting displacement or

velocity in two or three dimension although sometimes the interpretation of the particle pattern can be difficult due to the presence of either more wave types or noise in the recording. Therefore, particle motion provides a general insight about the components of the wave field but it doesn't allow them to be separated.

In comparison with the analysis of the particle motion, the polarization analysis, as it will be shown later in this section, is able to provide an in depth wave field assessment because it can separate between volumetric and surface waves and can be used to identify the source location too. On the one hand these features might help to improve the knowledge of the impact of the vibration on structures and people and on the other hand they might be used for a better understanding of the vibration source mechanisms.

The polarization is a property of certain types of waves that describes the orientation of their oscillations and is significant in areas of science and technology dealing with wave propagation, such as optics, geophysics, seismology, telecommunications and radar science.

Polarization analysis, at the end of the 50's, were applied for studying the propagation characteristics of electromagnetic fields in optics and radio transmission and a general description of the polarization theory can be found in Kanasewich [138]. Then, polarization studies were undertaken in geophysics for studying the Earth's magnetic field and in seismology for investigating the propagation characteristics of the seismic waves. The latter induce oscillation in the ground with a distinct direction in the three dimensional space and therefore are suitable for this kind of analysis. In fact, Both P and S waves exhibit a linear degree of polarization because their particle motion acts on one direction: for P waves this is parallel to the direction of the propagation whereas for S waves it is orthogonal. Surface waves of Rayleigh type are generally elliptical polarized in the vertical-radial plane, the fundamental modes displaying retrograde particle motion and the higher modes prograde or retrograde. Surface Love waves are also found to be rectilinearly polarized, but in a horizontal plane orthogonal to the direction of wave propagation (Kanasewich [138]). Microseismic background

noise is generally elliptical polarized, but with little preferred directionality. Signal generated noise can be also polarized but with a random direction (Kanasewich [138]).

The study of the polarization characteristics of seismic wave is mainly achieved using covariance matrix diagonalization techniques (Greenhalgh et al. [139]). The basis of this approach can be found in Flinn [140] for seismic direction finding (SDF) in the time domain. The general idea of the method, which will be explained in detail in section 7.3.3, is that the polarization analysis can be achieved by treating a time windows of a single-station triaxial recording as a covariance matrix, and performing a diagonalization that produces the principal components analysis (PCA) of the energy in the time window (Jackson et al. [141]). The objective of the PCA, explained in detail in section 7.3.2, is to construct linear combinations of the original variables in such a way as to minimize the new variables needed to predict the data (Samson [142]). In this way the receiver is oriented in the reference system of the direction of the propagation of the disturbance and the different modes of propagation can be distinguished. Another way to derive polarization attributes is to use Singular Value Decomposition (SVD) as showed by Jackson et al. [141].

The polarization properties of the seismic signals are described in the work of Samson [143] providing a matrix algebra similar to the one used in quantum mechanics. The same author [142] extended the polarization analysis in the frequency domain. Other methods for estimating the polarization in frequency domain can be found in Esmeroy [144] and Parker et al. [145] who developed a method for frequency dependent polarization analysis using multitapered spectral estimation.

Vidale [146] provided the basis for the complex polarization analysis using the analytic signal. In the time frequency domain, a wavelet approach of the polarization analysis can be found in Kulesh et al. [147] whereas Moriya and Niitsuma [148] provided an approach in the time frequency domain based on the Choi-Williams distribution. Polarization analysis can be carried out using array of

sensor and different approaches have been developed during the years. It is worth mentioning the work of Jurkevics [149], Wagner and Owens [150] and Rutty and Greenlagh [151].

The simplest application of the polarization analysis, as suggested by Vidale [146], would consist of rotating the motion into vertical radial and transverse components and inspect them visually. One can estimate the direction of polarization and perhaps, with some care and patience, determine whether the components are in phase for particular arrivals. This analysis can be used for seismic event location like in Bataille and Chiu [152] and Palo et al. [153].

Since polarization analysis might allow body waves (rectilinear polarization) to be distinguished from surface waves (elliptical polarization) (Jackson et al. [141]), its main application is to devise filters that can be used for extracting a particular wave type of wave from a noisy background (Kanasewich [138]). In seismic exploration, for example, polarization filtering is used for enhancing or rejecting a particular arrival in order to have a better interpretation of reflection or refraction survey like in the work of De Franco and Musacchio [154]. Other applications of the polarization filtering can be found in Perelberg and Hornbostel [155].

The exploitation of polarization characteristics has been used by several researchers for phase identification schemes which are important in automatic trigger algorithms for event detection and localization, like in White et al. [82] , Magotra et al. [156] or Patane and Ferrari [157], or for detecting split shear waves important for the study of anisotropy (Greenhalgh et al. [139]).

As mentioned above, polarization analysis is largely used in seismology and geophysics for analysing the propagation characteristics of seismic events such as earthquakes or volcanic explosions or by active sources, but few applications of this technique can be found for analysing vibration induced by manmade processes where the particle motion analysis seems to be preferred. The techniques presented above have been mainly used for solving geophysical and seismological problems whereas vibrations caused by manmade processes can be

better identified in the category of geotechnical problems: the differences between these two are well explained by Lai [105].

Following Lai [105], the first and most important difference is the scale factor. For seismologists the layer thickness of their stratified Earth is on the order of kilometres, instead geotechnical engineers deal with layers whose size is two or even three order of magnitude smaller. The frequency range involved in the two disciplines is different: seismology has a frequency range on the order of 0.1 whereas geotechnical engineering analyses waves up to 200 Hz fully containing the range of physical perception of vibration. Then, the high frequency seismology range that goes from 1 to 100 Hz coincides with the acoustic low frequency range.

Furthermore, there is a substantial difference in seismology and geotechnical engineering, concerning the distances over which surface waves are detected and recorded with seismometers and geophones. As a result of different spatial and temporal scales involved in these two disciplines, the phenomenon of wave propagation will assume certain unique and distinctive features. In seismology for example, the modes of propagation are in most cases well defined and separated from each other, and seismologists can determine them from the interpretation of time-history records. On the contrary, in geotechnical engineering the wave modes are mostly superimposed rather than separated from each other. It is therefore natural to expect based on these observations, different methods of interpretation.

The second difference between the problems faced by seismologists and geotechnical engineers is that seismologists do not have control over the source of wave energy: earthquakes occur at times, locations and with characteristics (duration, frequency content, source mechanism, etc.) that to this date are not predictable. On the other hand, this is not true for geotechnical/ground borne problems where the occurrence, the location and the features of the source is always known.

Considering the differences highlighted above, in sections 7.4 and 7.5 an early investigations into the polarization properties of the manmade processes considered in this dissertation it will be presented.

6.6 GROUND INDUCED VIBRATIONS IN BUILDINGS

In the source path receiver scheme described in section 3.3.3, the receiver is defined as one a nearby property including its foundation and the soil in the immediate vicinity, which interacts with the foundation. Usually, vibration is strongest in the top floor and increases with the number of floors in the building. At the lower floor levels, vertical vibration tends to dominate, while horizontal vibration becomes stronger higher up. The propagated free field vibration in the ground is transferred to the building foundation through a dynamic soil/foundation interaction, is further propagated and usually amplified through the building structures (Madshus et al. [41]).

The interaction between the vibration generated by source and the building is simply explained below by Dawn and Stanworth [69]. The latter discusses whether the local propagation velocity may play an important role in determining whether or not significant disturbance is caused within a particular building. Considering λ the wavelength of an incoming wave travelling in the ground towards a property, if λ is long compared with the width of the building then its excitation will be purely translational. A similar result could be expected if an integral number of wavelengths match the building width $\lambda = n\Gamma$. On the other hand, the natural sway frequency of the building is expected when $\lambda = \left(n - \frac{1}{2}\right)\Gamma$. Practically, a combination of effects would occur, and several modes of vibration would be available for excitation, including those involving in distortion of the building shell.

The important point highlighted by the authors is that if a building mode is excited, then the correct frequency must be present in the ground vibrations, but also the wavelength in the ground must be properly matched to the building dimension. Therefore, in order to respond at the excitation spectra provided by the ground perturbation a building needs to have appropriate modal frequencies available, the right size, orientation and the correct local propagation velocity in the ground.

The estimation of building response goes through the analysis of the soil-structure-interaction, and the reader can find more information about this topic in Kausel [158] and Wolf and Song [159]. Those methods are based on the approximate soil/foundation impedance functions and lumped mass-spring models of the building, often applied for simpler buildings to simulate the transmission and amplification in the receiver region. For more complex structures, more involved dynamic finite element or boundary methods are needed. Complex numerical models have been created for describing the response of the building under the impact of wave fields generated by road and rail traffic and some examples can be find in Chua et al. [160], Francois et al. [161] and Fiala et al. [162].

A direct estimation of the soil-structure interaction can be obtained with measurement. The latter consists of evaluating the transmissibility between accelerometers: one placed on the ground outside the building and one inside. An overview of the transmissibility measurement is given in section 8.2. Although the measurement methodology based on the transmissibility is suggested, in U.K., by standards such as BS ISO 4866:2010 [58] and guidelines like ANC [27], only limited literature exists for the application of this technique.

D.J. Martin [163] provides a table of floor vibrations in various buildings near to sheet piling operation. In the table an amplification ratio is declared as the ratio between the peak velocities measured inside and outside the building. The same approach can be found in Athanasopouls & Pelekis [89].

In the study conducted by Hunaidi and Tremblay [164] regarding traffic-induced vibration in buildings in Canada, transfer functions were determined between rms acceleration values, in 1/3 octave frequency bands from 8 to 25 Hz, at the following measurement points inside and outside of buildings: between midpoint of first-storey floor and the ground in front of buildings, between midpoint of first-storey floor and the external foundation wall facing the road, and between midpoint of second-storey floor and midpoint of first-storey floor.

Transmissibility measurements across a resilient isolation pad in the column of a building were presented in Newland and Hunt [165] in order to evaluate the vibration isolation caused by railway traffic vibration.

Jakobsen [166] carried out a project for investigating the connection between the vibration level in the ground outside a building and that on the floors of the building. Based upon measurement results from six buildings, a set of typical transfer functions between a point in the ground and points inside buildings were determined.

De Avillez et al. [167] compared, as a method of evaluating a building transfer function, an impact method with actual rail pass-bys and recently collected response with published generalised response curves. The results suggested that, when using the impact method excitation process (point source), the distance of impact location to the building foundation was critical, drastically affecting the resulting transfer function. In addition when using train pass-bys as the excitation process, train length had an influence on the transfer function assessed. The pre-published data were also shown to have limitations for more recent types of construction.

With and Bodare [168] presented a study for using transfer functions to predict vibrations inside a building due to train-induced ground vibrations. It was proposed that knowing the transfer function of a building, the vibrations inside a similar building could be predicted given a known ground motion outside. A comparison was conducted between predicted and measured vibrations inside a building in south-western Sweden due to freight and passenger trains. The transfer function was derived by using a stationary vibrating source. The average particle velocity (1s - r.m.s.) inside the house was calculated with the transfer functions with an average error of 10%, 0.02 mm/s. Prediction was achieved with a standard deviation of 23%, 0.06 mm/s when no filtering of the data was used.

Gallipoli et al. [169] used the HSVR technique for evaluating the soil-structure interaction in estimates of site response of tall buildings. It confirmed that HVSR is

able to detect building fundamental modes and, once known the building frequency, it is also possible to detect the presence of soil-structure interaction.

6.7 CONCLUSION

In this section the soil as the medium of propagation for vibration in residential environment has been considered. The vibration generated by manmade processes can be considered in first approximation as a "Lamb problem" and on the free surface two types of waves can exist: body and surface waves. The main parameters involved in the complex propagation process are: soil profile, constitutive behaviour, water contents, non-homogeneity and anisotropy. The understanding of this problem can be approached either through the assessment of the soil properties, especially in terms of the soil profile constitution, or with the investigation of the propagation characteristics. Generally these two methods can be seen as complementary because the knowledge of the propagation characteristics can be linked to the knowledge of the soil property.

The microtremor features are extensively used in the seismology-geophysics related field, but it has not be completely exploited for the sources considered in this work where active methods or semi empirical approaches are preferred for inferring soil properties. On the other hand, the few applications found in literature (Harutoonian et al. [124], Motazedian et al. [125]) have provided interesting results especially in the determination of the soil amplification factor which affects the propagation of vibration in occupied environment (Dawn and Stanworth [69] , Svinkin [87]).

A direct estimation of the propagation characteristic of the wave field generated by manmade processes can be achieved with the estimation of the particle motion. The particle motion can be estimated using triaxial sensors plotting the displacement, or the velocity on two axes for the interpretation of the wave type generated by the disturbance. Wave field analysis can be improved by exploiting the polarization characteristics of the vibration as it has already been done in seismology and geophysics. In comparison with the particle motion analysis, the polarization analysis is able to provide an in depth wave field assessment which

can help to improve the knowledge of the impact of the vibration on structures and people and to provide a better understanding of the vibration source mechanisms.

7 WAVE FIELD ANALYSIS

7.1 INTRODUCTION

In chapter 5 a semi empirical propagation model has been introduced in order to assess the vibration exposure from construction sources. One of the assumptions made for the model was that Rayleigh waves were dominating the propagation field. Rayleigh waves are considered the dominant component of the wave field generated by manmade processes in the far field where the propagation is mainly dominated by the soil response.

The near field region, instead, is defined as the region where volumetric waves significantly influence the surface vibration level (Arcos et al. [137]). In this area the source mechanisms are still influencing the propagation field generating a different vibration impact on structure and people.

The extent of the near field region can be assessed using an analytical approach, as shown in Arcos et al. ([137]), but in real condition the wave field generated by manmade processes is quite complex phenomena depending on the source mechanism, soil profile and by their interaction. As a consequence, a better understanding of the wave fields generated by manmade process is potentially useful for vibration exposure assessment.

A first step in this direction can be achieved using a detailed wave field assessment. It is common practice, in the case of vibration induced by manmade processes, to evaluate the wave field through the particle motion which can be defined as the motion of the particle of the soil when subjected to the vibration field generated by the source. The particle motion is a powerful tool which permits to have a direct estimation of the field using a tri-axial accelerometer.

Another approach based on the analysis of the evolution of the particle motion is called polarization analysis which is widely used in seismology and geophysics. Polarization analysis is going be applied, for the first time in this chapter, to

disturbance generated by construction sources in order to provide more information about their wave field.

The background and the objectives of the analysis are presented in 7.2, whereas the tools necessary for the analysis are described in 7.3. Then, the results of the early investigation of the polarization properties of piling and railway vibrations can be found in section 7.4 and 7.5. Conclusions are drawn in 7.6.

7.2 BACKGROUND AND OBJECTIVES

An application of the polarization analysis is presented here for analysing the different phases generated by piling and railway vibration using two approximations: the former will be considered as a seismic pulse and the latter as a microtremor.

The seismic pulse can be seen as the simplest disturbance, acting at and below the free surface generated, by manmade vibration generating body and surface waves as shown in Achenbach [99] and Ewing et al. [101]. This approximation is used for performing the polarization analysis on pile induced vibration.

On the other hand, some authors like Bencat [170] and Gaohang et al. [171] have started to refer to train-induced vibration as a 'microtremor'. As explained in section 6.3.2, microtremors are considered as part of the seismic noise which is used in geophysics, seismology and geotechnical engineering to identify the ambient vibrations with frequencies above 1 Hz generated by cultural sources, like railways; it is a powerful tool for investigating the soil amplification factor.

According to Bonnefoy-Claude et al. [117], the microtremor is a mixture of body and surface waves and this definition agrees well with the experimental observations of Kim and Lee [135] and Motazedian et al. [125], presented in section 6.5.1, on the wave field generated by induced vibration from railway conducted using the particle motion analysis. Therefore, in this scenario, railway vibration will be considered as a microtremor. The nature of this propagation field can be seen in the interpretation of the source, considered as train and railway

line, as a mixture of point and line loads which can be found, among others, in Madshus et al. [41] and Kim and Lee [135].

Polarization analysis is a tool that permits a better interpretation of the particle motion by distinguishing body waves from surface waves (Kanasewich [138]). The objective of this chapter is to present an application of this technique for analysing the propagation characteristics of piling and train vibration which can be considered as novel since no previous cases have been found in literature for these two vibration sources. The main aim of the polarization analysis is to identify the body wave motion included in the microtremor generated by these processes. Three reasons are provided for supporting this choice:

1. Body waves are related with a high value of the degree of polarization which means that one dimension is enough to identify their motion. This means that body waves are seismic phases "easy" to identify and can be localized in terms of azimuth and incidence angle.
2. The identification of the body waves can be useful for the understanding of the propagation characteristics of manmade vibrations in the near field.
3. The identification of the near field region can be used for the localization of the vibration sources and for an investigation of the vibration source mechanisms. The latter, especially for railway sources, are not completely understood and are still one of the main points in the European roadmaps for vibration proposed by The European Rail Research Advisory Council (ERRAC) [172].

7.3 ANALYSIS TOOLS

In this section, the tools necessary for performing the polarization analysis are presented. For analysing the variation of the frequency content over the time of the vibration signals a time frequency representation, see 7.3.1, will be used focussing the attention on the Wigner Ville distribution. Then in order to perform the polarization analysis, explained in section 7.3.3 in time and frequency domain, the concept of principal component analysis is illustrated in section 7.3.2.

7.3.1 TIME FREQUENCY REPRESENTATIONS

The description of how the spectral content of a signal changes with time is possible using its time frequency representation. According to Cohen [173], the power of standard Fourier analysis is that it allows the decomposition of a signal into individual frequency components and establishes the relative intensity of each component. The energy spectrum does not, however, tell us when those frequencies occurred. This information can be obtained by computing the Fourier transform with a temporally shifted window. This approach to time-frequency analysis is known as the Short Time Fourier Transform (STFT). The window function is commonly parameterized by window size, overlap, and taper. Once the window function has been chosen for the STFT, temporal and spectral resolutions are fixed for the entire time-frequency map (Liu et al. [174]). This last characteristic can be seen as a limitation of this approach especially if the spectral contents of the signal changes rapidly because SFTF cannot precisely present a spectrum that changes with time (Moriya and Niitsuma [148]). In order to overcome this problem, work has been carried out on alternative methods of studying time-varying frequency spectra which involves ways of calculating joint time frequency distributions with no loss of resolution.

One of these methods was introduced in signal processing in 1948 by Ville who introduced a quadratic form studied by Wigner in a 1932 article on quantum thermodynamic:

$$P_{WVD}[x(t,f)] = \int_{-\infty}^{\infty} x\left(t+\frac{\tau}{2}\right)x^{*}\left(t-\frac{\tau}{2}\right)e^{-i\tau 2\pi f}d\tau \tag{7.1}$$

The Wigner-Ville distribution (WVD), in (7.1), is a time frequency energy density based on the use of the autocorrelation function of the signal x for calculating the power spectrum. WVD varies resolution in the time-frequency plane by providing good temporal resolution at high frequencies and good frequency resolution at low-frequency (Cohen [173]). Among the properties of the WVD, which are discussed in detail in Auger [175] and Mallat [176], it is important to mention the covariance under time and frequency translation:

$$x(t) = g(t - t_0) \Rightarrow P_{WVD}\left[x(t, f)\right] = P_{WVD}\left[g(t - t_0, f)\right] \tag{7.2}$$

$$x(t) = e^{i2\pi f_0 t} g(t) \Rightarrow P_{WD}\left[x(t, f)\right] = P_{WD}\left[g(t, f - f_0)\right] \tag{7.3}$$

Therefore if x is translated in time or frequency, its WVD is also translated. The WVD is unitary, which implies energy conservation properties, but it misses one fundamental property of an energy density: positivity (Mallat [176]). WVD seems to be an ideal tool for analysing the time frequency features of a signal but due to the quadratic properties of the distribution can create interferences (Mallat [176]). These spurious values, which are due to the so-called cross terms, are particularly prevalent for multi component signals (Cohen [173]). Let $x = x_1 + x_2$ be a composite signal, its WVD can be expressed as follow,

$$P_{WVD}\left[x(t, f)\right] = P_{WVD}\left[x_1(t, f)\right] + P_{WVD}\left[x_1(t, f)\right] + I\left[x_1(t, f), x_2(t, f)\right] \tag{7.4}$$

$$I\left[x_1(t, f), x_2(t, f)\right] = P_{WVD}\left[x_1(t, f), x_2(t, f)\right] + P_{WVD}\left[x_2(t, f), x_1(t, f)\right] \tag{7.5}$$

Where $I\left[x_1(t, f), x_2(t, f)\right]$ is the interference term and $P_{WVD}\left[x_1(t, f), x_2(t, f)\right]$ is the cross WVD of two signals

$$P_{WVD}\left[x_1(t, f), x_2(t, f)\right] = \int_{-\infty}^{\infty} x_1\left(t + \frac{\tau}{2}\right) x_2^*\left(t + \frac{\tau}{2}\right) e^{-i\tau 2\pi f} d\tau \tag{7.6}$$

Equation (7.5) may lead to an erroneous visual interpretation of the signal's time-frequency structure (Auger and Fladrin [177]) creating non-zero values at unexpected locations of the time frequency plane. These interferences can be removed by averaging the WVD with appropriate kernels which yield positive time-frequency densities. The use of kernels might reduce the time-frequency resolution but open up to the creation of several time frequency distributions which make possible to apply WVD in real situation.

Cohen introduced a general class of quadratic time frequency distributions which satisfy the time translation and frequency modulation invariance properties (7.2) and (7.3) (Mallat [176]). This approach characterizes time-frequency distributions

by an auxiliary function called the kernel function. The properties of a particular distribution are reflected by simple constraints on the kernel which implies that it is possible to choose those kernels with prescribed and desirable properties. Both STFT and WVD fulfil (7.2) and (7.3) belonging to Cohen's class. The latter admits at least three equivalent definitions (Auger [175]). The one used in this dissertation is called Time-frequency parameterization, via $\phi_{t-f}(t, f)$:

$$C\left[x(t,f)\right] = \int_{-\infty}^{\infty}\int_{-\infty}^{\infty} \phi_{t-f}(t-v, f-u) P_{WVD}\left[x(v,u)\right] dv du = \phi_{t-f}(t,f) \otimes P_{WVD}\left[x(t,f)\right] \quad (7.7)$$

where $P_{WVD}\left[x(t, f)\right]$ is the WVD (equation (7.1)), that is the simplest distribution of the Cohen's Class (Cohen [173]), whereas $\phi_{t-f}(t, f)$ is the kernel. As a consequence, the Cohen's class is obtained by low-pass filtering (symbol $\otimes$ stands for convolution) the WVD in time and frequency (Mallat [176]).

Choi and Williams found a kernel for which the non-zeroes values are minimal and succeeded in devising a distribution that behaves remarkably well, and that reduces to a large extent the spurious cross terms for multi component signals (Cohen [173]). The kernel $\phi_{CW}(t, f, \sigma)$ is:

$$\phi_{CW}(t, f, \sigma) = e^{-f^2 t^2/\sigma} \quad (7.8)$$

σ is a scaling factor: $\sigma > 1$ is used for signals whose amplitude and frequency are changing quickly whereas $\sigma \leq 1$ is recommended for signals whose amplitude and frequency are changing slowly. Using (7.7), the Choi-Williams distribution (CWD) can be express as:

$$P_{CWD}\left[x(t, f)\right] = \phi_{CW}(t, f) \otimes P_{WD}\left[x(t, f)\right] \quad (7.9)$$

Applying a kernel $\phi_{t-f}(t, f)$ such that:

$$\phi_{t-f}(t, f) = g(t)H(f) \quad (7.10)$$

,where $H(f)$ is the Fourier transform of $h(t)$, in (7.7) allows a progressive, independent control in both time and frequency of the smoothing applied to the

WVD. This approach is also known as the Smoothed-Pseudo-Wigner-Ville distribution (SPWVD), reported in (7.11), which corresponds to the windowed version in time and frequency of the WVD.

$$P_{SPWVD}\left[x(t,f)\right]=\int_{-\infty}^{\infty}h_1(\tau)\int_{-\infty}^{\infty}h_2(u-t)x_a\left(u+\frac{\tau}{2}\right)x_a^*\left(u-\frac{\tau}{2}\right)due^{-i\tau 2\pi f}d\tau \qquad (7.11)$$

Where x_a is the analytic signal of x, h_1 and h_2 are two real even windows, like hanning windows, with $h_1(0)=h_2(0)=1$ (Auger and Flandrin [177]). The compromise of the SFTF between time and frequency resolution introduced at the beginning of the section, it is now replaced by a compromise between joint time-frequency resolution and the level of interference terms.

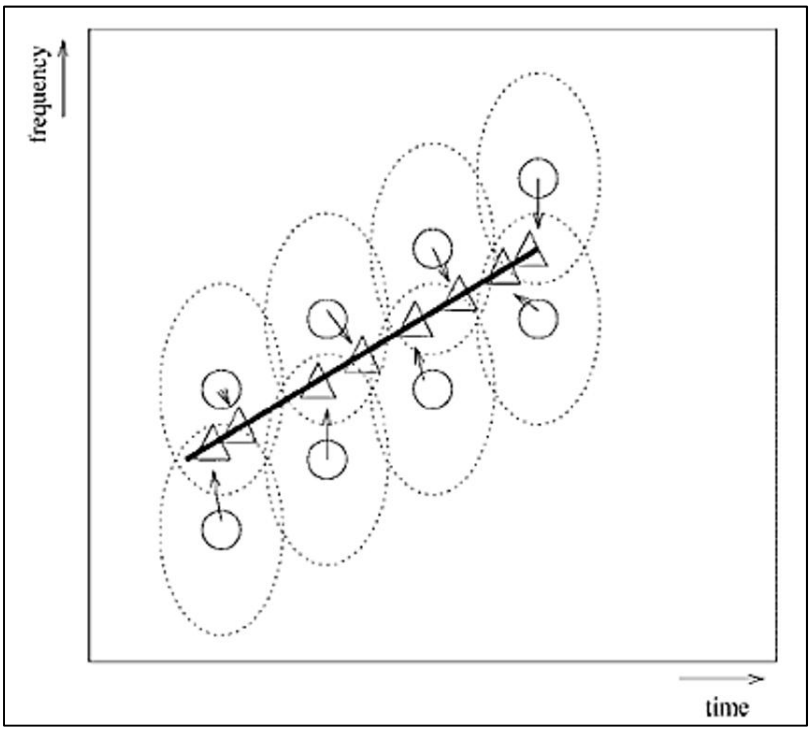

FIGURE 65 - PRINCIPLE OF REASSIGNMENT METHOD (FROM LAND [179]) .

An improvement of the time frequency estimation of a signal using the WVD can be achieved using the reassignment method developed by Auger et al. [177] assuming that there are no physical reasons for the energy distribution to be symmetric in the vicinity of each time-frequency point. According to Flandrin et al. [178], a much more meaningful choice is to assign the total mass of the centre of gravity of the distribution within the domain.

The principle of the reassignment method is explained in Figure 65 for a linear chirp. The dashed ellipse represents the analysis window in the time frequency domain. The circle represents the point of allocation of the energy calculated by the joint time frequency energy distribution, in our case the SPWVD, and the triangle is the point of the reallocation close to the centre of gravity of the energy of the signal.

Therefore at each point in the time frequency (f,t) where the SPWVD, equation (7.11), value is computed, the two quantities are calculated as well:

$$\begin{cases} \hat{t}(f,t) = t - \dfrac{P_{SPWVD}(f,t;h_1,t\times h_2)}{2\pi P_{SPWVD}(f,t;h_1,h_2)} \\ \hat{f}(f,t) = f + j\dfrac{P_{SPWVD}(f,t;\dfrac{dh_1}{dt},t\times h_2)}{2\pi P_{SPWVD}(f,t;h_1,h_2)} \end{cases} \tag{7.12}$$

Which define the local centroids of the SPWVD distribution centred in the windows h_1 and h_2. The SPWVD value is then moved from the point (f,t), circle in Figure 65, where it has been computed to the centroid $\left(\hat{f}(f,t),\hat{t}(f,t)\right)$, triangle in Figure 65, leading to define the Reassigned-Smoothed-Pseudo-Wigner-Ville Distribution (RSPWVD):

$$P_{RSPWVD}[x(t,f)] = \int_{-\infty}^{\infty} P_{SPWVD}(u,\tau,h_1,h_2)\delta\left(u-\hat{f}(f,t),\tau-\hat{t}(f,t)\right)dud\tau \tag{7.13}$$

The improvement on to the readability of the time frequency distribution brought using the RSPWVD can be seen in Figure 66 where the differences among the time frequency distribution in (7.1), (7.11) and (7.13) can be noted. Indeed, the simplified model displayed in the top left subplot of Figure 66 makes apparent the coexistence of two FM components (one sinusoidal and one linear) and one logon (Gaussian wave packet of effective duration dt). The purpose of the time frequency analysis is therefore to produce a picture as close to this idealized model as possible, given the observed three-component signal, of a priori unknown structure. In the WVD of the signal (top right of Figure 66), whereas individual

components are rather sharply described, the overall readability is hampered by cross-components interference mentioned earlier in the section. The SPWD (bottom left of Figure 66) contains much less cross terms, but this image cleaning is obtained at the expense of a smearing of the TF signatures of the individual components. Instead, the application of the RSPWVD results in a picture (bottom right of Figure 66) that is almost identical to the idealized starting model.

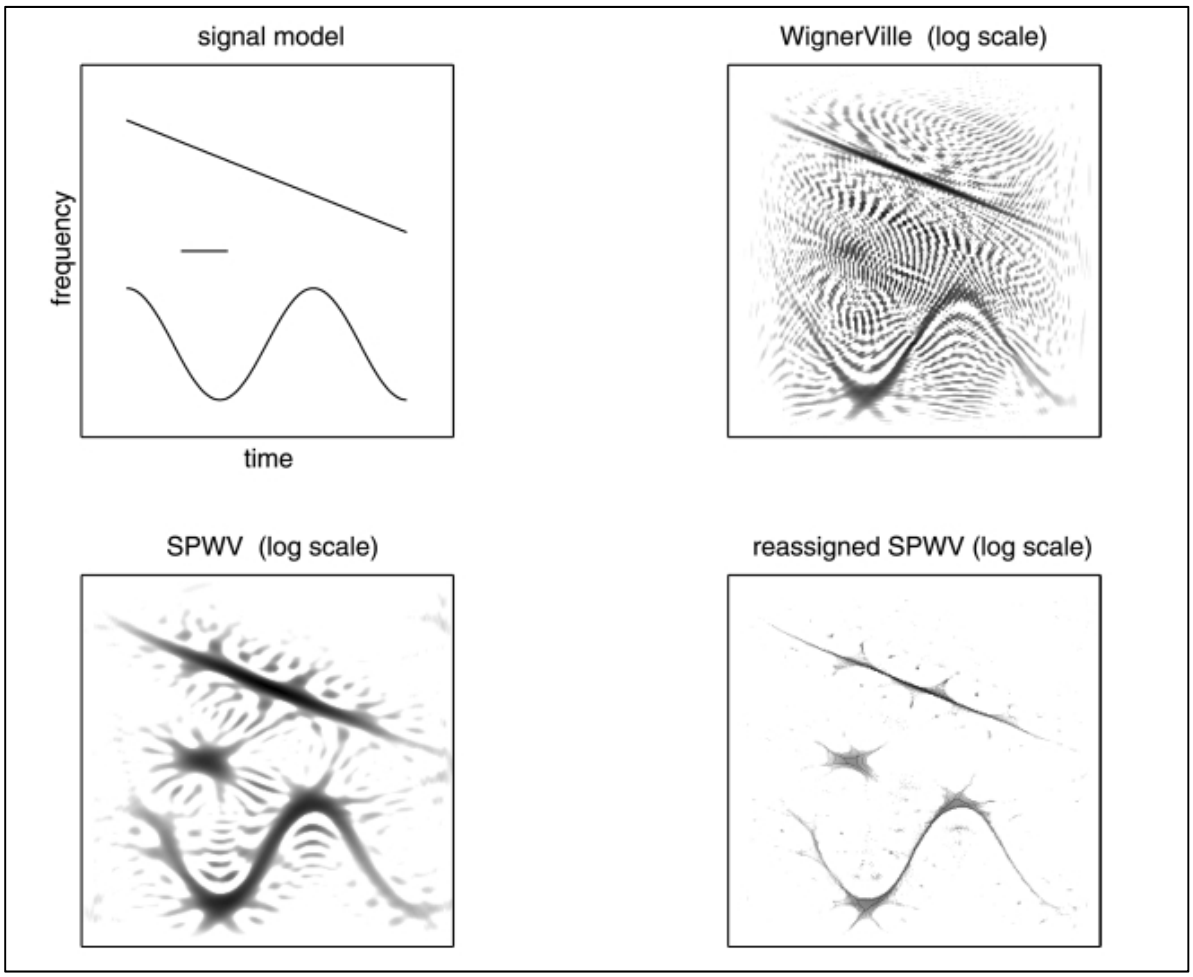

FIGURE 66 – IMPROVEMENT IN READIBILITY OF TIME FREQUENCY REPRESENTATION. TOP LEFT SIGNAL MODEL: TOP RIGHT WVD REPRESENTATION; BOTTOM LEFT SPWVD REPRESENTATION; BOTTOM LEFT RSPWVD REPRESENTATION (FROM FLANDRIN ET AL. [178]).

7.3.2 PRINCIPAL COMPONENT ANALYSIS

Principal component analysis (PCA) analyses a data set representing observation described by several dependent variables, which are, in general, inter-correlated. Its goal is to extract the important information from the data set and to express this information as a set of new orthogonal variables called principal components.

The aim of the PCA is to eliminate the redundancy in the data set revealing its underlying dynamics. The assumptions used for performing the PCA are:

1. Linearity.
2. Probability distribution of original values must be Gaussian so that mean and variance entirely describes the distribution.
3. Principal components with larger associated variances represent interesting dynamics, while those with lower variances represent noise.
4. Principal components are orthogonal implying that PCA is soluble with linear algebra techniques.

Let us define X as our original set of data arranged in a $p \times n$ matrix, where p are the observations and n are the variables. The goal of PCA is to find a linear transformation U, i.e. an orthonormal matrix, able to re-represent our new data set Y such that:

$$Y = UX \tag{7.14}$$

U is the eigenstructure that makes the covariance matrix $R_C \equiv \frac{1}{m-1} X^T X$ diagonal.

$$R_C = UD_M U^T \tag{7.15}$$

Where D_M is a diagonal matrix containing the principal component. An alternative way of calculating the PCA is to evaluate the Singular Value Decomposition (SVD) of the data set X.

$$X = P\Delta Q^T \tag{7.16}$$

The columns of matrix Q^T are the eigenvectors of the R_C. The singular values (diagonal elements of Δ) are the positive square roots of the eigenvalues of R_C. The PCA is an important tool for the identification of the wave types present in the vibration signal generated by manmade processes through the polarization analysis. The latter is explained in the next section 7.3.3.

7.3.3 POLARIZATION MEASUREMENTS

Polarization measurements are important in many areas of seismology in many ways, as shown in section 6.5.2, and a single triaxial geophone or accelerometer can provide estimates of the polarization state of a seismic arrival (Perelberg and Hornbostel [155]).

Obviously, an instantaneous triaxial signal does not provide polarization information therefore it is necessary to observe the signal for some time defining the polarization analysis over a time window (Greenhalgh et al. [139]). According to Jackson et al. [141] three requirements constrain the choice of analysis window: first, the window should contain only one arrival; second, the window should be such that the ratio of signal energy to noise energy is maximized; and third, the window should be as long as possible to allow discrimination of noise from signal. Of course polarization estimates lose their reliability with increasing noise levels.

The length of the window is related to the dominant period of the disturbance that is analysed. According to Kanasewich [138], the window length could be specified so as to be consistent with one or two cycles of the dominant period and one common approach in seismology is to band-pass filter with a zero phase shift digital filter before rotation so that the spectral content of the record is restricted. According to Jurkevics [149], the quality of particle-motion information obtained for a given arrival depends critically on the positioning of the analysis window and choice of frequency interval. The choice of both window length and bandwidth are subject to the usual trade-offs between resolution and estimation variance. Short windows and narrow bands are required to avoid smearing information between close arrivals and to capture the frequency-varying properties of polarization. However, longer windows and wider frequency bands yield more stable and reliable estimates. The nature of the signals being processed as well as the objectives of the particular analysis must determine the resolution settings.

In time domain, the polarization analysis is achieved by performing the PCA on the time window of the triaxial recording as a matrix. Therefore for each time window q an eigenanalysis, or an SVD, of the cross-energy matrix M is done.

$$M = \frac{X^T X}{N_q} = \frac{1}{N_q} \sum_{i=1}^{N_q} \begin{bmatrix} x_e(i)^2 & x_e(i)x_n(i) & x_e(i)x_z(i) \\ x_n(i)x_e(i) & x_n(i)^2 & x_n(i)x_z(i) \\ x_z(i)x_e(i) & x_z(i)x_n(i) & x_z(i)^2 \end{bmatrix} \tag{7.17}$$

Where $x_e(i)$, $x_n(i)$ and $x_z(i)$ are the three signals of the triaxial recording in the time window and N_q is the length of time windows used in the analysis. A better interpretation of the polarization parameter can be obtained overlapping the time window with a number of points $o \leq N_q$.

For each time window q the eigenvalues λ_1^q, λ_2^q and λ_3^q of the cross energy matrix M, in (7.17), are ordered such that $\lambda_j^q \geq \lambda_k^q$ for $j < k$. Purely rectilinear ground motion has only one nonzero eigenvalue $\lambda_j^q = 0$, $j \neq 1$. Purely elliptical polarization has two nonzero eigenvalue, $\lambda_1^q \geq \lambda_2^q$, $\lambda_3^q = 0$. In reality, all three eigenvalues are generally nonzero and no equal, so the polarization is ellipsoidal. The degree of rectilinearity $RL(q)$ defined by Flinn [140]:

$$RL(q) = 1 - \frac{\lambda_2^q}{\lambda_1^q} \tag{7.18}$$

This is unity when there is only one nonzero value, as for body waves. On the other hand pure Rayleigh-wave motion is elliptical and the particle motion is confined within a plane. A measure of the degree of planarity $PL(q)$ is:

$$PL(q) = 1 - \frac{2\lambda_3^q}{\lambda_1^q + \lambda_2^q} \tag{7.19}$$

Esmersoy [144] provided a formal proof that the direction of maximum projected power is the eigenvector of the covariance matrix corresponding to the largest

eigenvalue, and that this direction is the minimum variance estimate of the bearing in the presence of isotropic white noise.

The azimuth of the propagation can be estimated from the horizontal orientation of rectilinear motion, given by the eigenvector u_1^q corresponding to the largest eigenvalue:

$$\vartheta(q) = \tan^{-1}\left(\frac{u_{21}^q \, \mathrm{si}\, gn(u_{11}^q)}{u_{31}^q \, \mathrm{si}\, gn(u_{11}^q)}\right) \tag{7.20}$$

where $u_{j1}^q \quad j = 1\ldots 3$ are the three direction cosines of eigenvector u_1^q. The sign function is introduced to resolve the 180° ambiguity by taking the positive vertical component of u_1^q. In the same way, the apparent incident angle of rectilinear motion, as measured from vertical between 0 and 90°, may be obtained from the vertical direction cosine of u_1^q:

$$\varphi(q) = \cos^{-1}\left|u_{11}^q\right| \tag{7.21}$$

It is worth mentioning that the azimuth and incident angle are well defined in the presence of high rectilinear motion therefore in the presence of body waves since their oscillation only acts on one dimension. The distinction of body waves from surface waves is generally achieved by fixing a threshold in the value of rectilinearity which is generally greater than 0.8 while the differentiation between P and SV waves is done by evaluating the incidence angles: SV waves exhibit an angle close to 90° whereas P wave have an angle less than 90 °.

An application of polarization measurement in time domain will be presented in section 7.4 for analysing the wavefield components generated by piling vibrations. As already said in section 6.5.2, polarization measurements have been extended in the frequency domain with the work of Samson [142] [143] which will be briefly presented below.

Considering $x^T(t)$ a row vector of a triaxial recording

$$x^T(t_k) = [x_e(t_k), x_n(t_k), x_z(t_k)](k = 0, N-1) \tag{7.22}$$

The corresponding vector $x(f)$ in frequency domain will be

$$x(f) = (2\pi)^{-1} \sum_{k=0}^{N-1} x(t_k) e^{-ift} \tag{7.23}$$

An estimation of the spectral density matrix (SDM) $S(f)$ at a certain frequency f_0 is given by:

$$S(f_0) = \xi\{x(f)x^T(f)\} \quad f_0 - \Delta f < f < f_0 + \Delta f \tag{7.24}$$

where ξ indicates an expectation value which implies smoothing over f_0 for narrowband analysis (Wagner and Owens [180]). $S(f)$ can be obtained by applying a moving average to the density matrix to smooth it. The length of the window used for the smoothing is related, as in the time domain case, to the resolution of the analysis. The spectral density matrix is Hermitian and plays a role analogous to the cross-energy matrix *M* (7.17) presented for the time domain approach. The diagonal elements of the covariance matrix provide a measure of the power flux density, and the standardized off-diagonal elements provide a measure of the channel-wise coherence (Wagner and Owens [150]). The degree of the polarization $P(f)$ as a function of the frequency f is expressed by Samson [142] as:

$$P(f) = \frac{n_C\left(trS^2(f) - \left(trS(f)\right)^2\right)}{(n_C - 1)\left(trS(f)\right)^2} \tag{7.25}$$

Where *tr* is the trace of the matrix and n_C is the number of channels, in this case three. This parameter can be computed without having to diagonalize the SDM and its definition of polarization contains the desired characteristics, since, in the case of linearly polarized waves $P(f)$ is 1 whereas it is 0 for unpolarised or circularly polarized wave. Diagonalizing the SDM, the incidence and the azimuth

angle of the direction of the propagation can be computed in similar ways to that obtained in the time domain.

Moriya and Niitsuma [148] extended the concept of polarization in the time frequency domain for analysing downhole three components microseismic data. Following Samsom's approach, they treated the SDM as a joint function of time and frequency, called $S_p(t_k, f_0)$, and its formulation is reported below for a frequency f_0 at a t_k time.

$$S_p(t_k, f_0) = \begin{bmatrix} S_{ee}(t_k, f_0) & S_{en}(t_k, f_0) & S_{ez}(t_k, f_0) \\ S_{ne}(t_k, f_0) & S_{nn}(t_k, f_0) & S_{nz}(t_k, f_0) \\ S_{ze}(t_k, f_0) & S_{zn}(t_k, f_0) & S_{zz}(t_k, f_0) \end{bmatrix} \tag{7.26}$$

Where $S_{lm}(t_k, f_0)(l, m = e, n, z)$ are the auto and cross spectra evaluated of the triaxial recording $x^T(t_k)$ in the time frequency domain. The elements of the $S_p(t_k, f_0)$ can be obtained with any kind of time frequency distribution. In their work, Moriya and Niitsuma [148] used the Choi-Williams distribution, see (7.9), and the time frequency approach was derived for building a precise detector of P wave for monitoring the microseismic activity of a geothermal field. On the other hand, the approach presented here is slightly different because its aim is the observation of the polarization attributes in the time frequency domain. As said at the beginning of the section, the polarization is meaningless as an instantaneous value therefore an average estimation of the $S_p(t, f)$ is needed. Following Moriya and Niitsuma's [148] approach a smoothed estimation of $S_p(t, f)$ can be achieved applying a moving average process in the time domain. For a time instant t_k the average estimator $\overline{S_p(t_k, f_0)}$ for each frequency $f_o \in f$ is:

$$\overline{S_p(t_k, f_0)} = \frac{1}{N_q} \sum_{j=k-1}^{k-N_q} \overline{S_p(t_k, f_0)} \quad \forall f_0 \in f \tag{7.27}$$

Where N_q is the length of the time window which can be overlapped in order to have a better resolution in time of the averaged SDM. Even in this case the length

of the time windows is related to the resolution of the analysis. Once the $\overline{S_p(t_k, f_0)}$ is obtained the polarization parameters such as the degree of polarization, the azimuth and the incidence angle can be calculated for each time instant t_q and each frequency f_0 belonging to the set of frequencies f. The time frequency polarization measurement is applied to induced train vibrations in section 7.5.

7.4 POLARIZATION ANALYSIS OF PILING VIBRATIONS

7.4.1 ANALYSIS STRATEGY

The polarization analysis will be conducted on the piling activity recorded during the project "Human response to vibration in residential environments" for assessing the human exposure from construction vibration as explained in chapter 5.

Most specifically, the measurements at the so called Site A, see section 5.3.3, will be considered where an array of 4 accelerometers, at measurement positions $M1 \ldots M4$ were used for measuring vibration coming from 4 piling positions called $P1 \ldots P4$. The measurement layout is already presented in Figure 37. The first step of the analysis strategy is to identify which measurement and pile positions need to be used for the analysis. The latter needs to be conducted on sensors affected as little as possible by the "presence" of the residential environment for obtaining a polarization signature representative of the ground motion.

Athanasopoulos and Pelekis [89] already highlighted the difficulty to carry vibration measurement in urban environment where the seismic waves propagate in a soil medium that incorporates buried objects and is covered by pavements and sidewalk structures which could generate multiple reflections and wave interference and result in complicated time history records. Moreover, the problems of measuring vibration in occupied environments are extensively treated in section 8.2. It has been already shown in section 5.4.2 that positions $P3$ and $P4$

cannot be used because they suffer from scattering generated by the interaction between the wavefield and the building foundation. For the same reason, positions $M2, M3, M4$ from piles $P2, P1$ are not considered. As a consequence, the remaining positions are: $M1$ from $P1$ and $M1$ from $P2$. The former is discarded because it suffers from a local effect that is shown in Figure 42 therefore the latter will be used for the analysis. The distance between the sensor $M1$ and the pile $P2$ has been estimated as 21 m, Table 7, and the azimuth angles from North have been estimated as 76 degrees. The pile position has been extrapolated using GPS position and digital maps like Google Earth.

The polarization analysis will be mainly conducted in the time domain trying to identify the seismic phases involved in the vibration from piles. Furthermore, a comparison with the particle motion plot analysis will be presented.

7.4.2 EVENT IDENTIFICATION

Since the analysis will be conducted from every pile hit, the strategy for identify the event is a little bit different from the one used for railway vibration. First of all, an STA with a time window of 1 sec on the time z component of the vibration time history is performed, and then three percentiles from the STA time history are chosen: 95%, 75% and 35%. Taking advantage of the periodicity of the signal, these percentages are used as cut off points for identifying each hit in the time history. Once identified the triggering points of the event on the z component, the same points have been used for the event extraction on the north and east component too.

7.4.3 TIME DOMAIN POLARIZATION AND PARTICLE MOTION

Let's consider a triaxal event e from the set H of the pile hits identified with the process described above.

$$e = \left[x_e(t_k), x_n(t_k), x_z(t_k) \right] \quad k = 1 \ldots N_e \tag{7.28}$$

Where $N_e = 571$ is the length of the event for all the elements of H. As highlighted in Figure 67, the pile hit can be divided in two phases: between 0 and

1 s the ram is raised by hydraulic pressure which generates high pressure waves into the soil and between 1 and 2 s the pile is hit. Both phases will be analysed separately in terms of particle motion and polarization.

In Figure 68 the auto spectrum of the three components in the time frequency domain is presented. From the figure, the impulsive characteristic of the signal from the hit between 1 and 2 seconds can be observed with the maximum concentration of the energy around 20 Hz. On the other hand, the rise of the ram, between 0 and 1 s, has the energy mainly distributed between 20 and 40 Hz.

The time frequency auto spectra are obtained using Reassigned-Smoothed-Pseudo-Wigner-Ville Distribution (RSPWVD) defined in (7.13) using the time frequency toolbox by Auger et al. [181] with $N_{fbin} = 256$ frequency bins with a time smoothing windows h_2 of $N_{fbin}/10$ points and a frequency smoothing windows h_1 of $N_{fbin}/4$ as suggested in the authors' routine. Both h_1 and h_2 windows are Hanning. As pointed out in Auger et al. [177], the readability of the RSPWVD depends on a suitable trade-off between good interference attenuation and good time-frequency concentration. This trade-off is determined by the choice of the windows parameters. The latter proposed by Auger et al. [181] in the toolbox provide a suitable "smoothing" in the time frequency domain for the identification of the most energetic part of the signals considered in this work as shown in Figure 68 for piling vibration.

Considering that the most energetic part of the signal is around 20 Hz, the time domain polarization analysis, already explained in section 7.3.3., for piling vibrations will be conducted with an optimal length of the time widows Δt of 40 points, corresponding to 0.2 s, and an overlap of 90 %. Let's start to analyse the first phase of the piling event in Figure 67 between 0 and 1 s, identified as the raising of the ram, first in terms of particle motion and then in terms of polarization analysis.

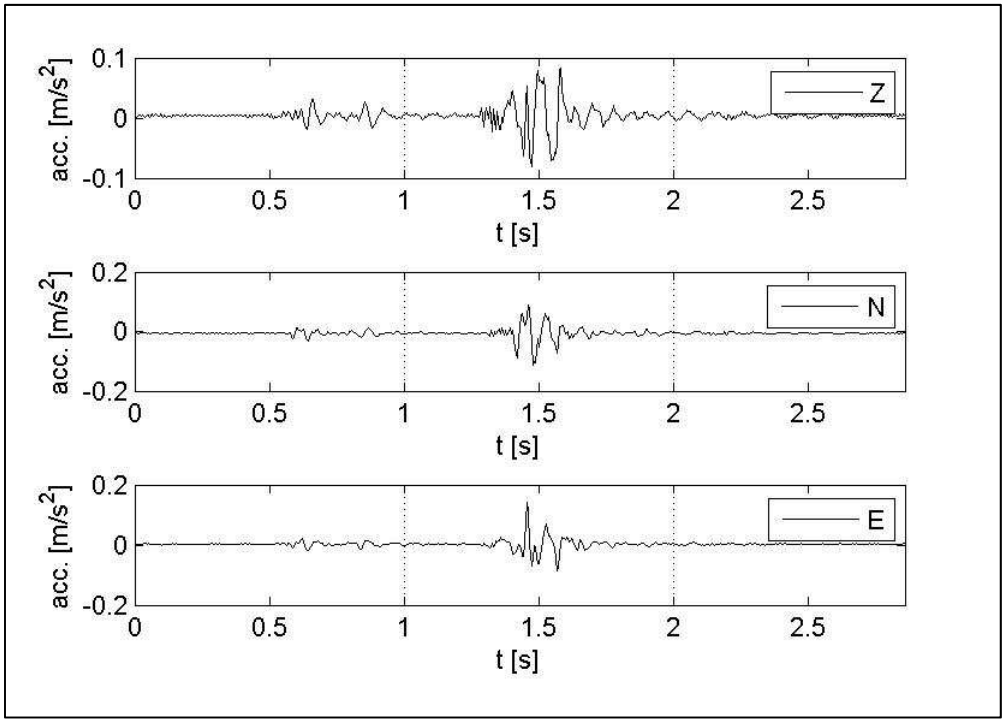

FIGURE 67 – VIBRATION SIGNAL FROM PILE INDUCED VIBRATION. FROM THE UPPER TO THE LOWER PANEL: Z, N AND E COMPONENTS.

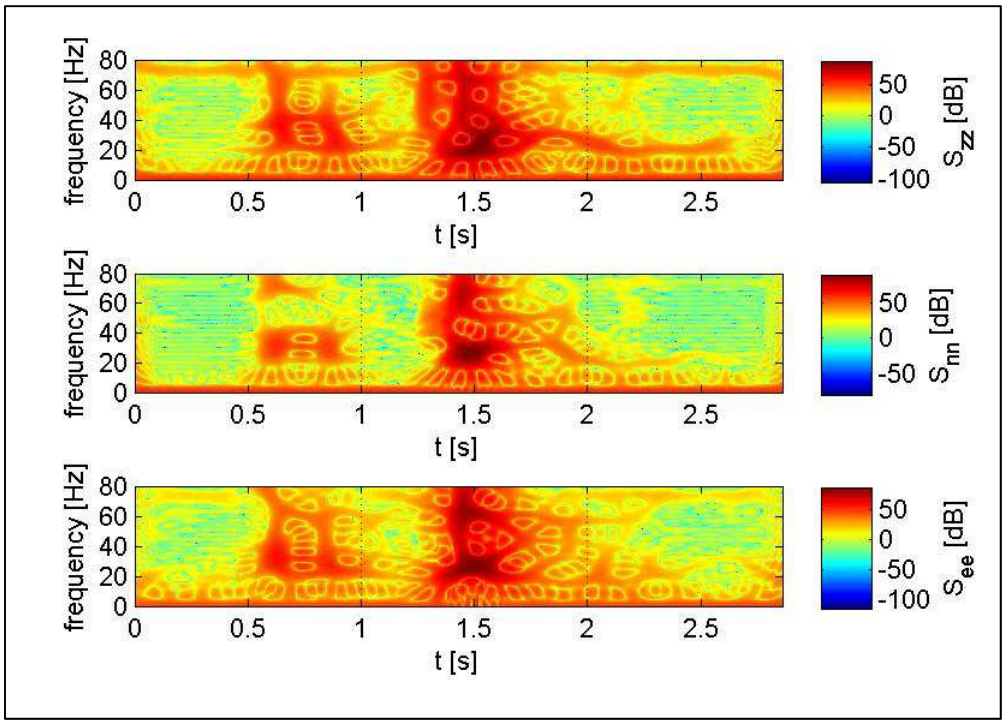

FIGURE 68 - VIBRATION SIGNAL FROM PILE INDUCED VIBRATION: TIME FREQUENCY REPRESENTATION. FROM THE UPPER TO THE LOWER PANEL: Z, N AND E COMPONENTS. AUTOPOWER EXPRESSED IN DB WITH REFERENCE ACCELERATION 10^{-6} M/S^2

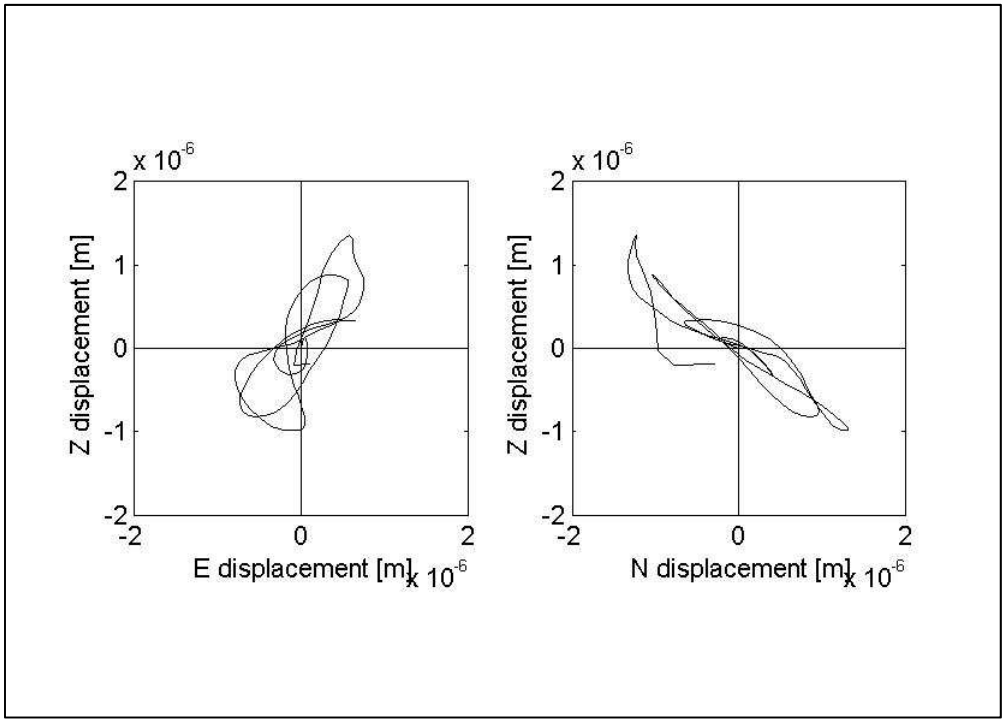

FIGURE 69 - DISPLACEMENT PARTICLE MOTION OF THE RAISING OF RAM. FROM THE LEFT TO THE RIGHT PANEL: EAST Z PLANE AND NORTH Z PLANE.

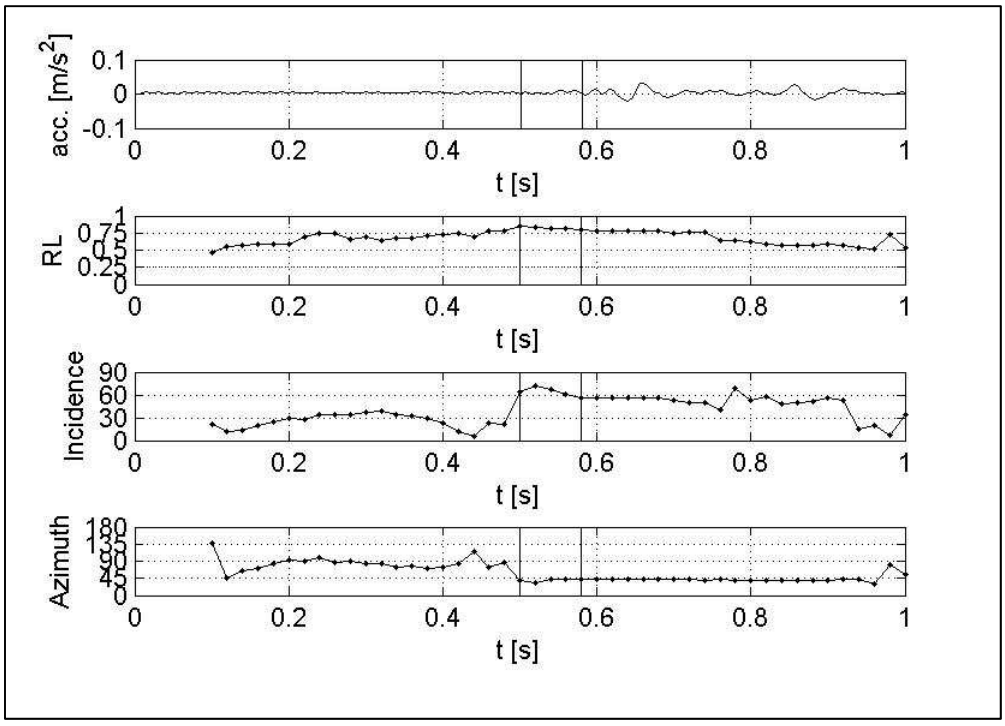

FIGURE 70 – POLARIZATION ANALYSIS FOR THE RISING OF RAM. FIRST PANEL FROM THE TOP TIME HISTORY Z COMPONENT. SECOND PANEL RECTILINEARITY. THIRD PANEL INCIDENCE ANGLE. FOURTH PANNEL AZIMUTH ANGLE.

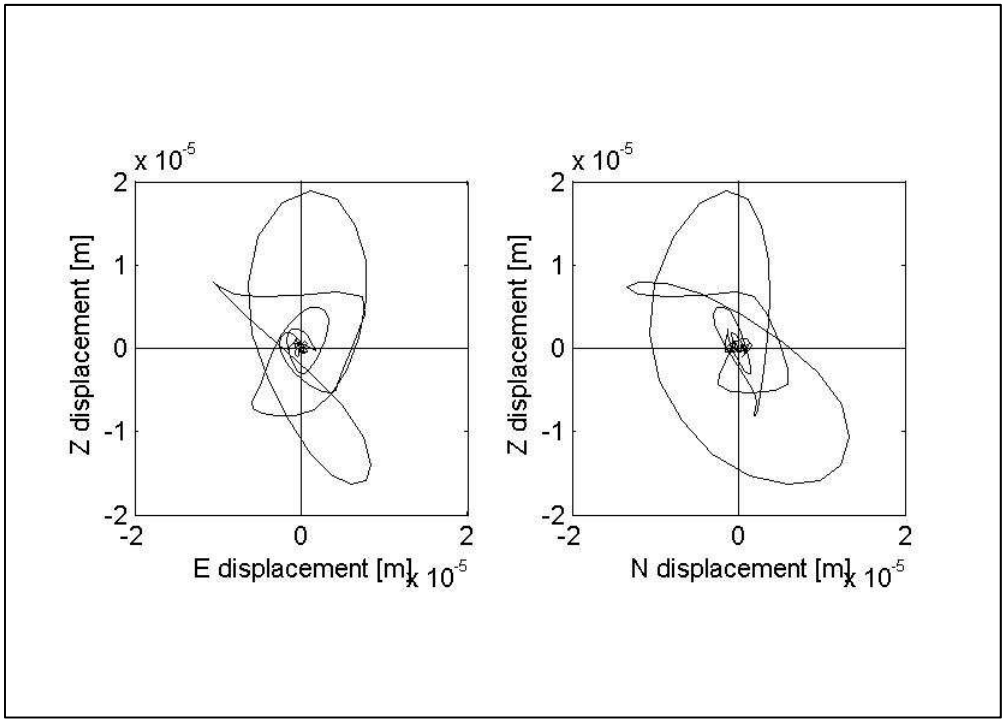

FIGURE 71 – DISPLACEMENT PARTICLE MOTION OF THE PILE HIT. FROM THE LEFT TO THE RIGHT PANEL: EAST Z PLANE AND NORTH Z PLANE.

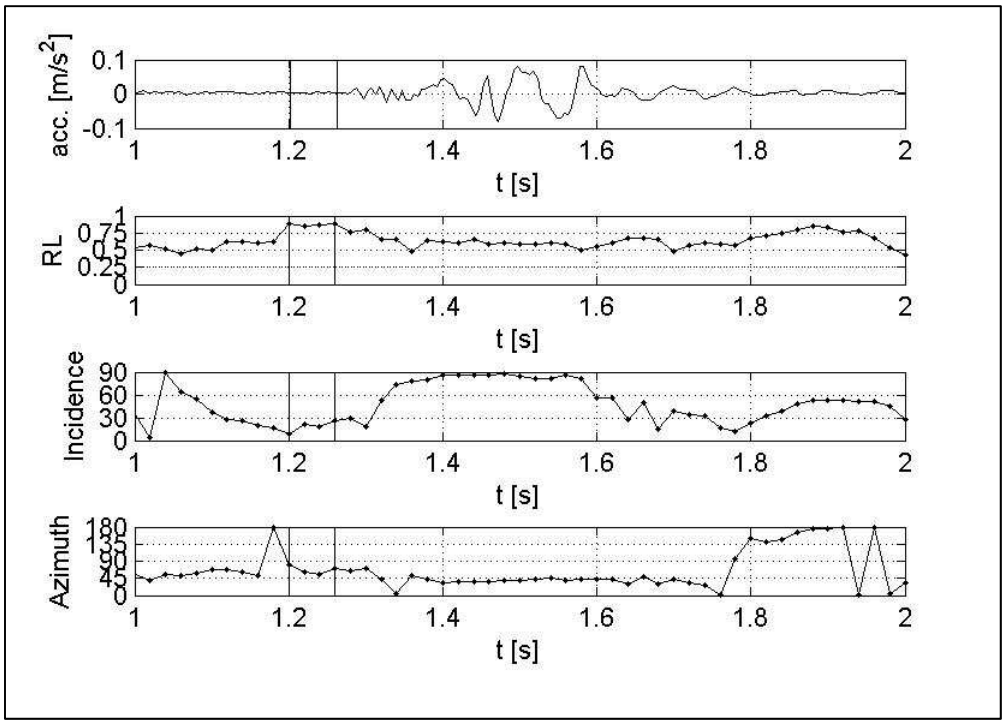

FIGURE 72 - POLARIZATION ANALYSIS FOR THE PILE HIT. FIRST PANEL FROM THE TOP TIME HISTORY Z COMPONENT. SECOND PANEL RECTILINEARITY. THIRD PANEL INCIDENCE ANGLE. FOURTH PANNEL AZIMUTH ANGLE.

Following the standard approach explained in 6.5.1 used for the analysis of wave fields created by manmade processes, in this work the particle motion plot is obtained through a double integration of the entire tri-axial acceleration time series containing the pile hit. The low-frequency drift problem rising from the integration processes has been avoided by applying a high pass filter at 3 Hz after the double integration.

In Figure 69 shows the particle motion of the raising of the ram is presented. From Figure 69 it can be seen that the particle motion is linear in both panels, therefore the first phase of the piling, between 0 and 1 s, can be considered as a P-wave. Still considering the phase related to the raising of the ram, in Figure 70 its polarization analysis is shown. In the second panel of Figure 70 the evolution over the time of the rectilinearity parameter is presented.

In fact, as already said in section 7.3.3, high values of rectilinearity (close to 1) are associated with linear polarization which is characteristic of body wave type. Following an approach usual in the field, linear polarized values are "declared" if the value is above a certain threshold decided by the "interpreter" of the polarization signature. In literature this threshold is 0.8 or above (Chichowicz [182], Patane and Ferrari [157], De Lauro et al. [183]).

In Figure 70 the area between the two vertical black lines indicates the zone where $RL(q)$ remains above 0.8 and in this time interval, 0.5 to 058 s, the average values, following the Fisher statistic, of the incidence and azimuth angle are 64 degree and 40 degree respectively. In the region of high rectilinearity, the incidence angle shows that the wave is not superficial: as a consequence this phase can be considered as a P-Wave. It can be noted that even using a threshold of 0.75 the incidence and azimuth angles are quite steady around the average values at 0.8, therefore the P-Wave phase can be broadened from 0.5 to 0.75 s.

In this case both particle motion and polarization analysis provide the same interpretation about the wave type of the disturbance, i.e. P-Waves, but the latter gives back more information such as the start of the seismic phase and the polarization attributes which can be useful for building polarization filters.

Now the same approach is going to be used for analysing the triaxial event between 1 and 2 s identified as the pile hit. Figure 71 shows the displacement particle motion of the pile hit in the E Z and N Z plane. The particle motion in both panel of Figure 71 highlights an elliptical motion which can be interpreted mainly as a Rayleigh waves, but another seismic phase it may be involved in the propagation process of the disturbance.

From Figure 72 the region where the $RL(q)$ exceed 0.8 is between 1.2 and 1.23 s with an average azimuth and incidence angle of 60 and 30 degrees respectively. The latter is quite deep and this phase of the polarization signature can be considered as a P-wave, on the other hand the former is reasonably consistent with the actual direction of the source estimated at 72 degrees. Considering 0.75 as the threshold, the P-wave phase can be widened from 1.2 to 1.3 s. Furthermore, between 1.4 to 1.8 s a steady behaviour of $RL(q)$ around 0.6 can be seen, which means that 2 directions are involved in the motion, with a fixed depth of 90 degrees in the zone between 1.4 to 1.6 s and a fixed azimuth around 45 degree: this phase is a superficial elliptical motion indicating a Rayleigh wave.

Even in this case the description of the wave field generated by the piling activity is more "rich" compared with the one provided by the only inspection of the particle motion especially in the identification of the body wave part of the seismic pulse.

The event analysed in Figure 72 can be considered as "raw" because it is only low pass filtered at 80 Hz which is the maximum frequency that the instrument can acquire and the polarization analysis has provided good results even with the signal in the full frequency range of the instrument.

Let's consider now, the effect of filtering the time history on the polarization analysis especially on the identification of the body waves. As already shown in Figure 68, the energy of the signal is around 20 Hz therefore the polarization analysis, with the same parameters defined above, will be applied to the signal low pass filtered at 40 and 20 Hz.

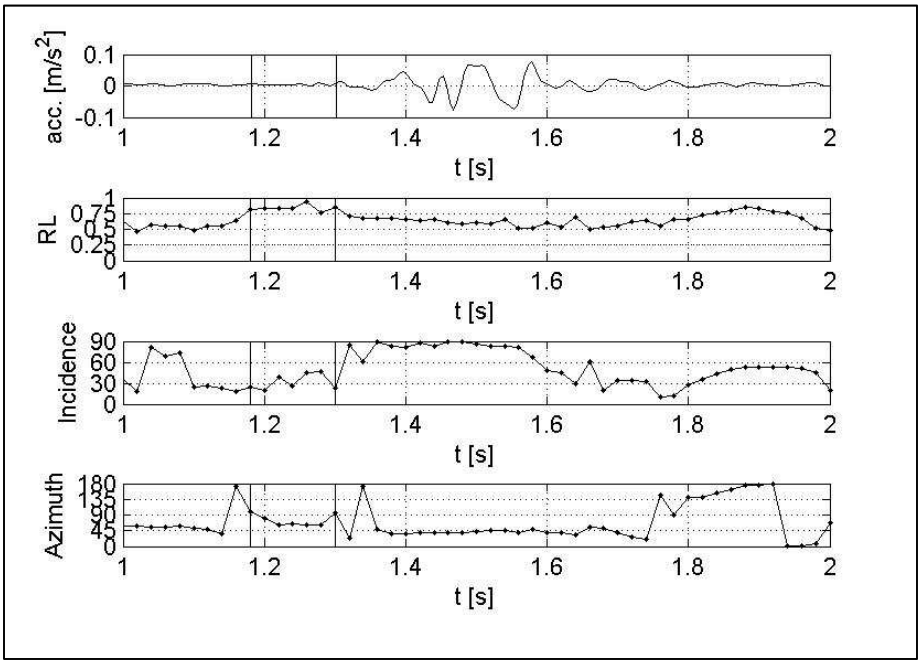

FIGURE 73 – POLARIZATION ANALYSIS FOR THE PILE HIT LOW PASS FILTERED AT 40 HZ. FIRST PANEL FROM THE TOP TIME HISTORY Z COMPONENT. SECOND PANEL RECTILINEARITY. THIRD PANEL INCIDENCE ANGLE. FOURTH PANNEL AZIMUTH ANGLE.

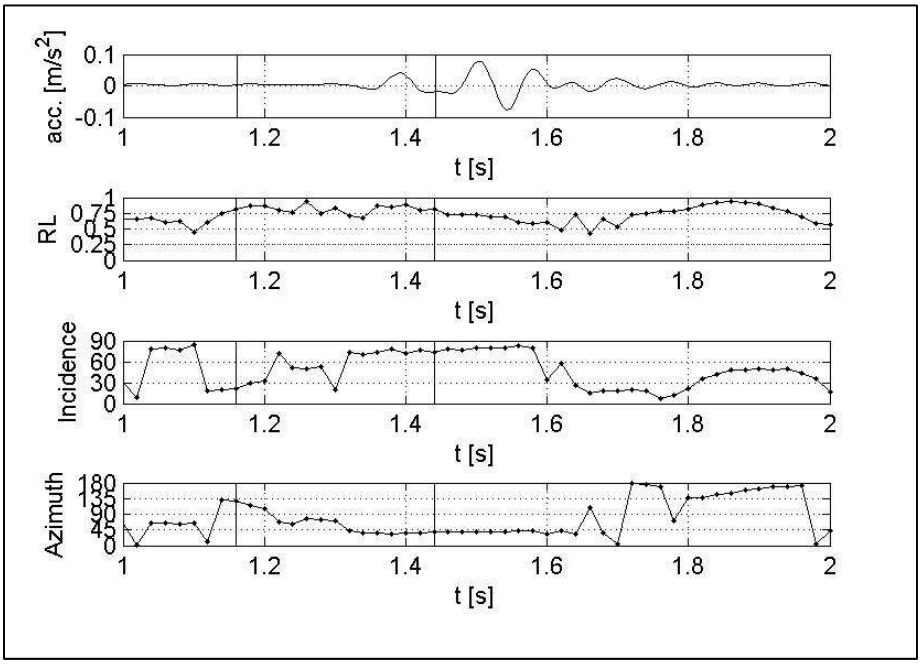

Figure 74 - Polarization analysis for the pile hit low pass filtered at 20 hz. First panel from the top time history z component. Second panel rectilinearity. Third panel incidence angle. Fourth pannel azimuth angle.

Specifically, the entire tri-axial acceleration time series is filtered in the forward direction and then the filtered signal is reversed and run back through the same filter in order to ensure a zero-phase distortion as suggested by Kanasewich [138]. The results of the polarization applied on the filtered signals are shown respectively in Figure 73 and Figure 74.

From Figure 73 and Figure 74 it can be noted that the filtering broadens the phase with high rectilinearity with respect to the "raw" case. With a 40 Hz low pass filters, Figure 73, the average azimuth is 75 degree and the incidence is 31 degree. Instead, at 20 Hz, Figure 74, the average azimuth is 62 degrees whereas the incidence angle is 55 degree. Therefore filtering the time series, as also explained in section 6.5.3, can improve the polarization signature of the event. This also highlights a possible frequency dependence of the polarization attributes which will be better investigated with the vibration induced by railway vibration.

As already pointed out by Magotra et al [156], the location provide by a single triaxial receiver will of course be cruder than those achievable with data from several receivers surrounding the sources.

7.4.3.1 WAVE FIELD ASSESSMENT

The signal analysed in the previous section is the first pile hit of a series of 94. Considering that for each hit of the ram, the pile goes further into the ground, it can be useful to understand how the polarization attributes, especially those related to the location of the source like the incidence angle, changes with the depth. In this way a wave field assessment of the entire piling activity can be performed. In order to achieve this aim, the process explained in the previous section needs to be iterated for each triaxial pile hits k belonging to the set H. The analysis is performed on the set of pile hits H low pass filtered at 40 Hz. In fact, as already shown, in the previous section, filtering the event can improve the polarization signature. For each hit k the time interval t_{HR}^{k} where the rectilineraity $RL^{k}(i)$ exceeds the 0.8 can be defined as:

$$t_{HR}^{k} = \left[i \in [1, N_H] / RL^{k}(i) \geq 0.8 \right] \quad \forall k \in H \tag{7.29}$$

t_{HR}^{k} is declared if at least 4 consecutive time instants are found otherwise is set as zero. The choice of the duration threshold has been done considering the impulsive nature of the pile which implies a short duration of the body wave phase as shown in the previous section in Figure 72. Once t_{HR}^{k} is different from 0, the average value of rectilinearity, azimuth $\overline{\vartheta_{HR}^{k}}$ and incidence $\overline{\varphi_{HR}^{k}}$ can be defined. Of course, the polarization attributes are set to zero when t_{HR}^{k} is zero.

$$\overline{RL_{HR}^{k}} = \left\langle RL^{k}(i) \right\rangle_{i \in t_{HR}^{k}} \quad \forall k \in H \tag{7.30}$$

$$\overline{\vartheta_{HR}^{k}} = \left\langle \vartheta^{k}(i) \right\rangle_{i \in t_{HR}^{k}} \quad \forall k \in H \tag{7.31}$$

$$\overline{\varphi_{HR}^{k}} = \left\langle \varphi^{k}(i) \right\rangle_{i \in t_{HR}^{k}} \quad \forall k \in H \tag{7.32}$$

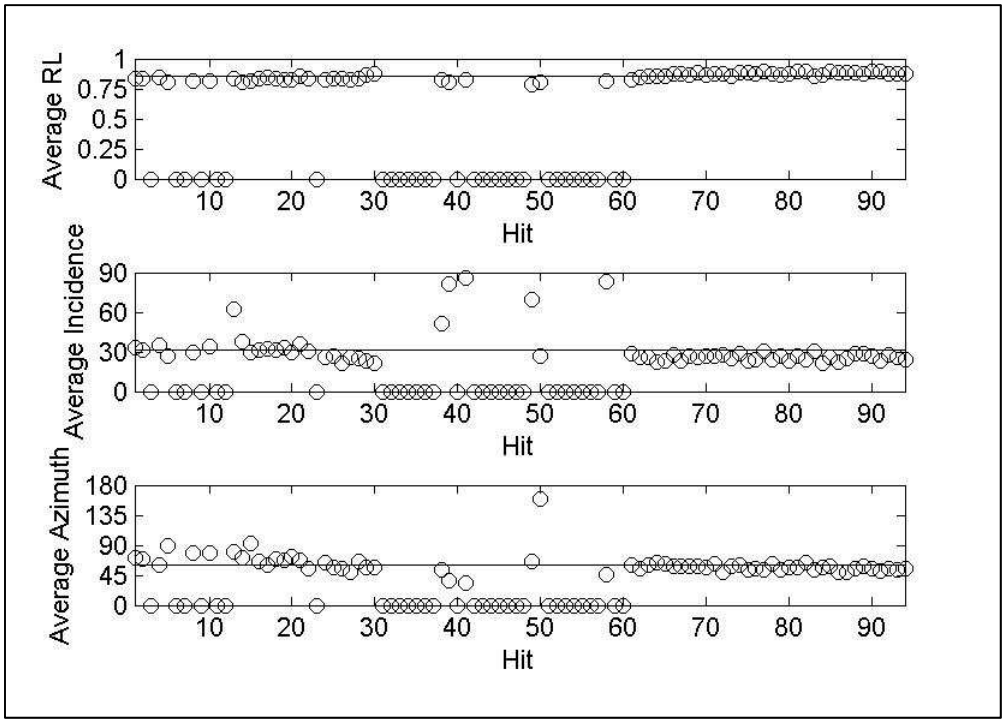

FIGURE 75 - HIGH RECTLINEAIRITY POLARIZATION ATTRIBUTES IN FUNCTION OF THE PILE HIT LOW PASS FILTERED AT 40 HZ. FROM THE TOP TO THE BOTTOM PANEL: AVERAGE RECTLINERAITY, AVERAGE INCIDENCE AND AVERAGE AZIMUTH.

It can be observed from Figure 75 that 67% of the pile hits have a polarization above 0.8 with an average value of 0.85 confirming the near field nature of the wave field. The average $\overline{\vartheta_{HR}^{k}}$ over the number of hits is 60 degrees whereas the

average $\overline{\varphi_{HR}^{k}}$ is 31 providing a satisfying localization of the vibration source. Considering the average values of the polarization attributes over the hit pile, P waves are still present in the majority of the pile hits coming from position $P2$ showing that the first sensor of the array is still in the near field of the source. This information it might be used in the future for an improvement of the propagation model of the vibration exposure introduced in section 5.

7.5 POLARIZATION ANALYSIS OF INDUCED TRAIN VIBRATIONS

7.5.1 ANALYSIS STRATEGY

The exposure assessment from railway vibration, as explained in chapter 4, consists of two measurement types: a long term measurement known as control position (CP) and a short term measurement taken inside or outside the property where the interview has been taken.

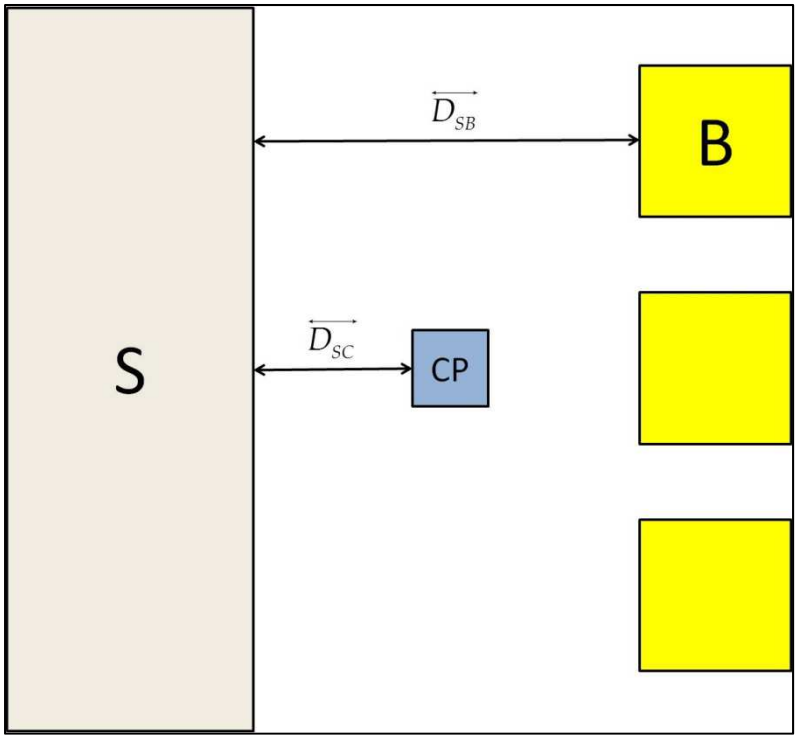

FIGURE 76 – LAYOUT OF CONTROL POSITION MEASUREMENT

The latter is not suitable for the analysis because the vibration recorded will be mostly dominated by the building behaviour and therefore the polarization will be applied on the control position. A layout of the control position measurement is

shown in Figure 76. The following distances have been defined as well: $\overline{D_{SC}}$ is the distance between the source and the CP and $\overline{D_{SB}}$ is the distance between the source and the building. Control positions have been acquired, when available, using the gps positions from the antenna of the transducer or provided by Smartphone and both $\overline{D_{SC}}$ and $\overline{D_{SB}}$ are measured at the boundary of the source such as after the closest railway line to the residential environment. All the distances mentioned above have been measured using digital maps tools like Google Maps and Google Earth.

Considering the difficulty related to the installation of the CP described in 3.5.6 and 8.2, the microtremor recorded at this position is complex and likely to contain the wave propagating from the source plus some reflection belonging to the interaction between the wave field and the line of the houses. Moreover, due to the soil's heterogeneity and the superficial nature of the source the tremor will be affected by mode conversions, multipathing, anisotropy, and scattering. The complexity of the recording presented above is similar to the one highlighted by Bataille and Chiu [152] for the polarization analysis of high frequency three components seismic data[10]. According to Bataille and Chiu [152] the polarization in frequency domain it may resolve the problem of two simultaneous arrivals from different directions but in the presence of superposition of direct, refracted, reflected and scattered waves there is no guarantee that the polarization waves are constant in frequency as pointed out by Park et al. [145] who also emphasized that in the presence of strong scattering it also possible to obtain high degrees of polarization at any frequency.

If the wavefield is not so complex, the polarization in frequency domain can be a good candidate for the analysis. In the approach proposed here the polarization attributes will be analysed in the time frequency (TF) domain following an approach, explained in section 7.3.3., similar to the one developed by Moriya and Niitsuma [148] for downhole accelerometers for geothermal microseismic

[10] The seismic high frequency range goes from 1 to 100 Hz and therefore fully contains the frequency response of the instrument and the evaluation range of the human exposure that is between 1 to 80 Hz.

monitoring and the authors showed that the method permits a very precise identification of P-Wave and the resolution of multiple arrivals.

The last thing that needs to be decided in this measurement strategy is which part of the recording analyse. It has already been said that we need to reduce the complexity of the wavefield produced by the tremor to a minimum in order to identify its body wave component. In seismology body waves are generally identified in the first arrivals of the event (Flinn [140]) , that we are going identify as the 'rise', and the same approach, which is explained in the following sections, will be used for the analysis of train vibration. Another approach used for conducting polarization analysis is analysing the coda, which is the Italian word for tail, of the event. In few words after an event the reverberation of the ground will produce coherent scattered arrivals whose signature can be interpreted with a well-defined polarization that varies with frequency (Park et al. [145]). Since the polarization properties of a signal are determined by the propagation characteristics of the medium through which the waves have travelled, Chichowicz et al. [182] , among others, investigated the polarization properties of the coda in order to infer some physical properties about the medium through which the waves had passed. Since the control position acquires train passages for a minimum of 24 hours a statistical analysis of the rise can be done in order to infer the polarization characteristics of the wavefield generated by the railway line in the residential environment.

7.5.2 SITE OVERVIEW

The measurement site is shown in Figure 77. According to the scheme presented in Figure 76 $\overline{D_{SC}}$ is 20 m (blue line in Figure 77) and $\overline{D_{SB}}$ is 29 m (yellow line in Figure 77). The CP was installed in a garage and acquired data for 24 hours.

FIGURE 77 - MEASUREMENT SITE

7.5.3 RISE & CODA IDENTIFICATION

As said in section 7.5.1, the polarization analysis for train will be conducted using the rise of the event and the process to identify those phases is given here. From the control position described in the previous section, let's consider the time history $x(t)$ of a train event, upper panel Figure 78, identified with the procedure explained in section 4.5.2 without the "10dB down point cut" constrain used for deriving the exposure response relationship. A short term average (STA) is applied to the signal with a time window of 0.25 s and a further smoothing of the waveform is obtained by convolving the STA with a Hanning window of 3 s. Then, from the smoothed STA (SSTA) explained above the normalized logarithmic SSTA (LSSTA), shown in lower panel Figure 78, is obtained using the following formula

$$LSSTA = 20\log_{10}\left(\frac{SSTA}{a_{ref}}\right) - \max\left(20\log_{10}\left(\frac{SSTA}{a_{ref}}\right)\right) \tag{7.33}$$

Where a_{ref} is the reference acceleration quantified in $10^{-6}\,\mathrm{m/s^2}$.

Considering the LSSTA, we are going to define:

1. $[on_H, off_H]$ (vertical red line Figure 78) the interval where $LSSTA \geq -1dB$

2. $[on_L, off_L]$ (vertical black line Figure 78) the interval where $LSSTA \geq -20dB$

For the event $x(t)$ the three signal phases can be defined as follow:

$$\begin{aligned} Rise &= x(on_L, on_H) \\ Body &= x(on_H, off_H) \\ Coda &= x(off_H, off_L) \end{aligned} \tag{7.34}$$

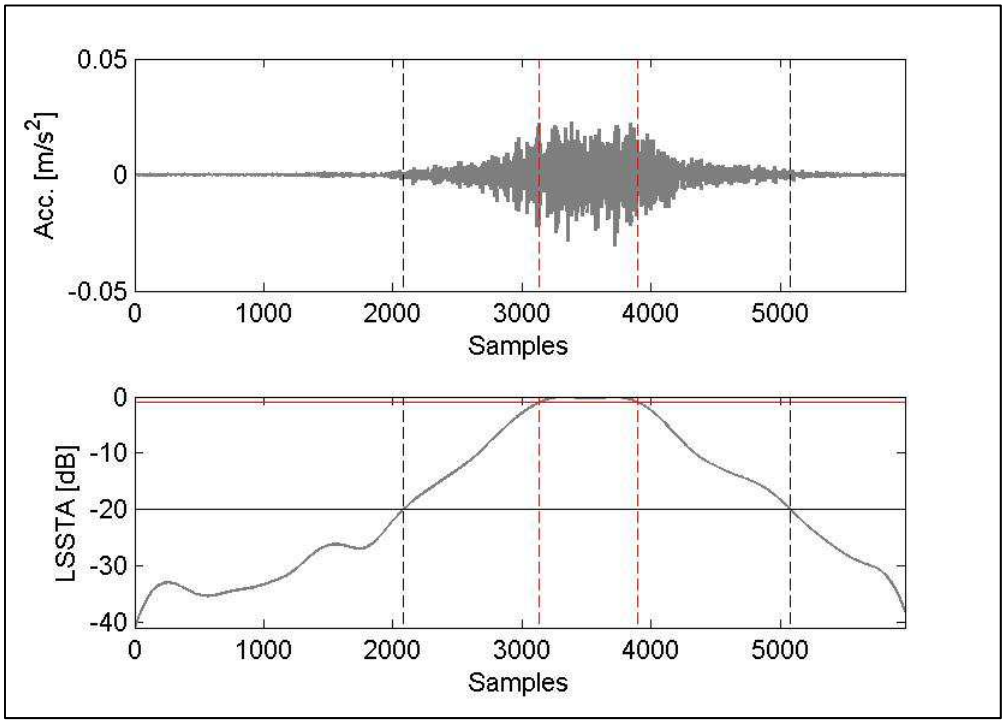

FIGURE 78 - TRAIN EVENT. UPPER PANEL TIME HISTORY. LOWER PANEL 20LOG10 SHORT TERM AVERAGE REPRESENTATION

The event body, as shown in the lower panel of Figure 78, is the most energetic phase of the event and therefore mainly dominated by Rayleigh waves (Richart et al. [86]). Due to the moving nature of the source, in this region waves are coming from every direction, caused by several source mechanisms, producing a complex wavefield not suitable for the polarization analysis as explained in section 7.5.1. As a consequence, our attention from now on will be focussed only on the rise of the events. Since the polarization analysis it will be conducted on all the events recorded at the CP, the cut off points at -1dB and -20dB have been founded to provide an acceptable identification for the rise with a signal to noise ratio of at least 20 dB.

7.5.4 TIME FREQUENCY POLARIZATION FOR PASS BY

Once identified, the event's phases suitable for the analysis, polarization measurement for first arrivals, or rise, can be performed. As already pointed out in the analysis strategy, section 7.5.1, the polarization will be conducted in the TF domain following the approach explained in 7.3.3.

Considering the event showed in Figure 78, its triaxial event's rise signal is defined as:

$$r^T = \left(x_e(t_k), x_n(t_k), x_z(t_k)\right) \quad k = 1 \ldots N_r \tag{7.35}$$

Where N_r is the length of the rise. From (7.35) the elements of the time frequency spectral density matrix (SDM) $S_p(t_k, f_o)$, defined in (7.26), known as $S_{lm}(t_k, f_o)$

$$S_{lm}(t_k, f_o) \quad l, m = e, n, z \quad k = 1 \ldots N_r \quad f_0 = 0 \ldots 80 \tag{7.36}$$

are obtained using Reassigned-Smoothed-Pseudo-Wigner-Ville Distribution (RSPWVD) defined in (7.13) with the same approach explained in section 7.4.3. In the lower panel of Figure 79, the element S_{zz} of the SDM is shown. Considering $S_p(t_k, f_o)$, its smoothed estimator $\overline{S_p(t_k, f_o)}$ defined in (7.27) is obtained by averaging over a time window with a length $N_q = 100$ points with a 90% overlap. Once obtained the $\overline{S_p(t_k, f_o)}$ at each time t_k for each frequency f_0 the polarization degree $P(t_k, f_0)$ is obtained using the Samson's formulation in (7.25) while the azimuth $\vartheta(t_k, f_0)$ and Incidence $\varphi(t_k, f_0)$ angles are obtained doing the SVD of (7.27). Their evolution in the time frequency domain is shown in Figure 80.

From the first panel in Figure 80, it can be seen that the polarization degree $P(t_k, f_0)$ between 1 and 3 s around 20 Hz has a value greater than 0.8 indicating the presence of linear polarized wave type with an incidence between 30 and 60 degree. This phase can be interpreted as a P-Wave.

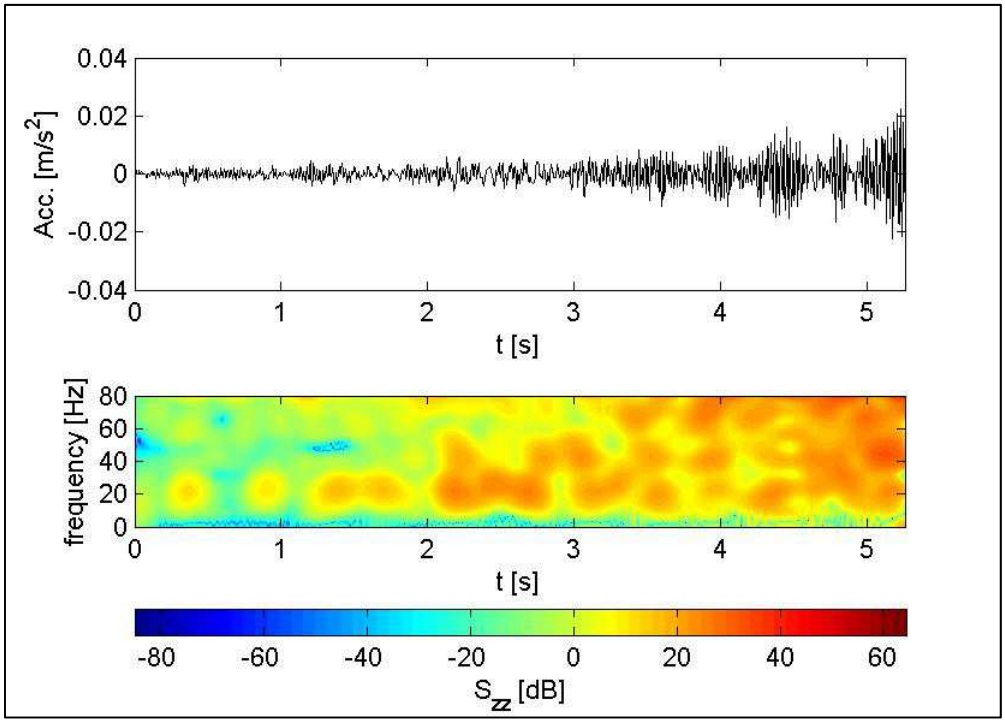

FIGURE 79 – TIME FREQUENCY REPRESENTATION. UPPER PANEL TIME HISTORY EVENT 'S RISE Z COMPONENT. LOWER PANEL: AUTOPOWER OBTAINED WITH REASSIGNED PSEUDO SMOOTHED WIGNER VILLE DISTRIBUTION. AUTOPOWER EXPRESSED IN DB WITH REFERENCE ACCELERATION 10^{-6} M/S

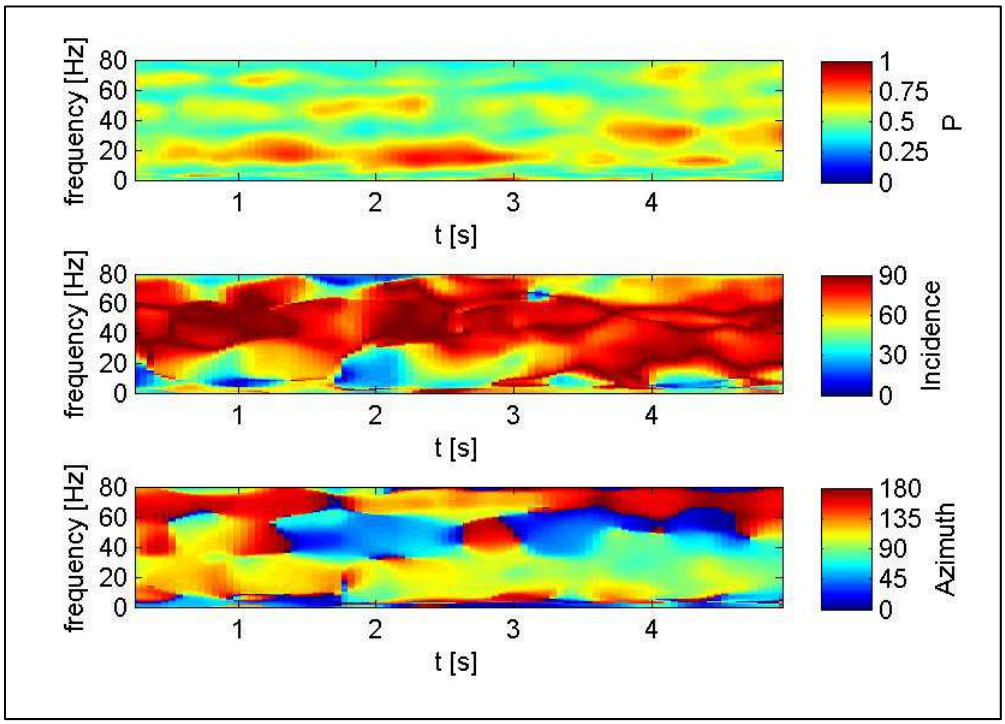

FIGURE 80 – TIME FREQUENCY POLARIZATION OF A TRAIN RISE

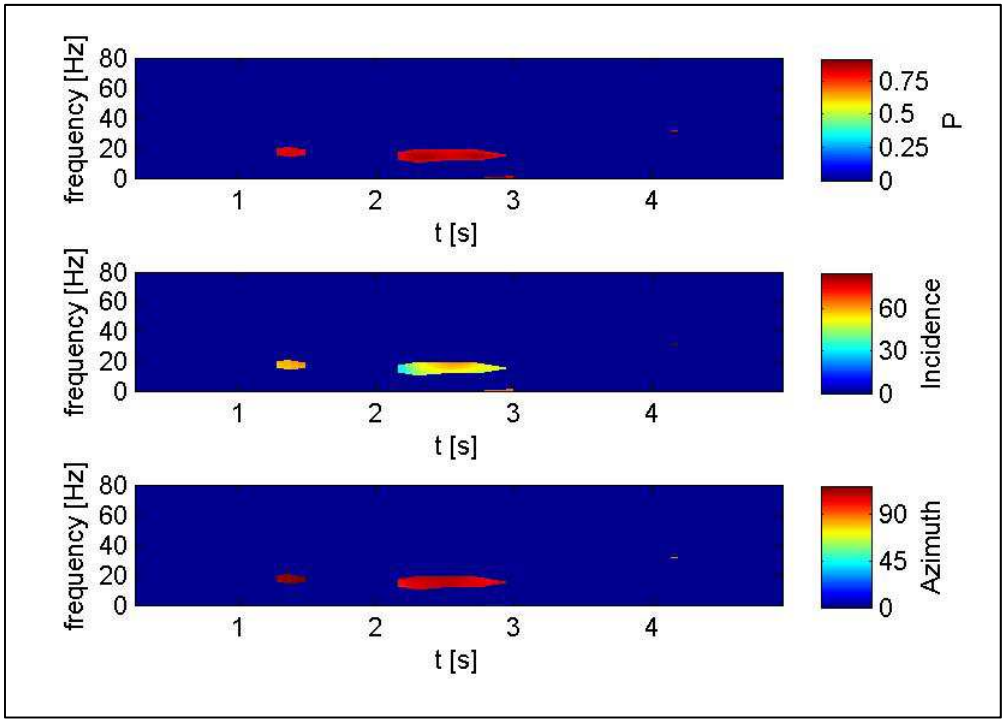

FIGURE 81 – FILTERED HODOGRAM

As stated in section 7.2 the aim of the analysis is the identification of body waves in the railway tremor. Therefore an improvement in the readability of the hodogram, the plot that described the evolution of the particle motion through the polarization parameters, in Figure 80 can be achieved thereby isolating the contribution of these phases. The latter is obtained defining a threshold in the polarization and analysing the evolution of the polarization parameter above this value.

Following the Chicowicz's approach [182] the polarization threshold is fixed at 0.8 and the filtered hodogram is shown in Figure 81 where the P-Wave phase already identified in Figure 80 is now better defined especially in terms of Incidence and Azimuth angles: the former is between 50 and 60 degree and the latter is between 90 and 100 degree. A better identification of the body waves can be achieved performing a statistic on the TF representation of the polarization attributes. This approach is going to be very useful for the CP wave field assessment explained in the next section. Let's consider W_r the set of N_R triaxial rise events j identified with the process explained in section 7.5.3 over the long term monitoring period.

$$W_r = [j] \quad j = 1 \ldots N_R \tag{7.37}$$

Therefore, the event analysed in Figure 80 belongs to W_r and is identified with e. For each frequency f_0, between 0 a 80 Hz, the statistical method is essentially based on identifying the time bins $t_0^e(f_0)$ such that:

$$t_0^e(f_0) = \left[t_k \in t \,/\, P^e(t_k, f_0) \right] \quad \forall f_0 \in [0, 80] \tag{7.38}$$

At each frequency f_0, the number of time bins $N_0^e(f_0)$ that exceed the polarization threshold is defined as the dimension of $t_0^e(f_0)$.

$$N_0^e(f_0) = \dim\left[t_0^e(f_0) \right] \quad \forall f_0 \in [0, 80] \tag{7.39}$$

$N_0^e(f_0)$ is coded as zero if $\dim\left[t_0^e(f_0) \right] \leq 5$. Considering that the TF polarization measurement is carried out on $N_{\Delta t}^e$ overlapped time windows, the probability $P_{HP}^e(f_0)$ that the frequency bins exceed the polarization threshold is defined as:

$$P_{HP}^e(f_0) = \left[\frac{N_0^e(f_0)}{N_{\Delta t}^e} \right] \quad \forall f_0 \in [0, 80] \tag{7.40}$$

In the same way $P_{MP}^e(f_0)$ can be defined as the probability that the frequency bins have a polarization level $P^e(t_k, f_0)$ between 0.5 and 0.8 which can be useful as an indication of the surface waves components of the railway microtremor. Both $P_{HP}^e(f_0)$ and $P_{MP}^e(f_0)$ are reported in Figure 82 which shows that only the 20% of the frequency bins between 10 and 20 Hz have a degree of polarization above 0.8. A better knowledge of the railway wavefield can be achieved considering also the information provided by azimuth and incident angles which can be treated in a statistical way too.

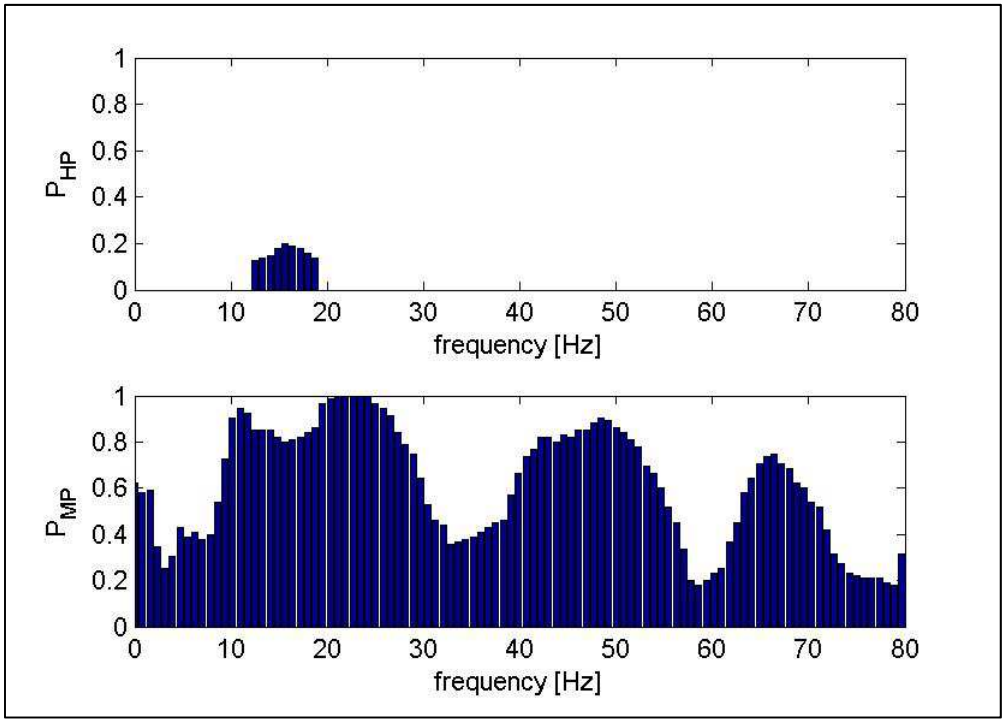

FIGURE 82 – UPPER PANEL PROBABILITY THAT THE FREQUENCY BINS HAVE A POLARIZATION LEVEL ABOVE 0.8. LOWER PANEL PROBABILITY THAT THE FREQUENCY BINS HAVE A POLARIZATION BETWEEN 0.5 AND 0.8

Considering the set $t_0^e(f_0)$ defined in (7.38) the average angles $\overline{\vartheta_{HP}^e(f_0)}$ and $\overline{\varphi_{HP}^e(f_0)}$ are defined as follow:

$$\overline{\vartheta_{HP}^e(f_0)} = \left\langle \vartheta^e(t_k, f_0) \right\rangle_{t_k \in t_0^e} \quad \forall f_0 \in [0,80] \tag{7.41}$$

$$\overline{\varphi_{HP}^e(f_0)} = \left\langle \varphi^e(t_k, f_0) \right\rangle_{t_k \in t_0^e} \quad \forall f_0 \in [0,80] \tag{7.42}$$

the average angles are obtained using the Fisher statistics as done by Patané and Ferrucci [157]. The equations (7.41) and (7.42) are coded as zero if $\dim\left[t_0^e\right] \le 5$.

Using this statistical approach, the polarization analysis in the TF domain is reduced to an analysis in the frequency domain using the parameters: $P_{HP}^e(f_0)$, $\overline{\vartheta_{HP}^e(f_0)}$ and $\overline{\varphi_{HP}^e(f_0)}$. The latter are presented in Figure 83 showing that the 20% of the frequency bins between 10 and 20 Hz have a degree of polarization greater than 0.8 with an average incidence angle around 50 degree and an average

azimuth respect to the North direction of 100 degree. As already shown Figure 61, the first arrival generated by this train event can be considered as a P-Wave type.

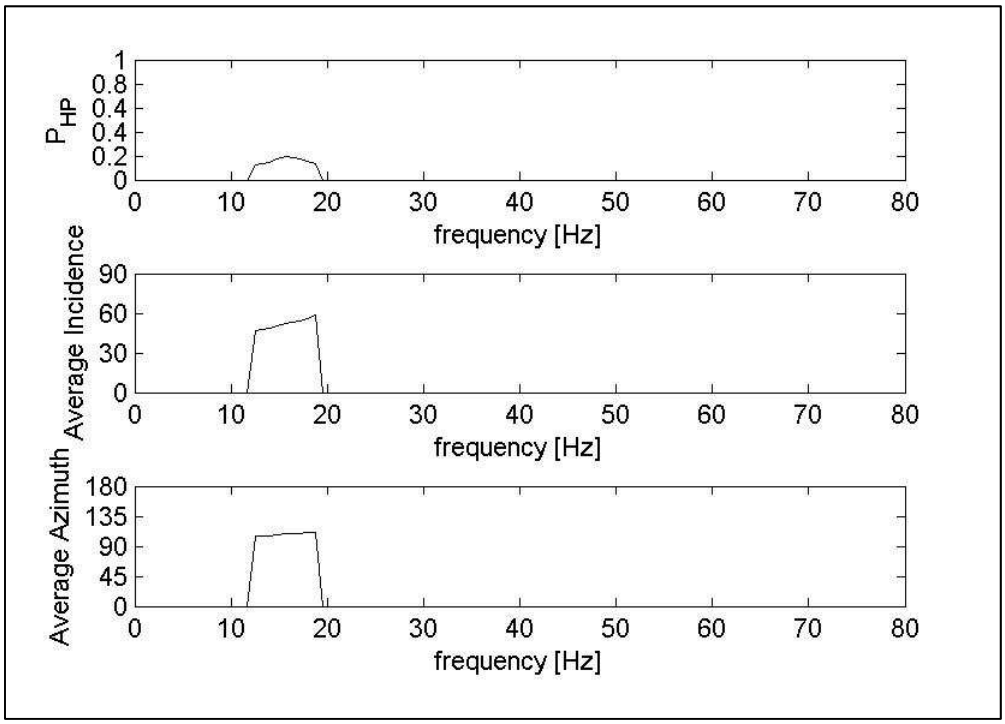

FIGURE 83 – STATISTICAL TF POLARIZATION ANALYSIS IN FREQUENCY DOMAIN. UPPER PANEL PROBABILITY THAT THE FREQUENCY BINS HAVE A POLARIZATION LEVEL ABOVE 08. MIDDLE PANEL AVERAGE INCIDENCE ANGLE. LOWER PANEL AVERAGE AZIMUTH ANGLE

7.5.5 WAVE FIELD ASSESSMENT FOR CONTROL POSITION

In the previous section with the time frequency polarization analysis from the first arrival, or rise, of the railway tremor it is possible to identify its part due to body waves. Of course, each train passage, during the 24 hour long term monitoring, will generate a different rise which will depend from its specific static and dynamic load. As a consequence, each rise is going to contain different polarization attributes, and averaging all of them acquired at CP will enhance some common propagation characteristics providing an estimation of the microtremor's wave field generated by the railway traffic in the resident environment. In this section a description of the wave field assessment is given for the control position described in section 7.5.2.

Let's consider the set W_r of N_T triaxial rise events defined in (7.37). For each event e belonging to W_r, at each frequency f_0 between 0 and 80 Hz, it's possible to

define the following polarization attributes $N_0^e(f_0)$, $P_{HP}^e(f_0)$, $\overline{\vartheta_{HP}^e(f_0)}$ and $\overline{\varphi_{HP}^e(f_0)}$ which are defined in the previous paragraph in (7.39), (7.40), (7.41) and (7.42). All the rises have been analysed with a moving time windows of 100 points, corresponding to 0.5 seconds, with an overlap of 90 %. The simplest estimator of the degree of the polarization for all events can be obtained considering the set of $P_{HP}^e(f_0)$ and applying an average at each frequency $f_0 \in [0,80]$. This estimator is defined as $\overline{P_{HP}(f_0)}$:

$$\overline{P_{HP}(f_0)} = \left\langle P_{HP}^e(f_0) \right\rangle_{\forall f_0 \in [0,80]} \quad \forall e \in W_r \tag{7.43}$$

The drawback of applying (7.43) is that for some $j \in W_r$ at certain frequencies $f_p \in [0,80]$, $P_{HP}^j(f_p)$ may be zero because $N_p^j(f_p) = 0$. This problem can be avoided by implementing an estimator that average only the $P_{HP}^j(f_o)$ where the $N_0^j(f_0) \neq 0$. This estimator is defined as $\overline{P_{HP}^{N0}(f_p)}$

$$\overline{P_{HP}^{N0}(f_p)} = \left\langle P_{HP}^j(f_0) \right\rangle_{\forall f_0 \in [0,80]/N_0^j(f_0)} \quad \forall j \in W_r \tag{7.44}$$

Since each $P_{HP}^j(f_0)$ is evaluated using different numbers of time bins $N_0^j(f_0)$ depending on the number of overlapped time windows $N_{\Delta t}^j$ used for the analysis, the estimator needs to be built for taking into account this important feature. This estimator, defined as $\overline{P_{HP}^W(f_0)}$, can be built as a weighted average considering $N_0^j(f_0)$ as a weighting.

$$\overline{P_{HP}^W(f_0)} = \left\langle N_0^j(f_0) P_{HP}^j(f_0) \right\rangle_{\forall f_0 \in [0,80]} \quad \forall j \in W_r \tag{7.45}$$

This estimator naturally manages the problem of the zeroes contained in $N_0^j(f_0)$. An idea of the maximum variation of the distribution of the $P_{HP}^j(f_0)$ over the frequency ranges can be done by defining a "peak hold" type estimator defined as $\overline{P_{HP}^{MAX}(f_0)}$:

$$\overline{P_{HP}^{MAX}(f_0)} = \max\left[P_{HP}^{j}(f_0)\right]_{\forall f_0 \in [0,80]} \quad \forall j \in W_r \tag{7.46}$$

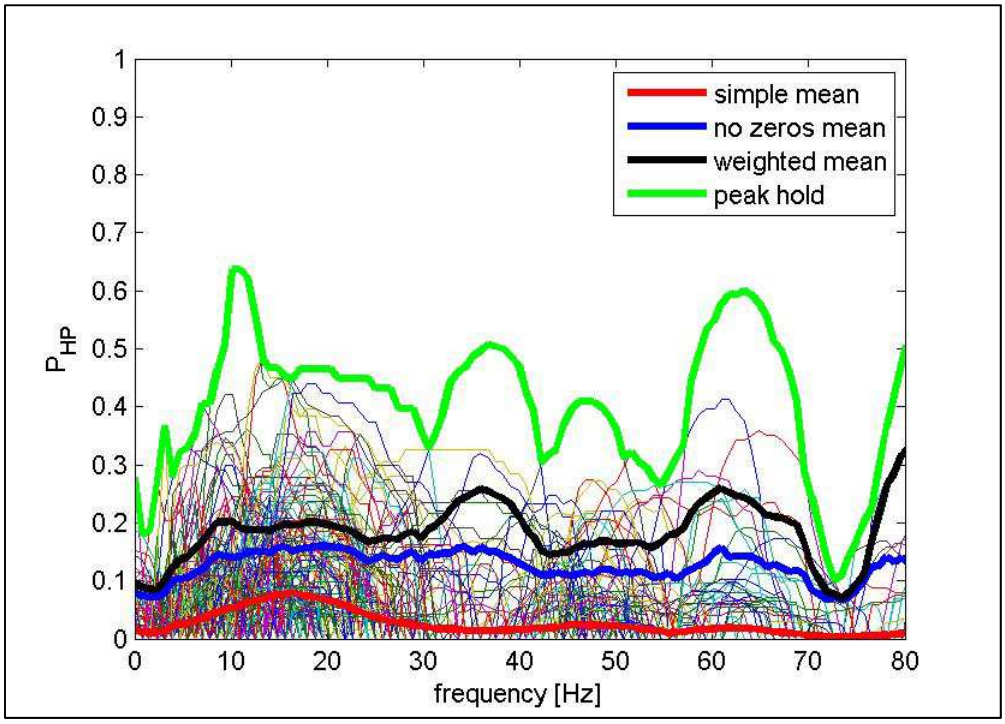

FIGURE 84 – DISTRIBUTION OF 219 $P_{HP}^{j}(f_o)$ AS A FUNCTION OF FREQUENCY OVER 24 HOUR MONITORING. THICK RED LINE REPRESENTS THE SIMPLE AVERAGE ESTIMATOR, THICK BLU LINE DESCRIBES THE AVERAGE ESTIMATOR WHICH EXCLUDES THE ZERO VALUES, THICK BLACK LINE IS THE WEIGHTED AVERAGE ESTIMATOR AND THE THICK GREEN LINE IS THE PEAK HOLD ESTIMATOR.

The distribution of all the 219 $P_{HP}^{j}(f_0)$, acquired in 24 hours at the CP, as a function of the frequency $f_0 \in [0,80]$ is plotted in Figure 84 with all the polarization degree estimators $\overline{P_{HP}(f_0)}$ (thick red line in Figure 84), $\overline{P_{HP}^{N0}(f_0)}$ (thick blue line in Figure 84), $\overline{P_{HP}^{W}(f_0)}$ (thick black line in Figure 84) and $\overline{P_{HP}^{MAX}(f_0)}$ (thick green line in Figure 84) defined above. It can be noted the effects on the zeroes on $\overline{P_{HP}(f_0)}$ is strong: with this estimator just the frequency range between 10 and 20 Hz has a probability of less than 10% to have a polarization degree above 0.8. On the other hand, $\overline{P_{HP}^{N0}(f_0)}$ and $\overline{P_{HP}^{W}(f_0)}$ have a similar behaviour across the frequency range with the latter providing slightly greater values than the former probably due to the effect of the weighting. Therefore $\overline{P_{HP}^{W}(f_0)}$ takes better into consideration the distribution of all the $P_{HP}^{j}(f_0)$ and therefore is going

to be used as estimator of the polarization degree for the wavefield generated by the railway traffic over 24 hours.

The wavefield assessment will be completed defining the estimator of incidence and azimuth angles. Even these two estimators will be an average over the entire set of $\overline{\vartheta_{HP}^{j}(f_0)}$ and $\overline{\varphi_{HP}^{j}(f_0)}$ with the same issues already discussed for the definition of the estimator for the polarization degree. Therefore as already done for the set $P_{HP}^{j}(f_0)$, the estimators for the incidence and azimuth angles will be a weighted average, using Fisher statistics, considering $N_0^{j}(f_0)$ as a weighting. The $\overline{\vartheta_{HP}^{W}(f_0)}$ and $\overline{\varphi_{HP}^{W}(f_0)}$ are defined as following:

$$\overline{\vartheta_{HP}^{W}(f_0)} = \left\langle N_0^{j}(f_0)\,\overline{\vartheta_{HP}^{j}(f_0)} \right\rangle_{\forall f_0 \in [0,80]} \quad \forall j \in W_r \tag{7.47}$$

$$\overline{\varphi_{HP}^{W}(f_0)} = \left\langle N_0^{j}(f_0)\,\overline{\varphi_{HP}^{j}(f_0)} \right\rangle_{\forall f_0 \in [0,80]} \quad \forall j \in W_r \tag{7.48}$$

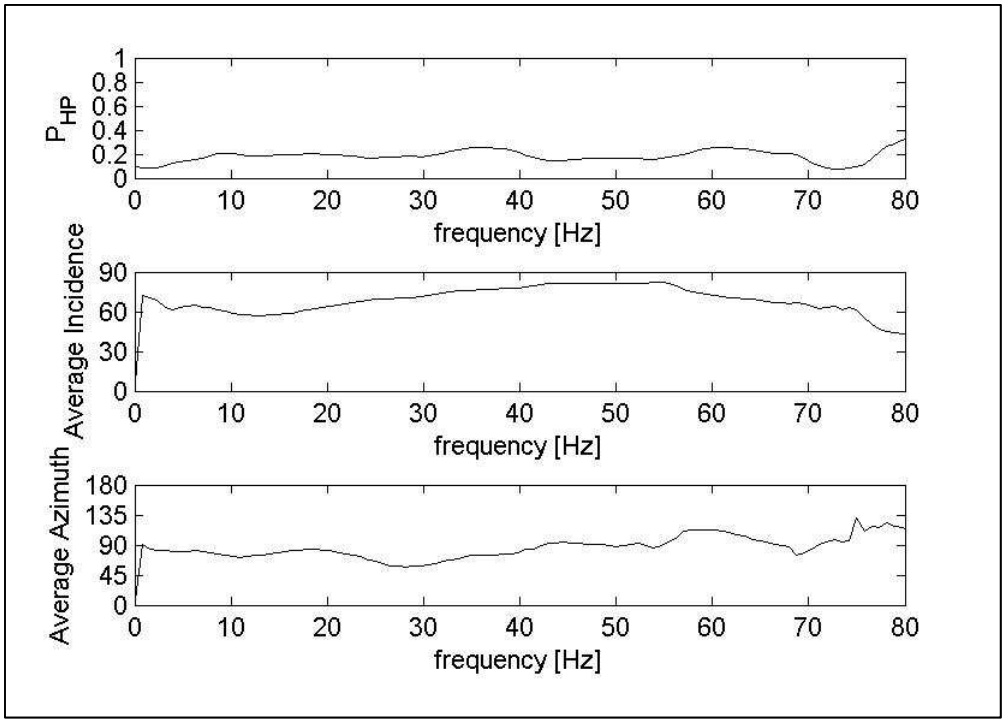

FIGURE 85 - WAVE FIELD ASSESSMENT OVER 24 HOUR MONITORING IN THE FREQUENCY DOMAIN. UPPER PANEL: PERCENTAGE OF FREQUENCY BINS WITH A POLARIZATION ABOVE 0.8. MIDDLE PANEL: AVERAGE INCIDENCE ANGLE. LOWER PANEL: AVERAGE AZIMUTH ANGLE.

Finally, the estimation of the body wave component of the wave field for the railway traffic is done considering the following estimators: $\overline{P_{HP}^{W}(f_0)}$, $\overline{\vartheta_{HP}^{W}(f_0)}$ and $\overline{\varphi_{HP}^{W}(f_0)}$ as a function of the frequency $f_0 \in [0,80]$. The latter are presented in Figure 85 as product of an average processes over 219 events. Considering Figure 85, it can be said that across the frequency range there is an average probability $\overline{P_{HP}^{W}(f_0)}$ of 20 % of to have a polarization above 0.8.

Then, a distinction between P and S waves can be done observing the behaviour of $\overline{\varphi_{HP}^{W}(f_0)}$ (middle panel Figure 85) as a function of frequency. With respect to the analysis of the single pass by, in the previous section, where only some frequency regions have polarization attributes different from zero, see Figure 83, the effect of the averaging on all events recorded during 24 hours gives back a sort of continuum. In this "continuum" it's possible to identify distinctively two frequency regions with two different characteristics. In the frequency range between 8 and 20 Hz, with a constant $\overline{P_{HP}^{W}(f_0)}$ of 20 %, the estimator of the incidence angle $\overline{\varphi_{HP}^{W}(f_0)}$ has a value around 60 degree and an azimuth angle $\overline{\vartheta_{HP}^{W}(f_0)}$ around 80 degree considering this phase as a SV wave type.

The method proposed here provides an estimation of the wave field generated by the entire railway traffic recorded in 24 hour long term monitoring which might lead to some information about the source mechanism of the vibration coming from the rail system

7.6 CONCLUSION

The polarization properties of vibration from railway construction and operation have been considered, for the first time, in this chapter.

It has been shown that the exploitation of the polarization characteristics was able to provide more detailed information of the wave field generated by railway and piling in comparison with the particle plot, which is an established method for the wave field assessment from manmade vibration.

Both approaches provided an interpretation of the wave types belonging to the wave field but the polarization analysis was also able to identify the exact starting point and the duration of the seismic phase. The particle motion plot performed well only if a single wave type was presented in the wave field whereas the polarization analysis was able to identify more than one wave type and the transition among the wave types. In addition, the polarization analysis allowed an estimation of the direction of the propagation of the perturbance which could be useful for localizing the vibration source as shown for piling vibration in section 7.4.3.

Generally, construction sources can be either fixed like piling or moving like compaction. Current vibration monitoring systems for construction vibration are not able to discriminate this source feature which can be resolved implementing the polarization analysis. Therefore, this method can be used for improving the vibration monitoring in order to better control and quantify the vibration impact on structure and people caused by construction sources

There were some computational advantages related to the implementation of the polarization analysis which was applied straight away on a tri-axial acceleration time history whereas the particle motion plot was generally obtained through a double integration process. Both methodologies presented here gave an interpretation of the wave field provided by an operator and suffered by the presence of noise but the polarization provides a more detailed analysis of the propagation characteristic of the pertubance generated by manmade processes.

The preliminary results presented in this chapter are encouraging for providing an in depth wave field assessment using vibration measurement which can improve both the assessment of vibration on people and structure and the investigation of the vibration source mechanisms.

8 TRANSMISSIBILITY ANALYSIS

8.1 INTRODUCTION

In the exposure assessment methodologies introduced in the framework of the project "Human response to vibration in residential environments", the transmissibility is a key tool that has been used to characterise the propagation from outside to inside the property in order to estimate the internal long term exposure. The use of ground-to-building transmissibility, is encouraged in the U.K; for example in BS 6472-1:2008 [18], the British Standard for predicting internal building vibration for assessing human exposure to vibration in buildings.

However, clear guidelines for its application are not provided. Generally in literature, the use of the transmissibility is "hidden" in measurement methodologies and models for assessing vibration induced in buildings (Martin [163], Hunaidi and Tremblay [164], Newland and Hunt [165], Nelson [184], Hunt [185]) but a few papers (Jakobsen [166], De Avillez et al. [167], With and Bodare [168]) treat the problem of the transmission of railway vibration into buildings. Furthermore, Sica et al. [83] and Villot et al. [186] explicitly treat the use of ground to building transmissibility function in order to predict exposure in buildings and estimate annoyance. On the other hand, the problem of the transfer function can be also found in the dual channel analysis where different formulations have been introduced (Randall [187], Amini [188]).

In the research objectives of this dissertation, see section 1.2, the study of the ground-to-building transmissibility is a topic correlated to NANR209 and the objectives of this chapter are: to identify the most suitable way to calculate the transmissibility for determining the human exposure, to validate the database of transmissibilities, to assess the uncertainty of the exposure estimation and to show some results for various property types. One of the possible applications of this large collection of buildings Frequency Response Functions (FRFs) could be in the prediction of the internal vibration exposure as sanctioned by the BS 6472-1:2008 [18].

In section 8.2 an overview of the transmissibility measurement is given. In section 8.3 the tools for the transmissibility analysis (section 8.5 and 8.6) are presented and conclusions are drawn in section 8.7.

8.2 OVERVIEW OF TRANSMISSIBILITY MEASUREMENT

In both exposure measurement methodologies presented in the chapters 4 and 5, the assessment of the internal exposure is done using two time synchronised accelerometer, one outside the property and one inside, for measuring the ground-to- building frequency response function (FRF) or transmissibility where the internal measurement point is at the 'point of entry'. This approach (see 4.4 and 0) has been used in order to satisfy the suggestion from the standard of obtaining the 24 hour internal exposure estimation.

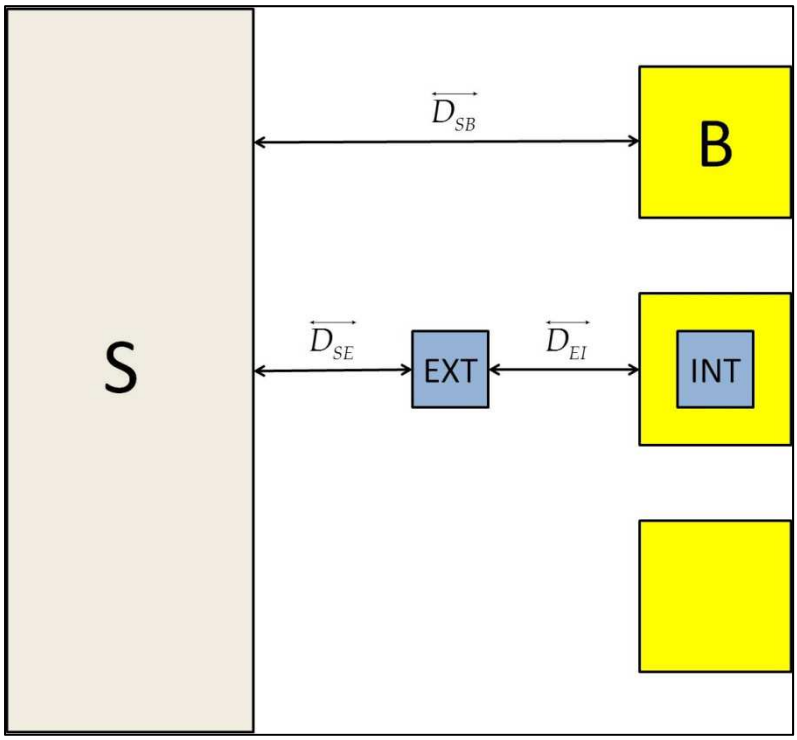

FIGURE 86 - SCHEME ILLUSTRATING THE GROUND-TO-BUILDING TRANSMISSIBILITY MEASUREMENT

The measurement setup is summarised in Figure 86 where *EXT* refers to the accelerometer outside the house[11] whereas *INT* is the one inside and S stands for

[11] In this framework both control position from railway traffic and construction sources are considered as an external measurement together with the elements of the external array for construction.

the vibration source. The following distances have been defined as well: $\overline{D_{SB}}$ is the distance between the source and the building, $\overline{D_{SE}}$ is the distance between the source and the accelerometer placed externally to the property and $\overline{D_{EI}}$ is the distance between the two sensors.

It is worth noting that $\overline{D_{SB}}$ and $\overline{D_{SE}}$ are measured at the boundary of the source such as after the closest railway line to the residential environment for the railway traffic methodology. On the other hand, for obtaining $\overline{D_{SB}}$ and $\overline{D_{EI}}$ the distance of the building has been measured at the most exposed facade. All the distances have been measured using digital maps tools (Google Maps and Google Earth) and, when available, the gps positions from the antenna of the *EXT* position or provided by Smartphone.

The standard BS ISO 4866:2010 [58] highlights the difficulty to measure ground-to-building FRF correctly in urban areas as the one surveyed by the project "Human response to vibration in residential environments". Generally, the *EXT* accelerometer should not be installed too close to the excitation point such as the railway track because in this way the ground motion will be influenced by the source mechanisms. This means that an ideal position of the transducer should be outside the near field of the source where compression and surface waves are generated. Even if it's difficult to evaluate the extent of the near field, some indications are given in the literature especially for railway sources. Madshus et al. [41] quantified the effect of the near field as 15 meters from the sources whereas Hannelius (in Bahrekazemi [68]) gave a figure 20 meters. On the other hand, the *EXT* transducer cannot be too close to the building as suggested by With and Bodare [168] who also advise that the transducer on the ground must not be in close proximity to large objects like cellars or boulders. The close proximity of the building can be quantified as less than 2 meters from the building or 1/10 of the dominant wavelength, generated by the source, away from the building as reported in the ANC guidelines [27]. Furthermore, the amplitude of vibration may be affected by reflection at the front of the foundation (with respect to the

travelling wave) and decreased at the rear side by dissipation and front side reflection (BS ISO 4866:2010 [58]).

All the observations mentioned above have been taken into consideration for the installation of the long term monitoring position albeit with some practical constraints. Primarily, the need to put the instrumentation in a secure place created some limitations in choosing a position not too close to the source or to the building. Another difficulty experienced was when the distance $\overleftrightarrow{D_{SB}}$ was too close to the source: in this way the *EXT* transducer was likely to be in the near field of the source. The installation of the *INT* accelerometer is generally done at a point: on the mid span of the floor of the room where a complaint originates or where the greatest adverse comment can be predicted according to BS 6472-1. Of course, the accessibility to the best measurement point is related with the resident's interest and cooperation with the study.

8.3 ANALYSIS TOOLS

In this section, theory is provided regarding the tools used for conducting the transmissibility analysis. First of all, a hypothesis on the nature of the process involved is needed; we are going to consider our vibration signals $\{X_n\}$ as a stochastic process, where the index n denotes the time $t = n\Delta t$ at which the observation is made and Δt is the sampling interval.

The concept of stochastic process is too general to be used, therefore $\{X_n\}$ will belong to a more restrictive class of random process: the stationary process. This means that even if the actual observables vary in time, the underlying statistical description is time invariant. A further approximation is needed; the process will be stationary in a wide sense or so called weakly stationary (Parker [189]). A process $\{X_n\}$ is weakly stationary if its mean is constant

$$\langle X_n \rangle = \mu$$

And in our case μ is considered zero; another property of $\{X_n\}$ is that its autocorrelation R_X depends on $\tau = m - n$, where τ is called the lag.

$$R_X(\tau) = R_X(m-n)$$

The autocorrelation is an even function $R_X(-\tau) = R_X(\tau)$ and $R_X(0) = \left\langle \{X_n\}^2 \right\rangle = \sigma_X^2$ where σ_X^2 is the variance of the process. The process $\{X_n\}$ needs to be ergodic too. A random process is ergodic when the ensemble average can be replaced by a time average.

8.3.1 SPECTRUM, AUTO SPECTRUM AND CROSS SPECTRUM

The spectrum of the signal $\{X_n\}$ is obtained using a segment averaging method as already pointed out in 4.5.3. The signal contains N samples which are segmented in q time windows of length N_q overlapped by o points. The spectral estimate $X_q(f)$ for each slice will be:

$$X_q(f) = \sum_{T=0}^{N_q-1} w_T X_T e^{-2\pi f T} \tag{8.1}$$

where w_T is the windowing function. The averaging process will enhance the underlying behaviour of the signal such that the variability will be reduced (Shin & Hammond [190]). The spectrum $X(f)$ of the signal $\{X_n\}$ will be.

$$X(f) = \frac{1}{q}\sum_{i=1}^{q} X_i(f) \tag{8.2}$$

For an acceleration time history $\{X_n\}$ of finite length, the choice of the segment length N_q influences the random error associated with $X(f)$, the frequency resolution and lowest reliable frequency component of the spectral estimation. If railway induced vibration is assumed to be a weakly stationary process, the normalised RMS random error associated with this analysis is inversely

proportional to the square root of the number of averages (Bendat and Piersol, [191]).

The number of averages is a function of the length of the time record *N*, the length of the windowed segments N_q, and the proportion of the overlapped points *o* in the windowed segments which is 50 % as stated in section 4.5.3. From all events identified from the 24-hour external measurement data, the average duration of an event is 7 s (standard deviation 5 s over 14143 train events identified) which is equal to 13 averages per event using N_q =200 and o =100. On average, five synchronised internal and external events were available for each case study therefore a normalised RMS random error of 13% can be found. For a 200 point segment length, the lowest frequency at which the length of a full cycle is less than the window length is 1 Hz. Below this frequency estimates of $X(f)$ will be highly unreliable and the vibration energy generated by railway vibration in this frequency region would be imperceptible to human subjects. Therefore 200 point Hanning window with 50% overlap can be considered a reasonable choice for the spectral analysis of this chapter and the one proposed in 4.5.3.

Keeping consistency with the system described in 8.2, we are going to consider two signals $\{E_n\}$ and $\{I_n\}$, recorded at the same time at *EXT* and *INT* position, with sliced spectra $E_q(f)$ and $I_q(f)$ as in (8.1) such that the cross spectrum $G_{EI}(f)$, single sided, between the above series is:

$$G_{EI}(f)=\frac{2}{q}\sum_{i=1}^{q}E_i^*(f)I_i(f) \tag{8.3}$$

Generally the cross spectrum $G_{EI}(f)$ would have the same amplitude but opposite phase. It's also worth mentioning the auto spectra, single side, of both $\{E_n\}$ and $\{I_n\}$: $G_{EE}(f)$ and $G_{II}(f)$ respectively.

$$G_{EE}(f)=\frac{2}{q}\sum_{i=1}^{q}E_i^*(f)E_i(f) \tag{8.4}$$

$$G_{II}(f)=\frac{2}{q}\sum_{i=1}^{q}I_i^*(f)I_i(f) \tag{8.5}$$

Now that cross and auto spectra functions are defined, it's possible to introduce, in the following sections, two important concepts in the field of dual channel analysis: coherence and frequency response function.

8.3.2 COHERENCE

The coherence function between the two signals $\{E_n\}$ and $\{I_n\}$ is equal to the cross spectrum $G_{EI}(f)$ divided by the square root of the product of the two auto spectra [192].

$$\gamma_{EI}(f)=\frac{G_{EI}(f)}{\sqrt{G_{EE}(f)G_{II}(f)}} \tag{8.6}$$

The coherence is a normalized cross-spectral density function and the magnitude-squared coherence (MSC) defined as

$$C_{EI}(f)\equiv\left|\gamma_{EI}(f)\right|^2 \tag{8.7}$$

Lies in the range

$$0\le C_{EI}(f)\le 1 \tag{8.8}$$

For a single estimate the MSC $C_{EI}(f)$ would always be unity (Randall [187]), therefore its calculation is based on average functions. In order to reduce the bias and variance in the estimation of the coherence a moving average with a 50 % overlap, using an Hanning window, has been considered following the approach suggested in Carter et al. [193]. Bendat and Persol [191] identified the following reasons for having a MSC less than unity:

1. Extraneous noise is present in the measurements.
2. A non-linear relationship between $\{E_n\}$ and $\{I_n\}$
3. $\{I_n\}$ is an output due to an input $\{E_n\}$ as well other inputs.

The last point is an important mechanism which contributes to poor coherence measurements for railway vibration as found, for example, in Bahrekazemi [68], Newland and Hunt [165] and De Avillez et al. [167]. In fact, the vibration transmission from the ground to the house can be modelled as a Multiple Input Multiple Output (MIMO) system. The railway can be described as a mix of incoherent point sources and line source (Madshus et al. [41]) and the time histories recorded by the receivers, employed in the transmissibility measurement in Figure 86, are the product of the interaction among these multiple sources. This phenomenon, here defined as MIMO effect, tends to decrease the cross correlation between the measurement points providing a coherence value less than unity.

The coherence function has uses in several areas, such as system identification, measurement of signal-to-noise ratio and determination of time delay.

8.3.3 VIRTUAL COHERENCE

As already explained in the previous section, a system contaminated by noise will have a coherence function $C_{EI}(f)$ between 0 and 1. Generally, if the coherence is less than 0.8 the system should be modelled as having more than one input, and a multiple input single output should be used for describing our system (Price & Bernhard [194]).

This problem is commonly encountered in automotive engineering for optimizing the interior road noise in a multiple input environment (Vanderbroeck and Hendrix [195]) . In fact the noise inside the car is induced by incoherent excitation caused by the wheels rolling over the road surface. The amount of energy transferred from the wheels to the car's interior depends on the dynamic properties of the suspension and car body. In this framework an analysis of the energy transmitted from the wheels to the interior of the car has been developed with the objective of separating the data into sets of "uncorrelated phenomena". In this section we are going to discuss this approach. The latter consists of a linear transformation which will condition the measured input spectra to identify how many incoherent sources exist. The technique will provide a frequency spectrum of each incoherent source which is an image of the real source. A coherence

function is generated as the portion of the energy output due to each incoherent source. This function is referred to as virtual coherence.

Considering the system described in section 8.2 with an *EXT* accelerometer outside the building and *INT* accelerometer inside, we are going to define for each tri-axial receiver the auto power matrices $EE_{ij}(f)$ and $II_{ij}(f)$.

$$EE_{ij}(f) = G_{E_iE_j} = \frac{2}{q}\sum_{k=1}^{q} E_{jk}^{*}(f)E_{ik}(f) \quad i,j = 1\ldots3 \tag{8.9}$$

$$II_{ij}(f) = G_{I_iI_j} = \frac{2}{q}\sum_{k=1}^{q} I_{jk}^{*}(f)I_{ik}(f) \quad i,j = 1\ldots3 \tag{8.10}$$

The cross power spectra matrix $IE_{ij}(f)$ needs to be defined as well:

$$IE_{ij}(f) = G_{I_iE_j} = \frac{2}{q}\sum_{k=1}^{q} I_{jk}^{*}(f)E_{ik}(f) \quad i,j = 1\ldots3 \tag{8.11}$$

Considering the *EXT* accelerometer as the reference of our system, its "incoherent sources" are found from an eigenanalysis of its cross spectrum matrix $EE(f)$. The latter can be rewritten in the following way:

$$EE_{ij}(f) = U^{T}(f)D_{M}(f)U(f) \tag{8.12}$$

Where $D_M(f)$ identify the principal component or "incoherent sources" of the reference: it is a diagonal matrix with a 3 x 3 dimension corresponding to the x, y and z axes measured by the accelerometer. $U(f)$ is the matrix of the eigenvectors which identify the direction of the new reference system that maximize the variance of $EE(f)$. The eigenstructure matrix $U(f)$ is used for rotating the cross spectrum matrix $IE(f)$ in the basis of the "incoherent sources" identified at the reference. In this way the virtual cross power spectra matrix $IE'(f)$ between physical signal at *INT* and principal component at *EXT* can be calculated:

$$IE'(f) = IE(f)U(f) \tag{8.13}$$

The virtual coherence function $C_{I_iD_{Mj}}(f)$ is defined as the ordinary coherence between the i-th $I_i(f)$ signal at *INT* and the j-th principal component $D_{Mj}(f)$ at *EXT*.

$$C_{I_iD_{Mj}}(f) = \frac{\left|IE'_{ij}(f)\right|^2}{I_i(f)D_{Mj}(f)} \quad i,j = 1\ldots3 \tag{8.14}$$

An application of the virtual coherence for solving ground-to-building transmissibility problems is shown in section 8.6.

8.3.4 FREQUENCY RESPONSE FUNCTION

The most important use of the dual channel analysis is the measurement of frequency response function (FRF) or as it is called in the framework of this work transmissibility. Throughout the text these terms will be used interchangeably. The transmissibility is a sort of "black box" which represents the ratio of the output-to-input of the system in the frequency domain (Randall [187]). In our case the output is the vibration $\{I_n\}$ inside the property measured at the *INT* position whereas the input is the incoming vibration $\{E_n\}$ recorded at the *EXT* position. Therefore the system considered is the portion of soil which interacts with the building foundation and the sub-structures linked with the foundation like floors, walls and cellars. The FRF provides a correct description of the system considered if the latter is stable, linear, time-invariant and noise free (Randall [187]). Therefore in our case, the FRF will provide an approximation of the behaviour of the system.

Several estimators exist in literature for calculating the FRF. Considering the system described in 8.2 and the values defined in (8.3), (8.4) and (8.5), the first estimator $H(f)$ can be obtained from:

$$H(f) = \sqrt{\frac{G_{II}(f)}{G_{EE}(f)}} \tag{8.15}$$

This estimator has been used in the project "Human response to vibration in residential environments" for calculating the soil-to-building transmissibility. A similar approach has been used by Hunaidi and Tremblay [164], Jakobsen [166] and De Avillez et al. [167] with the difference that their analysis was carried out in octave bands. In Newland and Hunt [165] and Hunt [185] the equation (8.15) is referred to as total transmissibility. The second estimator is defined as $H1(f)$

$$H1(f) = \frac{G_{EI}(f)}{G_{EE}(f)} \tag{8.16}$$

the noise at the input contaminate $H1(f)$: its effect is significant in the vicinity of resonance (Amini [188]). The $H1(f)$ estimator, is also called as the direct transmissibility in Newland and Hunt [165] and Hunt [185], and With and Bodare [168]. The last estimator considered is $H2(f)$

$$H2(f) = \frac{G_{II}(f)}{G_{IE}(f)} \tag{8.17}$$

which is considered by Mitchell to be sensitive to the output noise and its effect is pronounced in the anti-resonant region (Amini [188]). It can be seen that the ratio between $H1(f)$ and $H2(f)$ is equal to the MSC.

In a noise free scenario all the FRF formulations provide the same result; however the presence of noise corrupts the results instead. In this framework, the sources of noise considered are the same mentioned in section 8.3.2 for the coherence analysis: uncorrelated noise between the input and/or output, non-linearity and MIMO effect. In fact in a noisy environment, for a given frequency *f*, the cross spectrum tends to decrease therefore $H1(f)$ will decrease whereas $H2(f)$ will increase (See right side Figure 87) considering (8.16) and (8.17).

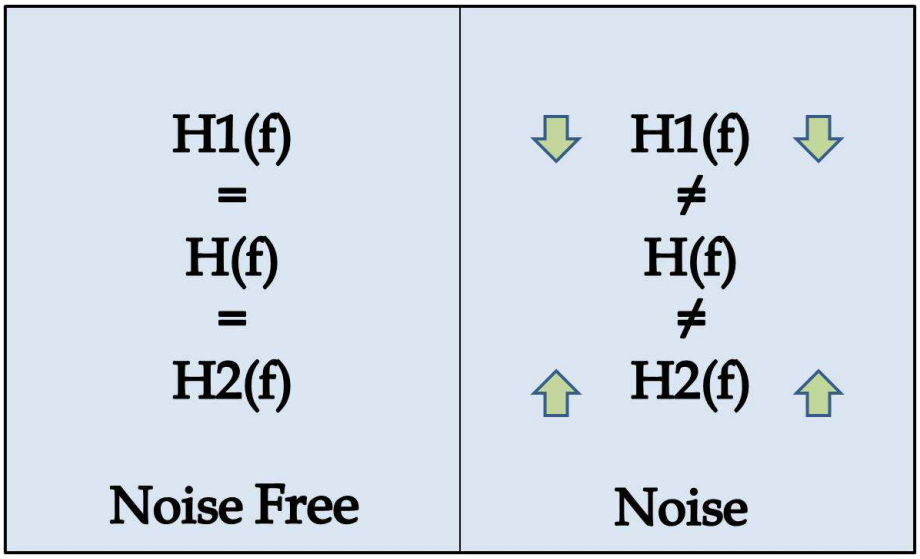

FIGURE 87 - EFFECT OF NOISE ON THE DIFFERENT FRF FORMULATIONS

Before considering the transmissibility analysis, section 8.5, a quick description of the selection of the site used is given in the following section.

8.4 SITE SELECTION

In this section the selection of the sites used for the transmissibility analysis is presented. As already explain in section 4.3.2 measurement sites can have different configurations depending on the orientation of the line of the houses with respect to the vibration source and for this analysis measurement sites parallel to the railway have been considered. Using online map service and the Excel file, 43 such houses have been identified.

8.5 ANALYSIS OF TRANSMISSIBILITY

Bearing in mind the scenario depicted in 8.2, in this section we are going to consider the analysis steps necessary for evaluating the transmissibility between two synchronized accelerometers: one placed outside the house called *EXT* and one placed internally close as possible to the point of entry named *INT*. The measurement is realized considering several train passages - a minimum of five.

First of all, the events are identified using the STA\LTA algorithm as shown in 8.5.2, then in 8.5.3 the propagation time between the events is removed. In 8.5.4 a method for assessing the linearity of the measurement is presented based on the

coherence whereas the issue of the averaging is considered in 8.5.5. Finally the use of transmissibility for assessing the human exposure is presented in 8.5.6. For a better understanding of the problem, the analysis steps will be applied in a detailed way to a single case study belonging to the collection of measurements from the project NANR209. For this reason the site characteristics are presented in 8.5.1. Following the approach presented in this section, further transmissibility analyses are presented in appendix E.

8.5.1 SITE OVERVIEW

The site considered for the analysis, also referred as site 0, is shown in Figure 88.

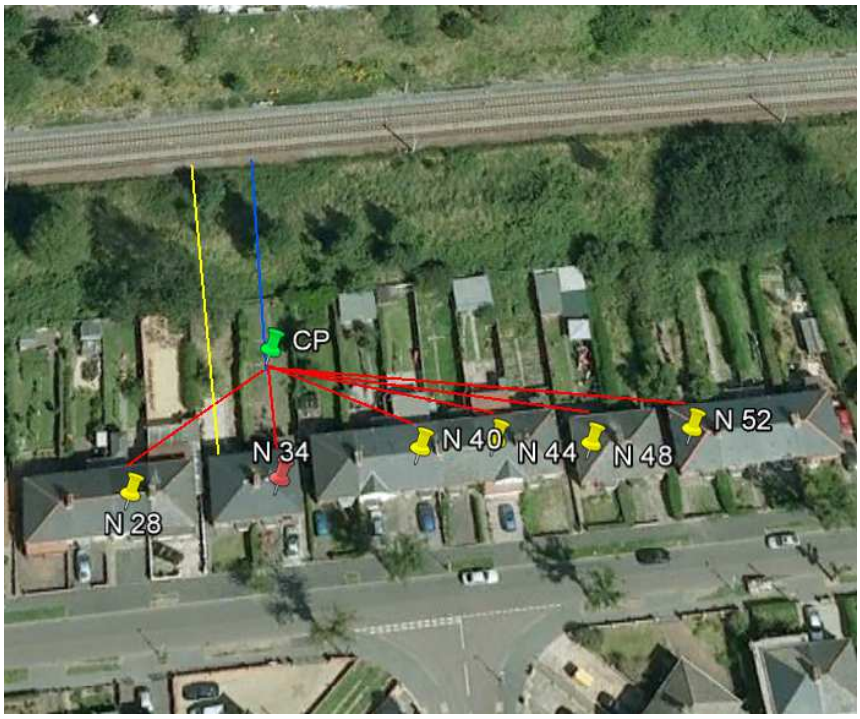

FIGURE 88 – SITE 0

The distance between the source and the control position, *EXT* accelerometer in the scenario described in Figure 86, $\overline{D_{SE}}$ (blue line in Figure 88) is 33.9 meters whereas the distance between the source and the line of the buildings $\overline{D_{SB}}$ (yellow line in Figure 88) is 45.2 meters. For this site 6 houses have been surveyed.

The characteristics of the measurement site such as house number, distance from control position (red lines in Figure 88), house type, room, floor, mounting method and numbers of trains are reported in Table 16.

House N°	Distance CP (m)	Type	Room	Floor	Mounting	N° Trains
28	22.7	Semi detached	Living Room	Ground	Direct	6
34	12.1	Semi detached	Kitchen	Ground	Plate	12
40	21.8	Semi detached	Living Room	Ground	Direct	17
44	32.1	Semi detached	Living Room	Ground	Direct	4
48	45.1	Semi detached	Corridor	Ground	Direct	5
52	58.5	Semi detached	Kitchen	Ground	Direct	4

TABLE 16 - CHARACTERISTICS OF THE MEASUREMENT SITE 0

8.5.2 EVENT IDENTIFICATION

The routine for identifying the events simultaneously recorded at the two measurement positions is the one already discussed in section 4.5.2.

8.5.3 ALIGNMENT

Once the events have been identified, an intermediate step is needed before performing the dual channel analysis. In fact for obtaining a better definition of

the coherence and transmissibility measurements, the propagation time between the waveforms has been removed.

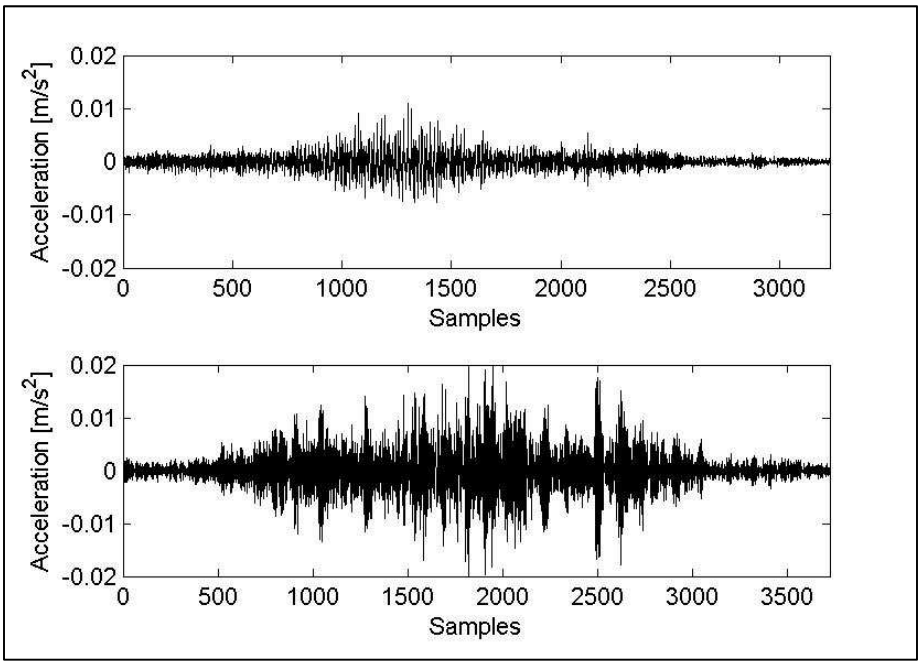

FIGURE 89 – ACCELERATION TIME HISTORIES OF A TRAIN PASSAGE. UPPER FIGURE *EXT* POSITION, LOWER FIGURE *INT* POSITION.

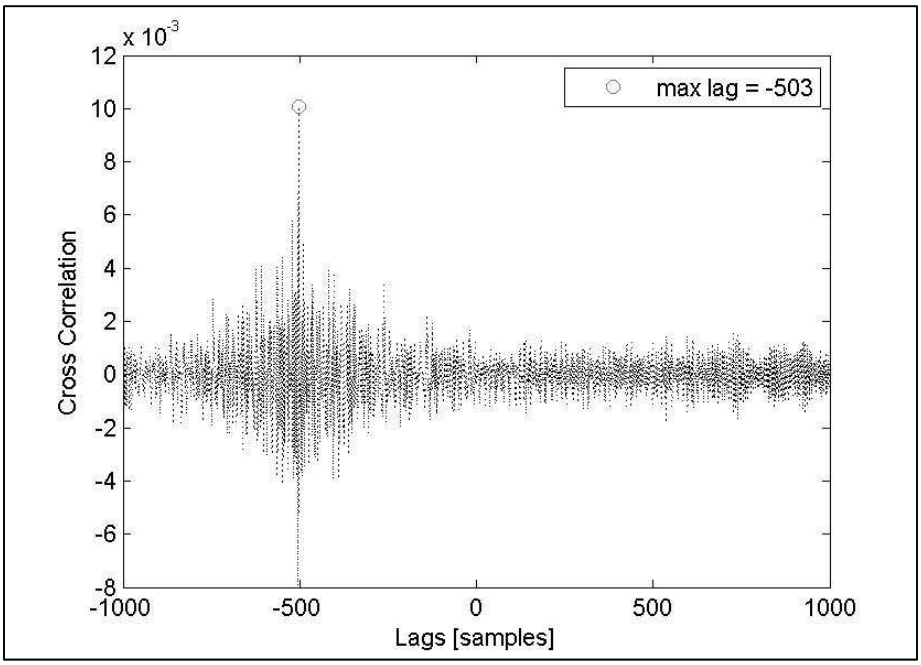

FIGURE 90 - CROSS CORRELATION FUNCTION BETWEEN THE SIGNALS RECORDED AT *EXT* AND *INT* POSITION.

An estimation of the propagation time is obtained evaluating the time lag corresponding to the maximum of the cross correlation function between the two

signals: the reference signal of the *EXT* accelerometer and one component of the *INT* accelerometer. Any waveform alignment is always conducted using the z component of the *EXT* accelerometer as reference.

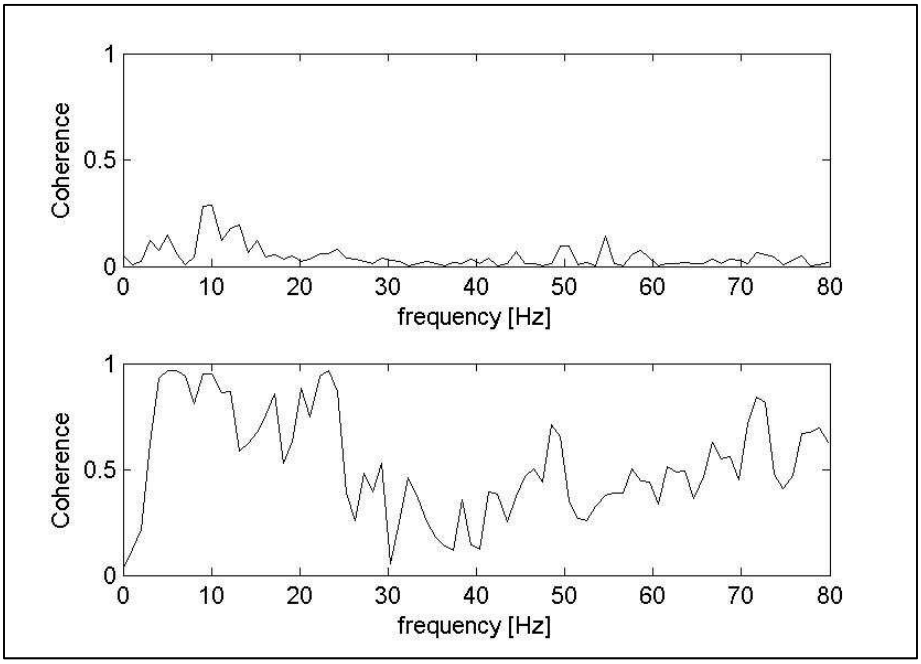

FIGURE 91 - COMPARISON BETWEEN MSC FUNCTIONS. UPPER FIGURE COHERENCE EVALUATED WITHOUT ALIGNEMENT. LOWER FIGURE COHERENCE EVALUATED WITH ALIGNEMENT

As example, we are going to consider a train passage recorded, at the site described above, at the same time in both CP as *EXT* position at the house number 34 as *INT* position (See Figure 88). Both time histories are presented in Figure 89. In Figure 90 a detail of the cross correlation function is shown. From the figure, it can be noted that the maximum of the function is reached when the time lag is negative with a value of -516 samples. Finally, the effect of the waveform alignment on the coherence estimation is shown in Figure 91 between the signals shown in Figure 89. It can be seen, from the lower part of figure, that this procedure can produce a significant improvement in the coherence estimation.

8.5.4 LINEARITY OF THE MEASUREMENT

One of the objectives of this chapter is to identify which transmissibility formulations, introduced in 8.3.4, is the most suitable for the evaluation of the human exposure to vibration. From Figure 87 it can be seen that the different FRF formulation are comparable in a noise free scenario therefore, considering the

cause of noise stated in 8.3.2 and 8.3.4, when there is no noise in the measurement system, the system is linear and only the input is responsible for the output. A tool that can help to identify the features described above is the coherence.

As described in Randall [187], the coherence gives a measure of the degree of linear dependence between the two signals, as a function of frequency. The higher the linear relation between the signals detected by the *INT* and *EXT* receivers, the higher the coherence (Foti [104]). According to Bendat and Piersol [191] coherence values between 0.8 and 0.9 indicate that the input of the system *EXT* contributes strongly to its output *INT*. On the other hand, values with low coherence, as already stated in section 8.3.2, generally indicate that the output of the system is a contribution from its input plus other inputs. The same picture is proposed by Price and Barnard [194] who identified coherence values less than 0.8 for modelling the system as having more than one input. This situation is very typical for railway excitations due to their multi inputs nature which implies poor ground to building coherence measurement (Newland and Hunt [165]). Therefore a threshold of 0.8 in coherence, based on the theory and the practical experience, can be used for identifying the frequency ranges where the dual channel measurement identifies a linear relationship between input and output with a high signal-to-noise ratio.

An application of this approach is shown in Figure 92 for the train passage in Figure 89. The set of frequencies for the *j* dual channel measurement where there is linearity is identified by L_j in (8.18) (which can be empty).

$$L_j = \left\{ f_i \in f \,/\, \left| \gamma_j \left(f_i \right) \right| \geq 0.8 \right\} \tag{8.18}$$

Considering the couple of receivers CP as *EXT* position and the Internal measurement at the house number 34 as *INT* position (green and red Pin in Figure 88), a contour map of the coherence as a function of frequency for all the events recorded at both receivers can be useful for identifying the frequency zones where the coherence is greater than 0.8. In fact from Figure 93 it can be found that these frequency zones are between 5-25 Hz and 70-80 Hz.

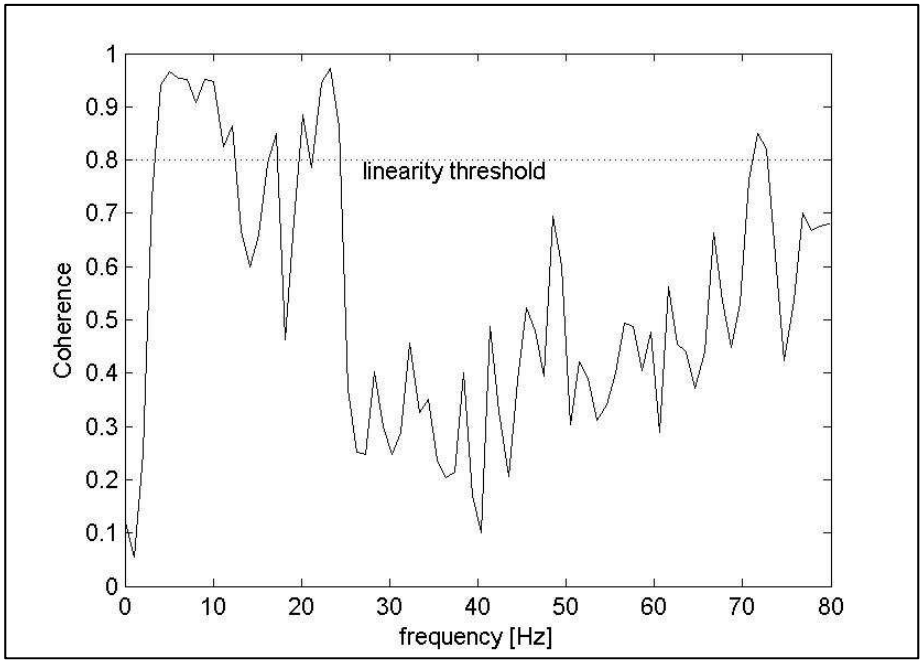

FIGURE 92 – COHERENCE AS A FUNCTION OF FREQUENCY WITH LINEARITY THRESHOLD

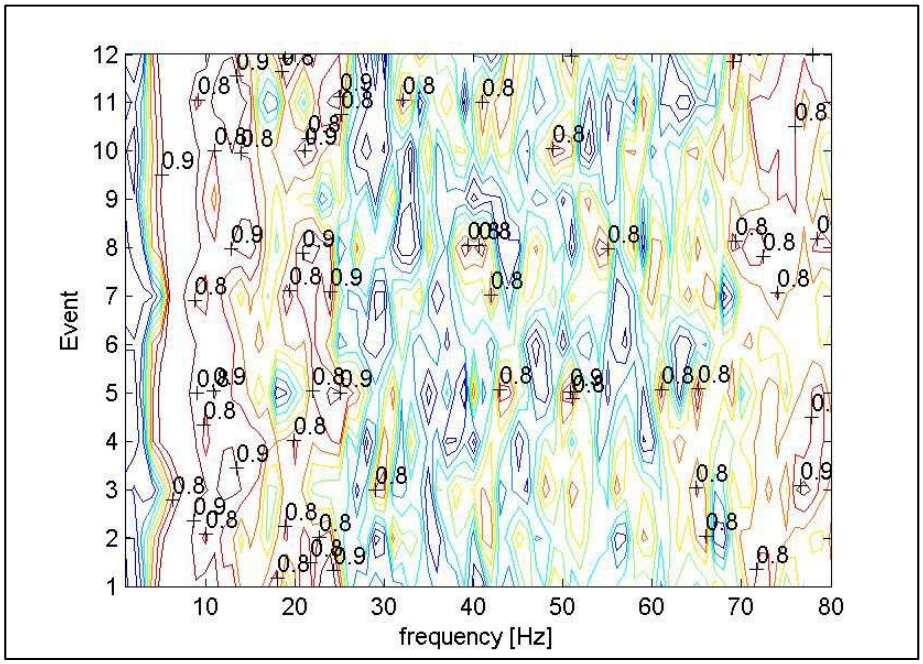

FIGURE 93 – COUNTOUR MAP OF THE COHERENCE FUNCTION BETWEEN THE Z COMPONENTS AT CP AND HOUSE NUMBER 48 FOR ALL THE EVENTS

If all the events measured at both receivers are considered, for each dual channel measurement j will be associated a L_j, where L is defined as the set of all the L_j

$$L = \{L_1, L_2, \ldots, L_N\} \tag{8.19}$$

Where N are the number of events. Knowing L, it is possible to build the distribution of the frequency bins above the coherence threshold as a function of the frequency as shown in Figure 94.

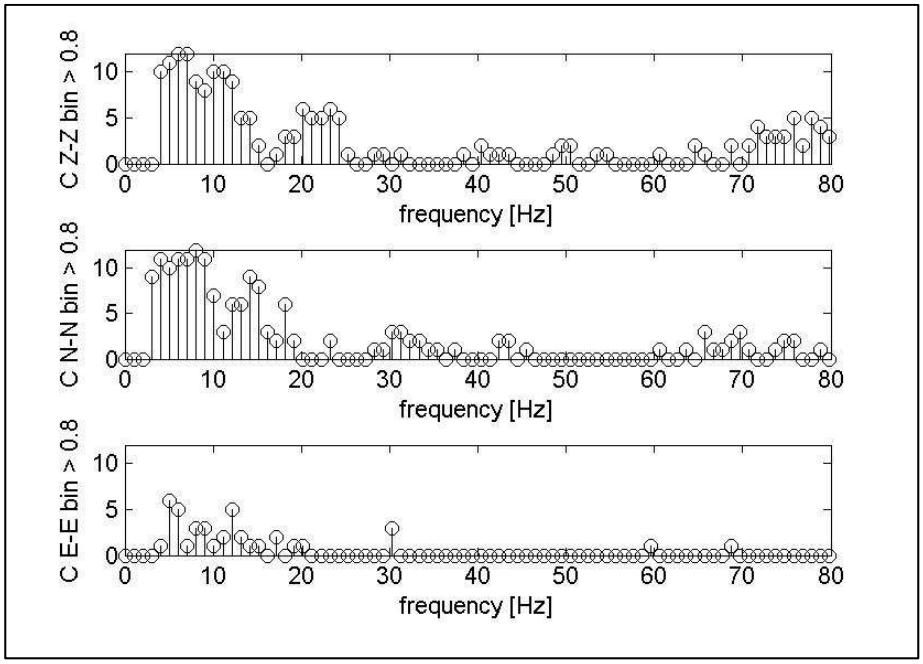

FIGURE 94 – NUMBER OF THE FREQUENCY BINS OF THE COHERENCE FUNCTION (C) WITH A VALUE ABOVE 0.8 IN FUNCTION OF FREQUENCY. IN THE UPPER PANEL THE COHERENCE BETWEEN THE Z COMPONENT IN *EXT* AND Z COMPONENT IN *INT* IS CONSIDERED. MIDDLE PANEL COHERENCE BETWEEN N AND N. LOWER PANEL COHERENCE BETWEEN E AND E

Considering the coherence between the z components of the two receivers, it can be seen in Figure 94 that 9 events or more have frequency bins above the threshold in the frequency range between 5 and 11 Hz. The same behaviour can be observed for the coherence between the n components in the frequency range between 4 and 9 Hz. For each event, it is also possible to count the frequency bins that are above the fixed threshold in coherence. This parameter can be related to the length of the event recorded at the *EXT* position in order to understand which events can provide a good coherence measure.

For the site considered, the coherence between the *EXT* position and the other *INT* positions has been investigated and no frequency bins above the 0.8 threshold have been found. In the following section, a new method for averaging cross spectra based transfer functions will be introduced based on the assessment of the linearity of the dual channel measurement.

8.5.5 AVERAGING AND COMPARISON

In framework of NANR209, the ground-to-building transmissibility estimation is obtained with a linear averaging of the FRF, in its *H* formulation shown in (8.15), for each event recorded at both measurements positions as explained in 4.5.3. On the other hand, the transmissibility function can also be obtained with a linear average of cross spectra based transfer functions such as *H1* (8.16) or *H2* (8.17). The three different transmissibility formulations are represented, for the couple of receivers CP and House number 34, in Figure 95. From Figure 95, it can be understood that the three formulations of transmissibility, between the z component outside and the one inside the property, are close to each other in the frequency range between 5-20 Hz and 70-80 Hz. Outside these ranges, the formulations provide different results with a discrepancy of several dBs. As already pointed out in section 8.3.4, this discrepancy might be related to noise as shown in Figure 87.

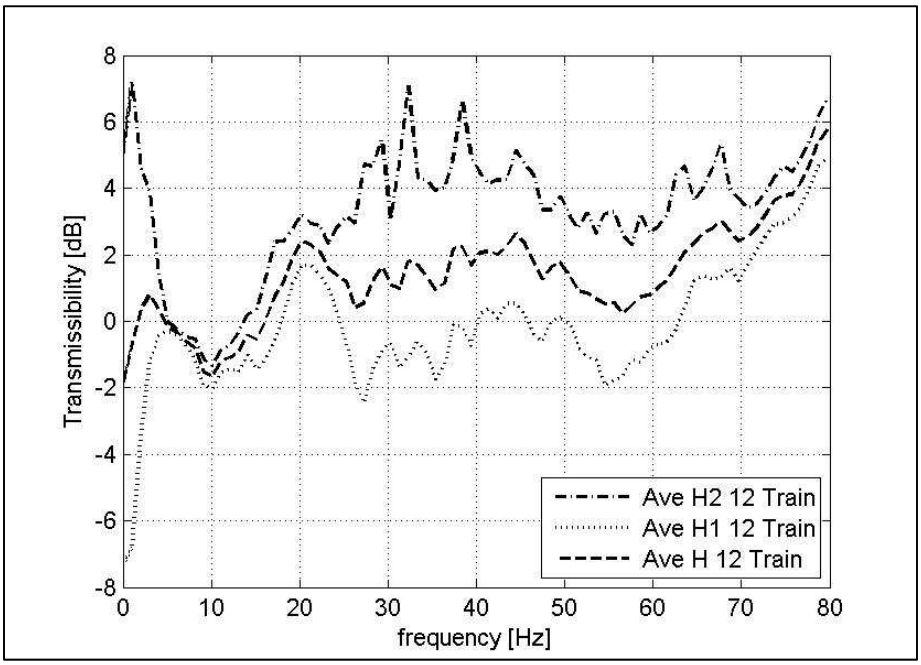

FIGURE 95 – TRANSMISSIBILITY OF THE HOUSE NUMBER 34 BETWEEN Z COMPONENTS AS A FUNCTION OF FREQUENCY. UPPER CURVE H2 FORMULATION, MIDDLE CURVE H FORMULATION AND LOWER CURVE H1 FORMULATION

As already explained in this section, the transmissibility is obtained with a linear average processes, but in the averaging the linearity of the measurement is not

taken in account. In fact, as shown in Figure 94, there are some frequency ranges where the majority of the events have a high linearity whereas for other frequencies this characteristic is less evident or missing.

Since cross spectra based transfer functions, $H1(f)$ (8.16) and $H2(f)$ (8.17), share the same coherence function according to Randall [187], an alternative way of averaging is considered taking into account the linearity of the dual channel measurement. This method consists of averaging only the frequency bins of the transfer function where the coherence between the two receivers is more than 0.8 creating the transfer functions $H1_Q$ and $H2_Q$.

$$H1_Q = \langle H1(f_i) \rangle \quad f_i \in L \tag{8.20}$$

$$H2_Q = \langle H2(f_i) \rangle \quad f_i \in L \tag{8.21}$$

In this way, the transmissibilities are defined only for the frequency bins that belong to L. $H1_Q$ and $H2_Q$ formulations have been proposed as a tool for comparing the transmissibilities obtained with different formulations.

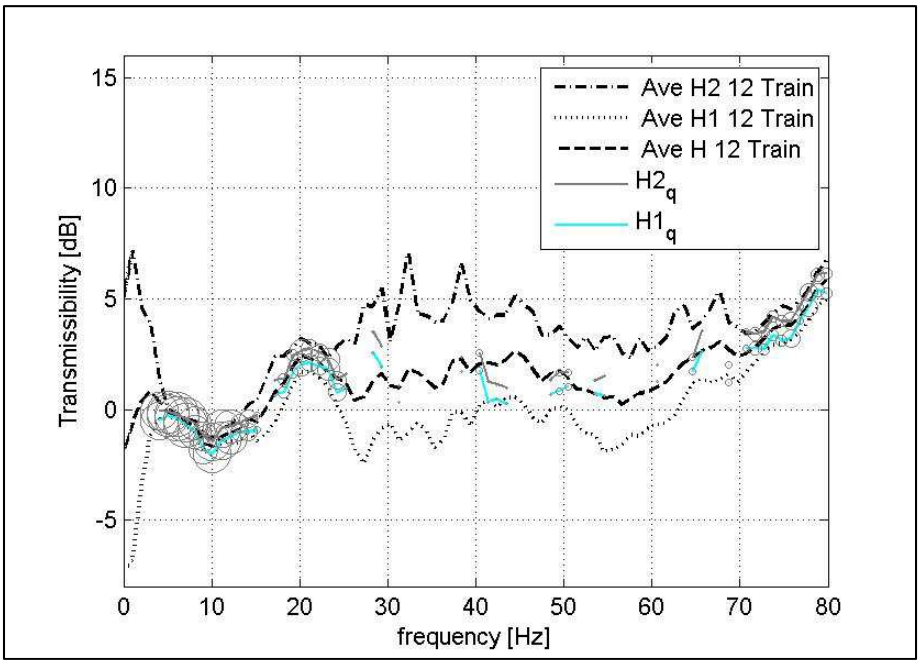

FIGURE 96 – TRANSMISSIBILITY HOUSE NUMBER 34 BETWEEN Z COMPONENTS AS A FUNCTION OF FREQUENCY. FROM THE TOP CURVE: H2, $H2_Q$,H,$H1_Q$ AND H1 FORMULATION.

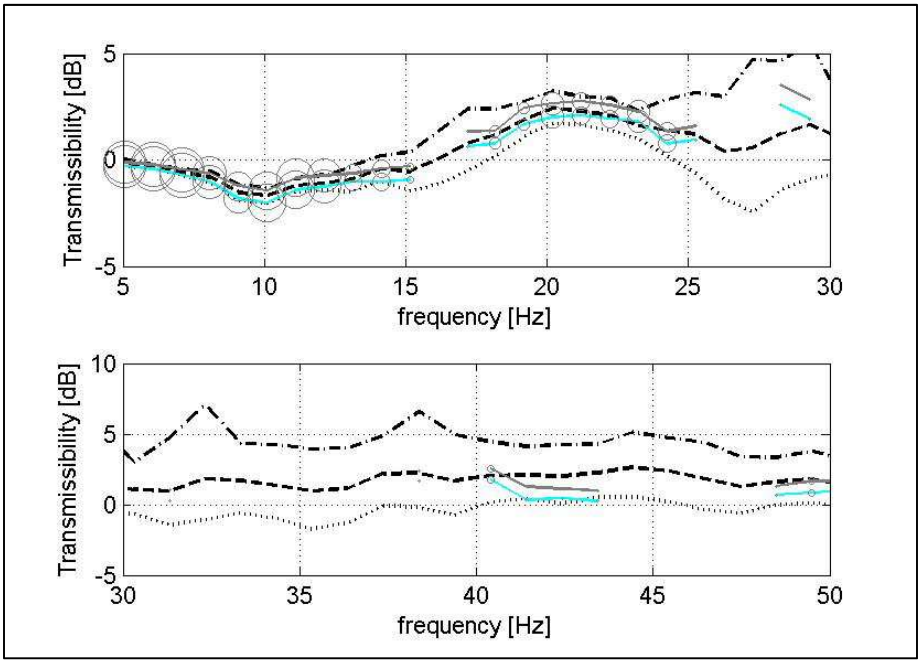

FIGURE 97 - TRANSMISSIBILITY HOUSE NUMBER 34 BETWEEN Z COMPONENTS AS A FUNCTION OF FREQUENCY: PARTICULAR. LEGEND SIMILAR TO FIGURE 96

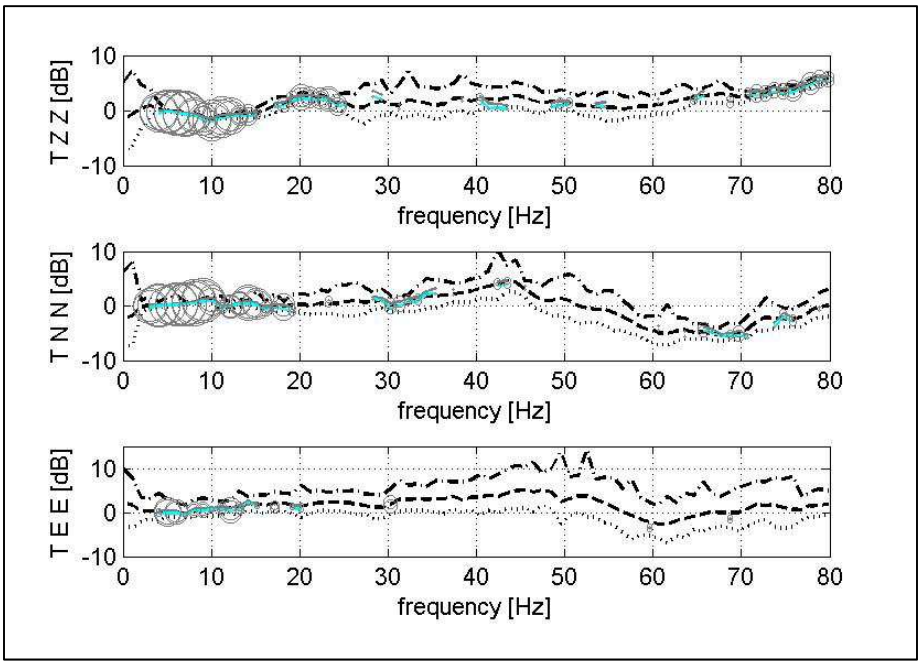

FIGURE 98 – TRANSMISSIBILITY HOUSE NUMBER 34 AS A FUNCTION OF FREQUENCY. FROM THE UPPER PANEL: TRANSMISSIBILITY BETWEEN Z, N AND E COMPONENTS. IN EACH FIGURE FROM THE TOP CURVE: H2, $H2_Q$,H,$H1_Q$ AND H1 FORMULATION. LEGEND SIMILAR TO FIGURE 96

Figure 96 shows the different formulations for the transmissibility, and each frequency bin belonging to L is highlighted with a circle. The diameter of the circle is proportional to the number of the bins, as shown in Figure 94, used for building $H1_Q$ and $H2_Q$ at that specific frequency. Therefore, in the area when the

circle is large, see Figure 97 upper panel in the frequency range 4-14 Hz, all the transfer functions are similar providing the same transmissibility value. This is because in that frequency ranges the measurement is noise free and all the formulations are close to each other. On the other hand, when the circles are small, see Figure 97 upper panel in the frequency range 15-25 Hz, not all the frequency bins contribute to the average and the $H1_Q$ and $H2_Q$ values are generally included between the *H1* and *H2* values. It is worth noting that, in this situation the discrepancy between the transmissibility formulation is larger than the case when the majority of the frequency bins contribute to $H1_Q$ and $H2_Q$.

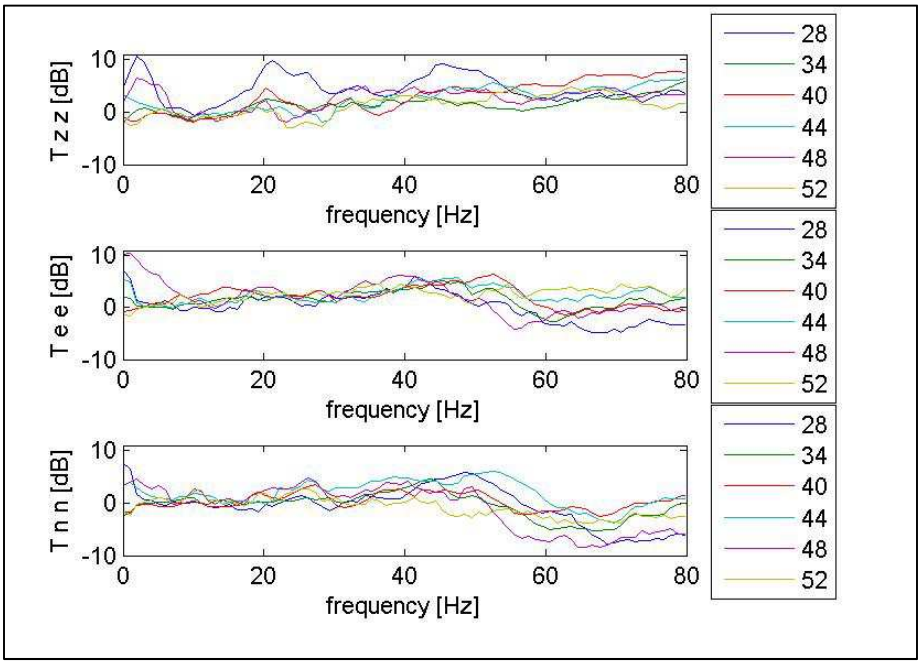

FIGURE 99 - TRANSMISSIBILITY COMPARISON BETWEEN HOUSES ON SITE 0. UPPER PANEL TRANSMISSIBILITY Z COMPONENTS, MID PANEL TRANSMISSIBILITY E COMPONENTS AND LOWER PANEL TRANSMISSIBILITY N COMPONENTS.

When there is no coherence, see Figure 97 lower panel in the frequency range 30-40 Hz, $H1_Q$ and $H2_Q$ don't exist. In these areas, there is a large discrepancy between the transfer function formulations and this observation is confirmed in Figure 98 where the comparison of transmissibilities for the three components is presented. This means that noise is present between the two channels or that more than one source is involved in the propagation process, as a consequence, cross

spectrum FRFs, in this condition, may introduce error in the estimation of the transmissibility.

From Table 16 it can be noted that six houses have been measured in site 0. Using the *H* formulation, a comparison between the transmissibility functions between the CP and the residences is shown in Figure 99. Despite the differences in the numbers of trains used for the averaging, the inter-distance between sensors and the positions of the receiver inside the house, it can be noted from Figure 99 that for all the components the transmissibility functions seem to follow the same trend in the frequency range between 10 and 80 Hz.

8.5.6 TRANSMISSIBILITY FOR EXPOSURE ASSESSMENT

As shown in the section above, the coherence can be used as tool for assessing the goodness of the transmissibility. The absence of coherence implies that noise or several excitation sources might be involved in the propagation process, as a consequence it is difficult to assess the linearity between the two receivers. In this scenario cross spectra based FRFs can introduce error in the estimation of the ground-to-point-of-entry transmissibility, therefore the latter can be better assessed just using magnitude based FRF for the evaluation of the human exposure. This hypothesis will be tested estimating the internal exposure using the three different transmissibility approaches.

In section 4.5.4.1 the use of the transmissibility for propagating the activity from the *EXT* to *INT* accelerometers in order to assess the internal exposure is explained. If we define $E(f)$ the double sided "non smoothed" Fourier spectrum of the time history $e(t)$ or $\{E_n\}$ recorded at the *EXT* position, the predicted internal spectra $I_{pred}(f)$ is carried out interpolating the double sided transmissibility $H(f)$ to the length of $E(f)$ obtaining $H_{est}(f)$ and multiplying both the quantity according to the expression:

$$I_{pred}(f) = H_{est}(f)E(f) \tag{8.22}$$

Once $I_{pred}(f)$ is obtained, the prediction of the time history $i_{pred}(t)$ is achieved by applying the inverse Fourier transform and the estimation of the internal exposure metric can be done.

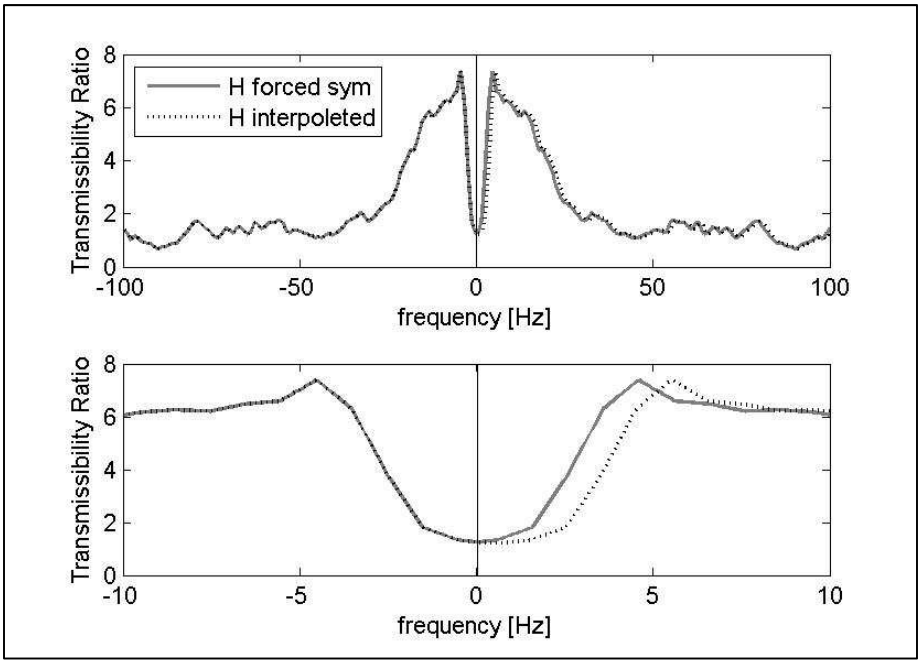

FIGURE 100 – TRANSMISSIBILITY RATIO AS A FUNCTION OF FREQUENCY. EFFECTS OF THE INTERPOLATION. GREY LINE H TRANSMISSIBILITY INTERPOLATED, BLACK LINE H TRASMISSIBILITY INTERPOLATED WITH "FORCED" SYMMETRY.

The critical part of the procedure described above is the interpolation of the transmissibility. In fact as shown in Figure 100, one problem that arises with this operation is the loss of the symmetry in the interpolated $H_{est}(f)$: as a consequence, $i_{pred}(t)$ will be complex. The problem can be avoided by "forcing" the symmetry of $H_{est}(f)$. Since $H_{est}(f)$ is double sided, only the first half of the spectrum is considered and reflected on the other half except for the first element of the spectrum. In this way the 'reality' of $i_{pred}(t)$ is preserved. Sometimes the edge of the transmissibility function may introduce artefacts, such as very low frequency trends, in the estimated internal time history. Therefore before interpolating the FRF, the edge effects are reduced by windowing the double sided transmissibility function $H(f)$.

In the railway traffic methodology, equation (8.22) is repeated for each event recorded at the *EXT* transducer for obtaining the long term estimation of the internal exposure.

An evaluation of the uncertainty on the exposure estimation can be obtained considering the events recorded simultaneously at the both measurement positions. The uncertainty can be defined as the relative error ε_{exp} between the true value of the internal exposure e_r and the one predicted by the method expressed in (8.22) e_p.

$$\varepsilon_{\text{exp}} = \frac{e_p - e_r}{e_p} \tag{8.23}$$

Considering the measurement site described in 8.5.1, the relative error in percentage is calculated for the following exposure metrics (See Table 10): Weighted Peak, Weighted RMS, VDV and Weighted RMQ. The metrics are calculated, for the z component of the acceleration W_b weighted, for each of the houses where measurements were taken and the vibration propagation from the control position inside the houses is obtained using the *H* formulation (8.15) of the transmissibility.

The results are shown in Figure 101. From Figure 101, it can be observed that using a magnitude only transmissibility function provides at most a 10 % relative absolute error in the prediction of weighted RMS, for the other exposure metrics a maximum of 20 % is achieved for the relative absolute error. In Figure 102 the error on the prediction of the internal weighted RMS obtained with different transmissibility formulations is shown at each house of the measurement site. It can be seen that the minimum error for the *H1* and *H2* is reached at the house number 34 with -26% and 36%. For the other houses the *H2* estimate provides a large error between 150% (house number 40) and 350% (house number 52) whereas the *H1* estimate provides an underestimation of the exposure metric around -50 %.

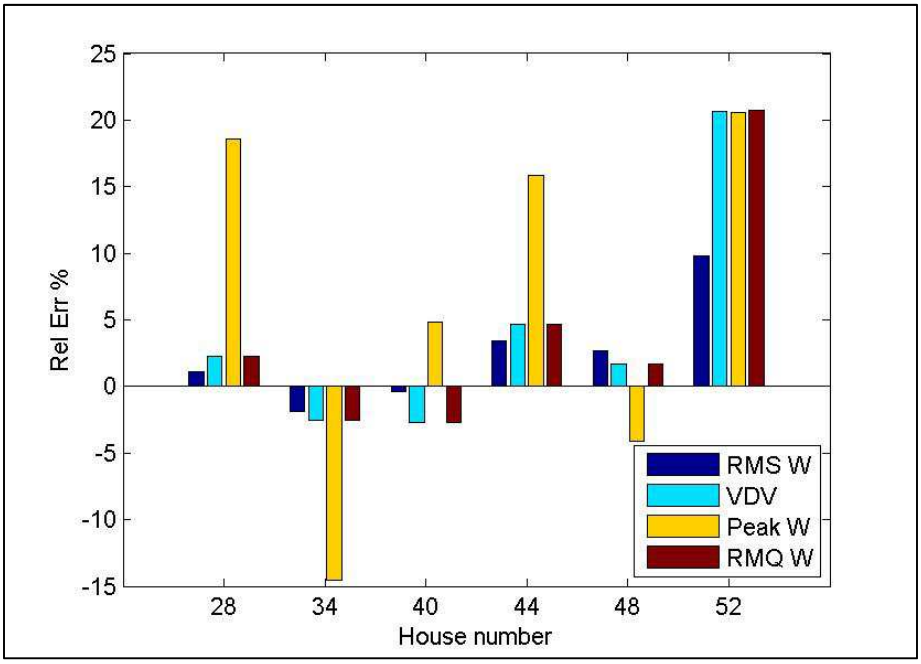

FIGURE 101 – RELATIVE ERROR IN PERCENTAGE ON THE EXPOSURE METRICS FOR DIFFERENT HOUSES. METRICS CONSIDERED: W RMS, VDV, W PEAK AND W RMQ.

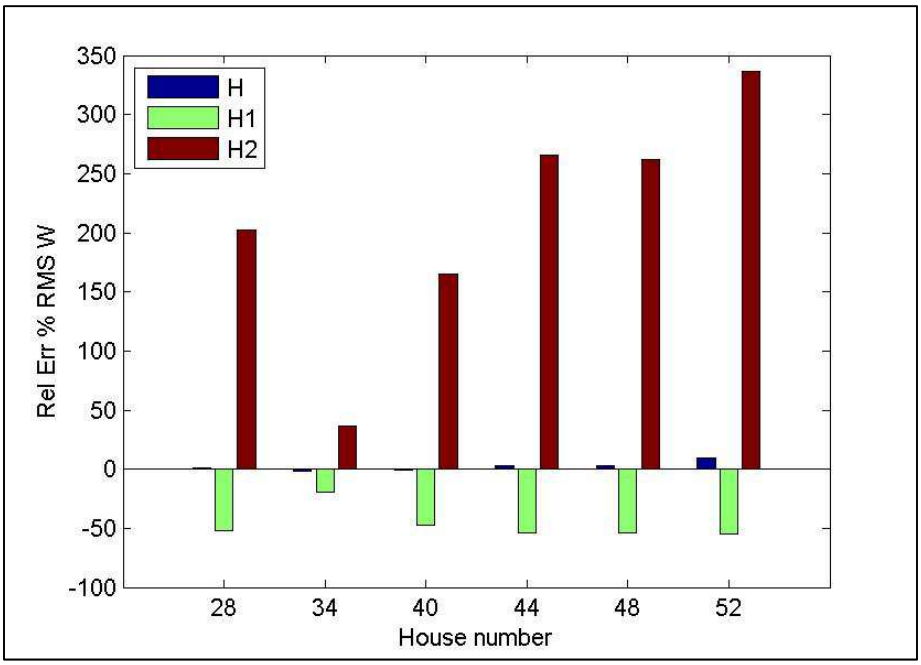

FIGURE 102 - RELATIVE ERROR IN PERCENTAGE ON WEIGHTED RMS FOR HOUSE NUMBER USING DIFFERENTS TRANSMISSIBILITY FORMULATIONS: H, H1 AND H2.

Considering that the same trends have been found for the other metrics, the hypothesis introduced at the beginning of the section is confirmed: cross spectra based transmissibility measurement can introduce a greater error in the evaluation of the internal human exposure as compared with magnitude only estimators. For

this reason magnitude only transmissibility measurement are preferred because even when there is lack of coherence in the dual channel measurement the uncertainty due the exposure estimation is much lower than for the case of cross spectra transfer functions.

8.6 VIRTUAL ANALYSIS

In this section the application of the virtual analysis for describing ground-to-building-transmissibility problem is discussed. It can be seen as an extension of the problem treated in the previous section 8.5. Since seismic technique such as polarization, see section 6.5.2, allow the identification of the ground motion through its principle components, the virtual coherence can be used for quantifying how the components recorded outside the house at the *EXT* position influence the acceleration measured inside the property at the *INT* position.

For consistency with section 8.5, we are going to consider the measurement site described in 8.5.1 focussing our attention on the following receivers: CP as *EXT* and house number 34 as *INT*. Considering the events in Figure 89, the virtual coherence between the principal components outside the building and the vertical component inside compared with ordinary coherence is shown in Figure 103.

It can be noted from Figure 103 that the second and third component of the motion has a small influence on the acceleration measured inside the building. However, good coherence has been found between the first principal component outside and the z component inside the building instead. Moreover, it can be observed that there are some similarities with the ordinary coherence between the z components and the two formulations are indistinguishable in the frequency range between 8 and 25 Hz. On the other hand, the high coherence between 0 and 8 Hz found in the normal coherence does not exist using the virtual coherence formulation.

Considering a train passage for the control position and house number 48, the virtual coherence and coherence for the z components are shown in Figure 105. From the figure, it can be said that only the first principal component, for the

measurement configuration used has influence on the acceleration measured inside the property.

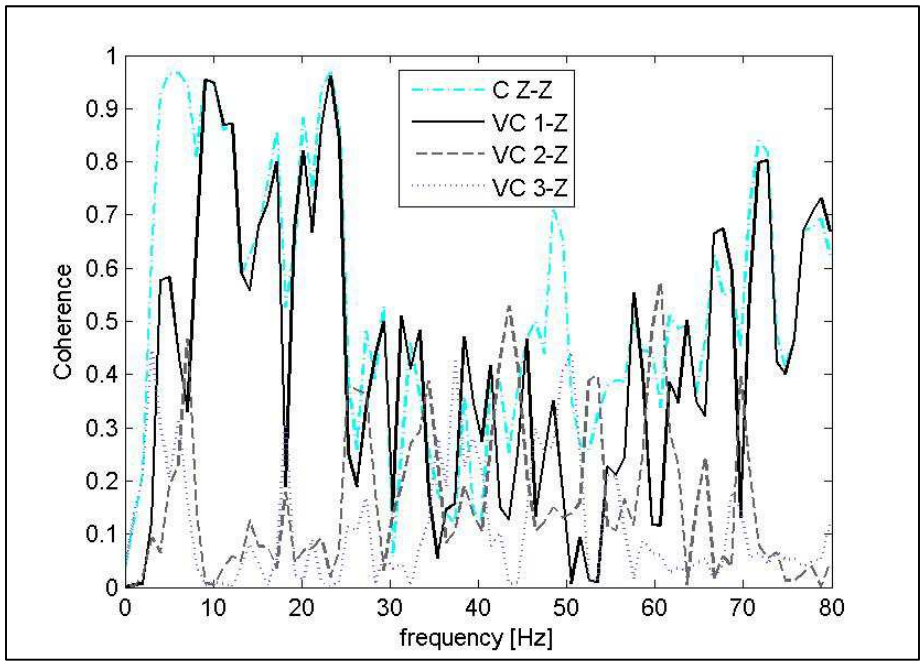

FIGURE 103 – COMPARISON BETWEEN COHERENCE FUNCTIONS TRAIN PASSAGE CP HOUSE NUMBER 34. MSC BETWEEN Z COMPONENTS (CYN DASH DOT LINE). VC BETWEN FIRST PRINCIPAL COMPONENT OUTSIDE AND Z INSIDE (BLACK LINE). VC BETWEN SECOND PRINCIPAL COMPONENT OUTSIDE AND Z INSIDE (GREY DASHED LINE). VC BETWEN THIRD PRINCIPAL COMPONENT OUTSIDE AND Z INSIDE (LIGHT GREY DOTTED LINE).

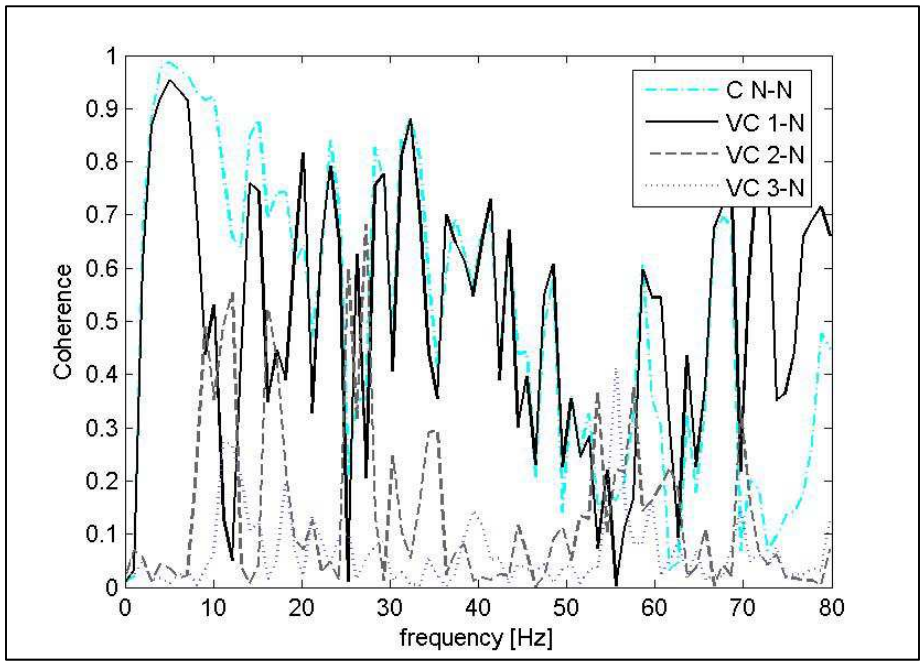

FIGURE 104 - COMPARISON BETWEEN COHERENCE FUNCTIONS TRAIN PASSAGE CP HOUSE NUMBER 34. MSC BETWEEN N COMPONENTS (CYN DASH DOT LINE). VC BETWEN FIRST PRINCIPAL COMPONENT OUTSIDE AND N INSIDE (BLACK LINE). VC BETWEN SECOND PRINCIPAL COMPONENT OUTSIDE AND N

INSIDE (GREY DASHED LINE). VC BETWEN THIRD PRINCIPAL COMPONENT OUTSIDE AND Z INSIDE (LIGHT GREY DOTTED LINE).

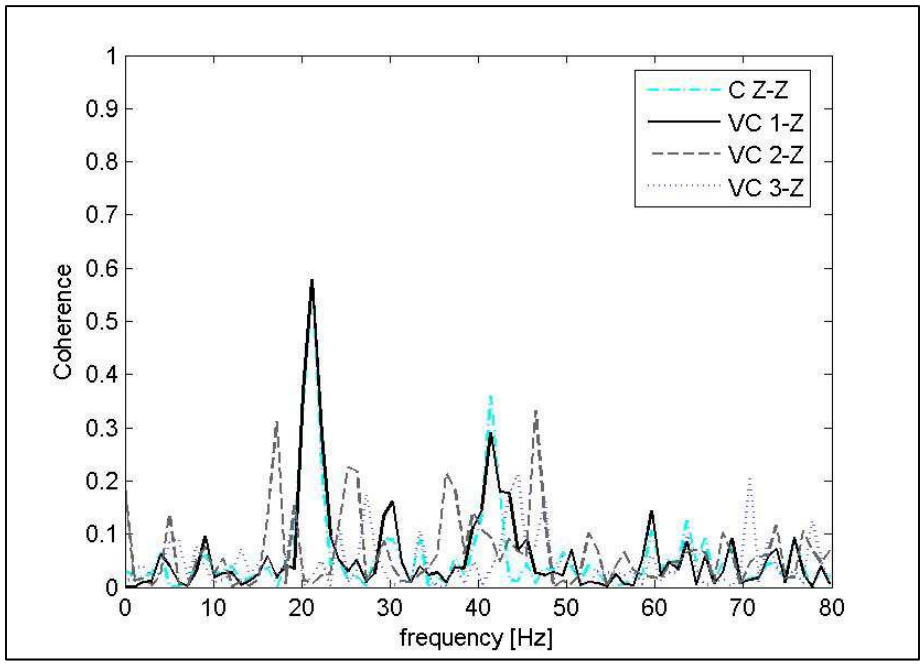

FIGURE 105 - COMPARISON BETWEEN COHERENCE FUNCTIONS TRAIN PASSAGE CP HOUSE NUMBER 48. MSC BETWEEN Z COMPONENTS (CYN DASH DOT LINE). VC BETWEN FIRST PRINCIPAL COMPONENT OUTSIDE AND Z INSIDE (BLACK LINE). VC BETWEN SECOND PRINCIPAL COMPONENT OUTSIDE AND Z INSIDE (GREY DASHED LINE). VC BETWEN THIRD PRINCIPAL COMPONENT OUTSIDE AND Z INSIDE (LIGHT GREY DOTTED LINE).

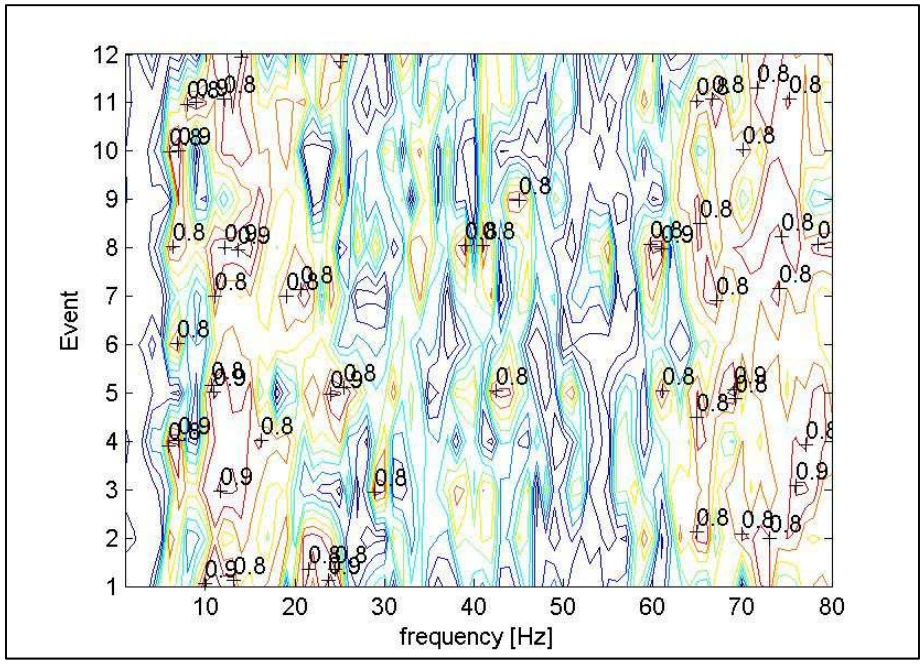

FIGURE 106 – COUNTOUR MAP OF THE VIRTUAL COHERENCE (VC) BETWEEN THE FIRST PRINCIPAL COMPONENTS OUTSIDE AND THE Z COMPONENT INSIDE FOR ALL THE EVENTS RECORDED AT CP AND HOUSE NUMBER 34

Furthermore, considering Figure 103 and Figure 104, it can be added that the virtual coherence approach may define well some frequency areas with respect to the ordinary coherence: in the virtual approach the coherence is calculated with respect to the reference system identified by the incoming wave recorded at the control position whereas in the ordinary coherence the reference system used is the one identified by the instrument which may not identify the "right" direction of the ground motion. Coming back to the CP and house number 34, the map of the virtual coherence between the first component of the ground and the z component acceleration inside the property for all the events recorded is shown in Figure 106.

In analogy to the *H* and *H2* formulation introduced in 8.3.4, a FRF between the first principal component outside the property and the physical components inside can be introduced as $H_{VI_i}(f)$ and $H2_{VI_i}(f)$:

$$H_{VI_i}(f) = \sqrt{\frac{G_{I_iI_i}(f)}{D_{M1}(f)}} \quad i = n, e, z \tag{8.24}$$

$$H2_{VI_i}(f) = \frac{G_{1I_i}(f)}{G_{I_iI_i}(f)} \quad i = n, e, z \tag{8.25}$$

In Figure 107 the virtual transmissibility, in $H_{VI_i}(f)$ and $H2_{VI_i}(f)$ formulation, between CP and house number 34 obtained averaging 12 train passages. It can be noted that the discrepancy between the formulations, even in this case, can be linked to the lack of virtual coherence in some frequency ranges.

In fact if the virtual transmissibility between the first principal component on the ground and the z component inside the property is considered (top panel Figure 107), good agreement between $H_{VI_i}(f)$ and $H2_{VI_i}(f)$ can be found in the frequency ranges between 10 and 20 Hz and 65 and 80 Hz. In those areas the virtual coherence is above 0.8 as shown in Figure 106.

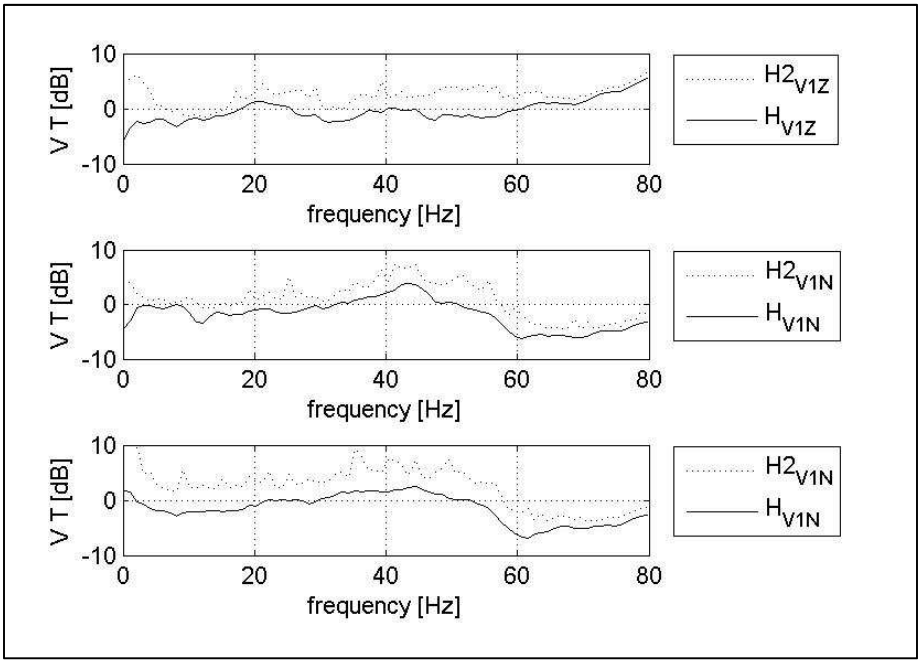

FIGURE 107 – VIRTUAL TRANSMISSIBILITY (VT) HOUSE NUMBER 34 AS A FUNCTION OF FREQUENCY. FROM THE UPPER PANEL: VT BETWEEN FIRST PRINCIPAL COMPONENT OUTSIDE AND Z, N, E COMPONENTS INSIDE. IN EACH FIGURE FROM THE TOP CURVE: $H2_{V1Z}$ (DOTTED GREY LINE), H_{V1N} (BLACK LINE).

Therefore as happened in 8.5.5 for the ordinary transmissibility formulation, even in the virtual analysis, transmissibility magnitude-only formulation like $H_{VI_i}(f)$ are preferred to virtual cross power spectra formulation.

8.7 CONCLUSION

In this chapter the ground-to-building transmissibility has been considered, based on measurement from a couple of time synchronised receivers, one on the ground and one inside the property, in order to assess human exposure caused by railway vibration. Magnitude-only and cross spectrum FRF formulations were compared for understanding which was the most suitable method for the evaluation of the human exposure. For this purpose, the concept of linearity for the dual channel measurements has been defined as the set of frequency bins where the coherence function is above 0.8. Considering several train passages the linearity of the dual channel measurement was used for identifying the frequency ranges where the system behaviour was linear, noise free and Single Input Single Output (S.I.S.O). In this scenario a cross spectrum averaging transfer function based on the linearity

of the measurement was defined for comparing the different transmissibility formulations.

When the linearity of the measurement was high then all the transmissibility formulations were very close to each other as in the noise free case, on the other hand in the absence of coherence a big discrepancy of several dB was found between the methods. The absence of coherence implied that noise or several excitation sources might be involved in the propagation process, as a consequence it was difficult to assess the linearity between the two receivers. For this reason, cross spectra based transfer functions introduced error in the estimation of the ground to point of entry transmissibility; the latter was better assessed just using magnitude based transfer function for the evaluation of the human exposure.

In order to validate both methodology and the transmissibility database, the error in the estimation of the internal exposure was evaluated using the transmissibility approach as a filter for propagating the vibration activity from the ground to inside the property. It has been found that magnitude only transfer function provided the lowest error for all the exposure metrics considered. From the results presented the maximum absolute error on the exposure metrics estimation was quantified as 20 %.

In the chapter a transmissibility analysis based on the principal component analysis has been described too. This approach was based on the identification of the reference system in agreement with the ground motion recorded outside the property which was used for rotating the cross power spectra matrix between the two receivers. In this way coherence between the principal components of the ground and the physical component of the building was defined.

The advantage of using this approach was that it was possible to understand how the principal components of the ground motion were distributed between the three physical components inside the property. The analysis showed that only the first principal component of the ground motion propagates significantly into the house. Of course, virtual transmissibilities were defined too and likewise the

ordinary approach magnitude only transmissibility was preferred to virtual cross power formulation.

9 CONCLUSIONS AND RECOMMENDATIONS

9.1 CONCLUSIONS

Human response to vibration is an important factor in both the construction and operation of railways, and a better knowledge of the topic can be achieved by assessing the response of the community to the vibration source with an exposure-response relationship.

New measurement strategies are needed in this field to collect reliable experimental data for the derivation of robust exposure-response relationships for railway operations, railway construction and a full investigation into the most suitable vibration metric for describing annoyance.

In this scenario, the first part of this dissertation has aimed to describe the design and implementation of a measurement methodology for estimating both exposure and response in a large number of dwellings in order to provide sufficient data for the development of exposure-response relationships for vibration from both rail construction and operations. The design of the field methodology to collect this socio-vibrational data required: a careful site selection, a questionnaire for the assessment of the response, two novel methodologies for the assessment of vibration exposure and coordination between teams from different disciplines.

The site selection allowed the social data to be gathered through a personal interview, rather than postal or telephone questionnaires, which permitted the collection of a large number of internal vibration measurements ensuring a wide range of exposures. The high success rate in obtaining permission to conduct internal measurements was mainly due to the rapport, which can be built between the interviewer and the respondent when conducting face-to-face interviews.

Considering the large number of case studies in the study, the requirement of a portable and compact instrumentation was vital for the assessment of the vibration exposure. For this reason, the advantages of modern seismic instrumentation have been exploited for the first time for large-scale socio-

vibrational surveys. In particular, the wide dynamic range offered by force feedback accelerometers and the ability to synchronise several instruments to within a few samples have been exploited. Furthermore, the ability to synchronise remote units without cables creates the possibility of using transducer arrays in rather flexible ways. This feature has been exploited in the measurement methodologies developed for railway and construction vibration by employing the idea of a control position accelerometer to capture the full time history of vibration at a fixed point. The method of filtering this signal for assessing the long term internal exposure differs for the two different sources: for railway vibration the filtering is based on measured vibration in individual dwellings; for the construction case it is based on a simple vibration propagation law with semi-empirically derived soil properties. Therefore, the exposure assessment is driven by the nature of the source. The type of source also influences the approach of the researchers collecting questionnaires and therefore the coordination between the two research teams.

The implementation of the field survey to measure vibration exposure and response confirmed the feasibility of the methodologies presented in this work. A large amount of measured data has been collected showing an ordinal relationship between exposure and response expressed in terms of annoyance.

A convenient by-product of this extensive field work is the generation of one of the biggest databases of vibration caused by railway vibration in the world. The second part of this dissertation exploits this database and is oriented towards the preliminary analysis of two problems linked with the exposure assessment: the wave field assessment and the ground-to-building transmissibility.

Wave field assessment aims to identify the wave types involved in vibration propagation and is estimated experimentally by analysing the particle motion through polarization analysis. The latter, extensively used in seismology and geophysics, has been applied, apparently for the first time, to the vibration sources considered in this work. In comparison with the particle motion plot commonly used in the field, the polarization analysis provides a quantitative description of

the wave field supplying the following information: the type of seismic phase involved in the propagation and an estimation of the source location. This suggests the use of this technique for the identification of the body waves, which are important for identifying the near field of the source, as indicated by the interesting results provided for piling and railway vibration. The work conducted here illustrates that there may be some scope for developing this approach, which will be discussed in the next section.

The transmissibility is a key tool that has been used for characterizing the propagation of vibration from outside to inside the property. It has been shown that the magnitude-only formulation provides a better assessment of the long term internal exposure in comparison with cross spectrum formulations. It has been found that, in the scope of the work reported in this dissertation, cross spectrum formulations can introduce large errors in the estimation of the ground to point of entry transmissibility used for the estimation of the internal exposure.

9.2 RECOMMENDATIONS FOR FURTHER RESEARCH

The work provided in this dissertation opens up several scenarios for further research oriented towards the improvement of the current knowledge on the human response to environmental vibration caused by railway construction and operations, which can be still considered as a novel research field. Keeping consistency with the thesis structure, the topics covered in this section will be: Design and strategy, Implementation of measurement methodology and Analysis. The latter is divided into understanding of soil through measurement, study and classification of building transmissibility function and organization of the data.

9.2.1 DESIGN AND STRATEGY

In terms of standards and guidelines, there are several methods for the evaluation of the human response to vibration but, as explained in this work, all these approaches need to be adapted for a large scale survey. As a consequence, a standardization and harmonization among the current methodologies is needed not only in terms of where and what to measure but also how.

The large body of policies developed for environmental noise, like directive 2002/49/EC, has brought specific strategies for the harmonization of noise exposure measurement through noise action planning and tools like noise map (Licitra [196]). As a consequence, much attention has been focused on the impact of noise from railways but the consideration of railway-induced vibration has often been neglected. With the future increase of railway construction and operations, noise and vibration needs to be taken into account in future environmental policies in order to ensure quality of life and well-being of inhabitants living in the vicinity of route paths (Peris et al. [197]). The first step in this direction will be the good practice guide on the assessment of the human response to vibration in residential environments, which will provide a set of practical tools to assess the human impact of "steady state" railway vibration primarily in terms of annoyance and sleep disturbance (Moorhouse et al. [51]).

The design stage of a large scale survey is a very important topic which is generally overlooked in the literature (Sica et al. [198]). The strategies related to the data collection of both exposure and response and the instrumentations employed are important elements, which need to be standardized in order to obtain a better comparison among studies. A harmonization of the methodologies is needed for "non steady state" problems too like vibration hotspot, which has been defined in the framework of RIVAS project by Stiebel et al. [199], and vibration from large railway construction.

In order to gain a better characterization of residential environments, research should be addressed towards strategies for the identification of exposure and response related parameters of large areas to provide a better vibration impact assessment not only in the detailed stage. In analogy with noise, the concept of vibration zonation should be introduced in order to characterize the vibration exposure. From the response side, a parameter that shows the annoyance distribution across the area may be helpful, and in this sense an approach similar to the airport index (Brink et al. [200]) used for aircraft noise could be implemented for railways too.

Peris [201] has shown that non acoustical factors played an important role in the annoyance from railway vibration. This implies that a reduction of the annoyance might be achieved through a management of the human response oriented towards a better engagement with the local communities.

9.2.2 IMPLEMENTATION OF MEASUREMENT METHODOLOGY

The railway exposure methodology presented in this work has demonstrated that intensive field work can be used for obtaining a better estimation of the internal exposure caused by vibration induced from railway traffic with an approach based on the use of two measurement positions. An improvement of the methodology may be achieved using a further short term measurement position for monitoring the foundation of the building. In this way, a better definition of the transmissibility from the ground to the point of entry, through the foundation, and a harmonization with the current approaches (see Villot et al. [186]) may be achieved.

The validation of the construction methodology for the assessment of the internal exposure in both frequency domain and single figure parameter has shown that Barkan's law can be used as a propagator of the vibration exposure. However, further research is needed to extend this approach to any semi empirical propagation model if possible, to other construction sources not treated in this work and for a full wave field generated by the vibration source.

Considering that annoyance increases when noise and vibration are both present, a better quantification of the human response may be achieved through an experimental vibro-acoustics characterization of the residential environment implying the extension of the frequency range of the analysis from 1 to 80 Hz to at least 1 to 250 Hz for assessing groundborne noise as well. The frequency range for investigating groundborne noise can be partially investigated with the current sensor configuration because force feedback loop has not been designed to measure vibration above 200 Hz. On the other hand, the configuration can be updated in terms of sample frequency in order to obtain better details of the vibration time history together with an improvement in the instrument

connectivity. Therefore, at the moment, the instrumentation can be improved further on the acquisition and connectivity side instead of the actual hardware. An improvement in the exposure assessment can be achieved by designing a measurement methodology where noise and vibration measurements are synchronized.

9.2.3 UNDERSTANDING OF SOIL THROUGH MEASUREMENT

The results from both laboratory and field study carried out by Woodcock [202] on the perception of railway induced vibration has shown the importance of the energy content of the vibration in the frequency range below 32 Hz. These findings reinforce the need for better investigation of soil and its propagation, which are influenced by local amplification factor characteristics through measurement, as already explained by the author in chapter 6 and 7.

In this framework, the encouraging results provided by the polarization analysis can take the analysis of groundborne vibration to a new level but further research is needed. The analysis of the first arrival could be useful for the identification of body wave and the near field region whereas the coda analysis could provide a better insight about the interaction between the source and soil.

In comparison with seismic sources, manmade processes are localized and are capable of producing significant amounts of vibration. As a consequence, better analysis tools can be implemented not only for seismic/geophysical exploration but also for obtaining better knowledge of the generation mechanisms for vibration. The source mechanisms for railway vibration are not completely understood and are still one of the main points in the European roadmaps for vibration proposed by ERRAC. Instead an exploration approach can be beneficial especially for the assessment of soil property on a large scale and seismic noise methods, as shown in section 6.3.2, can be a cost effective solution for achieving this goal.

Passive seismic can improve the current determination of vibration background measurements, which are generally used for the planning of new railway lines like

HS2 in the U.K (Arup and URS [203]), providing soil data and not just the vibration level. Passive seismic is already used for the seismic microzonation and can be a good candidate for the vibration zonation of large urbanized area mentioned in 9.2.1. Of course, research is needed for understanding which technique is more suitable for railway construction and operation. Vibration zonation using passive seismic methods can be a sustainable way for assessing soil properties, which are not only used for the impact assessment but for a better planning and construction of the infrastructure.

9.2.4 STUDY AND CLASSIFICATION OF BUILDING TRANSFER FUNCTIONS

One of the main consequences of a better wave field assessment is a better understanding of the building response especially if the receiver is in the near field of the source or if the latter has point source behaviour. In this sense, further research is needed for the use of the virtual analysis for describing ground-to-building transmissibility. One advantage of this method is to link the principal component of the ground, which can be assessed with the polarization, to the physical component acquired inside the building. For example, identifying only the ground-to-building transmissibility due to the Rayleigh waves will make possible a comparison of the different transmissibility functions for each measurement site of the exposure railway methodology leading to the definition, for each site, of a sort of "standard transfer function" (STF).

Then, extra information related to the building such as foundation type and soil type can be integrated to the STF in order to create a classification of the property close to the railway line and research should be pursued for achieving this goal. Building classification using STF can be useful for different purposes. From an impact assessment point of view, it will update the English property types, which are not included in the Transportation Noise Reference Book and FTA guidelines. Furthermore, a better classification of the property types can be useful for improving the uncertainty associated with the ground-to-building transmissibility for predicting the exposure from an external measurement.

In has been observed that the response of the building changes under different train loads and that especially freight trains provide a different ground-to-building FRF in comparison to other trains. Generally, freight trains are slower, longer and heavier than passenger trains. Furthermore, freight trains do not have secondary suspension. All these characteristics generate a frequency spectrum richer in energy in the low frequency region, between 4 and 30 Hz (Jones and Block [204]), in comparison with passenger trains. In this sense, algorithms for the classification of the train traffic, like the one proposed by Sharp et al. [205], can help to understand how the response of the building changes under different train loads. For example, ground-to-building FRF generated by freight traffic can be a very useful tool for the investigation of the human exposure during the night time.

9.2.5 ORGANIZATION OF THE DATA

In order to manage and preserve the large amount of data collected in the study "Human response to vibration in residential environments" a database should be built. In fact, a better determination of the exposure and response could be achieved considering extra information related to the residential environments like property type, soil, railway distance, railway elevation and rail type alongside the vibration measurement. The database should also integrate the response data exploiting the benefit of the GIS (Geographic Information System). In literature a reference to this problem can be found in Madshus et al. [41] and Glickman [206].

REFERENCES

[1] H. Xia, N. Zhang, and Y. M. Cao, “Experimental study of train-induced vibrations of environments and buildings,” *Journal of Sound and Vibration*, vol. 280, no. 3–5, pp. 1017–1029, 2005.

[2] T. J. Schultz, “Synthesis of social surveys on noise annoyance,” *The Journal of the Acoustical Society of America*, vol. 64, no. 2, pp. 377–405, Aug. 1978.

[3] P. Ellias and M. Villot, “Rivas Project, Del 1.4 - Review of existing standards, regulations and guidelines as well as laboratory study concerning human exposure to vibration,” *UIC*, 2012. [Online]. Available: http://www.rivas-project.eu/fileadmin/documents/rivas_cstb_wp1_d1_4_v03_assesment_human_response.pdf. [Accessed: 31-Aug-2013].

[4] D. Waddington, A. Moorhouse, A. Steele, J. Woodcock, J. Condie, E. Peris, G. Sica, and Z. Koziel, “Human Response to Vibration in Residential Environements (NANR209), Final Project Report,” Defra, London, 2011.

[5] “BS ISO 14837-1:2005 Mechanical vibration. Ground-borne noise and vibration arising from rail systems. Part 1: General guidance,” International Standard Organization, 2005.

[6] Y. Matsumoto and M. Griffin, “Mathematical models for the apparent masses of standing subjects exposed to vertical whole-body vibration,” *Journal of Sound and Vibration*, vol. 260, no. 3, pp. 431–451, 2003.

[7] G. Rasmussen, “Human body vibration exposure and its measurement,” *The Journal of the Acoustical Society of America*, vol. 73, no. 6, pp. 2229–2229, 1983.

[8] Y. Matsumoto and M. J. Griffin, “Comparison of biodynamic responses in standing and seated human bodies,” *Journal of Sound and Vibration*, vol. 238, no. 4, pp. 691–704, 2000.

[9] P. Holmund, R. Lundstrom, and L. Lindeberg, “Mechanical impedance of the human body in vertical direction,” *Applied Ergonomics*, vol. 31, no. 4, pp. 415–422, 2000.

[10] M. J. Griffin, *Handbook of human vibration*, 2nd ed. London: Elsevier, 1996, p. 988.

[11] Y. Matsumoto and M. J. Griffin, “Dynamic response of the standing human body exposed to vertical vibration: Influence of posture and vibration magnitude.,” *Journal of Sound and Vibration*, vol. 212, no. 1, pp. 85–107, 1998.

[12] G. H. M. . Subashi, Y. Matsumoto, and M. J. Griffin, “Apparent mass and cross-axis apparent mass of standing subjects during exposure to vertical whole-body vibration,” *Journal of Sound and Vibration*, vol. 293, no. 1–2, pp. 78–95, 2006.

[13] G. H. M. . Subashi, Y. Matsumoto, and M. J. Griffin, “Modelling resonances of the standing body exposed to vertical whole-body vibration: Effects of posture,” *Journal of Sound and Vibration*, vol. 317, no. 1–2, pp. 400–418, 2008.

[14] P. Holmlund, R. Lundstrom, and P. Holmund, “Mechanical impedance of the human body in the horizontal direction.,” *Journal of Sound and Vibration*, vol. 801, no. 4, pp. 801–812, 1998.

[15] J. Woodcock., E. Peris, J. Condie, G. Sica, A. Moorhouse, and D. Waddington, “Human Response to Vibration in Residential Environments (NANR209), Technical Report 6: Determination of Exposure-Response Relantionships.,” Defra, London, 2011.

[16] “ISO 2631-1:1997 Mechanical vibration and shock - Evaluation of human exposure to whole-body vibration - Part 1: General requirements,” International Standard Organization, 1997.

[17] H. Howarth and M. J. Griffin, “Human response to simulated intermittent railway-induced building vibration,” *Journal of Sound and Vibration*, vol. 120, no. 2, pp. 413–420, Jan. 1988.

[18] “BS 6472-1:2008 Guide to evaluation of human response to vibration in buildings (1 Hz to 80 Hz) - Part 1: Vibration sources other than blasting,” British Standards Institution, 2008.

[19] C. E. Hanson, D. A. Towers, and L. D. Meister, “Transit noise and vibration impact assessment FTA-VA-90-1003-06,” *Federal Transit Administration*, 2006. [Online]. Available: http://www.fta.dot.gov/documents/FTA_Noise_and_Vibration_Manual.pdf. [Accessed: 31-Aug-2013].

[20] “NS8176:1999 Vibration and Shock - Measurement of Vibration in Buildings from Landbased Transport and Guidance to Evaluation of its Effect on Human Beings,” Norwegian Council for Building Standardization, 1999.

[21] “DNR.S02-4235/SA60: Buller och Vibrationer, Fran Sparburen Linjetrafik.,” Banverket (Swedish Railway Administration), 2002.

[22] “DIN 4150-2:1999 Structural vibration - Part 2: Human exposure to vibration in buildings,” Deutsches Institut für Normung (German Institute for Standardization), 1999.

[23] “ISO 2631-2:2003: Mechanical vibration and shock - Evaluation of human exposure to whole-body vibration. Part 2: Vibration in buildings (1 Hz to 80 Hz).,” International Standard Organization, 2003.

[24] “ANSI S3.29-1983 (R2001) American National Standard to the Evaluation of Human Exposure to Vibration in Buildings,” American National Standards Institute, 2001.

[25] “NT-ACOU 082: Buildings: Vibration and shock, evaluation of annoyance.,” Nordtest (Nordic Strategy Group on Quality and Metrology), 1991.

[26] J. A. Zapfe, H. Saurenman, and S. Fidell, “TCRP Web-Only Document 48: Ground-Borne Noise and Vibration in Buildings Caused by Rail Transit,” *Transportation Research Board*, 2009. [Online]. Available: http://onlinepubs.trb.org/onlinepubs/tcrp/tcrp_webdoc_48.pdf. [Accessed: 31-Aug-2013].

[27] ANC, *Association of Noise Consultants Guidelines: Measurement and Assessment of Groundborne Noise and Vibration (ANC guidelines)*, 1st ed. London: Fresco, 2001, p. 173.

[28] Y. Hirao, S. Kunimatsu, and T. Hamamoto, “Development of wireless measurement system for ground-borne vibration in buildings and measurements for vibration amplifications of detached houses,” in *Internoise*, 2011.

[29] “ANSI S2.71-1983 (R2006) Guide To The Evaluation Of Human Exposure To Vibration In Buildings,” American National Standards Institute, 2006.

[30] “BS 6472-1:1992 Guide to evaluation of human response to vibration in buildings (1 Hz to 80 Hz) - Part 1: Vibration sources other than blasting,” British Standards Institution, 1992.

[31] C. Ostendorf, “Nine Years of Dutch Experience in the Evaluation of Vibrations in Relation to Nuisance,” *Journal of Low Frequency Noise, Vibration and Active Control*, vol. 21, no. 4, pp. 219–228, 2002.

[32] “SBR Richtlijn - Deel B: Hinder voor personen in gebouwen,” Stichting Bouwresearch Rotterdam (Foundation for Building Research), 2002.

[33] I. H. Turunen-Rise, “Assessment of vibration from landbased transport - a new norwegian standard.,” *Journal of Low Frequency Noise, Vibration and Active Control*, vol. 21, no. 1, pp. 21–28, 2000.

[34] “BS 5228-2:2009 Code of practice for noise and vibration control on construction and open sites - Part 2: Vibration,” 2009.

[35] G. R. Watts, “Traffic induced vibrations in buildings,” *TRRL Research Report*, vol. 246, 1987.

[36] G. R. Watts, “Vibration nuisance from road traffic - results of a 50 site survey,” *TRRL Laboratory Report*, vol. 1119, 1984.

[37] H. J. Woodroof and M. J. Griffin, “A survey of the effect of railway-induced building vibration on the community,” *Institute of Sound and Vibration Research Technical Report*, vol. 160, 1987.

[38] I. Turunen-Rise, A. Brekke, and L. Hårvik, “Vibration in dwellings from road and rail traffic--Part I: a new Norwegian measurement standard and classification system,” *Applied Acoustics*, vol. 64, no. 1, pp. 71–87, 2003.

[39] R. Klæboe, I. Turunen-Rise, L. Harvik, and C. Madshus, “Vibration in dwellings from road and rail traffic--Part II: exposure-effect relationships based on ordinal logit and logistic regression models,” *Applied Acoustics*, vol. 64, no. 1, pp. 89–109, 2003.

[40] R. Klaeboe, E. Ohrstrom, I. H. Turunen-Rise, H. Bendtsen, and H. Nykanen, “Vibration in dwellings from road and rail traffic--Part III: towards a common methodology for socio-vibrational surveys,” *Applied Acoustics*, vol. 64, no. 1, pp. 111–120, 2003.

[41] C. Madshus, B. Bessason, and L. Harvik, “Prediction model for low frequency vibration from high speed railways on soft ground,” *Journal of Sound and Vibration*, vol. 193, no. 1, pp. 195–203, 1996.

[42] S. Yokoshima, T. Morihara, Y. Sano, A. Ota, and A. Tamura, “Community response to Shinkansen Railway vibration,” in *Internoise*, 2011.

[43] J. Condie, A. Steele, N. Whittle, P. Brown, and D. Waddington, “Human Report to Vibration in Residential Environments (NANR209), Technical Reports 2: Measurement of response,” Defra, London, 2011.

[44] E. Peris, J. Woodcock., G. Sica, A. Moorhouse, and D. Waddington, “Factors influencing the human response to vibration from railways in residential environments,” in *IoA Noise in the Built Environment*, 2010.

[45] M. Ogren, E. Ohstrom, and T. Jerson, “Effects of railway noise and vibrations on sleep - experimental studies within the Swedish research program TVANE,” in *Euronoise 2009*, 2009.

[46] E. Ohstrom, M. Ogren, and T. Jerson, “Effects of railway noise and vibration in combination: field and laboratory study,” in *Euronoise 2009*, 2009.

[47] E. Elmenhorst, U. Mueller, V. Rolny, S. Penning, J. Quehl, M. Harmut, and M. Basner, “Impact of nocturnal railway and aircraft noise on awakening probability in the field,” in *ICBEN*, 2011.

[48] European Commission, “WHITE PAPER Roadmap to a Single European Transport Area – Towards a competitive and resource efficient transport system,” *European Commission*, 2011. [Online]. Available: http://ec.europa.eu/transport/strategies/doc/2011_white_paper/white_paper_com(2011)_144_en.pdf. [Accessed: 01-Sep-2013].

[49] RIVAS, “Railway Induced Vibration Abatement Solutions.” [Online]. Available: http://www.rivas-project.eu/. [Accessed: 23-Apr-2012].

[50] CargoVibes, “Attenuation of ground-borne vibration affecting residents near freight railway lines.” [Online]. Available: http://www.cargovibes.eu/Home. [Accessed: 23-Apr-2012].

[51] A. Moorhouse, D. Waddington, E. Peris, J. Woodcock., C. Sharp, and G. Sica, “Outline proposal for good practice guide on the evaluation of human response to

vibration from railways in residential environments," *Proceedings of Meetings on Acoustics*, vol. 19, pp. 040106–040114, 2013.

[52] J. Woodcock, E. Peris, G. Sica, A. Moorhouse, and D. Waddington, "Investigations to measure human exposure to vibration in residential environments," in *Euronoise 2009*, 2009.

[53] R. Perkins, C. Grimwood, C. Stanworth, and R. Thornley-Taylor, "Human response to vibration in residential environments: A seven year journey to establish exposure-response relationships.," in *ICBEN*, 2011.

[54] Arup Acoustics and Temple Group, "NANR172: Human response to vibration in residential environments.," Defra, London, 2007.

[55] J. Condie and A. Steele, "Human Report to Vibration in Residential Environments (NANR209), Technical Reports 5: Analysis of Social Survey Findings.," Defra, London, 2011.

[56] G. Sica, J. Woodcock, E. Peris, Z. Koziel, A. Moorhouse, and D. Waddington, "Estimation of vibration exposure in residential environments.," in *ICBEN*, 2011.

[57] E. Peris, G. Sica, J. Woodcock, Z. Koziel, A. Elliott, R. Venegas, A. Moorhouse, and D. Waddington, "Human Response to Vibration in Residential Environments (NANR209), Technical Report 1: Measurement of vibration exposure," Defra, London, 2011.

[58] "BS ISO 4866:2010 Mechanical vibration and shock - Vibration of buildings - Guidelines for the measurement of vibrations and evaluation of their effects on buildings," International Standard Organization, 2010.

[59] P. Bormann, *New Manual of Seismological Observatory Practice*, Rev. ed. Postdam: GFZ, 2009.

[60] Guralp, "CMG-3T/5T Borehole." [Online]. Available: http://www.guralp.com/datasheets/DAS-BHO-0006.pdf. [Accessed: 03-Aug-2012].

[61] Guralp, "CMG-5TD Digital accelerograph system user's guide.," Guralp System Limited, 2007.

[62] "BS ISO 16063-1:1998 Methods for the calibration of vibration and shock transducers. Basic concepts," International Standard Organization, 1998.

[63] "BS ISO 5348:1998 Mechanical vibration and shock. Mechanical mounting of accelerometers," International Standard Organization, 1998.

[64] A. Mayr and T. R. T. Nightingale, "On the mobility of joist floor and periodic rib-stiffed plates," in *Internoise*, 2007.

[65] S. J. J. XIN, "Simplified characterization of structure-borne sound source with multi-point connections.," University of Liverpool, 2003.

[66] G. Sica, J. Woodcock, E. Peris, A. Moorhouse, and D. Waddington, “Human Response to Vibration in Residential Environments (NANR209), Technical Report 3: Calculation of Vibration Exposure.,” Defra, London, 2011.

[67] D. Stiebel, “Rivas Project, Del 1.2 - Protocol for free field measurements of mitigation effects in the project RIVAS for WP 2, 3, 4, 5,” *UIC*, 2011. [Online]. Available: http://www.rivas-project.eu/fileadmin/documents/rivas_db_wp1_d1_2_v04_measuring_protocol.pdf. [Accessed: 01-Sep-2013].

[68] M. Bahrekazemi, “Train-Induced Ground Vibration and Its Prediction,” Royal Institute of Technology Stockholm, 2004.

[69] T. Dawn and C. Stanworth, “Ground vibrations from passing trains,” *Journal of Sound and Vibration*, vol. 66, no. 3, pp. 355–362, Oct. 1979.

[70] V. Krylov, “Vibrational impact of high speed trains. I. Effect of track dynamics,” *The Journal of the Acoustical Society of America*, vol. 100, no. 5, pp. 3121–3134, 1996.

[71] X. Sheng, C. J. C. Jones, and D. J. Thompson, “A comparison of a theoretical model for quasi-statically and dynamically induced environmental vibration from trains with measurements,” *Journal of Sound and Vibration*, vol. 267, no. 3, pp. 621–635, 2003.

[72] G. Kourosussis, O. Verlinden, and C. Conti, “Influence of some vehicle and track parameters on the environmental induced by railway traffic,” *Vehicle System Dynamics*, vol. 50, no. 4, pp. 619–639, 2012.

[73] A. A. Mirza, A. Frid, J. C. O. Nielsen, and C. J. C. Jones, “Ground vibration induced by railway traffic - the influence of vehicle parameters,” in *10th International Workshop on Railway Noise*, 2010, pp. 245–252.

[74] N. Triepaischajonsak, D. J. Thompson, C. J. C. Jones, and J. Ryue, “Track-based control measures for ground vibration - the influence of quasi-static loads and dynamic excitation,” in *10th International Workshop on Railway Noise*, 2010, pp. 237–244.

[75] V. Krylov, “Generation of Ground Vibration by Superfast Trains,” *Applied Acoustics*, vol. 42, no. 2, pp. 149–164, 1995.

[76] T. Dawn, “Ground Vibration from Heavy Freight Trains,” *Journal of Sound and Vibration*, vol. 66, no. 3, pp. 355–362, 1983.

[77] G. Lombaert and G. Degrande, “Ground-borne vibration due to static and dynamic axle loads of InterCity and high-speed trains,” *Journal of Sound and Vibration*, vol. 319, no. 3–5, pp. 1036–1066, 2009.

[78] T. G. Gutowski and C. L. Dym, “Propagation of ground vibration: a review,” *Journal of Sound and Vibration*, vol. 49, no. 2, pp. 179–193, 1976.

[79] E. Rathe, “Note on two common problems of sound propagation,” *Journal of Sound and Vibration*, vol. 10, no. 3, pp. 472–479, 1969.

[80] L. Auersch and S. Said, “Attenuation of ground vibrations due to different technical sources,” *Earthquake Engineering and Engineering Vibration*, vol. 9, no. 3, pp. 337–344, 2010.

[81] M. J. Crocker, *Handbook of noise and vibration control*, 1st ed. New York: John Wiley and Sons, 2007, p. 1569.

[82] M. Withers, R. Aster, C. Young, J. Beiriger, M. Harris, S. Moore, and J. Trujillo, “A comparison of select trigger algorithms for automated global seismic phase and event detection,” *Bulletin of the Seismological Society of America*, vol. 88, no. 1, pp. 95–106, 1998.

[83] G. Sica, A. Moorhouse, J. Woodcock, E. Peris, C. Sharp, and D. Waddington, “Measurement of ground-to-building frequency response functions for assessment of human exposure to vibration from railway vibration,” in *ISMA*, 2012.

[84] J. Wiss, “Construction vibrations: state-of-the-art,” *Journal of the Geotechnical Engineering Division*, vol. 2, pp. 167–181, 1981.

[85] R. Woods, “Dynamic effects of pile installations on adjacent structures. A synthesis of highway practice,” *NCHRP Synthesis*, vol. 253, p. 96, 1997.

[86] F. Richart, J. Hall, and R. Woods, *Vibrations of soils and foundations*, 1st ed. Englewood Cliffs, New Jersey: Prentice-Hall Inc, 1970, p. 414.

[87] M. Svinkin, “Predicting soil and structure vibrations from impact machines,” *Journal of Geotechnical and Geoenvironmental Engineering*, vol. 128, no. 7, pp. 602–612, 2002.

[88] W. Clough and J.-L. Chameau, “Measured effects of vibratory sheetpile driving,” *Journal of the Geotechnical Engineering Division*, vol. 106, no. 10, pp. 1081–1099, 1980.

[89] G. A. Athanasopouls and P. C. Pelekis, “Ground vibrations from sheetpile driving in urban environment: measurements, analysis and effects on buildings and occupants,” *Soil Dynamics and Earthquake Engineering*, vol. 19, no. 5, pp. 371–387, 2000.

[90] C. Dowding, *Construction vibrations*, 3rd ed. Englewood Cliffs, New Jersey: Prentice-Hall Inc, 1996, p. 620.

[91] D. D. Barkan, *Dynamics of Bases and Foundations*, 1st ed. New York: McGraw-Hill Book Co., 1962, p. 434.

[92] G. A. Athanasopouls, P. C. Pelekis, and G. A. Anagnostopoulos, “Effect of soil stiffness in the attenuation of Rayleigh-wave motions from field measurements,” *Soil Dynamics and Earthquake Engineering*, vol. 19, no. 4, pp. 277–288, 2000.

[93] H. Amick, “A Frequency-Dependent Soil Propagation Model,” in *SPIE Conference on Current Developments in Vibration Control for Optomechanical Systems*, 1999.

[94] G. J. Rix, C. G. Lai, and A. Wesley Spang, “In Situ Measurement of Damping Ratio Using Surface Waves,” *Journal of Geotechnical and Geoenvironmental Engineering*, vol. 126, no. 5, pp. 472–480, 2000.

[95] R. D. Woods and L. P. Jadele, “Energy Attenuation Relationships for Construction Vibrations,” in *Vibrations Problems in Geotechnical Engineering*, 1985, pp. 229–246.

[96] G. Sica, J. Woodcock, E. Peris, A. Moorhouse, and D. Waddington, “On the assessment of the human exposure from vibration caused by railway construction,” in *Internoise 2012*, 2012.

[97] J. Woodcock., E. Peris, G. Sica, Z. Koziel, A. Moorhouse, and D. Waddington, “Human response to vibration in residential environments: Establishing exposure-response relationships,” in *ICBEN*, 2011.

[98] H. Lamb, “On the propagation of tremors over the surface of an elastic solid,” *Phil. Trans. Roy. Soc. London, Ser. A*, vol. CCIII, no. 1, pp. 1–42, 1904.

[99] J. D. Achenbach, *Wave propagation in elastic solids*, 1st ed. Amsterdam: North-Holland, 1973, p. 425.

[100] K. Aki and P. G. Richards, *Quantitave Seismology*, 2nd ed. University Science Books, 2002, p. 700.

[101] W. M. Ewing, W. S. Jardetzky, and F. Press, *Elastic waves in layered media*, 1st ed. New York: McGraw-Hill, 1957.

[102] W. Lowrie, *Fundamentals of Geophysics*, 1st ed. Cambridge: Cambridge University Press, 1997, p. 394.

[103] R. Woods, “Screening of surface waves in soils,” *Am Soc Civil Engr J Soil Mech*, vol. 94, no. SM4, pp. 951–979, 1968.

[104] S. Foti, “Multistation Methods for Geotechnical Characterization using Surface Waves,” Turin Politechnic, 2000.

[105] C. G. Lai, “Simultaneous Inversion of Rayleigh Phase Velocity and Attenuation for Near-Surface Site Characterization,” Georgia Institute of Technology, 1998.

[106] E. Kausel and J. M. Roesset, “Stiffness matrices for layered soils,” *Bulletin of the Seismological Society of America*, vol. 71, no. 6, pp. 1743–1761, 1981.

[107] L. V. Socco and C. Strobbia, “Surface-wave method for near-surface characterization: a tutorial,” *Near Surface Geophysics*, vol. 2, no. 4, pp. 165–185, 2004.

[108] S. W. Jones, “Ground Vibration from Underground Railways: How Simplifying Assumptions Limit Prediction Accuracy,” University of Cambridge, 2010.

[109] S. W. Jones and H. E. M. Hunt, “The effect of inclined soil layers on surface vibration from underground railways using a semianalytical approach,” *Journal of Physics: Conference Series*, vol. 181, no. 1, pp. 1–8, 2009.

[110] J. Houbrechts, M. Schevenels, G. Lombaert, G. Degrande, W. Rücker, V. Cuellar, and A. Smekal, “Rivas Project, Del 1.1 - Test procedures for the determination of the dynamic soil characteristics,” *UIC*, 2011. [Online]. Available: http://www.rivas-project.eu/fileadmin/documents/rivas_wp_13_d_11_v06.pdf. [Accessed: 01-Sep-2013].

[111] H. R. Masoumi, G. Degrande, and G. Lombaert, “Prediction of free field vibration due to pile driving using a dynamic soil-structure interaction formulation,” *Soil Dynamics and Earthquake Engineering*, vol. 27, no. 2, pp. 126–143, 2007.

[112] J. T. Nelson, “Prediction of ground vibration from trains using seismic reflectivity methods for a porous soil,” *Journal of Sound and Vibration*, vol. 231, no. 3, pp. 727–737, Mar. 2000.

[113] M. Biot, “Theory of Propagation of Elastic Waves in a Fluid Saturated Porous Solid. I. Low-Frequency Range,” *The Journal of the Acoustical Society of America*, vol. 28, no. 2, pp. 168–178, 1956.

[114] M. Biot, “Theory of Propagation of Elastic Waves in a Fluid Saturated Porous Solid. II. Higher Frequency Range,” *The Journal of the Acoustical Society of America*, vol. 28, no. 2, pp. 179–191, 1956.

[115] S. W. Jones and H. E. M. Hunt, “Predicting surface vibration from underground railways through inhomogeneous soil,” *Journal of Sound and Vibration*, vol. 331, no. 9, pp. 2055–2069, 2012.

[116] E. Larose, L. Margerin, A. Derode, B. Van Tiggelen, M. Campillo, N. Shapiro, A. Paul, L. Stehly, and M. Tanter, “Correlation of random wavefields: An interdisciplinary approach,” *Geophysics*, vol. 71, no. 4, pp. SI11–SI21, 2006.

[117] S. Bonnefoy-Claude, F. Cotton, and P. Bard, “The nature of noisewavefield and its applications for site effects studies: A literature review.,” *Earth-Science Reviews*, vol. 79, no. 3–4, pp. 205–227, 2006.

[118] F. J. Chavez-Garcia, M. Rodriguez, and W. R. Stephenson, “An Alternative Approach to the SPAC Analysis of Microtremors: Exploiting Stationarity of Noise,” *Bulletin of the Seismological Society of America*, vol. 95, no. 1, pp. 277–293, 2005.

[119] B. Choet, G. De Luca, G. Milana, P. Dawson, M. Martini, and R. Scarpa, “Shallow Velocity Structure of Stromboli Volcano, Italy, Derived from Small-Aperture Array Measurements of Strombolian Tremor,” *Bulletin of the Seismological Society of America*, vol. 88, no. 3, pp. 653–666, 1998.

[120] G. J. Rix, C. G. Lai, M. C. Orozco, G. L. Hebeler, and V. Roma, “Geotechnical Site Characterization using Surface Waves,” in *XV International Conference on Soil Mechanics and Geotechnical Engineering*, 2001.

[121] R. Carniel, F. Barazza, and P. Pascolo, “Improvement of Nakamura technique by singular spectrum analysis,” *Soil Dynamics and Earthquake Engineering*, vol. 26, no. 1, pp. 55–63, 2006.

[122] J. Lerno and F. J. Chavez-Garcia, “Are Microtremors Useful in Site Response Evaluation?,” *Bulletin of the Seismological Society of America*, vol. 84, no. 5, pp. 1350–1364, 1994.

[123] SESAME, “Site EffectS assessment using AMbient Excitations.” [Online]. Available: http://sesame-fp5.obs.ujf-grenoble.fr/index.htm. [Accessed: 12-Jun-2012].

[124] P. Harutoonian, C. J. Leo, T. Doanh, S. Castellaro, J. J. Zou, D. S. Liyanapathirana, H. Wong, and K. Tokeshi, “Microtremor measurements of rolling compacted ground,” *Soil Dynamics and Earthquake Engineering*, vol. 41, pp. 23–31, 2012.

[125] D. Motazedian, J. A. Hunter, S. Sivathayalan, A. Pugin, S. Pullan, H. Crow, and K. Khakeshi Banad, “Railway train induced ground vibrations in a low VS soil layer overlying a high VS bedrock in eastern Canada,” *Soil Dynamics and Earthquake Engineering*, vol. 36, pp. 1–11, 2012.

[126] Q. F. Chen, L.Li, G.Li, L.Chen, W. T. Peng, Y.Tang, Y.Chen, and F. Y. Wang, “Seismic features of vibration induced by train,” *Acta Seismologica Sinica*, vol. 17, no. 6, pp. 715–724, 2004.

[127] A. DITZEL, G. C. HERMAN, and G. G. DRIJKONINGEN, “SEISMOGRAMS OF MOVING TRAINS: COMPARISON OF THEORY AND MEASUREMENTS,” *Journal of Sound and Vibration*, vol. 248, no. 4, pp. 635–652, 2001.

[128] H. H. Hung and Y. B. Yang, “A review of researches on ground-borne vibrations with emphasis on those induced by trains,” *Proc. Natl. Sci. Counc. ROC (A)*, vol. 25, no. 1, pp. 1–16, 2001.

[129] A. Mirza, J. Nielsen, and P. Ruest, “Rivas Project, Del 5.1 - Train Induced Ground Vibration – Influence of Rolling Stock State-of-the-Art Survey,” *UIC*, 2011. [Online]. Available: http://www.rivas-project.eu/fileadmin/documents/RIVAS_UIC__WP5_D5_1_V02_final_01.pdf.

[130] H. R. Masoumi, G. Degrande, and A. Holeyman, “Pile response and free field vibrations due to low strain dynamic loading,” *Soil Dynamics and Earthquake Engineering*, vol. 29, no. 5, pp. 834–844, 2009.

[131] E. C. Bovey, “Development of an impact method to determine the vibration transfer characteristics of railway installations,” *Journal of Sound and Vibration*, vol. 87, no. 2, pp. 357–370, 1983.

[132] J. T. Nelson and H. J. Saurenman, “A prediction procedure for rail transportation groundborne noise and vibration,” *Transportation Research Record*, vol. 1143, pp. 26–35, 1987.

[133] H. L. Singleton, “Vibration Transfer Mobility Measurements Using Maximum Length Sequences,” in *150th Meeting of the Acoustical Society of America/NOISE-CON 2005*, 2005.

[134] P. B. Attewell and I. W. Farmer, “Attenuation of Ground Vibrations from Pile Driving,” *Ground Engineering*, vol. 3, no. 7, pp. 26–29, 1973.

[135] D. S. Kim and J. S. Lee, “Propagation and attenuation characteristics of various ground vibrations,” *Soil Dynamics and Earthquake Engineering*, vol. 19, no. 2, pp. 115–126, 2000.

[136] J. H. Hwang and T. Y. Tu, “Ground vibration due to dynamic compaction,” *Soil Dynamics and Earthquake Engineering*, vol. 26, no. 5, pp. 337–346, 2006.

[137] R. Arcos, J. Romeu, A. Balastegui, and T. Pameis, “Determination of the near field distance for point and line sources acting on the surface of an homogenous and viscoelastic half-space,” *Soil Dynamics and Earthquake Engineering*, vol. 31, no. 7, pp. 1072–1074, 2011.

[138] E. R. Kanasewich, *Time Sequence Analysis in Geophysics*, Third. Alberta: The University of Alberta Press, 1981, p. 480.

[139] S. A. Greenhalgh, I. M. Mason, and B. Zhou, “An analytical treatment of single station triaxial seismic direction finiding,” *Journal of Geophysics and Enginneing.*, vol. 2, pp. 8–15, 2005.

[140] E. A. Flinn, “Signal analysis using rectilinearity and direction of particle motion,” *Proceedings of the IEEE*, vol. 53, pp. 1874–1876, 1965.

[141] G. M. Jackson, I. M. Mason, and S. A. Greenhalgh, “Principal component transforms of triaxial recordings by singular value decomposition,” *Geophysics*, vol. 56, no. 4, p. 528, Apr. 1991.

[142] J. C. Samson, “Pure states, polarized waves and principal components in the spectra of multiple, geophysical time-series,” *Geophysical Journal of the Royal Astronomical Society*, vol. 72, no. 3, pp. 647–664, 1983.

[143] J. C. Samson, “Matrix and Stokes vector representations of detectors for polarized waveforms: theory, with some applications to teleseismic waves,” *Geophysical Journal of the Royal Astronomical Society*, vol. 51, no. 3, pp. 583–603, 1977.

[144] C. Esmersoy, “Polarization Analysis, orientation and velocity estimation in three-component VSP,” in in *Vertical Seismic Profiling Part B: Advanced Concept*, London: Geophysical Press, 1984, pp. 236–255.

[145] J. Park, F. L. Vernon III, and C. R. Lindberg, “Frequency Dependent Polarization Analysis of High-Frequency Seismograms,” *Journal of Geophysical Research*, vol. 92, no. B12, pp. 12664–12674, 1987.

[146] J. Vidale, “Complex polarization analysis of particle motion,” *Bulletin of the Seismological society of America*, vol. 76, no. 5, pp. 1383–1406, 1986.

[147] M. Kulesh, M. S. Diallo, M. Holscheneider, K. Kurennaya, F. Kruger, M. Ohrmberger, and F. Scherbaum, “Polarization analysis in the wavelet domain based on the adaptive covariance method,” *Geophysical Journal International*, vol. 170, no. 2, pp. 667–678, 2007.

[148] H. Moriya and H. Niitsuma, “Precise detection of a P-wave in low S/N signal by using time-frequency representations of a triaxial hodogram,” *Geophysics*, vol. 61, no. 5, pp. 1453–1466, 1996.

[149] A. Jurkevics, “Polarization analysis of three-component array data,” *Bulletin of the Seismological Society of America*, vol. 78, no. 5, pp. 1725–1743, 1988.

[150] G. S. Wagner and T. J. Owens, “Broadband eigen-analysis for three component seismic array data,” *IEEE trans. Signal. Proc.*, vol. 43, no. 7, pp. 1738–1741, 1995.

[151] M. Rutty and S. A. Greenhalgh, “Correlation using triaxial data from multiple stations in the presence of coherent noise,” in in *Covariance Analysis in Seismic Signal Processing*, Tulsa: Society Exploration Geophysics, 1999, pp. 291–322.

[152] K. Bataille and J. M. Chiu, “Polarization analysis of high-frequency, three-component seismic data,” *Bulletin of the Seismological Society of America*, vol. 81, no. 2, pp. 622–642, 1991.

[153] M. Palo, J. M. Ibanez, M. Cisneros, M. Breton, E. Del Pezzo, E. Ocana, J. Orozco-Rojas, and A. M. Posadas, “Analysis of the seismic wavefield properties of volcanic explosions at Volc{á}n de Colima, M{é}xico: insights into the source mechanism,” *Geophysical Journal International*, vol. 177, no. 3, pp. 1383–1389, 2009.

[154] R. De Franco and G. Musacchio, “Polarization filter with singular value decomposition,” *Geophysics*, vol. 66, no. 3, pp. 932–938, 2001.

[155] A. I. Perelberg and S. C. Hornbostel, “Applications of seismic polarization analysis,” *Geophysics*, vol. 59, no. 1, pp. 119–130, 1994.

[156] N. Magotra, N. Ahmed, and E. Chael, “Single-Station Event Detection and Location,” *IEEE transaction on geoscience and remote sensing*, vol. 27, no. 1, pp. 15–23, 1989.

[157] D. Patane and F. Ferrari, “Seismpol: a visual-basic computer program for interactive and automatic earthquake waveform analysis,” *Computer and Geoscience*, vol. 23, no. 9, pp. 1005–1012, 1997.

[158] E. Kausel, “Early history of soil-structure interaction,” *Soil Dynamics and Earthquake Engineering*, vol. 30, no. 9, pp. 822–832, 2010.

[159] J. P. Wolf and C. Song, “Some cornerstones of dynamic soil–structure interaction,” *Engineering Structures*, vol. 24, no. 1, pp. 13–28, 2002.

[160] K. K. H. Chua, K. K. W. Lo, and T. Balendra, “Building Response due to Subway Train Traffic,” *Journal of Geotechnical & Geoenvironmental Engineering*, vol. 121, no. 11, pp. 747–754, 1995.

[161] S. Francois, L. Pyl, H. R. Masoumi, and G. Degrande, “The influence of dynamic soil–structure interaction on traffic induced vibrations in buildings,” *Soil Dynamics and Earthquake Engineering*, vol. 27, no. 7, pp. 655–674, 2007.

[162] P. Fiala, G. Degrande, and F. Augusztinovicz, “Numerical modelling of ground-borne noise and vibration in buildings due to surface rail traffic,” *Journal of Sound and Vibration*, vol. 301, no. 3–5, pp. 718–738, 2007.

[163] D. J. Martin, “Ground vibrations from impact pile driving during road construction,” *TRRL Supplementary Report*, vol. 544, p. 25, 1980.

[164] O. Hunaidi and M. Tremblay, “Traffic-induced building vibrations in Montreal,” *Canadian Journal of Civil Engineering*, vol. 24, no. 5, pp. 736–753, 1997.

[165] D. E. Newland and H. E. M. Hunt, “Isolation of Building from Ground Vibration: A Review of Recent Progress,” *Proceedings of the Institution of Mechanical Engineers, Part C: Journal of Mechanical Engineering Science*, vol. 205, no. 1, pp. 39–52, 1991.

[166] J. Jakobsen, “Transmission of ground-borne vibration in buildings,” *Journal of low frequency noise & vibration*, vol. 8, no. 3, pp. 75–80, 1989.

[167] J. De Avillez, M. Frost, S. Cawser, A. El-Hamalawi, P. Flemming, P. Shields, and C. Skinner, “Issues and Limitations on Measuring Building’s Transfer Function,” in *15th International Conference on Experimental Mechanics*, 2012.

[168] C. With and A. Bodare, “Prediction of train-induced vibrations inside buildings using transfer functions,” *Soil Dynamics and Earthquake Engineering*, vol. 27, no. 2, pp. 93–98, 2007.

[169] M. R. Gallipoli, M. Mucciarelli, R. R. Castro, G. Monachesi, and P. Contri, “Structure, soil-structure response and effects of damage based on observations of horizontal-to-vertical spectral ratios of microtremors,” *Soil Dynamics and Earthquake Engineering*, vol. 24, no. 6, pp. 487–495, 2004.

[170] J. Bencat, “Microtremors from Railway Traffic,” in *The eighth international conference on computational structures technology*, 2006.

[171] C. Gaohang, T. Xiaxin, C. Xianmai, and W. Futong, “Designed Micro-tremor Array Based Actual Measurement and Analysis of Environmental Vibration Induced by Urban Rail Transit,” in *International Conference on Intelligent System Design and Engineering Application*, 2010, pp. 596–599.

[172] C. Cheron, M. Walter, J. Sandor, and E. Wiebe, “ERRAC Roadmap. Towards 2030: energy, noise and vibration European railway roadmaps.,” *Procedia Social and Behaviour Science*, vol. 48, pp. 2221–2229, 2012.

[173] L. Cohen, “Time-frequency distributions-a review,” *Proceedings of the IEEE*, vol. 77, no. 7, pp. 941–981, 1989.

[174] G. Liu, S. Formel, and X. Chen, “Time-frequency analysis of seismic data using local attributes,” *Geophysics*, vol. 76, no. 6, pp. 23–34, 2011.

[175] F. Auger, *Time frequency Analysis*, 1st ed. London: ISTE, 2008.

[176] S. Mallat, *A wavelet tour of signal processing*, 2nd ed. London: Academic Press, 1999.

[177] F. Auger and P. Flandrin, “Improving the Readability of Time-Frequency and Time-Scale Representation by the Reassignement Method,” *IEEE transaction on signal processing*, vol. 43, no. 5, pp. 1068–1089, 1995.

[178] P. Flandrin, F. Auger, and E. Chassande-Mottin, “Time-Frequency Reassignment — From Principles to Algorithms,” in in *Applications in Time-Frequency Signal Processing*, A. Papandreou-Suppappola, Ed. CRC Press, 2003, pp. 179–203.

[179] B. Land, “Time-Frequency Reassigned Spectrogram.,” 2008. [Online]. Available: http://people.ece.cornell.edu/land/PROJECTS/ReassignFFT/index.html. [Accessed: 07-Apr-2013].

[180] G. S. Wagner and T. J. Owens, “Signal Detection Using Multi-Channel Seismic Data,” *Bulletin of the Seismological Society of America*, vol. 86, no. 1A, pp. 221–231, 1999.

[181] F. Auger, P. Flandrin, P. Goncalves, and O. Lemoine, “Time-Frequency Toolbox for use with Matlab – Tutorial,” *CNRS GdR Information, Image, Signal Vision (ISIS)*, 1995. [Online]. Available: http://tftb.nongnu.org/. [Accessed: 01-Jul-2012].

[182] A. Chichowicz, R. W. E. Green, and A. Van Zyl Brink, “Coda polarization properties of high-frequency microseismic events,” *Bulletin of the Seismological Society of America*, vol. 78, no. 3, pp. 1297–1318, 1988.

[183] E. De Lauro, S. De Martino, M. Falanga, and M. Palo, “Decomposition of high-frequency seismic wavefield of the Strombolian-like explosions at Erebus volcano by independent component analysis,” *Geophysical Journal International*, vol. 117, no. 3, pp. 1399–1406, 2009.

[184] P. M. Nelson, *Transportation noise reference book*, 1st ed. London: Butterworth & Co., 1987, p. 540.

[185] H. E. M. Hunt, “Modelling of rail vehicles and track for calculation of ground-vibration transmission into buildings,” *Journal of Sound and Vibration*, vol. 193, no. 1, pp. 185–194, May 1996.

[186] M. Villot, C. Guigou, P. Jean, and N. Picard, “Rivas Project, Del 1.6 - Definition of appropriate procedures to predict exposure in buildings and estimate annoyance,” *UIC*, 2012. [Online]. Available: http://www.rivas-project.eu/fileadmin/documents/rivas_cstb_wp1_d1_6_v04_procedures_exposure_annoyance.pdf. [Accessed: 01-Sep-2013].

[187] R. Randall, *Frequency analysis*, 3rd ed. Glostrup, Denmark: Bruel & Kjaer, 1987, p. 344.

[188] F. Amini, “Dynamic soil properties using improved transfer function methods,” *Soil Dynamics and Earthquake Engineering*, vol. 9, no. 6, pp. 274–278, 1990.

[189] B. Parker, “Chapter 1: Stochastic processes,” *GEOPHYSICAL DATA ANALYSIS Class Notes by Bob Parker*, 2010. [Online]. Available: http://igppweb.ucsd.edu/~parker/SIO223/chap1.pdf. [Accessed: 10-Apr-2012].

[190] K. Shin and J. Hammond, *Fundamentals of Signal Processing for Sound and Vibration Engineers*, 1st ed. Chichester, England: John Wiley & Sons, 2008, p. 416.

[191] J. S. Bendat and A. G. Piersol, *Random Data: Analysis and Measurement Procedures*, 4th ed. Hoboken, New Jersey: John Wiley & Sons, 2011, p. 640.

[192] G. C. Carter, “Coherence and Time Delay Estimation,” *Proceedings of the IEEE*, vol. 75, no. 2, pp. 236–255, 1987.

[193] G. C. Carter, C. H. Knapp, and A. H. Nuttall, “Estimation of the Magnitude-Squared Coherence Function Via Overlapped Fast Fourier Transform Processing,” *IEEE transactions on audio and electroacoustics*, vol. 21, no. 4, pp. 337–344, 1973.

[194] S. M. Price and R. J. Bernhard, “Virtual coherence: a digital signal process technique for incoherent source identification,” in *4th International Modal Analysis Conference*, 1986.

[195] D. Vandenbroeck and W. S. F. Hendricx, “Interior road noise optimization in a multiple input environment,” *INSTITUTION OF MECHANICAL ENGINEERS CONFERENCE PUBLICATIONS*, vol. 3, pp. 53–58, 1994.

[196] G. Licitra, Ed., *Noise mapping in EU: models and procedures*. Boca Raton, Florida: CRC Press, 2013, p. 412.

[197] E. Peris, J. Woodcock., G. Sica, C. Sharp, A. Moorhouse, and D. Waddington, “Guidance for new policy developments on railway vibration,” *Proceedings of Meetings on Acoustics*, vol. 19, pp. 040037–040044, 2013.

[198] G. Sica, E. Peris, J. Woodcock, A. Moorhouse, and D. Waddington, “Design of measurement methodology for the evaluation of human exposure to vibration in residential environments,” *Science of the Total Environment*, 2013. [Online]. Available: http://dx.doi.org/10.1016/j.scitotenv.2013.07.006. [Accessed: 04-Sep-2013].

[199] D. Stiebel, R. Muller, E. Bongini, A. Ekblad, G. Coquel, and A. A. Alvaro, “Rivas Project, Del 1.5 - Definition of reference cases typical for hot-spots in Europe with existing vibration problems,” *UIC*, 2012. [Online]. Available: http://www.rivas-project.eu/fileadmin/documents/rivas_db_wp1_d1_5_v05_definition_hotspots.pdf. [Accessed: 01-Sep-2013].

[200] M. Brink, B. Shaeffer, D. Schreckenberg, and M. Basner, “Aircraft noise indexes - recent developments and current applications,” in *ICBEN*, 2011.

[201] E. Peris, “Human response to railway vibration in residential environments: exposure-response relationships and modifying factors.,” University of Salford, 2013.

[202] J. Woodcock., “Field and laboratory studies into the human response to groundborne vibration:exposure-response relationships, perceptual dimensions, and models of annoyance,” Univesity of Salford, 2013.

[203] Arup and URS, “HS2 London to West Midlands EIA Scope and Methodology Report,” *hs2*, 2012. [Online]. Available: http://assets.hs2.org.uk/sites/default/files/inserts/HS2 London to West Midlands EIA Scope & Methodology Report revised_0.pdf. [Accessed: 04-Sep-2013].

[204] C. J. C. Jones and J. R. Block, “Prediction of ground vibration from freight trains,” *Journal of Sound and Vibration*, vol. 193, no. 1, pp. 205–213, 1996.

[205] C. Sharp, D. Waddington, J. Woodcock., G. Sica, E. Peris, and A. Moorhouse, “Two algorithms for the sorting of unknown train vibration signals into freight and passenger train categories,” in *IOA Acoustics*, 2012.

[206] G. Glickman, “Getting more with more: leveraging project-available data to enhance ground-borne noise and vibration predictions,” in *Internoise 2012*, 2012.

[207] W. S. Heckman and D. J. Hagerty, “Vibrations Associated with Pile Driving,” *Journal of Construction Division*, vol. 104, no. CO4, pp. 385–394, 1981.

[208] C. B. Park, R. D. Miller, and J. Xia, “Multichannel analysis of surface waves,” *Geophysics*, vol. 64, no. 3, pp. 800–808, 1999.

[209] S. Nazarian and M. R. Desai, “Automated surface wave method: field testing,” *Journal of Geotechnical Engineering;*, vol. 119, no. 7, pp. 1094–1111, 1993.

[210] D. Yuan and S.Nazarian, “Automated Surface Wave Method: Inversion Technique,” *Journal of Geotechnical Engineering*, vol. 119, no. 7, pp. 1112–1126, Jul. 1993.

[211] S. A. Badsar, M. Schevenels, and G. Degrande, “The determination of the damping parameter of soils with the sasw method,” in *COMPDYN 2009 ECCOMAS Thematic Conference on Computational Methods in Structural Dynamics and Earthquake Engineering*, 2009.

[212] R. De Bolt, “Non-Destructive Evaluation of Railway Trackbed Ballast,” The University of Edinburgh, 2011.

[213] A. Samouelian, I. Cousin, A. Tabbagh, A. Braund, and G. Richard, “Electrical resistivity survey in soil science: a review,” *Soil and Tillage Research*, vol. 83, no. 2, pp. 173–193, 2005.

[214] J. Peterson, “Observation and modelling of background seismic noise.,” U.S.G.S., Albuquerque, New Mexico, 1993.

APPENDIX A: SEMI EMPIRICAL METHOD FOR ASSESSING PROPAGATION OF VIBRATION FROM MANMADE PROCESSES

The assessment of the vibration propagation using analytical models can be difficult due to the complexity of the source mechanisms. Therefore, another way to infer the propagation characteristics is to use theoretical assumptions for fitting experimental data: this approach is called semi empirical. The latter estimates the decrement of the vibration amplitude with the distance from the source also known as attenuation which is partly due to the geometry of the propagation of seismic waves, and partly due to the anelastic properties of the ground through which they travel (Lowrie [102]).

The geometric attenuation or geometric damping is essentially due to the expansion of the wavefronts, resulting in the spreading of energy over an increasing area (Houbrechts et al. [110]). Since body waves have different wavefronts from surface waves, the former is spherical the latter is cylindrical (Athanasopouls et al. [92]), they will provide different reduction of intensity with distance r : body waves attenuation is proportional to $1/r^2$ whereas the geometrical spreading of surface waves is proportional to $1/r$.

It can be found that for harmonic vibration the intensity of a wave-form is proportional to the square of its amplitude (Lowrie [102]). As a consequence, the corresponding amplitude attenuations of body waves and surface waves are proportional to $1/r$ and $1/\sqrt{r}$ for an in depth point source.

Only considering geometrical damping, the semi empirical propagation model can be written as follow:

$$A(r) = A_0\left(\frac{r_0}{r}\right)^n \tag{A.1}$$

$A(r)$ is the vibration amplitude at a distance r from the source whereas A_0 is the amplitude measured at r_0 from the source n is the geometric damping.

Gutowski and Dim [78], in 1976, provided a table, Figure 108 from Kim and Lee [135], with different values of the geometric damping, for different wave types, generated by several manmade processes modelled like point or line loads.

Physical sources	Type of source	Wave	Location	n
Highway/Rail line footing array	Line	Surface	Surface	0
		Body	Surface	1.0
Car in pothole, Single footing	Point	Rayleigh	Surface	0.5
		Body	Surface	2.0
Tunnel	Buried Line	Body	Interior	0.5
Buried explosion	Buried point	Body	Interior	1.0

FIGURE 108 – GEOMETRIC DAMPING FOR VARIOUS SOURCES

Another reason for attenuation is the absorption of energy due to imperfect elastic properties. If the particles of a medium do not react perfectly elastically with their neighbours, part of the energy is lost. This type of attenuation of the seismic wave is referred as damping (Lowrie [102]). Both geometric and material attenuation were combined in a semi empirical attenuation law by Bornitz [85].

$$A(r) = A_0 \left(\frac{r_0}{r} \right)^n e^{-\alpha(r-r_0)} \tag{A.2}$$

The Equation (A.2) is also known as Barkan's law [91]. The latter has been used by Clough and Chameau [88], among other, for assessing the propagation characteristics of vibratory sheet pile driving.

The terms A_0, r_0, $A(r)$, r and n are defined in the same way as the propagation model with geometric damping only but including a coefficient of attenuation α. Equation (A.2) provides an approximation

It is known that the attenuation coefficient due to material damping α depends on the type of soil and the frequency of vibration (Richart et al. [86]). A simplified analysis of the mechanics of seismic wave propagation in the ground leads to the following equation for estimating the values of coefficient α (Athanasopulus et al. [92]):

$$\alpha = \frac{2\pi fD}{V_R} \tag{A.3}$$

Where V_R is the propagation of Rayleigh waves, D the damping ratio of the soil and f the frequency of vibration. Equation (A.3) indicates that the value of attenuation coefficient α increases linearly with the frequency of vibration and with the damping ratio of the soil material whereas it is inversely proportional to the speed of Rayleigh waves.

Therefore α depends on the natural characteristics of the ground to attenuate elastic waves: softer materials generally have greater α values whereas harder materials have smaller values. In the case of steady state sources it is also possible to relate the α value to the soil characteristics using the classification proposed by Woods & Jadele [95] for earth materials shown in Table 17.

Class	Attenuation Coefficient α (1/m) 5 Hz	Description of Material
I	0.01 to 0.033	Weak or Soft Soils
II	0.0033 to 0.01	Competent Soils
III	0.00033 to 0.0033	Hard Soils
IV	< 0.00033	Hard, Competent Rock

Table 17 – Proposed classification of earth materials by attenuation coefficient

In Table 17 the coefficient of attenuation is frequency dependent. If α is known for one frequency f, α_1 can be computed for any other frequency f_1 using

$$\alpha_1 = \alpha\left(f_1/f\right) \tag{A.4}$$

Under the assumption that α is linearly dependent on f. This last hypothesis is not essentially true because the damping has a general function of frequency $\alpha = \alpha(f)$ [94]. In order to quantify the frequency dependence of the material damping the Barkan's Law can be extended in the frequency domain. This approach can be found in Amick [93] and Sica et al. [66] for construction sources.

Barkan's law is one of the most used semi-analytical models of propagation for describing the at-grade vibration problem (Arcos et al. [137]). Arcos et al. [137] highlighted that several authors have proposed laws similar to Barkan's for modelling the propagation of vibration induced by several sources: highway traffic (Watts [35]), railway traffic (Nelson [184]), construction processes (Kim and Lee [135]) or industrial machinery. The same law have been used in semi empirical models of railway vibration (Madshus et al. [41], Bahrekazemi [68]) for describing the propagation into the ground.

Kim and Lee [135] studied the propagation characteristics, using the Bornitz equation, of three manmade processes: train loading, blasting, friction pile driving and hydraulic compaction. For railway traffic Kim and Lee found that ground vibrations induced by shorter and faster train (8 cars, 135 km/h) was attenuated faster than that of longer and slower trains (24 cars, 71 km/h). Due to superposition effect of moving loads, the train loading of the shorter and faster train can be characterised as a combination of the point and line sources of body wave with a geometric damping coefficient n of 1.5. For the longer and slower train, it can be characterised as a line source of body wave with a geometric attenuation coefficient n of 1.0.

As already mentioned in section 5.4.1, semi empirical propagation models are largely used in construction especially for describing piling vibrations. Wiss [84] attempted to model attenuation from piling vibrations obtaining the best fit of field data in an equation of the form

$$V(d) = k(d)^{-n} \tag{A.5}$$

where $V(d)$ is defined as the PPV at distance d from the source, k is the value of velocity at one unit distance and n is the attenuation rate considered as a pseudo-attenuation coefficient. The last two values are obtained through a regression analysis. This approached can also be found in the work of Athanasopouls and Pelekis [89] who measured ground vibrations from sheet pile driving in urban environment. Attewell and Farmer [134] and Wiss [84] suggested an expression for including the source energy in the attenuation equation. The so called scaled-distance equation is expressed below where E is the energy of the source.

$$V(d) = k\left(d/\sqrt{E}\right)^{-n} \tag{A.6}$$

The value n generally lies between 1 and 2 with a common value of 1.5 (Wiss [84]). According to Woods [85], the pseudo attenuation approach is satisfactory for describing propagation characteristics of several construction sources from jackhammer to large dynamic-compaction (See Figure 35) whereas the Bornitz equation is the best representation of attenuation coefficient.

Heckman and Hagerty [207] pointed out the important effect of the pile impedance on the peak ground velocity and showed that a reduction of the pile impedance from 2000 to 500 kNs/m could increase the peak ground velocity by a factor of 8. As a consequence they modified the scaled-distance equation including a term called "K factor" that takes into account for the pile impedance.

APPENDIX B: PENETRATION AND LABORATORY TESTS

The first methods considered in section 6.3.1 belong to the category of in situ testing for collecting soil mechanical parameters such as resistance and slide friction that can help to obtain a stratigraphy of the soil profile. These methods are called penetration tests and can be divided into standard penetration tests (SPT) and cone penetration test (CPT).

The SPT uses a thick-walled sample tube, with an outside diameter of 50 mm and an inside diameter of 35 mm, and a length of around 650 mm. This is driven into the ground at the bottom of a borehole by blows from a slide hammer with a weight of 63.5 kg (140 lb) falling through a distance of 760 mm (30 in). The sample tube is driven 150 mm into the ground and then the number of blows needed for the tube to penetrate each 150 mm (6 in) up to a depth of 450 mm (18 in) is recorded. The sum of the number of blows required for the second and third 6 in. of penetration is termed the "standard penetration resistance" or the "N-value". In cases where 50 blows are insufficient to advance it through a 150 mm (6 in) interval the penetration after 50 blows is recorded.

The blow count provides an indication of the density of the ground, and it is used in many empirical geotechnical engineering formulae for estimating the wave speed as done in Athanasopolus et al. [92].

The CPT is an improvement of the SPT. The method is only applicable to soft soils extending, at most, to medium stiff soils, and without any sizeable proportion of medium to large gravel size particles. The main difference between CPT and SPT is that in the CPT the probe has a conical shape and is drive in to the ground at a controlled rate (between 1.5 -2.5cm/s). The resolution of the CPT in delineating stratigraphic layers is related to the size of the cone tip, with typical cone tips having a cross-sectional area of either 10 or 15 cm^2, corresponding to diameters of 3.6 and 4.4 cm. The piezocone penetration test (CPTU) is an electrical CPT, which includes additional instrumentation to measure the pore water pressure during penetration at the level of the base of the cone. Even in the case of CPT the

information gathered from the test can be linked to dynamic parameters of the soil through empirical relationships.

The soil samples collected in the penetration test can be used for estimating dynamic soil properties with laboratory tests. The most frequently used soil dynamic laboratory tests are the resonant column test, the bender element test, the cyclic shear test and the cyclic triaxial test which are described in Houbrechts et al. [110] and Lai [105]. These tests generate different levels of stress and deformation on the soil sample that are reached in to the ground; therefore they can measure dynamic properties of the soil with high accuracy. On the other hand, these tests have several drawbacks: the soil sampling leads to disturbance in the soil profile, the dynamic characteristics are valid just for the measurement point and they cannot be extended to the entire soil profile due to its heterogeneous nature. Furthermore, these tests are expensive to perform.

APPENDIX C: SEISMIC IN SITU MEASUREMENT

The other family of methodologies treated in section 6.3.1, following the scheme presented in Houbrechts et al. [110], are grouped in the category of seismic in situ measurement. These techniques allow knowing the dynamic soil properties in the region of small strain and are suitable for the characterization of soil properties for railway traffic and the far field of construction sources.

The assessment of soil properties through geophysical or seismic methods is based on the measurement of body waves like P or S wave depending on test that is performed. These techniques rely on a source, which can be on the surface or buried in the ground, that can be either impulsive or steady or random or an explosive which creates a perturbation in the soil that is recorded by receivers, seismometers or accelerometers, in array configuration. Once the data are acquired, some post processing may be necessary before finding the soil properties. This last step is called inversion where the post processed data are "transformed" into quantitative soil properties under some initial hypothesis about the system.

These approaches generally provide an overall description of the soil conditions which are representative of the test conditions because no information about the saturation of the soil is provided. The soil properties are derived through analysis or empirical relations and therefore uncertainties are introduced in these methods. Furthermore, other sources of uncertainty are, for example, the spatial variability of the properties, the inherent and induced anisotropy, the nonlinearity of the material, the soil disturbance due to drilling and sampling, and testing or interpretation errors. Some of these sources can be limited and quantified, others cannot.

1. Reflection/Refraction surveys

The first methods for retrieving soil properties take advantage of reflection or refraction of the seismic wave at the interface between two layers of the ground with different mechanical properties using Snell's law. Post processing technique

for identifying the direct waves at the measurement positions, such STA\LTA or polarization techniques (Whiters et al. [82]) , are used for having an estimation of the time travel of the perturbation across the array. The different slopes in the graph travel time versus distance provide information about the wave velocities in the layers and intersection between line segments gives information about the depth of the layers. Then the soil properties are obtained through inversion techniques. Further information can be found in Richart et al. [86] and Houbrechts et al. [110]. The seismic reflection or refraction surveys are popular methods for obtaining soil properties especially in exploration seismology because they are not expensive to implement. On the other hand, they work under the hypothesis that the soil profile is normally dispersive and horizontally layered which may lead to wrong interpretations of the arrival time.

2. Down/up/cross hole tests

Other categories of seismic test, which aims to measure the speed of P and S waves, are the down- and up-hole tests. In the former the vibration receivers are in a borehole and the source is on the surface whereas these locations are reversed in the latter. As for the methods explained above, an estimation of the travel time vs. distance, in this case depth, is obtained and an estimation of the wave speed can be obtained. An advanced method is called cross-hole testing where two boreholes are used: one for the sources and the other for the receiver. Since these techniques involve the creation of a borehole they are expensive and the accuracy of the methods depend on the distance between source and receivers which don't need to be too large in order to avoid that the ray path deviates considerably from the vertical. On the other hand, they provide good results in terms of wave speed and spatial resolution. In the case of the cross-hole testing an estimation of the damping can be obtained too.

Other methods for acquiring soil properties in borehole are the seismic penetration cone (SCPT) and the PS logging. Refer to Houbrechts et al. [110] for further information.

3. Spectral Analysis of Surface Waves (SASW)

The methods presented above are mainly based in the estimation of the P and S wave time travel for estimating the soil properties. The techniques shown below are based on the analysis of the surface waves. In fact, as said in section 6.2.3 surface waves have two main features: they carry almost 2/3 of the energy of a disturbance that is moving on the free surface and have a dispersive nature. These characteristics can be used for inferring near surface elastic properties (Park et al. [208]). The study of the surface waves started in the 1960's with the Steady-State-Vibration Technique (Richart et al. [86]) which evolved in the 1980's in the SASW with the work of Stokoe and Nazarian (Foti [104], Lai [105]) for pavement analysis. Later the SASW became a quite popular in situ seismic test for assessing dynamic soil properties and the methodology is well explain in the works of Nazarian and Desai [209] and Yuan and Nazarian [210] for dual the channel analysis. The approach was extended using arrays of sensors by Park et al. [208] and by Foti [104] among other.

The SASW method consists of three steps. First, an in situ measurement is performed where surface waves are generated by means of a falling weight device, an impact hammer, or a hydraulic shaker. The response is measured by means of accelerometers or geophones located at the soil's surface. Second, the experimental dispersion curve (i.e. the phase velocity as a function of the frequency) is determined from the measurement data. Different approaches for obtaining this curve can be found in Foti [104] and Houbrechts et al [110].

In the third step, an inverse problem is solved in order to find a soil profile corresponding to the experimental dispersion curves. A list of inverse algorithms is given in Lai [105] and Houbrechts et al [110]. The use of Rayleigh waves, at the small scale, for the determination of soil damping has been discussed by Lai [105], Rix et al [94] and Badsar et al. [211]. Several applications of the SASW to railway problems can be found in the work carried out by Prof. G. Degrande at K.U. Leuven.

APPENDIX D: IMAGING TECHNIQUES

Imaging techniques, treated in section 6.3.1, are the methods for procuring an image of the soil profile in one and more dimensions. The parameter reproduced is not only the stiffness, as in the methods presented in 6.3.1, but also other geophysical characteristics of the ground.

1. Seismic tomography

The first technique presented here can be used for assessing soil properties is the seismic tomography. This technique is used for producing velocity models of the portion of soil where the survey is undertaken by evaluating the propagation time of the elastic waves between the source and receivers. The latter can be estimated, for example, through a cross correlation analysis and the soil properties are inferred through an inversion algorithm. This method can be implemented, for example, with a measuring setup similar to the cross-hole method providing a high spatial resolution but it is an expensive technique and the inversion problem does not have a unique solution, like as in the SASW method.

2. Ground-penetrating radar (GPR)

Ground-penetrating radar (GPR) is a method that uses radar pulses to image the subsurface. This non-destructive method uses electromagnetic radiation in the microwave band (UHF/VHF frequencies) of the radio spectrum, and detects the reflected signals from subsurface structures. GPR can be used in a variety of media, including rock, soil, ice, fresh water, pavements and structures. It can detect objects, changes in material, and voids and cracks.

GPR uses high-frequency (usually polarized) radio waves and transmits into the ground. The principles involved are similar to reflection seismology, except that electromagnetic energy is used instead of acoustic energy, and reflections appear at boundaries with different dielectric constants instead of acoustic impedances.

GPR is mainly used in geophysical archaeology for detecting manufacture buried structures that are buried in the ground but it is also used in the railway

environment for assessing the performance of the structure below the rail track as shown in De Bolt [212].

3. Electrical Resistivity Tomography (ERT)

Another technique for obtaining soil imaging is called electrical resistivity tomography (ERT). The electrical resistivity of the soil can be considered as a proxy for the spatial and temporal variability of many other soil physical properties (i.e. structure, water content, or fluid composition). Because the method is non-destructive and very sensitive, it offers a very attractive tool for describing the subsurface properties. It has been already applied in various contexts like: groundwater exploration, landfill and solute transfer delineation, agronomical management by identifying areas of excessive compaction or soil horizon thickness and bedrock depth, and at least assessing the soil hydrological properties. The surveys, depending on the areas heterogeneities can be performed in one-, two- or three-dimensions and also at different scales resolution from the centimetre scale to the regional scale.

The purpose of electrical resistivity surveys is to determine the resistivity distribution of the sounding soil volume. Artificially generated electric currents are supplied to the soil and the resulting potential differences are measured. Potential difference patterns provide information on the form of subsurface heterogeneities and of their electrical properties. The greater the electrical contrast between the soil matrix and heterogeneity, the easier is the detection.

Therefore in comparison with seismic topography, the GPR and ERT investigate the soil properties by considering the electrical conductivity of the ground and their depth range is limited by the electrical conductivity of the ground, the transmitted centre frequency and the radiated power. As conductivity increases, the penetration depth decreases. This is because the electromagnetic energy is more quickly dissipated into heat, causing a loss in signal strength at depth. Higher frequencies do not penetrate as far as lower frequencies, but give better resolution. Optimal depth penetration is achieved in ice where the depth of penetration can achieve several hundred meters. Good penetration is also

achieved in dry sandy soils or massive dry materials such as granite, limestone, and concrete where the depth of penetration could be up to 15 m. In moist and/or clay-laden soils and soils with high electrical conductivity, penetration is sometimes only a few centimetres.

Furthermore, these methods are non-invasive, can provide soil imaging from one to three dimensions, can be implemented for survey on big portion of land, can detect discontinuities and they can estimate the water content.

The features listed above are useful for having a deeper understanding of the ground and a review of electrical resistivity survey in soil science can be found in Samouelian et al. [213].

APPENDIX E: TRANSMISSIBILITY ANALYSIS

In this appendix further results of the transmissibility analysis are presented for three measurement sites in section 1, 2 and 3. The analysis follows the approach already described in section 8.5. Therefore for each site the characteristics are presented together with the linearity of the dual channel measurement, the transmissibility of the house closest to the control position and the comparison between the transmissibility functions. Furthermore, the relative error on the internal exposure metrics is shown for each house of the measurement sites. Comments are presented in section 4.

1. Site A

The site considered for the analysis is shown in Figure 109.

FIGURE 109 – SITE A

The distance between the source and the control position (blue line in Figure 109) is 10.8 meter; the distance between the source and the line of the buildings (yellow line in Figure 109) is 23 meters. For this site 3 houses have been considered, their characteristics are in Table 18.

House Nº	Distance CP (m)	Type	Room	Floor	Mounting	Nº Trains
11	27.7	Semi detached	Living Room	Ground	Plate	9
15	12.5	Semi Detached	Living Room	Ground	Direct	5
17	13.2	Semi detached	Kitchen	Ground	Direct	4

TABLE 18 - CHARACTERISTICS SITE A

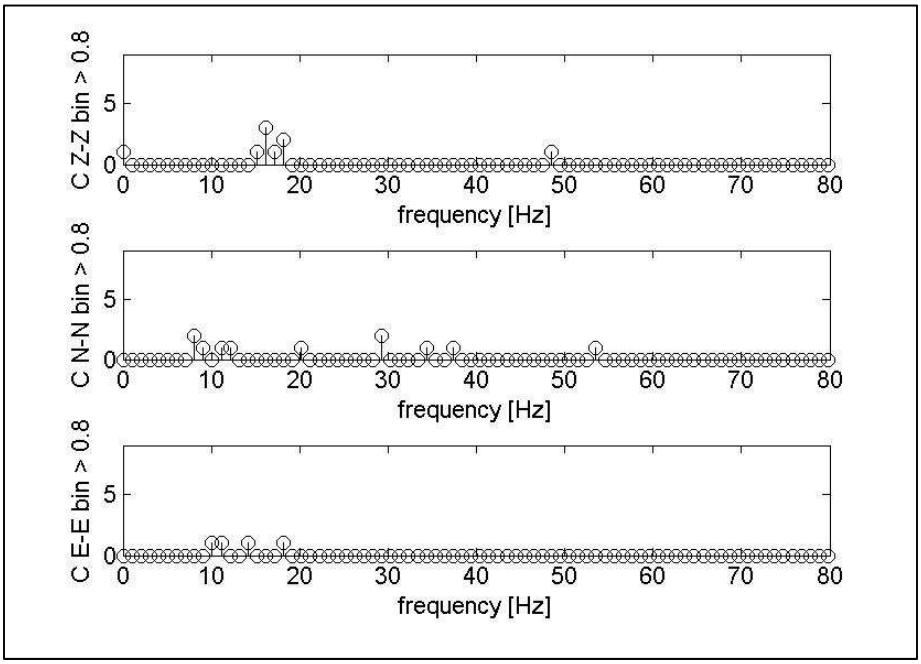

FIGURE 110 - SITE A HOUSE NUMBER 17. NUMBER OF THE FREQUENCY BINS OF THE MSC FUNCTION (C) WITH A VALUE ABOVE 0.8 AS A FUNCTION OF FREQUENCY. IN THE UPPER PANEL MSC BETWEEN THE Z COMPONENT IN *EXT* AND Z COMPONENT IN *INT* IS CONSIDERED. MIDDLE PANEL MSC BETWEEN N AND N. LOWER PANEL MSC BETWEEN E AND E

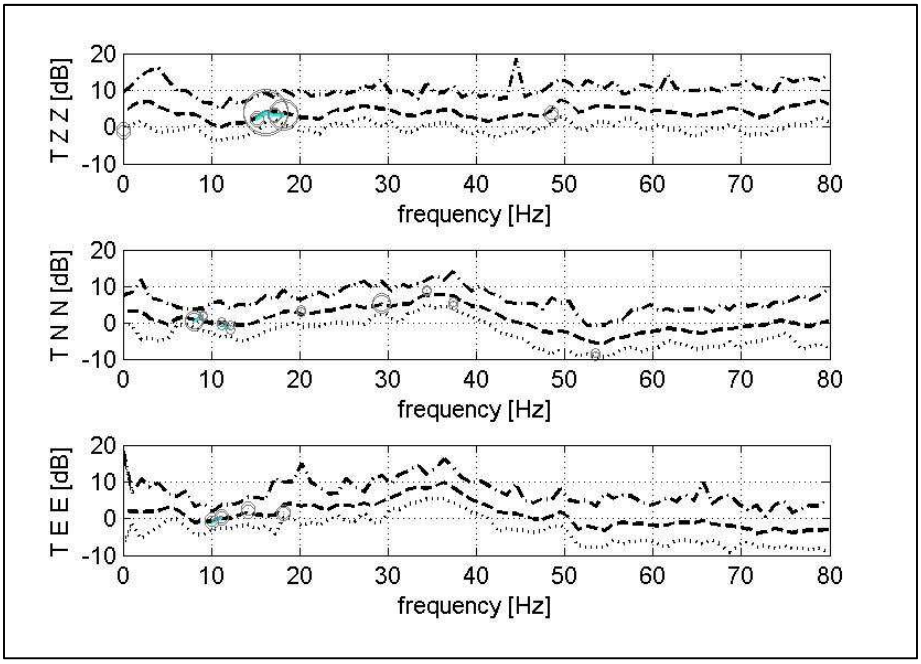

FIGURE 111 - SITE A HOUSE NUMBER 17. TRANSMISSIBILITY AS A FUNCTION OF FREQUENCY. FROM THE UPPER PANEL: TRANSMISSIBILITY BETWEEN Z, N AND E COMPONENTS. IN EACH FIGURE FROM THE TOP CURVE: H2, $H2_Q$,H,$H1_Q$ AND H1 FORMULATION. LEGEND SIMILAR TO FIGURE 96

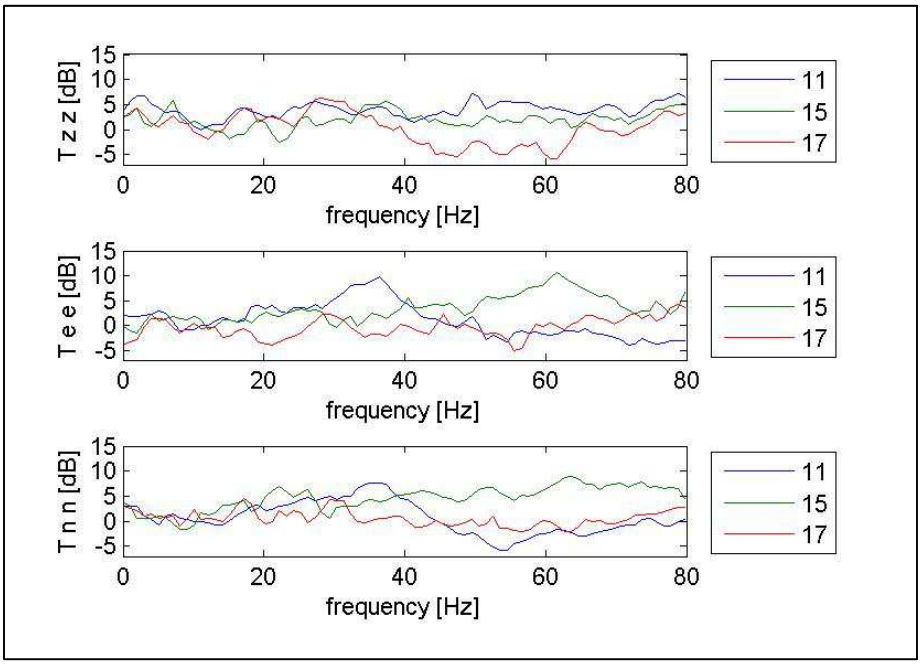

FIGURE 112 - TRANSMISSIBILITY COMPARISON BETWEEN HOUSES ON SITE A. UPPER PANEL TRANSMISSIBILITY Z COMPONENTS, MID PANEL TRANSMISSIBILITY E COMPONENTS AND LOWER PANEL TRANSMISSIBILITY N COMPONENTS.

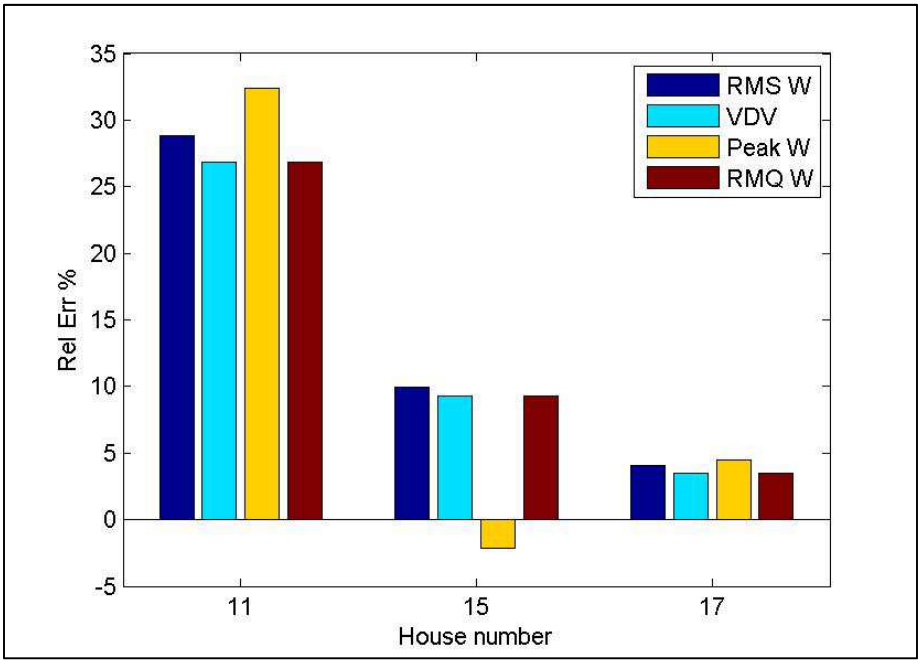

FIGURE 113 - SITE A. RELATIVE ERROR IN PERCENTAGE ON THE EXPOSURE METRICS FOR DIFFERENT HOUSES. METRICS CONSIDERED: W RMS, VDV, W PEAK AND W RMQ.

2. Site B

The site considered for the analysis is shown in Figure 114. The distance $\overline{D_{SC}}$ (blue line in Figure 114) is 10.8 meters; the distance $\overline{D_{SB}}$ (yellow line Figure 114) is 19.9 meters. For this site 2 houses have been considered, their characteristics are in Table 19.

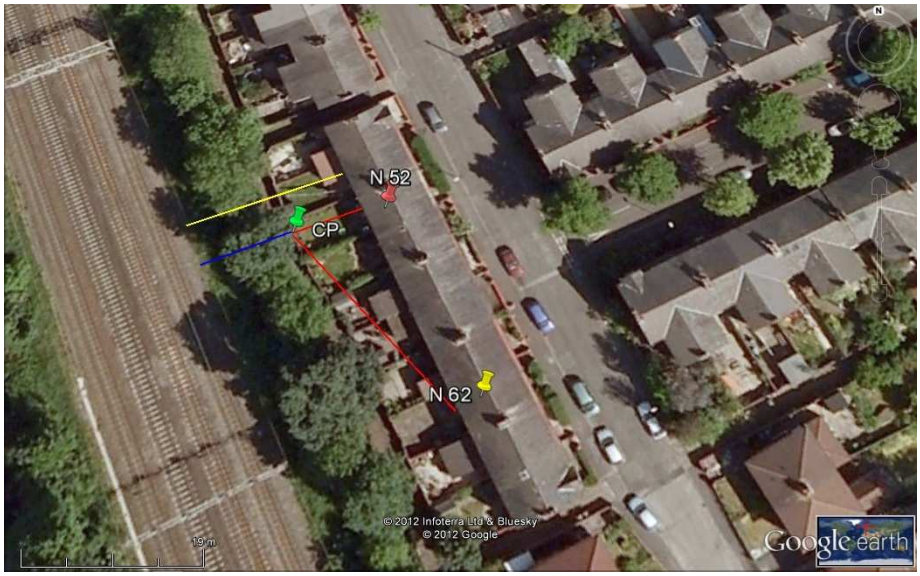

FIGURE 114 - SITE B

House N°	Distance CP (m)	Type	Room	Floor	Mounting	N° Trains
52	9	Terrace	Bedroom	First	Plate	7
62	29.2	Terrace	Kitchen	Ground	Direct	5

TABLE 19 - CHARACTERISTICS SITE B

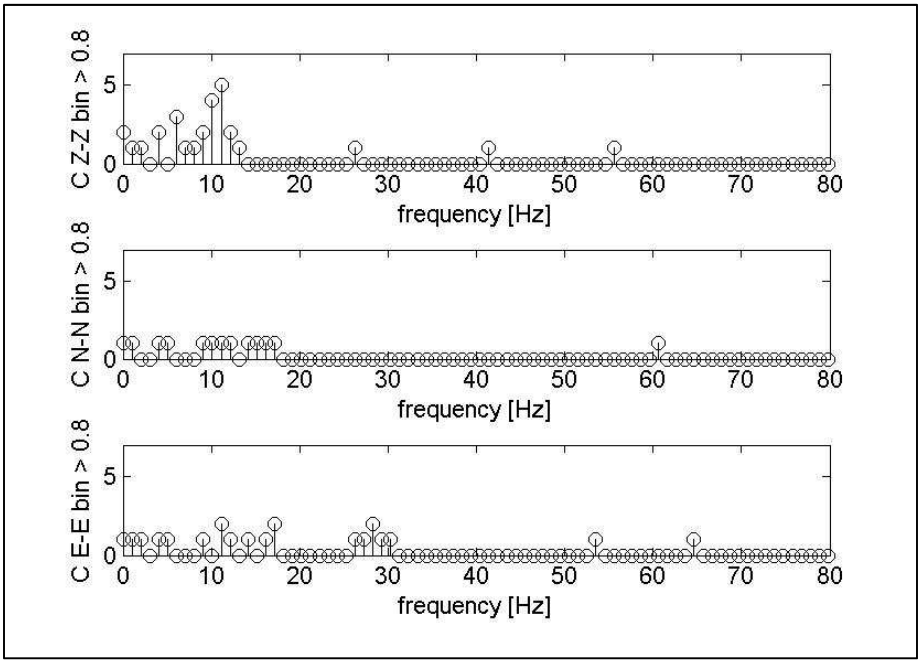

FIGURE 115 - SITE B HOUSE NUMBER 52. NUMBER OF THE FREQUENCY BINS OF THE MSC FUNCTION (C) WITH A VALUE ABOVE 0.8 AS FUNCTION OF FREQUENCY. IN THE UPPER PANEL MSC BETWEEN THE Z COMPONENT IN *EXT* AND Z COMPONENT IN *INT* IS CONSIDERED. MIDDLE PANEL MSC BETWEEN N AND N. LOWER PANEL MSC BETWEEN E AND E

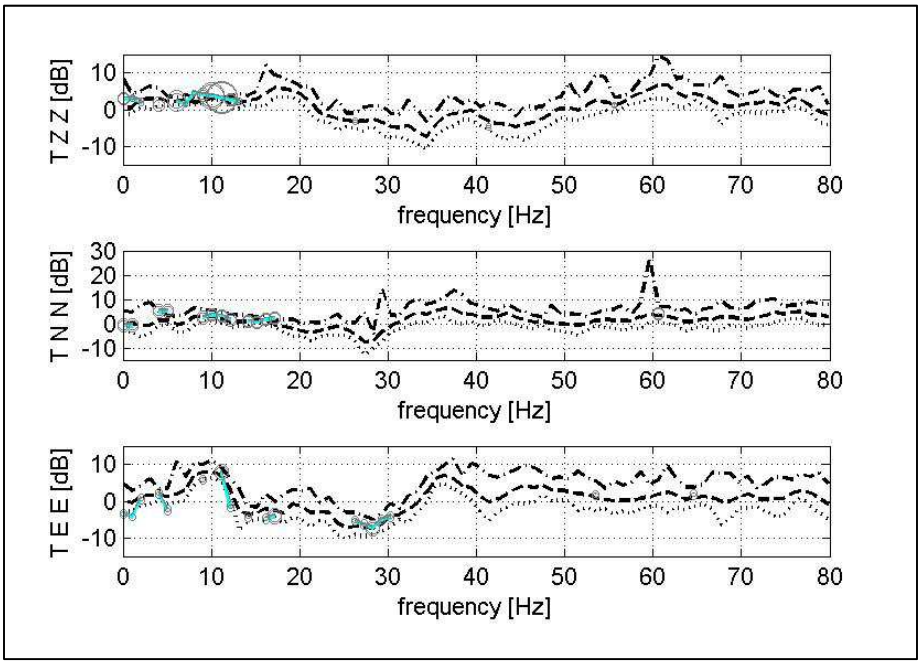

FIGURE 116 - SITE B HOUSE NUMBER 52. TRANSMISSIBILITY AS A FUNCTION OF FREQUENCY. FROM THE UPPER PANEL: TRANSMISSIBILITY BETWEEN Z, N AND E COMPONENTS. IN EACH FIGURE FROM THE TOP CURVE: H2, $H2_Q$,H,$H1_Q$ AND H1 FORMULATION. LEGEND SIMILAR TO FIGURE 96

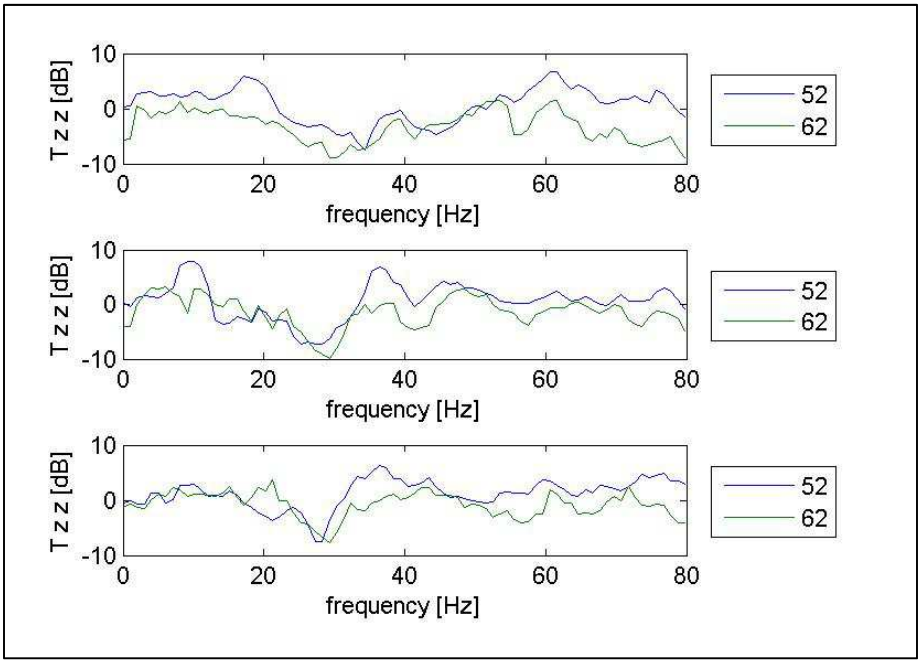

FIGURE 117 - TRANSMISSIBILITY COMPARISON BETWEEN HOUSES ON SITE B. UPPER PANEL TRANSMISSIBILITY Z COMPONENTS, MID PANEL TRANSMISSIBILITY E COMPONENTS AND LOWER PANEL TRANSMISSIBILITY N COMPONENTS.

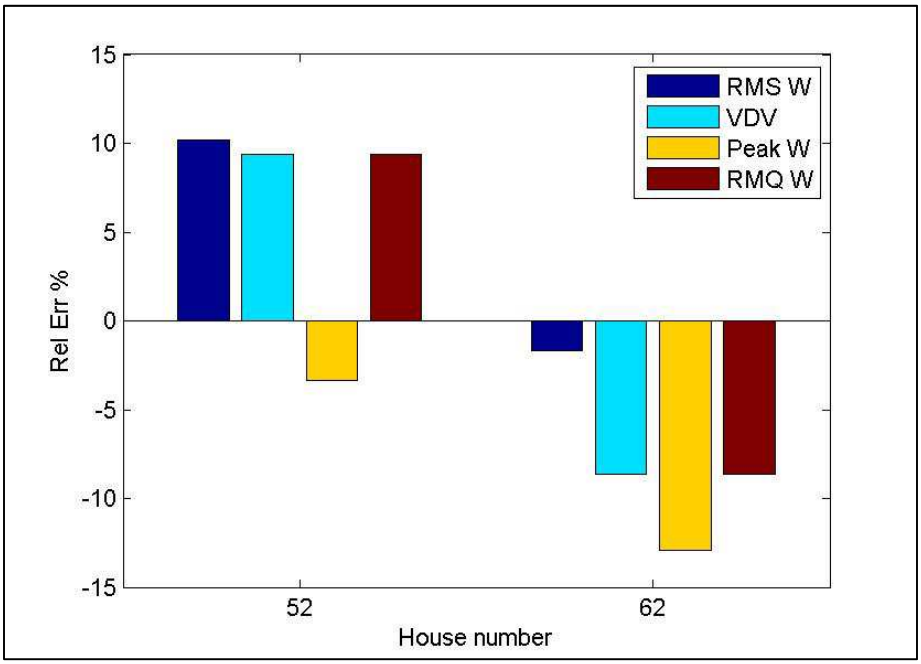

FIGURE 118 - SITE B. RELATIVE ERROR IN PERCENTAGE ON THE EXPOSURE METRICS FOR DIFFERENT HOUSES. METRICS CONSIDERED: W RMS, VDV, W PEAK AND W RMQ.

3. Site C

The site considered for the analysis is shown in Figure 119.

FIGURE 119 - SITE C

House N°	Distance CP (m)	Type	Room	Floor	Mounting	N° Trains
20	74.1	Terrace	Kitchen	Ground	Direct	5
44	13.7	Terrace	Kitchen	Ground	Direct	9
46	14.3	Terrace	Bedroom	First	Plate	6

TABLE 20 - CHARACTERSTICS SITE C

The distance $\overline{D_{SC}}$ (blue line in Figure 114) is 11.3 meters; the distance $\overline{D_{SE}}$ (yellow line Figure 114) is 27.9 meters. For this site 3 houses have been considered, their characteristics are in Table 20.

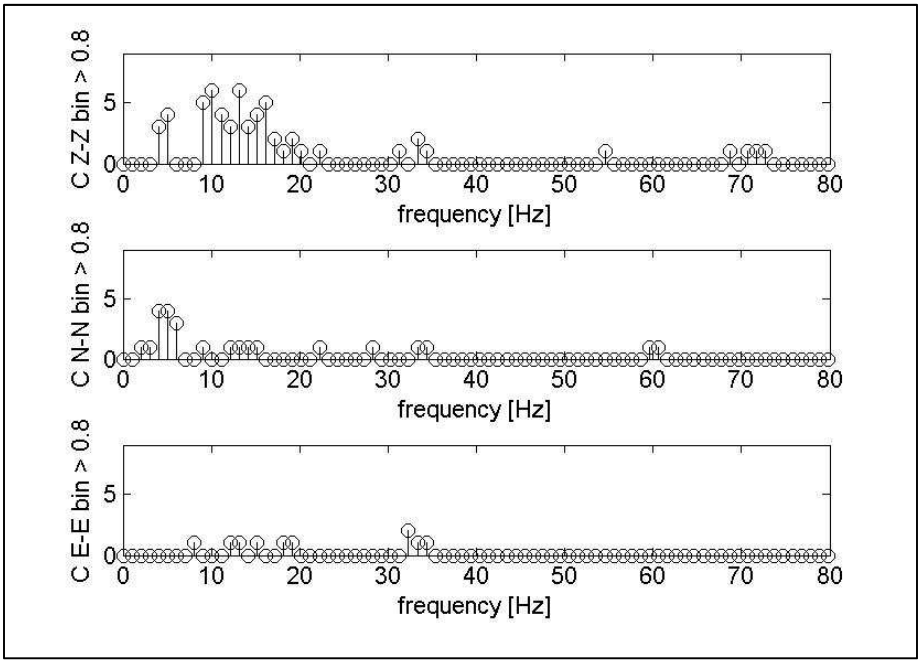

FIGURE 120 - SITE C HOUSE NUMBER 44. NUMBER OF THE FREQUENCY BINS OF THE MSC FUNCTION (C) WITH A VALUE ABOVE 0.8 AS FUNCTION OF FREQUENCY. IN THE UPPER PANEL MSC BETWEEN THE Z COMPONENT IN *EXT* AND Z COMPONENT IN *INT* IS CONSIDERED. MIDDLE PANEL MSC BETWEEN N AND N. LOWER PANEL MSC BETWEEN E AND E

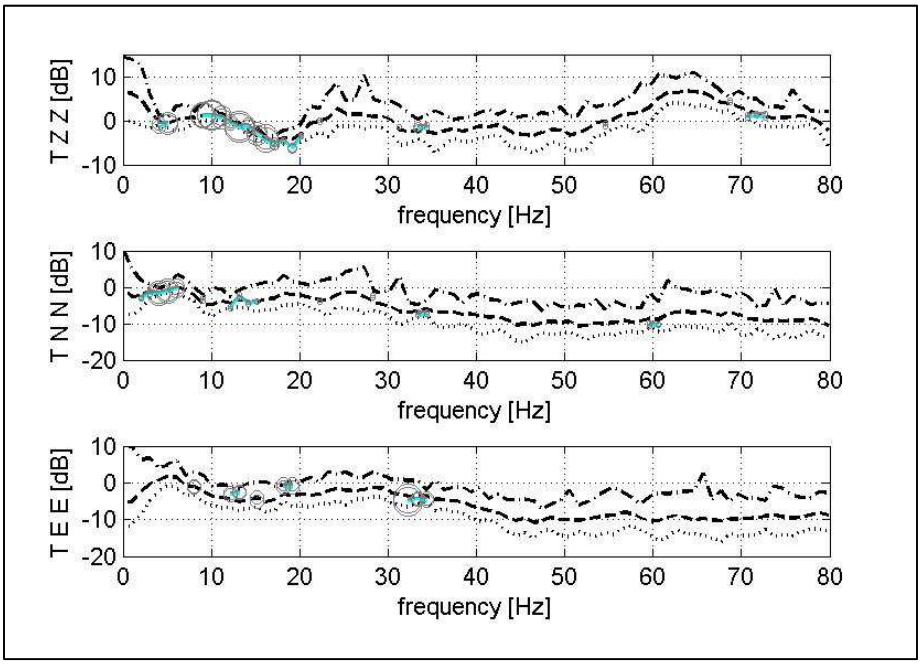

FIGURE 121 - SITE C HOUSE NUMBER 44. TRANSMISSIBILITY AS FUNCTION OF FREQUENCY. FROM THE UPPER PANEL: TRANSMISSIBILITY BETWEEN Z, N AND E COMPONENTS. IN EACH FIGURE FROM THE TOP CURVE: H2, $H2_Q$,H,$H1_Q$ AND H1 FORMULATION. LEGEND SIMILAR TO FIGURE 96

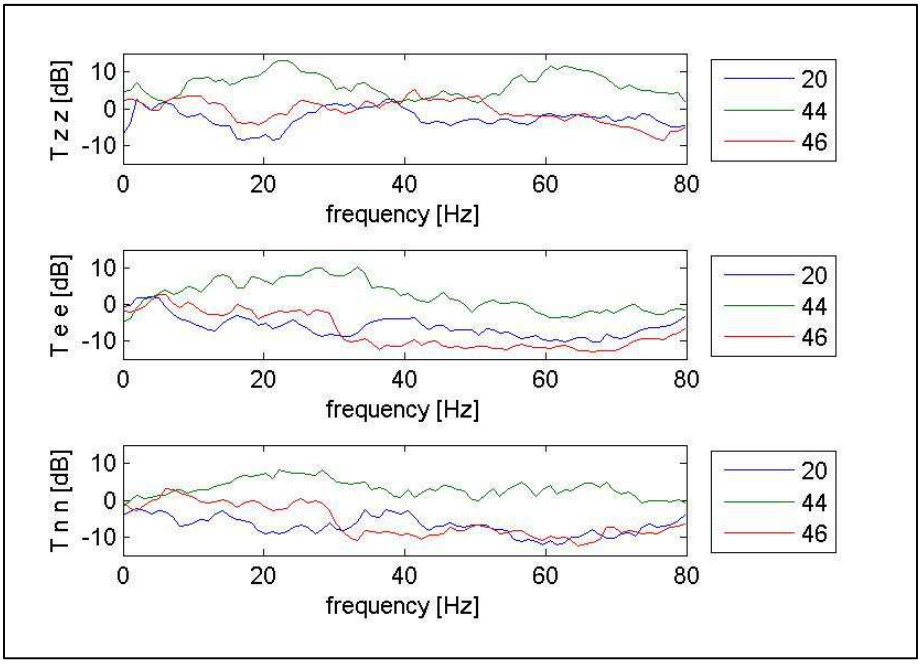

FIGURE 122 - TRANSMISSIBILITY COMPARISON BETWEEN HOUSES ON SITE C. UPPER PANEL TRANSMISSIBILITY Z COMPONENTS, MID PANEL TRANSMISSIBILITY E COMPONENTS AND LOWER PANEL TRANSMISSIBILITY N COMPONENTS.

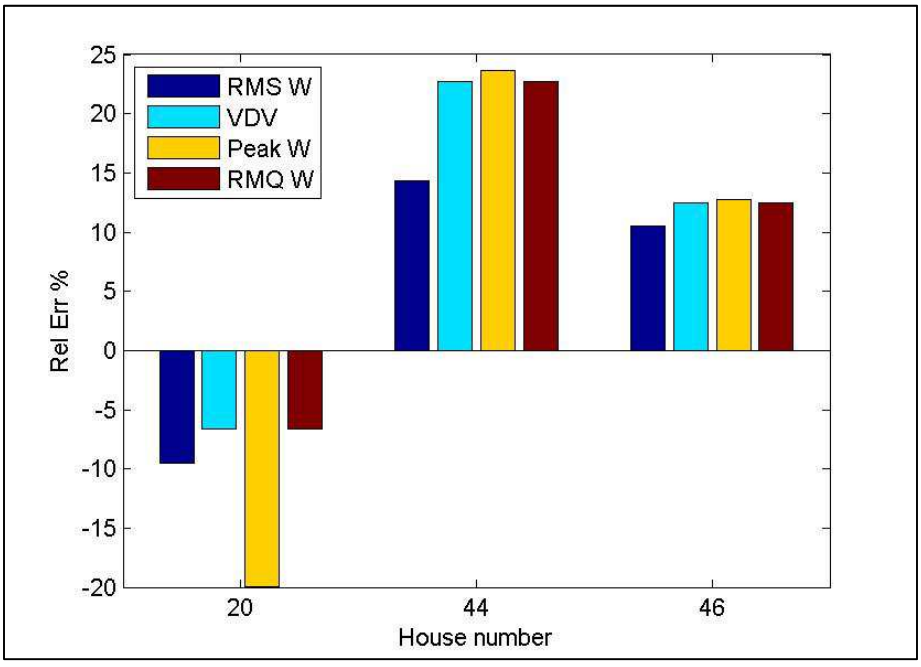

FIGURE 123 - SITE C. RELATIVE ERROR IN PERCENTAGE ON THE EXPOSURE METRICS FOR DIFFERENT HOUSES. METRICS CONSIDERED: W RMS, VDV, W PEAK AND W RMQ.

4. Comments

Apart the house number 11 in site A, the absolute value of the relative error for the internal exposure metrics for the other properties is below 20% as already found in section 8.5.6. Considering the results shows in 8.5.6 too, it can be noted that the number of trains for calculating the transmissibility may reduce the error on the internal exposure.

Other factors that can influence the error on the exposure metrics are: the noise at the measurement positions and the internal measurement position itself. Both elements may change the waveform inside the house especially the latter caused by the resonance of the structures in the property such us the floor.

Since the internal estimated event is obtained by filtering the event recorded outside the house, if the latter is similar to the internal event it's likely that the error on the internal exposure metric will be low. In this sense, further research is needed to establish the influence of the cross correlation on the error.

Then for each measurement site a comparison among the transfer functions of different houses have been presented. Only for site B (see Figure 117) a similar trend in the transmissibility functions can be easily recognised for all the three components as found in section 8.5.6 For the other two sites investigated (see Figure 117 and Figure 122), on the other hand, it is difficult to find a common trend in the behaviour of the transfer functions in function of frequency.